Spatial and temporal integration of granular inputs in the cerebellar cortex

Antoine Valera

UNIVERSITÉ DE STRASBOURG

Thèse de doctorat de l'Université de Strasbourg

Ecole Doctorale des Sciences de la Vie et de la Sante

Spécialité : Neurosciences

Présentée par Antoine VALERA

En vue d'obtenir le grade de docteur de l'université de Strasbourg

Spatial and Temporal Integration of Granular Inputs in the Cerebellar Cortex

Intégration spatiale et temporelle des entrées granulaires dans le cortex cérébelleux

Soutenue publiquement le 28 novembre 2013

Membres du jury

Pr. Henrik JÖRNTELL	Rapporteur externe
Dr. Dominique DEBANNE	Rapporteur externe
Pr. Rémy SCHLICHTER	Examinateur
Dr. Philippe ISOPE	Directeur de thèse

"Un bureau bien rangé est le signe d’un esprit dérangé"

Antoine de SAINT-EXUPERY

ACKNOWLEDGMENTS

First and foremost, I would like to thank my committee members Professor Henrik Jörntell, Doctor Dominique Debanne and Professor Rémy Schlichter for their precious time.

Merci à toi aussi Philippe pour tout le temps que tu m'as consacré depuis mon master en 2009 (et oui, 5 ans déjà !). Merci de m'avoir transmis ton enthousiasme pour les neurosciences et les analyses compliquées, mais surtout, merci pour la confiance que tu m'as accordée au cours de cette thèse à chaque fois que je voulais essayer une manip ou une analyse. Je crois que c'est cette liberté qui m'a le plus motivé pendant ces années.

Ensuite, je me dois de remercier infiniment la dream team. Merci à Laetitia pour toutes ces années passées à me supporter (depuis la L1, on attaque la 10ème année là !). Je te souhaite plein de bonnes choses pour la suite. Si tu te retrouves à Bale, ne prend pas l'accent suisse! Merci à Joseph, inébranlable, infatigable (sauf le matin), toujours prêt à filer un coup de main ! Et merci pour cette leçon de vie : un bureau peut effectivement rester rangé pendant toute une thèse. Respect ! Merci à ma Padawan, Anaïs, pour la joie, l'enthousiasme et le dynamisme que tu apportes dans notre bureau! Et puis bonne chance avec SynaptiQs... Merci aussi à la petite dernière, Flavia qui m'a sauvé des génotypages (et quand je dis sauvé, je le pense).

Merci aussi à tous les membres de notre chouette équipe. Tout d'abord, Jean-Luc, pour toutes ces passionnantes discussions politiques, culturelles et historiques qu'on a eu au cours de ces années. Et sache que Gustav Mahler m'a dignement accompagné durant cette rédaction! Merci aussi à Fred pour ta bonne humeur permanente, et ton stock secret de nourriture caché dans le placard du bas, porte de droite… (d'ailleurs il est vide, il faudrait que tu refasses les courses). Merci aussi à Bernard pour tes discussions précieuses, et tes connaissances encyclopédiques. Tu auras en tout cas réussi à me faire apprécier l'analyse de variance, et la chasse aux champignons. Merci aussi à tous les autres membres de l'équipe Jeff (prend soin de toi !), Didier, Jean, Jean-Louis. Grazie per la tua motivazione Super Francesca, e ricordati: non tocchi l'occhio!

Merci à tous les autres copains de l'institut avec qui j'ai passé tellement de soirées rock-happy-barbar…Merci à Coco, Pauline, Seb, Edith, David, Vy, Annie, Laureen, Marion, Aurélie, Audrey, JBS, et à tous les copains de la promo de master qui rôdent encore dans le coin ou qui viennent de partir : Alex, Romain, Michael, Paul, Laurent, Vivien, Bruce… Merci à tous ceux que je n'ai pas cité mais avec qui j'ai passé pleins de bons moments !

Merci à mes amis de longue date, que je devrais aller voir plus souvent (et qui me le rappellent régulièrement !) Julien, Noëlie, Tiphaine (nous sommes collègues désormais !), Lowik, Caro, Nono, Hélène, Sarah, Imane. Vous êtes les bienvenus à Londres ! Comme ça on est sûr de se croiser…

Pleins de merci à ma toute ma grande famille, et tout particulièrement à mes parents, mon petit frère Vincent, et à mes grands parents! Merci aussi à Armel, Carole et la Clara pour leur soutien.

Enfin, merci à ma Charline pour ta patience infinie, ta douceur, la force de tes convictions, et ta compréhension lorsque je rentre aussi tard qu'en ce moment. Zoubi la Nanine!

TABLE OF CONTENTS

TABLE OF FIGURES

ABBREVIATIONS

- A -

AMPA(R): 2-amino-3-(3-hydroxy-5-methyl-isoxazol-4-yl) propanoic acid (Receptor)

- D -

DAG: Diacylglycerol

DAO: Dorsal Accessory Olive

- E -

EAAT: Excitatory Amino Acid Transporter

EPSCs: Excitatory Postsynaptic Currents

- G -

GABA: *gamma*-Aminobutyric acid

GAD67: glutamic acid decarboxylase

$GlyT_2$: Glycine transporter 2

- H -

Hsp25: Heat shock protein 25

- I -

IP_3: Inositol triphosphate

- L -

LFD: Low frequency depression

LTD: Long term depression

LTP: Long term potentiation

- M –

MAO: Medial Accessory Olive

mGluR: metabotropic glutamate receptor

MPFA: Multiple-probability fluctuation analysis

- N -

Nfh: Neurofilament heavy chain

NMDA(R): *N*-Methyl-D-aspartate (Receptor)

nNOS: neuronal Nitric Oxyde Synthase

- P -

pcp2: Purkinje cell protein 2

PK: Protein Kinase

PLC: Phospholipase C

PP: Protein Phosphatase

- R -

RRP: Readily releasable pool

- S -

S1: Primary somatosensory cortex

- V -

VGLUT: Vesicular Glutamate Transporter

- Z -

ZII: Zebrin II

SUMMARY

The cerebellum is a structure involved in the control of posture, gait, motor coordination and motor learning. It integrates both sensory and motor information through two pathways: the climbing fibre-Purkinje cell pathway and the mossy fibre-granule cell-Purkinje cell pathway. Mossy fibre inputs carry sensorimotor context such as somesthesic information from specific receptive fields. Projections arrive in scattered locations in the cerebellar cortex which result in a fractured somatotopy. Sensory information carried by mossy fibres is transmitted to granule cells, which can fire high frequency bursts up to 1000 Hz. Many aspects of the spatiotemporal integration in the mossy fibre pathway structure are still unknown. During my PhD, I addressed two questions:

1: What are the short term plasticities that occur at the granule cell axon (parallel fibre) to Purkinje cell synapse during high frequency bursts and sustained trains? Is the information reliably transmitted in the whole physiological range of frequencies?

2: How are granule cell to Purkinje cell connections spatially organised? Are granule cells homogeneously connected along the mediolateral axis, or are there some hotspots of higher connection probability? Can we describe the cerebellar functional module, that is, the smallest processing unit, at the microcircuit level? This question was further extended to the other granule cell targets: molecular layer interneurons and Golgi cells.

Using whole cell patch clamp recordings in rat cerebellum acute slices, I found that high frequency information processed in the mossy fibre-granule cell pathway is conserved at the parallel fibre to Purkinje cell synapse. Small bursts of action potential could evoke strong Excitatory Postsynaptic Currents (EPSCs) at the Purkinje cell soma. The reliable transmission at the parallel fibre to Purkinje cell synapse can follow high frequency rates, with high initial release probability, paired-pulse facilitation up to 700 Hz, and sustained facilitation during tens of pulses. We found, by using variance mean analysis, that this fast release is possible during bursts through the recruitment of reluctant vesicles that boost vesicular release. Moreover, fast release can be sustained through fast vesicles reloading.

In a second study, by using precise RuBi-Glutamate uncaging onto granule cells, and by recording either Purkinje cells, molecular layer interneurons or Golgi cells, I found that in the anterior vermis of the mouse cerebellum, granule cell to Purkinje cell connection follows a precise spatial organisation. Specific sets of Purkinje cell, that can be identified using histochemical markers, receive inputs from small granule cell hotspots. Local granule cells generally elicit a strong input, but distal granule cells located in specific regions can also be strongly connected. The connection pattern between two neighbouring cells is highly correlated in a single animal. Inter-individual variability is important, probably because of individual motor learning performed in each animal, but similarities can be found, suggesting a shared general organisational map in the cerebellar cortex. Similar experiments performed on molecular layer interneurons showed an distinct pattern, suggesting that a given patch of granule cell either directly activate or indirectly inhibit distal Purkinje cells. Recordings of Golgi cells expressing glycine transporter 2 ($GlyT^{2+}$), a subpopulation of Golgi cells that are not homogeneously distributed, revealed that Golgi cells essentially receive inputs from local granule cells, whereas EPSCs from parallel fibres were weak and rare. This result suggests that basolateral dendrites and apical dendrites perform distinct computations in the network.

PREFACE

During my thesis, I worked on two main projects. The first one focused on short term plasticities that occur at the parallel fibre to Purkinje cell synapse in the cerebellar cortex, during high frequency bursts of action potentials. This work resulted in a first article *"Adaptation of granule cell to Purkinje cell synapses to high-frequency transmission"* (Valera et al., 2012). Frederic Doussau, in our team, continued this work and found further evidences supporting our data. I will describe some of these new results as supplementary results.

During the third and fourth year of my PhD, I started a second project that focused on the spatial organisation of the cerebellar cortex. The goal was to describe the cerebellar module, that is, the smaller functional unit of the cerebellum, at the microcircuit level. Could I delimitate its functional borders? And if it exists, which cells are actually included in this microcircuit, and which ones are not? This project required a long period of coding and technical adjustments. The result of this work is exposed in a second article, which has been recently written. It is thus presented in its non-definitive form.

In parallel, in the continuity of a previous PhD student, Heloïse Cruveiller, along with heroic histological quantifications of Jean-Luc Dupont, a third article is in preparation, which will be more focused on the spatial distribution of the different Golgi cells subtypes in the cerebellar cortex. In this project, which is complementary to my second paper, my contribution was essentially in data analysis. A small part of this work is presented in the second article of this manuscript.

For clarity, my two projects will be introduced in a non-chronological order. Thus, in the first chapter, I will describe the general organisation of the cerebellum, its main functions, the major cell types and subtypes, and some general consideration about the cortical network connectivity. The remarkable spatial organisation of the structure will be detailed in a second chapter, in which different somatotopical, histochemical and functional aspects of the cerebellar physiology will be detailed. Finally, in a third chapter, some temporal aspects of the neurotransmission will be developed: high frequency bursts and their consequences on firing patterns and short term plasticities.

INTRODUCTION

A SHORT HISTORY OF THE CEREBELLAR PHYSIOLOGY

The first known mention of the cerebellum dates back to the Greco-Roman literature from the 4th century B.C., when a structure distinct from the cerebrum was described. This structure, located at the back of the brain, was named *paracephalon* by Aristotle and Praxagoras, and *enpenkranis* by Erasistratus. Galen, in the 2nd century A.D. described the cerebellum with more details, and especially its medial part, later named *vermis*. Cerebellum was proposed to be the source of the cranial nerves and spinal cord. In accordance with the current opinion of that time, Galen suggested that the cerebellum could be a pump involved in the regulation of the flow of the *animal spirit*, that is, the liquid giving the movement to the muscles. Although Galen's observations were a big step forward at that time, their interpretation through the Greek theory of humorism restricted medical progresses for almost 15 centuries.

FIRST ANATOMICAL DESCRIPTIONS

Very little progress was made in neuroanatomy until Vesalius in the 16th century and his human anatomy textbook: *De humani corporis fabria,* published in 1543, when the work of Galen was reanalysed with new methodological approaches. Vesalius represented the human cerebellar structure, but without commenting on cerebellar function. His seminal work influenced all the following anatomists of the Renaissance. In 1575, Varolio brought more details in the external description of the cerebellum, and notably its link with the *pons*. One century later, Malpighi (1665) described the *cerebellar cortex* and the *white matter fibres,* noticing that they "*seem to have origin from the trunk of the spinal marrow contained within the cranium*". Raymond de Vieussens mentioned a few years after an "*ash grey glandular area*" that turned to be the *cerebellar nuclei*, a structure that Félix Vicq d'Azyr described more in details in 1805, although their modern names were only fixed later in the 19th century.

The first precise report on cerebellar cortex appears at the end of the 18th century in Malacarne work (1776). He described and named the lobes and lobules for the first time. He chose names based on lobule shape. Some of these names are still in use, like the lingula (from linguetta - "small tongue" in Italian), the uvula or the tonsil. This descriptive work was later refined by Reil (1807-1808) and Burdach (1819-1826). At this time, the first anatomical bases of the cerebellar anatomy were established.

EARLY CONCEPTS ON CEREBELLAR FUNCTIONS

All attempts to describe cerebellar function before the beginning of the 19th century were highly speculative. Rolando (1809), Flourens (1826), and later Luciani (1891) were the first to assess the link between cerebellum and motor functions, based on experimental research. Rolando, following

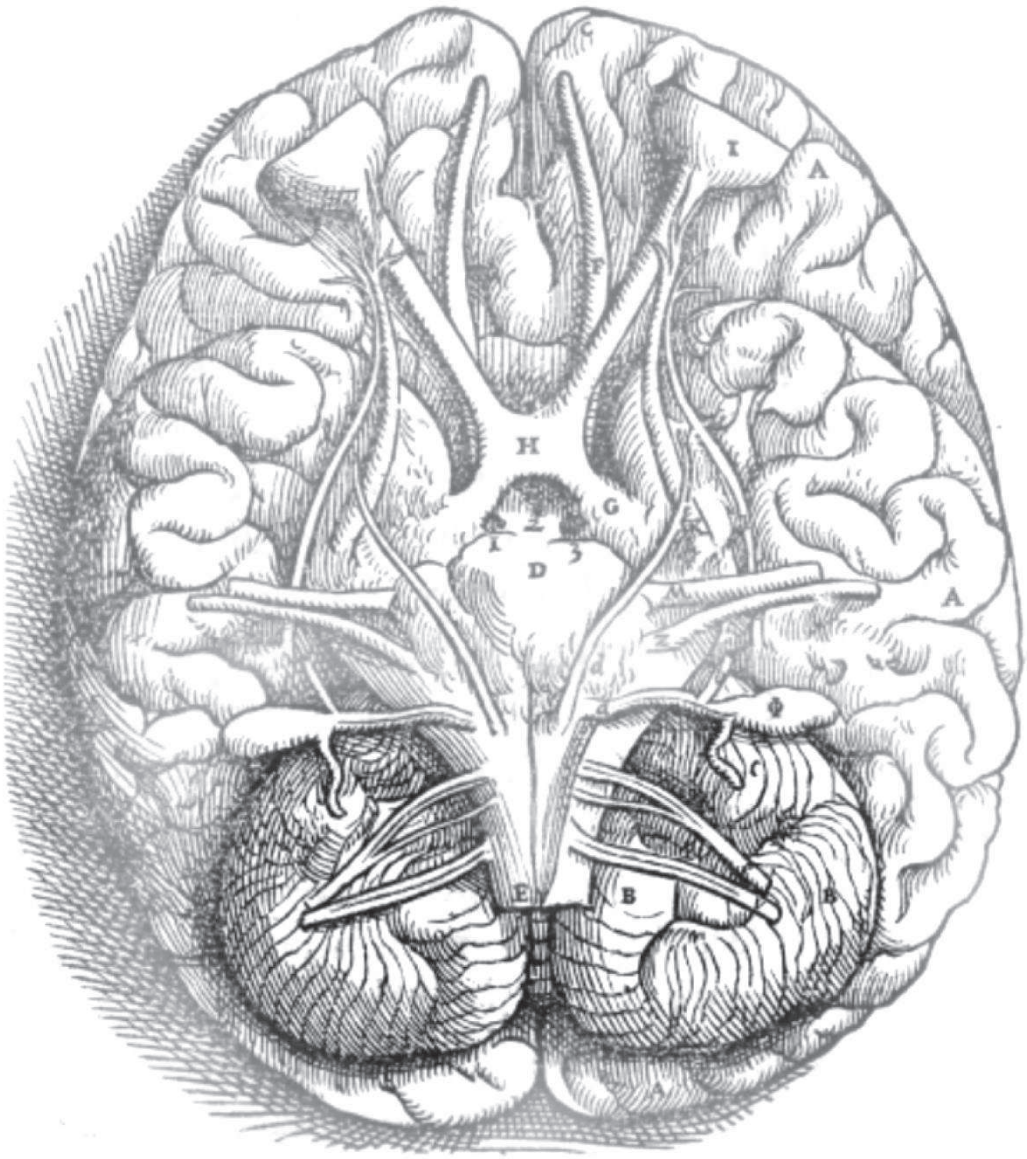

The first known illustration of the cerebellum, from De humani corporis fabrica, Andras Vesalius, 1543.
This illustration represents a ventral view of human brain. The cerebellum was darken.

partial and total ablation of the cerebellum, observed severe impairment of motor functions, but not of sensory or intellectual ones. He concluded from this work that the cerebellum was involved in the initiation of movements. One year after the translation of Rolando's work in French, Flourens (1924) developed the idea that movement initiation was actually not affected, but that regularity and coordination were lost. Thus, Flourens was the first to separate motor initiation from motor coordination, and to associate them with distinct brain regions. Luciani further detailed the semiology of cerebellar lesions, discriminating transient from permanent effects of a cerebellar lesion. According to Luciani, a cerebellar lesion is followed by an asthenia or muscular weakness, an atonia or lack of normal muscle tone, and an astasia or unstable muscular contraction. For him, these three symptoms explain all the behaviours associated with a cerebellar lesion, including "*tremor, titubation and rhythmically oscillating movements*". Later on, more precision in the symptoms were added by Babinsky (1902) like dysdiadochokinesis - the inability to perform rapid sequences of movements - or asynergia - the inability to coordinate groups of muscles in complex movements. These observations were confirmed and clarified in the following years by Holmes (1917, 1922) who studied soldiers wounded during the First World War, and patients with cerebellar tumours. He observed many occurrences of tremors and dyskinesia, and developed the concept of ataxia. At this time, the major implication of the cerebellum in the control of complex and voluntary movements was established.

The concept of functional organisation only emerged at the end of the 19th century in the cerebral cortex, and was extended to the cerebellum a few years later. After the early description of the cerebellar histology (Ramon y Cajal, 1911) and the first recordings of electrical activity in the cerebellum (Adrian, 1935), the idea of a structured cerebellar cortex was progressively refined, with major breakthrough at each technological progress. In the 60's, electronic microscopy allowed the description of the fine structure of the cerebellar tissue (Palay and Chan-Palay, 1974), while electrophysiological recordings permitted to describe the network and the cellular connections (Eccles et al., 1967). During the 70's and the 80's, the first precise maps of cerebellar somatotopy were performed, and immunohistochemistry revealed new cellular populations and cerebellar compartments (Voogd, 1967; Shambes et al., 1978b; Hawkes et al., 1985). More recently, patch clamp recordings and Ca^{2+} imaging techniques helped to understand synaptic integration, while genetically modified mice revealed the function of specific proteins in the cerebellar physiology.

Though, one century after the first description of the cerebellar circuitry, and despite the great number of laboratories that worked - and are still working - on the cerebellar physiology, the precise description of the cerebellar spatial organisation is yet in debate, like many other aspects of the cerebellar functions. To date, we probably lack an overview of all the cellular subtypes, the complete wiring diagram of the different cerebellar regions, the precise electrophysiological profile of the cerebellar neurons with their respective integration properties and metaplasticities profiles, as well as a comprehensive computational model of the cerebellar cortex, and even a full list of cerebellar functions such as its involvement in cognition.

1 GENERAL ANATOMY AND HISTOLOGY OF THE CEREBELLUM

1.1 CEREBELLAR FUNCTIONS

Most of the cerebellar functions are known from clinical observations, some of them for more than a century. Since then, pharmacological, lesion-induced, or more recently mutant animal models were developed to study cerebellar functions. In this chapter, I will present the main cerebellar function and the general circuitry of the cerebellar cortex. Then, in a second time, I will detail morphological and functional features of some of the cerebellar cell types, since we will discuss about cerebellar connectivity in the following chapters.

1.1.1 ROLES OF THE CEREBELLUM

The cerebellum is a structure related, first and foremost, to sensorimotor functions. It is considered to be involved in the control of gaze, gait and posture, fine motor coordination, motor learning, prediction of movements and correction of motor errors. To perform these tasks, the cerebellum integrates both sensory and motor signals coming from both the cerebral cortex and from multiple sensory receptors throughout the body, sometimes after multiple and complex integrative steps.

Sensory information coming from the whole body give contextual clues like skin pressure, muscle or skin stretch, articulations position or head inclination. Visual, auditory and somesthetic information are carried to the cerebellum by distinct pathways. In parallel to real-time sensory information, the cerebellar cortex receives inputs coming from several areas of the neocortex such as the prefrontal or the parietal cortex, carrying a copy of the motor command sent to the spinal cord termed *corollary discharges* (Sperry, 1950; Bell, 1981; Wolpert et al., 1998).

In order to efficiently control and adjust the movement while it is executed, the cerebellum is thought to predict the future sensory state of the body (Wolpert et al., 1998; Bastian, 2006). In this view, the prediction is then compared with the real sensory state, and any discrepancy would indicate a motor error or a novel sensory stimulus. In this process, the cerebellum is also able to adjust the movement, by sending a corrected motor order both to the motor cortex and to other motor structures like the red nucleus. In order to sort only relevant sensory information, the cerebellum is able to suppress the sensory feedback induced by the execution of self-generated movements (Blakemore et al., 1998).

1.1.2 SEMIOLOGY

Illustration of the cerebellar functions can come from the observation of cerebellar lesions. For example, a lesion in the flocculonodular lobe can result in a nystagmus, but also in impairments of the body balance. These symptoms illustrate the implication of that region of the cerebellar cortex in occulomotor reflexes and in the visual and vestibular control of movements. Lesions located in the

vermis essentially impair the gait ("drunken sailor" gait) whereas damages in the cerebellar hemispheres can result in ipsilateral impairment of voluntary multi-joint movements and intention tremor.

More surprising evidences suggest an implication of the cerebellum in various cognitive functions (Ivry et al., 1988; Ito, 2008; D'Angelo and Casali, 2012) like time perception, autonomous responses in fear conditioning, schizophrenia, dyslexia, autism and even tinnitus (Bauer et al., 2013). With the major difficulty that each lesion in the cerebellum can also induce motor disturbances, which can affect the measurement of the performances during cognitive tasks, these experiments revealed broader cerebellar functions than initially hypothesised. Several authors suggested that the cerebellum might use the same framework to perform cognitive tasks as those used for sensorimotor processes (Glickstein et al., 2011; D'Angelo and Casali, 2012).

1.2 GENERAL STRUCTURE OF THE CEREBELLUM

Inherited from the phylogenetic evolution of the vertebrates, the structure of the cerebellum essentially differs from one species to another in term of size and shape. It evolved from a leaf-like structure in amphibians and reptiles to the complexly foliated structure we can observe in upper mammals (Voogd and Glickstein, 1998). Nonetheless, the cerebellum is an evolutionary conserved structure, keeping striking similarities in development, histochemical compartmentation, structure and functions between vertebrates, suggesting its conserved involvement in sensorimotor tasks. In mammals, the size of the cerebellum is linearly correlated with the body surface, another argument for its role in sensorimotor processing (Sultan and Braitenberg, 1993; Heck and Sultan, 2002).

In all mammals, the cerebellum is composed of two main structures: three pairs of cerebellar nuclei and the cerebellar cortex, a three-layer cortex of about 500 µm thick. As an indication of its important foliation, in humans, the unfolded cerebellum is 15 cm large and 2 m long.

1.2.1 MULTIPLE ORGANISATION LEVELS IN THE CEREBELLAR CORTEX

The spatial organisation of the cerebellar cortex follows two main axes (Figure 1): the anterio-posterior one separates the cortex in lobes and lobules (Figure $2A_1$-$2A_3$) whereas the mediolateral one separates it between a vermis and two hemispheres (Figure 2B). The mediolateral axis is sometimes named *long axis of the folium*. This term actually embraces both the coronal and the horizontal/transverse plane (Figure $1B_2$, $1C_2$). Because of the cerebellar folding, acute slices in either coronal or horizontal/transverse plane have similar tissular organisation (Figure $1B_3$, $1C_3$, see also Figure 4). However, each slicing plane will allow the study of a different set of lobules. This point is of primary importance in my second article, in which the experiment required the recording of analogous cells (i.e. at the same set of parasagittal and mediolateral coordinates). More generally, the use of the horizontal plane is more convenient because it allows an easier recognition of the lobules, compared to the coronal plane which often results in twisted regions with more damaged cells.

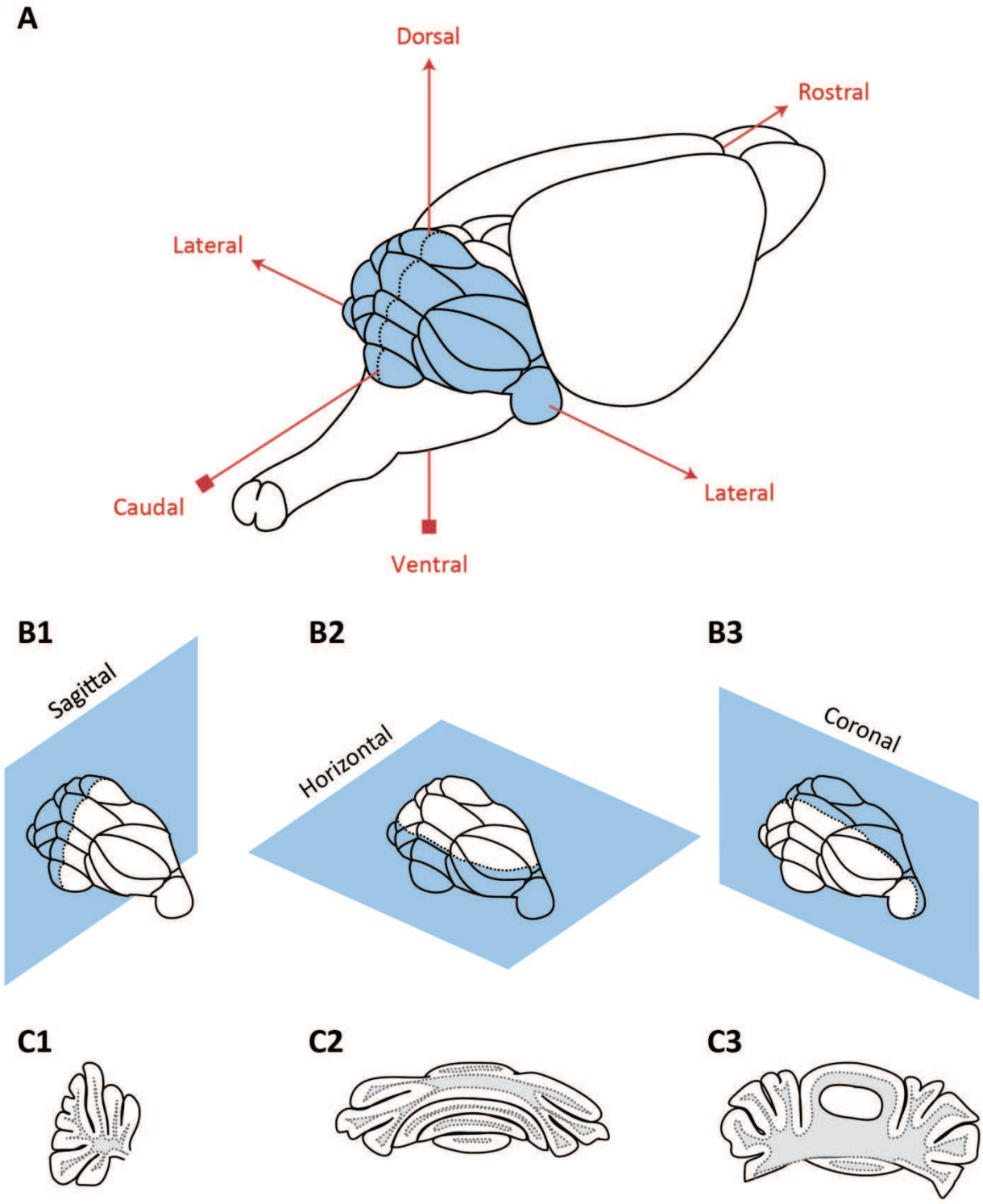

Figure 1 : Anatomical planes in the cerebellum.
A : Rostrocaudal, ventrodorsal and mediolateral axes. Representation of a mouse cerebellum (blue). The midline (dotted line) defines a mediolateral axis.
B : Three common orientation planes used *in vitro*. $\mathbf{B_1}$: Sagittal; $\mathbf{B_2}$: Horizontal; $\mathbf{B_3}$: Coronal.
C : Illustration of slices resulting from $\mathbf{C_1}$: Sagittal slicing; $\mathbf{C_2}$: Horizontal slicing; $\mathbf{C_3}$: Coronal slicing. Illustrations are based on experimental slices.

1.2.1.1 ANATOMICAL SEGMENTATION

Several grooves cross the cortex transversally, segmenting the cerebellum along the anterio-posterior axis. The two deepest ones divide the cerebellum in three lobes (Figure $2A_1$, $2A_2$, $2A_3$): the anterior lobe (anterior zone), the posterior lobe (central zone and posterior zone) and the flocculonodular lobe (nodular zone). A finer subdivision based on human anatomy (Larsell, 1952), splits the cerebellum in ten lobules, but the exact number of folia can actually vary from one species to another. For instance, in the mouse, lobules IV and V are fused whereas lobule VI is separated in VIa and VIb-c.

The mediolateral organisation (Figure 2B) separates the cerebellum in a vermal part, surrounded by two cerebellar hemispheres which can each be further split into an intermediate hemisphere or *paravermis*, and a lateral hemisphere.

1.2.1.2 FUNCTIONAL SEGMENTATION

A third approach to divide the cerebellum is based on a general segmentation of cerebellar functions. Inherited from the phylogeny, the cerebellum has three major regions, each one receiving major inputs from different regions of the nervous system, and each cortical region projecting to separate cerebellar nuclei (Figure 2C). Although often used, this segmentation can be misleading, because most regions actually receive inputs from several origins.

1.2.1.2.1 VESTIBULOCEREBELLUM

The oldest phylogenetic part, the *vestibulocerebellum* or *archeocerebellum*, is already present in the chondrichthyes (cartilaginous fishes). Besides vestibular information, the primitive cerebellum also receives cutaneous and proprioceptive inputs, especially from the lateral line. In higher vertebrates, this region corresponds to the *flocculonodular* lobe (Lobule X), which controls balance and eye movements. Because the posterior part of the Lobule IX performs similar functions, it is also considered as part of the vestibulocerebellum. The vestibulocerebellum projects directly out of the cerebellum, in the lateral vestibular nuclei (see Figure 3C).

1.2.1.2.2 SPINOCEREBELLUM

On the phylogenetic timescale, the second part of the cerebellum to appear is the vermis. Major inputs are coming from the spinal cord, giving the name of *spinocerebellum* to that region. The vermis receives somatic sensory inputs as well as visual, auditory and vestibular information, in order to control posture, locomotion and gaze. Efferences from the vermis of lobules I to $IX_{anterior}$ mainly target structures related to these functions, in the brain stem through the fastigial nucleus, directly to vestibular nuclei as in the flocculonodular lobe, and to the cerebral cortex (Sugihara, 2011). The muscles targeted by spinocerebellar outputs are principally located in the trunk and in the proximal parts of the limbs.

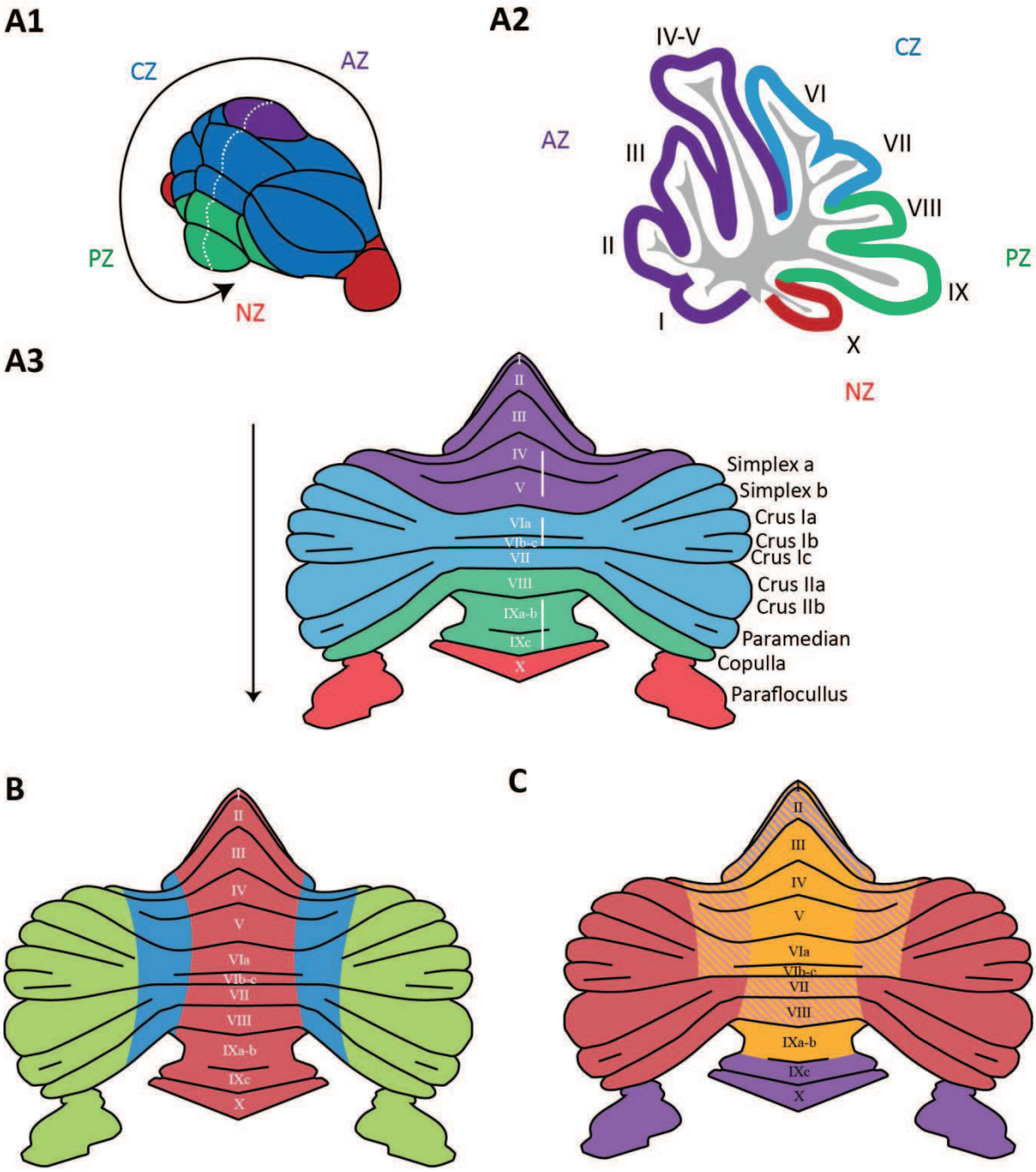

Figure 2 : General anatomy of the cerebellar cortex.

A : Anterioposterior segmentation: lobes and lobules. $\mathbf{A}_1$: Cerebellar cortex is divided in four zones : the anterior zone (AZ - purple), central Zone (CZ - blue), posterior zone (PZ - green) and nodular zone (NZ - red). $\mathbf{A}_2$: Sagittal view of the cerebellar cortex (corresponding to white dotted line in A_1). Cerebellar cortex is divided in 10 lobules, numbered I to X. $\mathbf{A}_3$: Unfolded view of the cerebellar cortex. Black arrow corresponds to black arrow in A_1. Names of the hemisphere lobules are indicated. Unfolded view adapted from (Sugihara and Shinoda, 2004).

B : Segmentation based on the mediolateral anatomy. The vermis (red) is surrounded by the paravermis (blue) and by the lateral hemispheres (green).

C : Anatomo-functional segmentation. Each region projects to different cerebellar nuclei. The vestibulocerebellum (purple) projects to the vestibular nuclei. The spinocerebellum (orange) projects to the fastigial (medial) nuclei for its most medial part, and to the interposed nuclei for its more lateral parts. The neocerebellum (red) projects to the dentate (lateral) nuclei. Hashed surfaces indicate that some regions receive different types of inputs.

The *paravermis* or lateral hemisphere can be considered as part of the spinocerebellum. This region integrates information coming from the limbs and projects first to the interposed nucleus, which in turn projects to the red nucleus or to the cortex through the thalamus.

1.2.1.2.3 CEREBRO-CEREBELLUM

The third part of the cerebellar cortex, the *neocerebellum* or *cerebrocerebellum* corresponds to the cerebellar hemispheres. Somesthetic, sensory and motor afferences coming from the cerebral cortex enter the cerebellum after a relay in the pontine nuclei. The cerebrocerebellum is particularly developed in primates in parallel to the massive development of the neocortex. The cerebrocerebellum sends back information to the cerebral cortex via the dentate nuclei.

1.2.2 CEREBELLAR INPUTS: INFERIOR OLIVE AND PRECEREBELLAR NUCLEI

Two main inputs project to the cerebellum, (Figure 3). Climbing fibres all originate from the inferior olive, an extensive nucleus located in the medulla, while mossy fibres are of various origins, grouped under the name of *precerebellar nuclei.*

The inferior olive receives sensory and motor information from very broad origins (cortex, spinal cord, precerebellar nuclei as well as a feedback from the cerebellar nuclei). It is an integrative structure that sends its projection to the cerebellum (Figure 3A). Its function is not clearly defined, but it was proposed to be involved in movement error detection and movement timing control (De Zeeuw et al., 1998; Llinás, 2009). Briefly the inferior olive is subdivided in three major subnuclei: Principal Olive, Dorsal Accessory Olive (DAO), Medial Accessory Olive (MAO) and four smaller subnuclei. Each part can be further subdivided based on its afferences and efferences.

Precerebellar nuclei (Figure 3B) carry sensorimotor information through mossy fibres either from the spinal cord, brainstem or from the cortex after a variable number of relays. Some precerebellar nuclei like the external cuneate nucleus or the gracile nucleus are direct relays of sensory information coming from the body whereas other nuclei like the pontine nuclei relay more integrated information coming from the cortex. The organisation of the inputs will be described more in details in chapter 2.

1.2.3 CEREBELLAR OUTPUTS: CEREBELLAR NUCLEI AND VESTIBULAR NUCLEI

The cerebellar nuclei (often: deep cerebellar nuclei) are the sole output of the cerebellum (Figure 3C). They receive collaterals from the cerebellar inputs, and are also targeted by all the axons leaving the cerebellar cortex from Purkinje cell axons. They are composed of three pairs of nuclei, located in the depth of the cerebellum, and surrounded by white matter. Cerebellar nuclei are named medial, interposed (anterior and posterior part) and lateral nuclei (respectively fastigial,

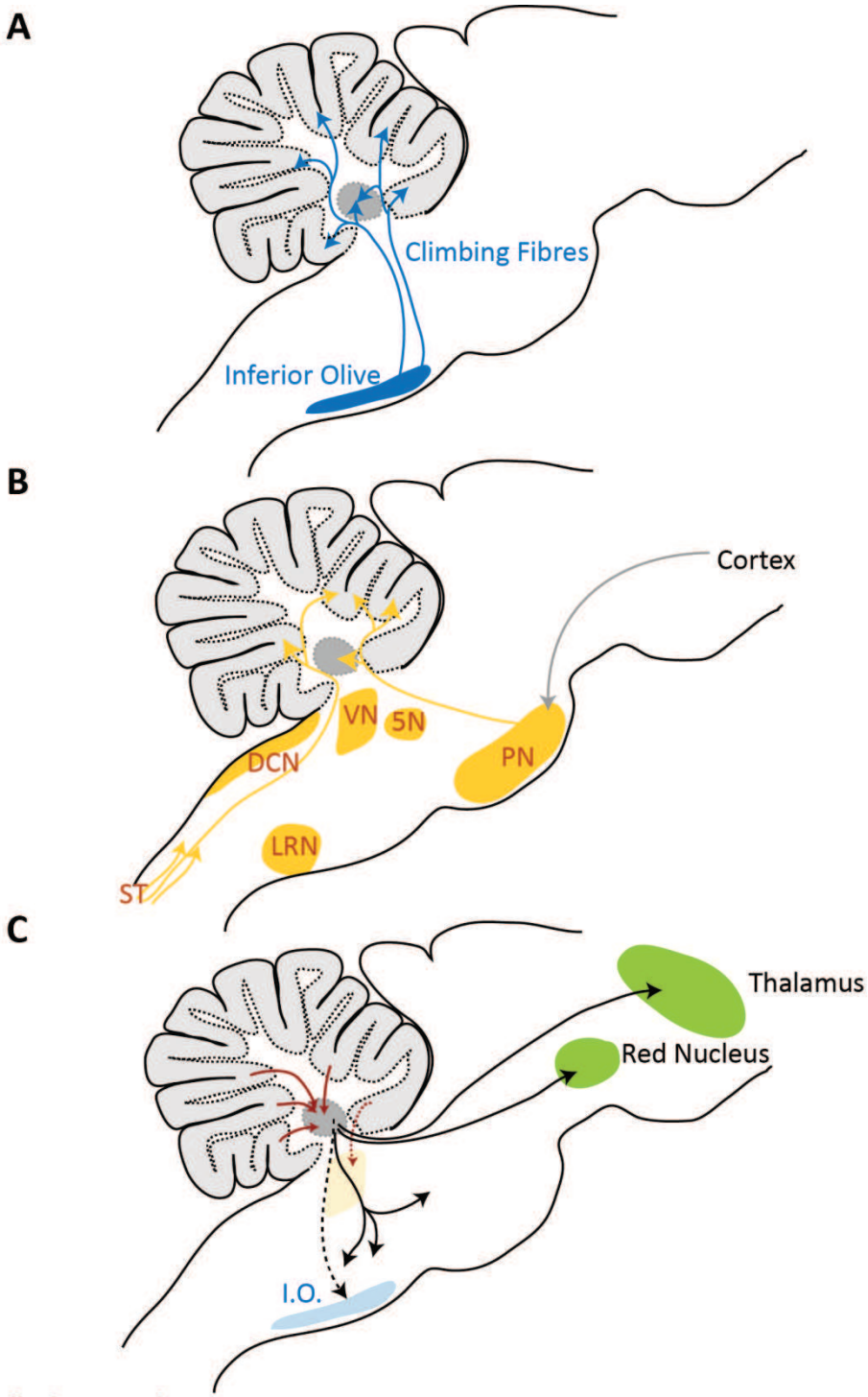

Figure 3 : Cerebellar inputs and outputs.
Sagittal view of medulla and cerebellum. The cerebellum is composed of the cerebellar cortex (light grey) and cerebellar nuclei (dark grey).
A : The inferior Olive (I.O.) is the only source of climbing fibres. They project to the cerebellar cortex and send collaterals to the cerebellar nuclei.
B : Mossy fibres inputs are coming from various precerebellar nuclei (ST : spinocerebellar tractus; DCN : Dorsal Column nuclei (see text); LRN : Lateral Reticular Nuclei; 5N : Trigeminal nuclei; VN : Vestibular Nuclei; PN : Pontine nuclei, which carry the inputs from the cerebral cortex. Mossy fibres projects to the cerebellar cortex and can send collaterals to the cerebellar nuclei.
C : Cerebellar output. Purkinje cells send axons (red arrows) to cerebellar nuclei (dark grey) or to the vestibular nuclei (dotted red arrow). Cerebellar nuclei project in various targets, such as the red nucleus, the cortex through the thalamus, or other reticular nuclei. A feedback (dotted black arrow) is sent to the inferior olive (light blue).

emboliform & globose and dentate in humans). To these three pairs of nuclei, we should add the vestibular nuclei, located at the junction between the cerebellum and the brain stem. Vestibular nuclei are similar to other cerebellar nuclei in the way that they receive both Purkinje cells and mossy fibres collaterals.

All these nuclei are topographically organised. They all receive projections from a specific part of the cerebellar cortex, and appear to be involved in separate processes. It must be noticed that except for some projections of the vestibulocerebellum, the deep cerebellar nuclei never project directly onto motoneurons, but rather to the motor cortex or to spinal local motor networks through the thalamus or the red nucleus (Figure 3C). This observation underlines the highly integrated position of the cerebellum in motor systems, which is involved in motor coordination and modulation but not in direct movement execution.

1.2.4 INTER-SPECIES VARIATIONS AND HOMOLOGY

Because of the apparent conservation of cerebellar structure across species, observation made in one animal model is often generalised to other models. My first project was performed on rats, whereas we used mice in the second project. Can we take into account observations performed in different species in a common cerebellar model?

Historical studies started with observations on humans, and the first animal models were essentially monkeys, cats and rabbits. In the 80's, the broader use of *in vitro* experiments introduced the rat model in the laboratories. The rat is a convenient animal model because of its fast reproduction rate, small size and homogeneous genetic background. Moreover, the animal is adapted to behavioural studies, although it cannot perform as complex tasks as monkeys do. Many of the initial observations in relation to the neuronal physiology in the cerebellum were performed in rats. Later, the development of transgenic mice pushed the lab to use the murine model. Fortunately, when experiments are realised in different species, similarities are striking. Sometimes inter-species or background-dependent discrepancies can be observed. For instance, it is possible to find very different firing frequencies for cerebellar nuclei neurons or for Purkinje cells between mice and rats (Rowland and Jaeger, 2005; Person and Raman, 2012a). However, when the study is performed in homogeneous conditions (same anaesthetics, same animal facility,…), values are remarkably similar (Shin et al., 2007). Most of the differences might be due to experimental variations. Some differences are however certain, like subtle variations in the protein expression patterns. For example between the rat and the mouse (Sugihara and Shinoda, 2004; Sugihara and Quy, 2007).

In this manuscript, I will give alternatively values coming from the cat, the rat and the mouse. When differences are documented, I will precise species in which the experiment was performed, but when no alternative data are available, we will have to postulate that the physiology between those species is close enough to allow generalisation. Based on the inter-species data already available, the risk is probably acceptable for the study of the cerebellar physiology because of the highly conserved features of that structure.

1.3 CELLULAR STRUCTURE OF THE CEREBELLAR CORTEX

In this section, I will briefly describe the cerebellar cortical structure and the cerebellar inputs. In a second time, I will detail the four cell types I recorded during my PhD, both in term of morphology and connectivity.

1.3.1 CELL TYPES AND INFORMATION PATHWAY

1.3.1.1 CELLULAR ELEMENTS OF THE CORTEX

Unlike the cerebral cortex, the architectonic and histological structure of the cerebellar cortex is constant throughout all lobules. This noteworthy feature led many authors to outline cerebellar cortex anisotropic, almost *crystalline* organisation. The number of morphologically distinguishable neuronal types is very low; only seven major types of neurons are described, all defined by a very specific morphology and localisation, and positioned precisely in one of the three cortical layers: Purkinje cells, granule cells, Golgi cells, basket cells, stellate cells, Lugaro cells and unipolar brush cells. A few other cell types were proposed, but for now they are still speculative, or too poorly characterised. In the seven identified neuronal types, several subtypes were described even if subtypes distinction remains essentially biochemical rather than functional or morphological. Except for unipolar brush cells, all the cell types are present all over the cerebellar cortex, without obvious variation in number, density or shape, strengthening this apparent homogeneity.

The three layer cortex is composed of, from the more internal to the more external layer: the granular layer, the Purkinje cells layer and the molecular layer (Figure $4A_1$, $4A_2$). Under the granular layer is the white matter, containing all the fibres entering and leaving the cerebellar cortex.

- The granular layer contains granule cells - which are by far the most numerous cells in the cortex (Figure $4B_1$) -, Golgi cells, Lugaro cells, and only in the posterior lobules, unipolar brush cells. Other cell types such as candelabrum or globular cells are sometimes mentioned in the literature (Lainé and Axelrad, 2002; Hirono et al., 2012). They are both supposed to be inhibitory interneurons, but they will not be developed here, as they are poorly characterised and impossible to identify in our experiments. In the rat, granular layer has an average thickness of 149 µm (Harvey and Napper, 1991), but unlike the molecular layer, this thickness is not perfectly constant and can present local variation in the sulcus or at the apex of each lobule (Braitenberg, 1967), probably because of the foliation itself.
- The Purkinje cells form a monolayer, sending their axon through the granular layer and their planar dendrites in a narrow parasagittal plane in the molecular layer (see Figure $4B_1$-$4B_3$ and $6A_2$).
- The molecular layer, the most external layer of the cerebellar cortex is around 225 µm thick (Harvey and Napper, 1991). It is composed essentially of the parallel fibres which are the axons of the granule cells, and the dendrites of Purkinje cells and Golgi cells. Two other major

cell types are present in this layer: basket cells and stellate cells, which will both be pooled under the name of molecular layer interneurons in this manuscript. The parallel fibres run along a mediolateral plane, crossing perpendicularly the flat dendritic tree of the Purkinje cells, the apical dendrites of the Golgi cells and the dendrites of the molecular layer interneurons. The molecular layer is bounded on its external part by the pia matter.

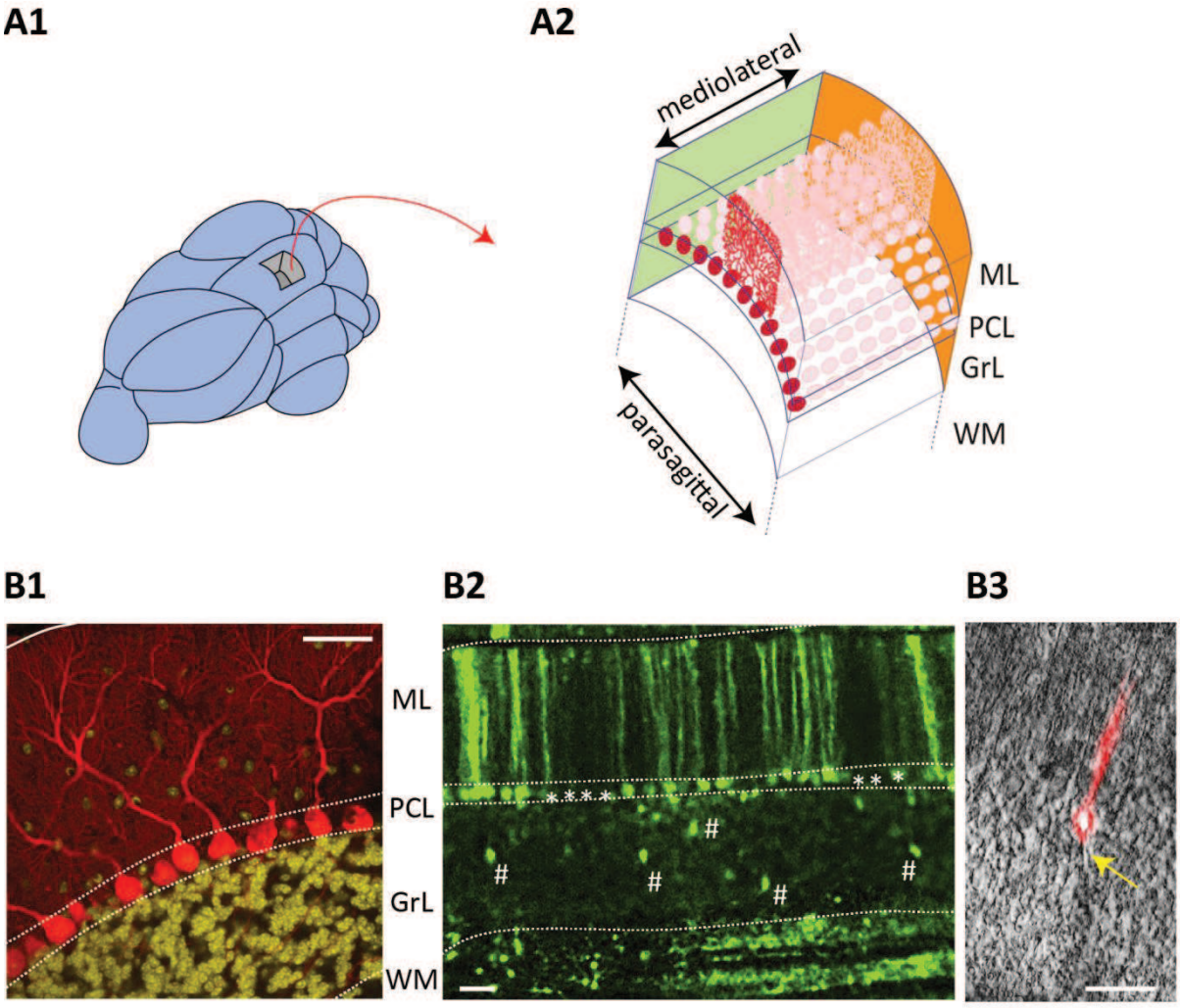

Figure 4 : Structure of the cerebellar cortex and cellular orientation depends on the slicing plane.
A_1 : A block of cerebellar cortex has the same structure anywhere in the cerebellum. A_2 : Organisation of the three layer cerebellar cortex. From outer to inner layer : Molecular layer (ML); Purkinje cell layer (PCL); Granular layer (GrL). Inputs and outputs to the cerebellar cortex form the white matter (WM). Purkinje cells (in red) have a flat dendritic tree that extends along the parasagittal axis, but poorly extends in the mediolateral axis. Orange plane indicates the sagittal plane (see B_1). Green plane indicate the coronal/transverse/horizontal plane (see B_2-B_3).
B : Impact of the slicing plane orientation on Purkinje cell morphology. Scale bar is 50µm. Dotted lines indicate the limit of the different layers. B_1 : Immunostaining on a sagittal slice of cerebellar cortex. Purkinje cells are labelled with calbindin (red); nuclei are labelled with Hoechst 33342 (yellow). Layers are indicated on the side (same legend than in A_2). Picture by Laetita Wioland. B_2 : Horizontal slice in lobule VIa in a transgenic mouse expressing a EAAT4-GFP fusion protein that labels a subset of Purkinje cells (unlabelled Purkinje cells are indicated by *) and GlyT2-GFP fusion protein that labels a subset of Golgi cells in the granular layer (some cells are indicated by #). B_3 : Montage of a horizontal slice in transmitted light (grey) during patch clamp experiment (yellow arrow indicates the patch pipette). The recorded Purkinje cell was filled with Alexa555 (red).

1.3.1.2 MOSSY FIBRES AND CLIMBING FIBRES

The information entering the cerebellar cortex follows two main pathways that are both converging onto Purkinje cells, the sole output of the cerebellar cortex (Figure 5A, 5B). Climbing fibres are coming from the inferior olive and projecting directly onto Purkinje cells, and indirectly through spillover to molecular layer interneurons (Szapiro and Barbour, 2007). Climbing fibre evokes a particular type of spike in the Purkinje cell, termed complex spike. Mossy fibres originating from various precerebellar nuclei project on granule cells and Golgi cells through a structure called glomerulus. Granule cells send their axon, the parallel fibre, in the molecular layer. A parallel fibre activates Purkinje cells, but also interneurons like Golgi cells, basket cells and stellate cells (Figure 5A,6B). Those four cell types will be described more in details in the following part of this chapter.

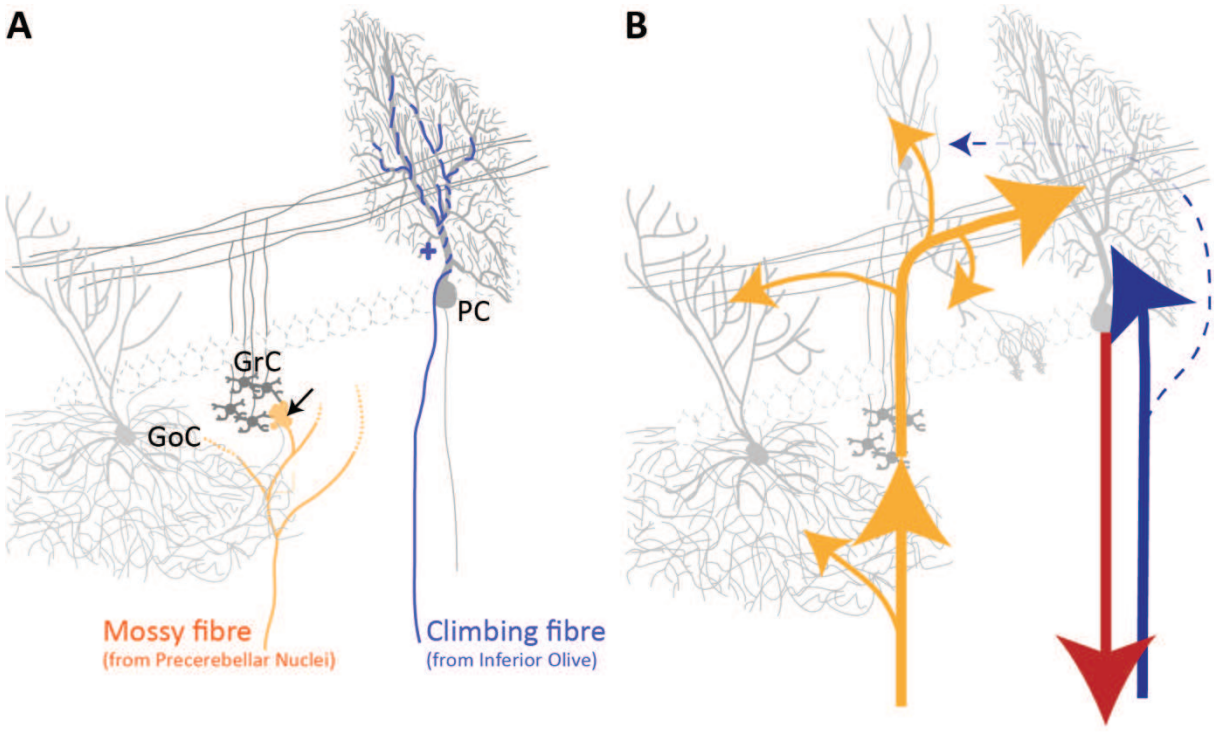

Figure 5 : Inputs and outputs of the cerebellar cortex.
A : One single climbing fibre (blue) originating from the inferior olive wrap around the primary dendrite of a Purkinje cell (PC). Numerous mossy fibres (yellow) from various precerebellar nuclei branch in the granular layer (collaterals are represented by dotted lines). Mossy fibres activate granule cells (GrC) and Golgi cells (GoC) in a particular synaptic structure named glomerulus (black arrow).
B : Information pathway. The mossy fibre pathway (yellow) can directly activate granule cells and Golgi cells, and indirectly Purkinje cells, Golgi cells and molecular layer interneurons through granule cell projections. The climbing fibre pathway (blue) can activate Purkinje cells, but also molecular layer interneurons through spillover (dotted arrow). Purkinje cell axon (red arrow) is the sole output of the cerebellar cortical network.

1.3.2 THE PURKINJE CELL

The Purkinje cell, discovered by the Czech physiologist Johannes Purkinje in 1837, is a central cell in the cerebellar circuitry. Indeed, this cell is the sole output of the cerebellar cortex and is therefore the final step in signal integration in the cerebellar cortex. Any relevant information computed in the cerebellar cortical network should have a detectable effect on its discharge (Figure 5B). Understanding how a given set of mossy fibres and climbing fibres inputs will modulate the Purkinje cell firing is a key point to understand how the cerebellar cortex compute sensorimotor information.

1.3.2.1 MORPHOLOGY

The Purkinje cell receives two excitatory inputs: one single climbing fibre coming from the inferior olive, and about 175 000 parallel fibres inputs coming from the granule cells (Napper and Harvey, 1988), themselves activated by mossy fibres (Figure 5A, $6A_1$). Inhibition on the Purkinje cell is performed by the molecular layer interneurons (Figure 6B) and neighbouring Purkinje cell collaterals (Figure $6A_1$).

Purkinje cells have a soma of about 20 µm in the rat, 15 µm in the mouse, forming a monolayer between the granular and the molecular layer (Figure $6A_1$, $6A_2$). The typical Purkinje cell has a tree-shaped planar dendritic tree of about 200 X 200 µm in the sagittal plane in rodents - 217 µm on average in the adult rat (Harvey and Napper, 1991) - , and a thickness of only 15 µm to 20 µm in the mediolateral plane (Figure $6A_2$). In higher mammals (cats, dogs or humans for instance), these cells can be twice as big as in rodents (Braitenberg and Atwood, 1958). Purkinje cells usually have one primary, more rarely two dendritic trunks that split in secondary and thin tertiary branchlets. These tertiary branchlets are covered with dendritic spines receiving only parallel fibre inputs and organised in a helical pathway with a short pitch (Palay and Chan-Palay, 1974; O'Brien and Unwin, 2006). These spines are rarely contacted by more than one parallel fibre (Napper and Harvey, 1988). Inhibitory molecular layer interneurons synapse preferentially on the dendritic shaft, and climbing fibres contacts directly smooth dendrites of the Purkinje cells on thorny spines, forming hundreds of release sites that appear to wrap the dendritic trunk (Palay and Chan-Palay, 1974) (Figure 5A).

1.3.2.2 TARGETS

The Purkinje cell is a GABAergic inhibitory projection neuron. It sends a myelinated axon that ultimately reaches several neurons in the cerebellar nuclei. Conversely, in the cerebellar nuclei, one neuron receives inhibition from several Purkinje cells. Thus, there are both a high degree of convergence and divergence of Purkinje cells onto cerebellar nuclei neurons (Person and Raman, 2012b).

The Purkinje cell axon can branch and form collaterals that contact other Purkinje cells (Palay and Chan-Palay, 1974; Orduz and Llano, 2007; Bornschein et al., 2013) and Lugaro cells (Palay and Chan-Palay, 1974; Hirono et al., 2012), but also basket cells (Palay and Chan-Palay, 1974; O'Donoghue et al., 1989), and possibly Golgi cells (Palay and Chan-Palay, 1974; Hirono et al., 2012) (Figure 6A).

Purkinje cell collaterals distribution is poorly understood. Briefly, two axonal plexus were described, one located just above or at the level of the neighbouring Purkinje cells, and a second deeper in the granular layer (Palay and Chan-Palay, 1974). The Purkinje cell collateral plexus was often described as more parasagittally oriented, but not exclusively. Purkinje cell collaterals can reach cells up to 200 µm in this axis (Braitenberg and Atwood, 1958). However, Richard Hawkes observed that Purkinje cells send collaterals up to five cells laterally (~80 to 100 µm) in the mediolateral axis, in the anterior lobe (Hawkes and Leclerc, 1989). A recent single cell reconstruction study (Sugihara et al., 2009) confirmed those early observations: even if most of the collaterals remains in a parasagittal axis, some of them occasionally travel along a mediolateral axis for short distances.

1.3.3 THE GRANULE CELL

If Purkinje cells are the sole output of the cerebellar cortex, granule cells are the major input stage cells, at least in number and density. Moreover, with the exception of unipolar brush cells in posterior lobules, granule cells are the only excitatory neurons in the cerebellar cortex. After migrating radially from the external granular layer between the first and the third postnatal weeks, granule cells establish their position in the inner part of the cerebellar cortex, forming the internal granular layer (Wang and Zoghbi, 2001). As we are working in the adult or juvenile (i.e. after P17) mouse or rat, any mention of the granular layer in this manuscript will thus refer to the inner granular layer.

1.3.3.1 MORPHOLOGY

The granule cells of the cerebellum are the most numerous neurons in the brain and might represent 60% of the neurons in the mouse brain and up to 70% in the rat brain. Granule cells are also among the smallest neurons, with an average somatic size of 4.82 µm (Harvey and Napper, 1991), and they have consequently a very high but constant density ($1.92.10^6$ cells mm^3 in (Harvey and Napper, 1988), 2.85 10^6 in (Palkovits et al., 1971)). They usually display 4 to 5 short dendrites terminating in the glomerulus (Cathala et al., 2003), which receives excitatory transmission form the mossy fibres (Figure 5A). On average, the granule cell dendritic extension is about 30 µm in the cat, and is probably almost the same in the rat and the mouse.

Granule cells send a very long axon in the molecular layer. This axon can be divided in two elements (Figure 6C): the ascending axon, which is the initial part of the axon rising vertically from the granule cell soma to the molecular layer, and the parallel fibre which run along the mediolateral plane in the molecular layer.

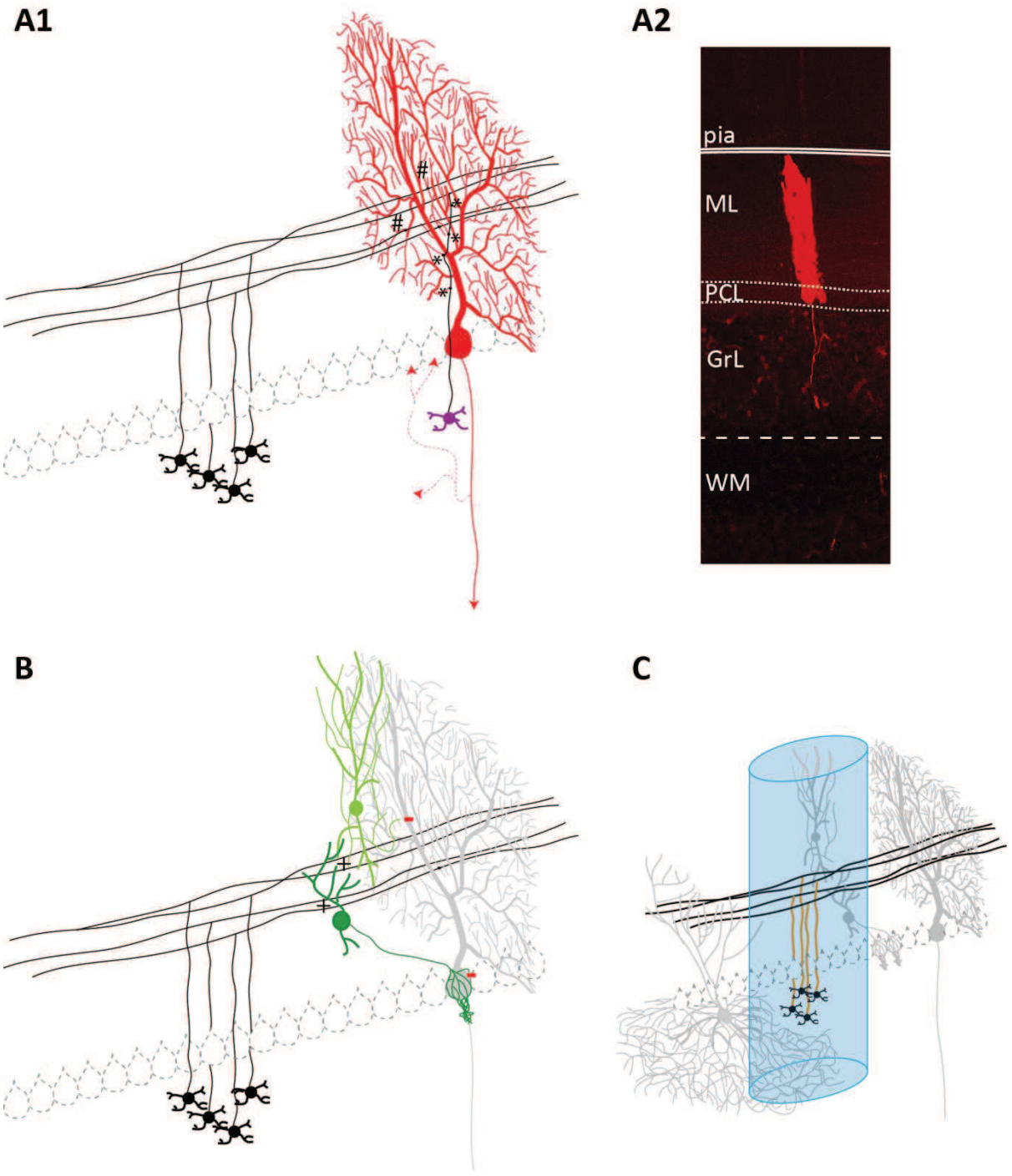

Figure 6 : Excitatory and inhibitory inputs onto Purkinje cells.
A_1 : Purkinje cells (red) can be contacted by distal granule cells (black) through parallel fibres synapses (#) or by local granule cells (purple) through ascending axon synapses (*). Purkinje cell sends its axon to cerebellar nuclei neuron (red arrow) or short collaterals to neighbouring Purkinje cells and presumably other cell types (dotted red arrows). **A_2** : Biocytin-filled patched cell in which the axon is visible.
B : Granule cells activate molecular layer interneurons. Stellate cells (light green) do feedforward inhibition onto Purkinje cells dendrites while basket cells (dark green) do feedforward inhibition onto Purkinje cell soma. Molecular layer interneurons can inhibit each other.
C : Ascending part of the granule cells axon (orange) can do several synapses with cells located above. Experimental evidences suggests the existence of a local network (blue barrel).

1.3.3.2 THE ASCENDING AXON

On an anatomical basis, the ascending part of the granule cell axon - *ascending axon* - makes several synapses before the parallel fibre bifurcation (Napper and Harvey, 1988; Gundappa-Sulur et al., 1999). The density of these synapses was estimated to be higher in the ascending axon (one synapse every 4.0 µm) compared to the density in parallel fibres (one synapse every 7.4 µm). As the ascending axon follow the dendritic plane of a unique Purkinje cell, it was estimated that one granule cell can do on average up to 31 synapses on a Purkinje cell (Gundappa-Sulur et al., 1999). Napper and Harvey proposed that 3% of the total granule cell to Purkinje cell synapses are coming from the ascending axon, whereas the value of 7 to 24% of the total granule cells inputs was proposed by a more recent study (Gundappa-Sulur et al., 1999). Although the exact number of synapses is still a matter of debate, even the lower estimate represent a significant number of synapses (3.5% would represent more than 6000 inputs per Purkinje cell). The high number of synapses does however not predict their functional properties. Finally, the Purkinje cell is not the only cell type to be contacted by the ascending part of the axon. Based on electronic microscopy, the ascending axon might also contact Golgi cells (Hámori, 1981) and molecular layer interneurons (Sultan and Bower, 1998).

1.3.3.3 THE PARALLEL FIBRES

Once in the molecular layer, the ascending axon bifurcates in a T-shaped manner. The two branches of the T run in the mediolateral plane, taking the name of parallel fibres. They are thin unmyelinated axons, making *en passant* synapses with Purkinje cells, stellate cells, basket cells and Golgi cells they cross. The exact longitudinal extend of the parallel fibres depends on species. Available data gives an estimated length between 4.2 and 4.7 mm in the rat (Pichitpornchai et al., 1994). The vermis measures 3 mm to 4 mm in the anterior lobules in the rat, and a quick estimate would suggest that although parallel fibres probably do not cross the whole cerebellum from one hemisphere to the other, most of the parallel fibres located on the midline are likely to be long enough to cross the vermis and even to reach the paravermis.

A study performed in 2005 (Zong et al., 2005) focused on the post-developmental final position of the granule cells coming from a single original clone during the development. It appeared that axons of granule cells coming from a same clone are bundled in the molecular layer in a restricted sublayer. On the other hand, their soma are scattered in all the depth of the granular layer. Neighbouring cells in the granular layer do not share neighbouring parallel fibres, but neighbouring parallel fibres come from the same clone. Determining whether neighbouring parallel fibres in the molecular layer correspond to a functionally related group of granule cells is actually a major technical concern, because many experiments use direct electrical stimulation of the parallel fibres to study granule cell input. In all my experiments, I always stimulated granule cells in the granular layer.

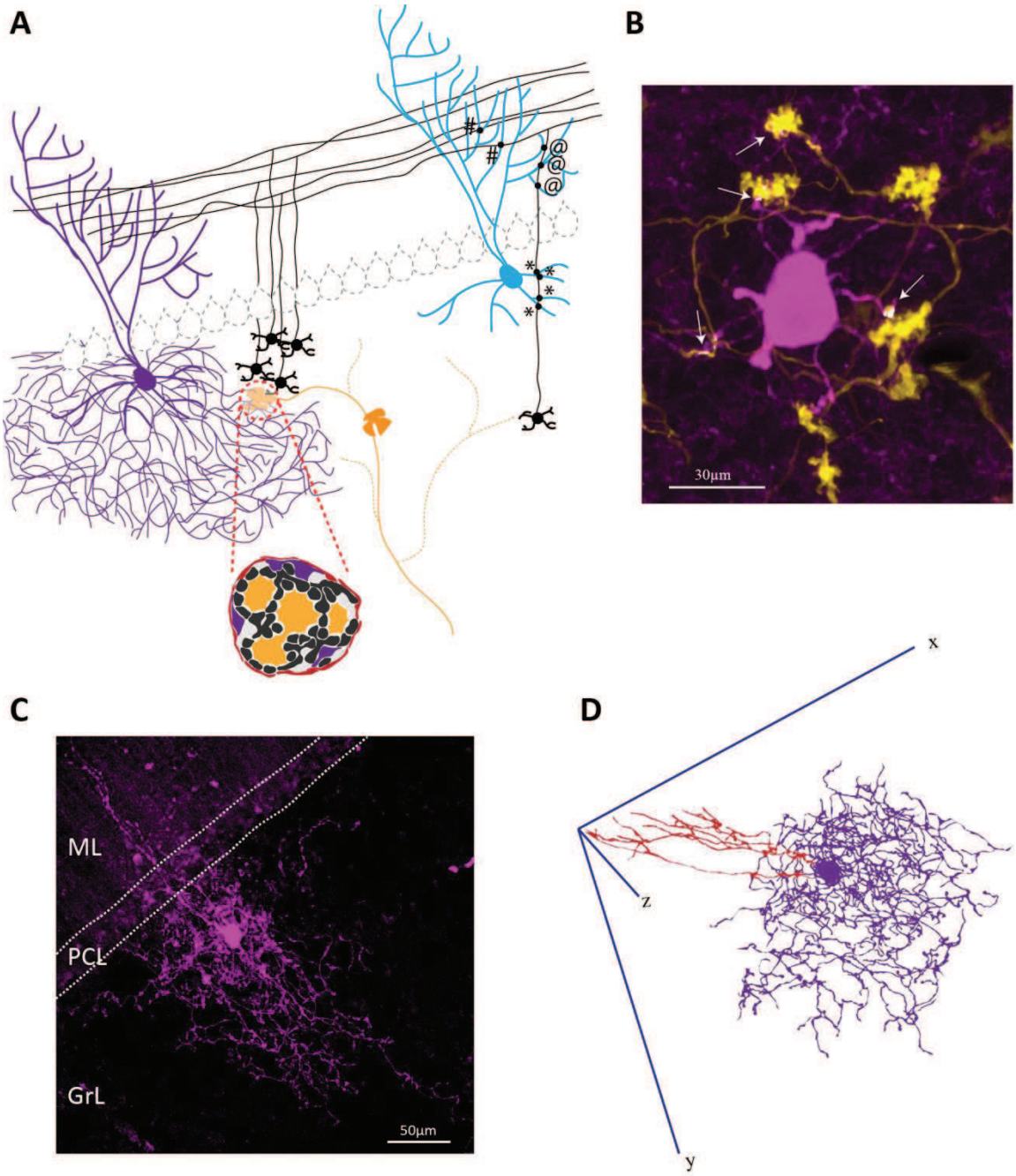

Figure 7 : Golgi cells morphology and connectivity.

A : Golgi cells dendrites (blue cell corresponds to a Golgi cell without axon) can be split into basolateral dendrites and apical dendrites. Granule cell ascending axon can contact basolateral dendrites (*) while virtually both ascending axon (@) and parallel fibres (#) can contact apical dendrites. The axonal plexus extend widely in the granular layer (purple Golgi cell). Mossy fibres terminals (yellow), granule cells dendrites (black) and Golgi cell axon (purple) interact in the glomerulus (dotted red circle). The glomerulus in ensheathed by glia. Glomerulus inset adapted from (Eccles, 1967).

B : Mossy fibre terminal is termed rosette. Neurogranin$^+$ Golgi cells is a subpopulation of Golgi cells. Immunolabelled neurogranin$^+$ Golgi cells (purple) are labelled mostly in the dendrites and soma, but also weakly in the axon. Mossy fibres injected with an adeno-associated virus in a precerebellar nucleus express GFP (in yellow for clarity). Mossy fibres terminals and Golgi axons colocalise within glomeruli (white arrows and white colocalisation mask). Virus injection performed by Francesca Binda and picture taken by Jean-Luc Dupont.

C : Recorded Golgi cell filled with biocytin for morphological study.

D : 3D reconstruction of another cell in Vaa3d free software.

1.3.3.4 PARALLEL FIBRE TO PURKINJE CELL SYNAPSE

In the molecular layer, parallel fibres cross orthogonally the dendritic tree of the Purkinje cells and make contact with more than half the Purkinje cells they pass through (Napper and Harvey, 1988) (Figure 6A, 6C). Electronic microscopy studies suggest that a parallel fibre contact one only, sometimes two dendritic spines in a Purkinje cell (double synapse in 2 to 11% of the cases, depending on the distance from the ascending axon bifurcation site (Pichitpornchai et al., 1994)). Dendritic spines contacted by two parallel fibres or more are on the other hand infrequent. A varicosity present in most cases one single active zone, with 8 docked vesicles, and 480 vesicles in the whole varicosity. The synapse is strongly ensheathed by glia (Xu-Friedman et al., 2001).

Thus, on a purely anatomical basis, a Purkinje cell can receive more contacts from a local granule cell through its ascending axon than from a distal granule cell through its parallel fibres, suggesting a dichotomy between inputs from the local network and distal inputs.

1.3.4 THE GOLGI CELL

The granular layer is considered as the input stage of the cerebellar cortex. Any attempt to model its functions will require a good understanding of all its cell types. If the major excitatory cell type is the granule cell, the major inhibitory interneuron in term of number and extension is the Golgi cell (Figure 7A, 7C, 7D).

1.3.4.1 MORPHOLOGY

In 1873, Camillo Golgi developed the silver nitrate method and opened the way to the morphological study of neurons. His first study focused on the cerebellum, in which he described two types of interneurons in the granular layer. The type I interneurons were described as “long and narrow cells irregularly fusiform” and were probably Lugaro cells. The type II interneurons were irregularly round or polygonal cells […] both these types have a large number of prolongations.” They were named Golgi cells by Ratzius in 1892. Santiago Ramon y Cajal gave more detailed description of their morphology in his *Histology of the Nervous System of Man and Vertebrate* (Ramon y Cajal, 1911), with particularly precise descriptions of the axonal plexus and dendrites. Far more details were brought by Palay and Chan Palay (Palay and Chan-Palay, 1974). Based on optical and electronic microscope observations, they tried to define the Golgi cell connectivity. They observed a single postsynaptic target, the granule cell, but multiple presynaptic inputs: mossy fibres, granule cells, climbing fibres, Purkinje cells collaterals, and basket and stellate cells.

The most impressive part of the Golgi cell is its extensive axonal plexus that branch hundreds, maybe thousands of times, inhibiting granule cells in a large volume of cerebellar cortex (Figure 7A, 7C, 7D). The mean extent of this plexus was estimated to be 650 µm sagittally and 180 µm mediolaterally in the mouse (Barmack and Yakhnitsa, 2008). The dendritic tree is actually separated between apical dendrites, which have, like Purkinje cells, an extensive parasagittal orientation but a poor mediolateral extension of only 82 µm (Sillitoe et al., 2008) and the basolateral dendrites, which are

restricted to the granular layer (Figure 7A). Basolateral dendrites spread also in the medio lateral axis, but their extent was never quantified. Since they are contained in the axonal plexus, we can only say that they are at most as long as the total neuritic extent (180 µm).

Golgi cells are directly activated by mossy fibres (Kanichay and Silver, 2008), evoking feedforward inhibition onto granule cells. Golgi cells can also be activated by granule cells, both on basolateral and apical dendrites (Midtgaard, 1992; Dieudonne, 1998; Cesana et al., 2013), and consequently perform feedback inhibition onto granule cells (Figure 7A). The existence of Golgi cell inhibition by molecular layer interneurons to Golgi cells was recently questioned by Wade Regehr (Hull and Regehr, 2012). Massive electrical stimulations or optogenetically-induced excitation of the molecular layer interneurons did not elicit inhibitory postsynaptic current that could be recorded in Golgi cells (Hull and Regehr, 2012). Moreover, since Palay and Chan-Palay study, new evidences suggest the existence of both Golgi cell to Golgi cell GABA transmission and Lugaro cell to Golgi cell corelease of GABA and Glycine (Dieudonné and Dumoulin, 2000; Dumoulin et al., 2001).

Finally, a major discovery is the strong electrical coupling between Golgi cells in the first part of the apical dendrites through connexin-36 gap junctions (Dugué et al., 2009; Vervaeke et al., 2012).

1.3.4.2 GOLGI CELL SUBTYPES

Golgi cells present important variations in size, shape or biochemical markers. One major difficulty is to distinguish Golgi cells from the other granular layer interneurons. No universal and specific marker has been identified yet. The most used markers also label Lugaro cells (polyclonal antibody rat-303), or some unipolar brush cells (somatostatin), or both some unipolar brush cells and Lugaro cells (calretinin) (Geurts et al., 2001).

Nevertheless, among the cells that are most probably Golgi cells, we can observe several subtypes based on both their molecular markers and their morphology (Figure 8).

For instance, most of the Golgi cells express the metabotropic glutamate receptor 2 ($mGluR_2$), but 10% express $mGluR_5$ instead (Neki et al., 1996). A further study suggested that $mGluR_2^+$ cells are $mGluR_3^+$ too, and that $mGluR_5^+$ cells are $mGluR_1^+$ too (Jaarsma et al., 1998).

Neurogranin, a calmodulin-binding protein that participates in the Protein Kinase C (PKC) signalling pathway, is another marker expressed in only a subset of Golgi cells of the mouse (Singec et al., 2003). Besides the fact that only one part of the Golgi cells express the protein, the authors observed spatial variations in the average density between the vermis and the hemispheres. In our morphological study, we performed a more detailed analysis of the distribution of this Golgi cell subtype.

Golgi cells can perform glycine uptake (Wilkin et al., 1981) or GABA uptake (Ottersen et al., 1987). The first team to study this aspect of cerebellar physiology indicated that 72% of the Golgi cells are immunopositive for both GABA and $GlyT_2$, whereas 14% are only GABAergic, and 14% only glycinergic (Ottersen et al., 1988). In this first study, Lugaro cells - which are 90% both GABAergic and glycinergic (Dumoulin et al., 2001; Crook et al., 2006) - were probably counted with Golgi cells, and integrated in the total number. GABAergic cells express glutamic acid decarboxylase (GAD67).

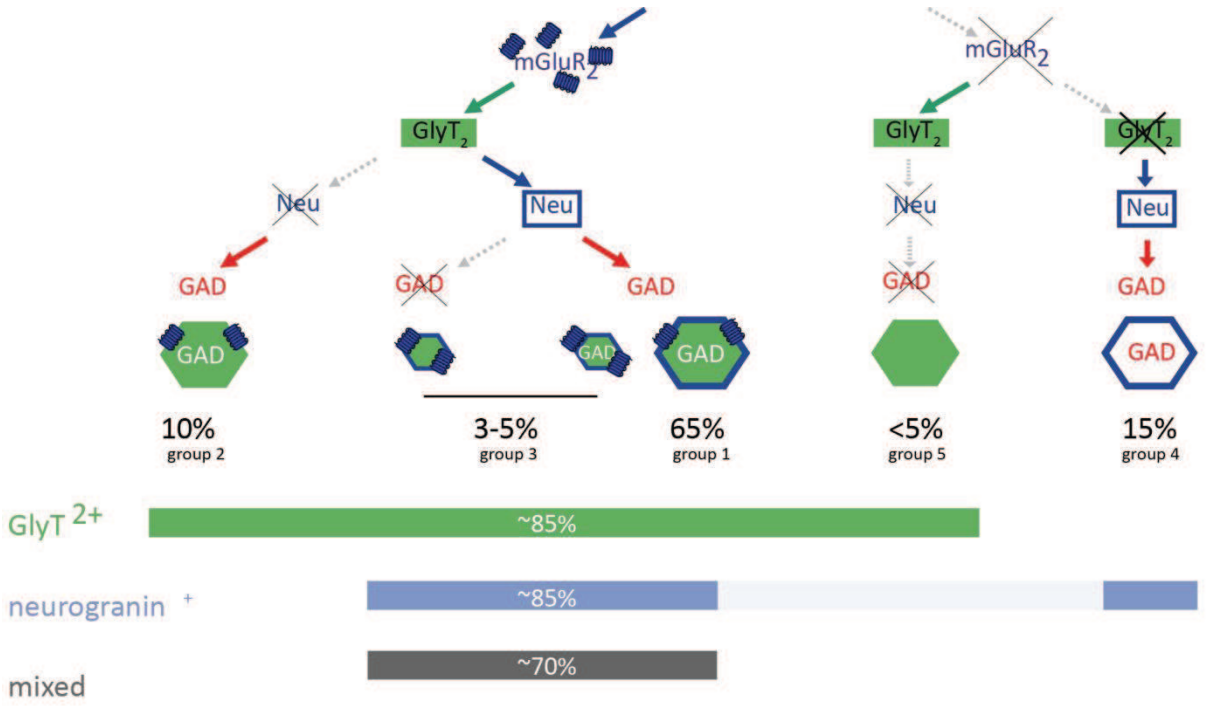

Figure 8 : Golgi cells subtypes.
Classification of Golgi cell subtypes in five groups based on 3 histochemical markers and cell mophology. $mGluR_2$ (Glutamate metabotropic receptor 2); neurogranin (Neu) and GAD (glutamic acid decarboxylase). Mixed cells are expressing both neurogranin ang $GlyT_2$. Adaptation from (Simat et al., 2007). Please note that $mGluR_2^-$ cells might be $mGluR_5^+$ and $mGluR_1^+$. $mGluR_2^+$ cells might be $mGluR_3^+$ too.

In a first attempt to classify Golgi cell subtypes, a classification in 5 groups was recently proposed (Simat et al., 2007) based on the presence of markers and on cell morphology (Figure 8).

- Group 1 cells (65% of the cells) are [$GAD67^+$, $GlyT_2^+$, $mGluR_2^+$ and Neurogranin+]
- Group 2 cells (10% of the cells) are [$GAD67^+$, $GlyT_2^+$, $mGluR_2^+$]. Group 1 and group 2 cells perform both GABA and Glycine release.
- Group 3 are small sized cells and correspond to 3 to 5% of the total. Cells are either [$GAD67^+$, $GlyT_2^+$, $mGluR_2^+$] like group 2 Golgi cells or only [$GlyT_2^+$, $mGluR_2^+$].
- Group 4 cells release only GABA, and constitute 15% of the total population. They are only [$GAD67^+$, $Neurogranin^+$].
- Group 5 cells are the last 5%, and are pure glycinergic cells [$GlyT_2^+$], expressing none of the three other makers.

Pure glycinergic cells do not express $mGluR_2$, and according to Neki (Neki et al., 1996), they are $mGluR_5^+$. It should be noticed that Neki found 10% of $mGluR2^-$ cells whereas Simat found 20%. These divergences between the results raise the question of a possible bias in such quantifications. There is no precise indication of the region of the cerebellum that were used (along the mediolateral axis, the whole cerebellar vermis was considered, but lobules were different in the two studies). Any spatial

heterogeneity in the subtype distribution would dramatically modify the values. We quantified these spatial heterogeneities for the $GlyT_2^+$ and Neurogranin$^+$ subpopulation (see second article).

Finally, we must keep in mind that this complex clustering of the Golgi cells is only based on the few identified markers that were shown to be heterogeneously expressed. As all proteins expressed in Golgi cells, it is possible that some other markers are expressed in specific subpopulations, either by respecting the subpopulation described above, or by clustering Golgi cells into even more subgroups.

1.3.5 THE GLOMERULUS

Now that mossy fibres, granule cells and Golgi cells are described, we should mention the particular structure in which all these three cell types interact: the glomerulus. When the myelinated mossy fibre enters the cerebellar cortex, it sends collaterals that will produce an axonal structure called rosette (Figure 7B). The rosette can either be an *en passant* synaptic structure, or the terminal part of the mossy fibre. The glomerulus was studied in details in the rat (Jakab and Hámori, 1988). It is a 10 µm spherical structure in which the mossy fibre terminal (the rosette), the granule cell dendrites and the Golgi cell axon tightly interact. The whole structure is wrapped with a glial sheet that isolates the glomerulus from the outside, and confers specific electrophysiological properties, favouring notably excitatory and inhibitory neurotransmitter spillover between synapses located within the glomerulus (Rossi and Hamann, 1998; DiGregorio et al., 2002) (Figure 7A, inset).

Granule cells send all their 4-5 dendrites in different glomeruli. Each dendrite further split into several protrusions (dendritic digits) in the glomerulus. Each granule cell dendritic digit receives one or more excitatory mossy fibre synapse (67%), inhibitory Golgi cell synapse (25%), or both (8%) (Jakab and Hámori, 1988). However, as there each dendrite has several digits, 60% of the dendrites is inhibited by at least one Golgi cell. On average one glomerulus can contact 53 granule cells, which indicates a high divergence in the transmission of the information carried by one single mossy fibre.

1.3.6 MOLECULAR LAYER INTERNEURONS

Until now, we only described Purkinje cells excitatory inputs, through parallel fibres, ascending axon, or climbing fibres. Molecular layer interneurons are dedicated to the inhibitory control of Purkinje cells, since they are their only source of inhibition, besides collaterals of other Purkinje cells. Moreover, according to recent study, Purkinje cells might be the only target besides other molecular layer interneurons (Hull and Regehr, 2012).

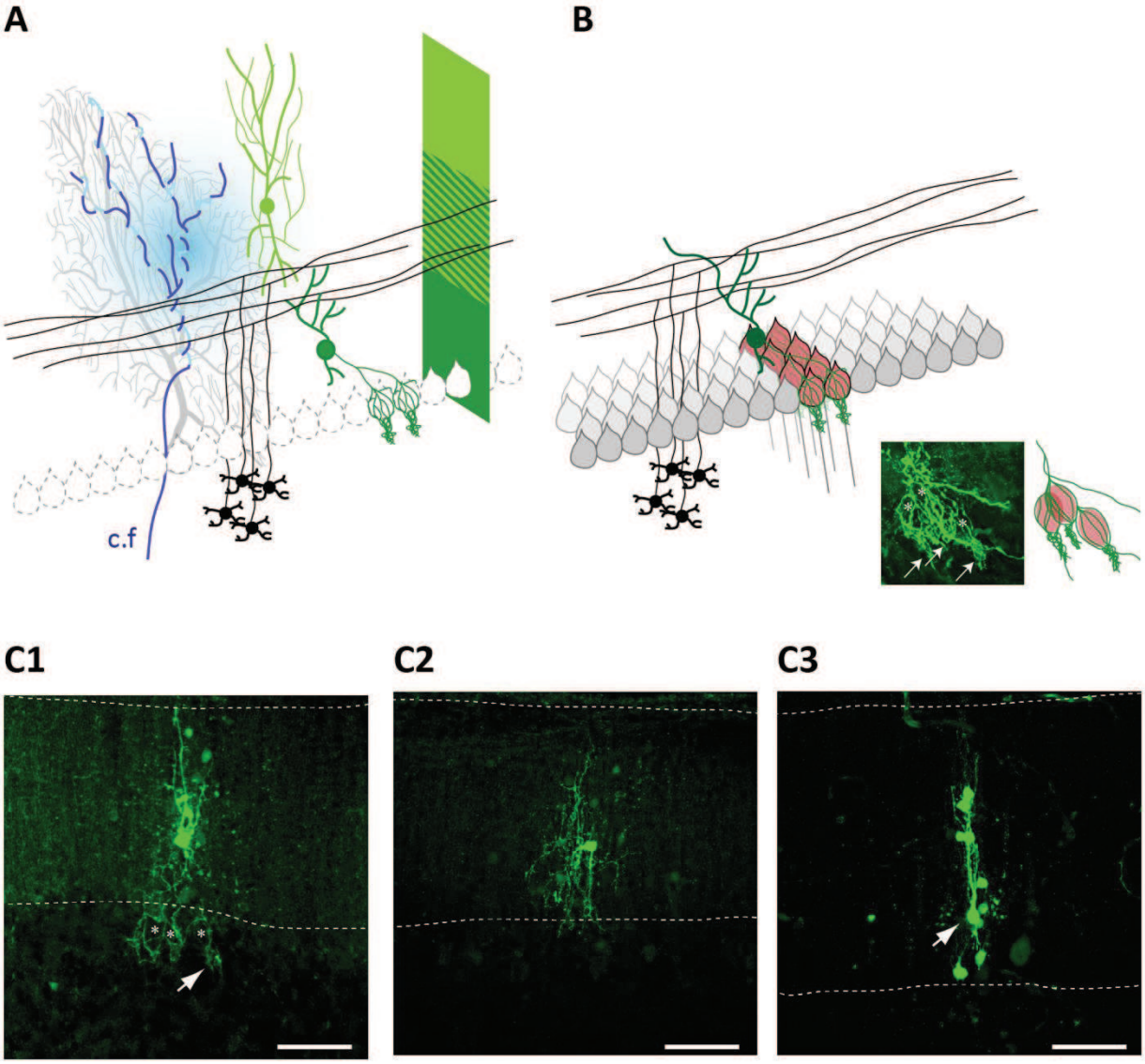

Figure 9 : Molecular layer interneurons.

A : Upper two third molecular layer interneuron (MLI) are mostly stellate cells (light green), while lower two third MLI are mostly basket cells (dark green). MLI are excited by parallel fibres (black) and inhibited by other MLI. Proximal climbing fibre (c.f., blue) can induce plasticity in the MLI through spillover.

B : Basket cells and stellate cells inhibit Purkinje cell along the parasagittal axis. Illustration for one basket cell (dark green). The basket contact several somas along the parasagittal axis. Inhibited Purkinje cells (red) are constrained in a parasagittal band. Inset: 3 baskets wrapping Purkinje cells soma (presumed position indicated by white stars), and 3 brushes (white arrow) from a biocytin-filled basket cell. Lower right panel: Interpretation scheme.

C : Biocytin-filled MLI (green). Scale bar is 50 µm, dotted line indicates the upper and lower limit of the molecular layer. $\mathbf{C_1}$: Biocytin-filled basket cell. Presumed position of Purkinje cells soma indicated by white stars. White arrow indicates a brush. $\mathbf{C_2}$: Biocytin-filled stellate cell. $\mathbf{C_3}$: In some cases, biocytin diffused from the recorded cell (white arrow) to neighbouring cells through gap junctions, however dye coupling remained in a parasagittal axis. Stellate cells and basket cells can be coupled.

1.3.6.1 MORPHOLOGY

Molecular layer interneurons were initially described by Ramon y Cajal (Ramon y Cajal, 1911). They are inhibitory interneurons displaying a parasagittally oriented axodendritic tree. The axon can project up to 450 µm from the cell body. Thus, when activated by a beam of parallel fibres, molecular layer interneurons perform lateral inhibition onto *off beam* targets (Eccles et al., 1967; Cohen and Yarom, 2000). The cellular morphology actually varies depending on the interneuron position in the molecular layer; cells located at the very top or at the very bottom show a more asymmetrical morphology. Molecular layer interneurons are classically distributed in two populations: stellate cells are located in the outer two-third of the molecular layer (Figure 9A, $9C_2$), whereas basket cells are located in the two inner thirds (Figure 9A, $9C_1$). Both basket and stellate cells perform feedforward inhibition following granule cells activation onto Purkinje cells and other molecular layer interneurons (Figure 6B, 9A). The basket cells present a supplementary axonal specialisation compared to stellate cells: lower part of the axon branches in the vicinity of a Purkinje cell and forms a basket around its soma (Figure 9B). The axon then wraps the axon initial segment, forming another structure called the brush (Figure 9B, inset). An interesting theory suggested that the brush does not contain any chemical contact, but rather acts directly through field potential to prevent action potential initiation without synaptic delay (Korn and Axelrad, 1980). This ephaptic contact would be very interesting in term of temporal coding as it would prevent Purkinje cell firing without synaptic delay. Basket cell contacts several Purkinje cells along the parasagittal axis, and sometimes two to three in the mediolateral one (Figure 9B). The separation of basket cells and stellate cells in two distinct populations is still in debate, with numerous authors suggesting a continuum of morphologies from purely stellate cells to purely basket cells (Ramon y Cajal, 1911; Palay and Chan-Palay, 1974; Sultan and Bower, 1998; Mittmann and Häusser, 2007; Schilling et al., 2008).

Molecular layer interneurons receive several hundreds of excitatory parallel fibres inputs (Palay and Chan-Palay, 1974) and between one and 20 inputs from other inhibitory interneurons (Lemkey-Johnston and Larramendi, 1968; Llano and Gerschenfeld, 1993). There are on average 10 molecular layer interneurons for one Purkinje cell, and *in vitro* recordings showed that one Purkinje cells receives on average 9 interneurons inputs (Häusser et al., 2004). Both their parasagittal morphology and their restricted connectivity suggest that molecular layer interneurons are contacting very few Purkinje cells, and that they are consequently restricted to a small local network.

1.4 FUNCTIONAL CONNECTIVITY IN THE CEREBELLAR CORTEX

1.4.1 MARR-ALBUS-ITO THEORY OF THE CEREBELLAR CORTEX

A few years after the first description of the cerebellar neuronal circuitry by John Eccles group (Eccles et al., 1967), David Marr developed a theoretical model of the cerebellar cortex (Marr, 1969) that was extended a few years later by James Albus (Albus, 1971) and functionally demonstrated by Masao Ito (Ito and Kano, 1982). In this theory, the cerebellum is described as a *perceptron* (Figure 10). Basically, a perceptron is a structure in which all the inputs are connected to the output in a feedforward manner, and in which the message is coded by a linear summation of the inputs

(Rosenblatt, 1958). If a threshold is reached, then the output cell fires and transmits the message to the next neuron in the network.

In Marr-Albus-Ito model, extended by Dean and Porrill (Dean et al., 2010), the network can compute supervised learning, which means that the selection of specific pattern is under the control of a *teaching signal*: the climbing fibre activity. Learning induces the selection of particular input patterns (*adaptative filter*), by changing the weight of the individual connections.

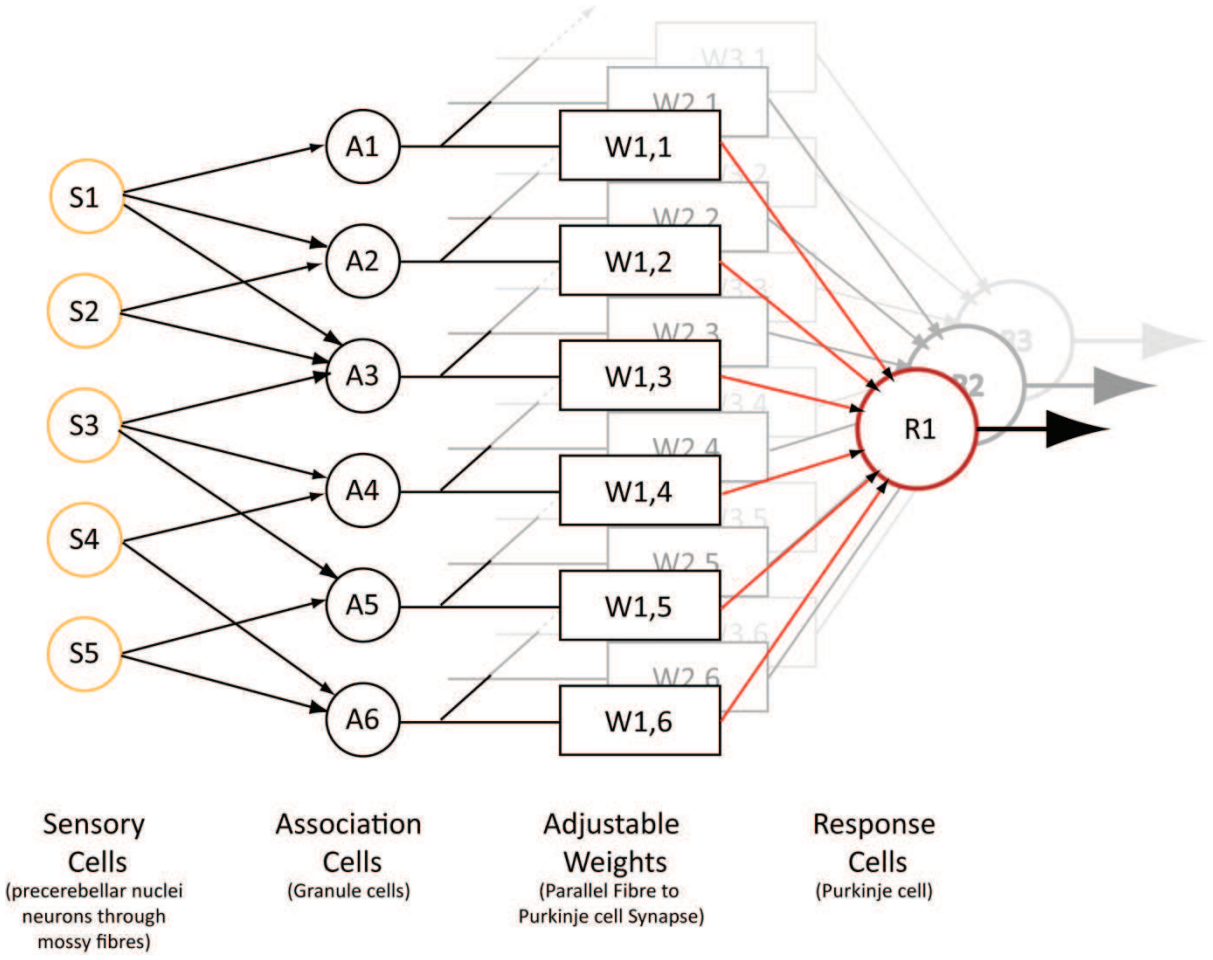

Figure 10 : Adapted perceptron in the cerebellar cortex. (Figure modified from Albus, 1971)
Different sensory modalities are carried by sensory cells (precerebellar nuclei) through the mossy fibres. The mossy fibres projections are highly divergent so that association cells (granule cells) are only activated by a specific combination of sensory inputs. The input stage of the cerebellum acts as a pattern classification device. Association cells (granule cells) project onto response cells (Purkinje cells, R1, R2, R3) which are the output of the network. Projections onto response cells have adjustable weights, which are individually tuned for each response cell, so that response cell only fires in specific sensorimotor contexts. In the cerebellar cortex, the weight adjustment is performed under the control of a response cell-specific teaching signal, carried by the climbing fibre.

In the cerebellar model, the Purkinje cell integrates sensorimotor contextual information carried by the parallel fibres. The relevance of the input is determined by the population of activated granule

cells, and by the synaptic weight of each of the corresponding parallel fibre to Purkinje cell excitatory synapse. The Purkinje cell firing is controlled by these input patterns, that is, the combination of activated and functional synapses. Climbing fibres are activated when a perturbation of a movement (Gilbert and Thach, 1977) or a nociceptive signal occurs (Ekerot et al., 1987), and carry an *error signal*. Consequently, in order to prevent the repetition of the same motor error, the parallel fibre to Purkinje cell synapses that were activated at this very moment must be depressed. In his theory of cerebellar cortex, David Marr proposed that the weight of the parallel fibre to Purkinje cell synapse should be adjustable, in order to store the information. James Albus perfected the model two years later by signalling that the coincidence signal should rather induce a depression in the cerebellar system. This early prediction was proved to be true in 1982 (Ito and Kano, 1982).

1.4.2 SILENT SYNAPSES AT THE PARALLEL FIBRE TO PURKINJE CELL SYNAPSE

An *in vivo* study (Ekerot and Jörntell, 2001) and an *in vitro* study (Isope and Barbour, 2002) showed that 85% to 97% of the connections are silent, displaying no detectable postsynaptic excitatory current (see also (Ekerot and Jörntell, 2001; Brunel et al., 2004; Ito, 2006)). Silent sites could be either “mute” (no released vesicles) or “deaf” (no postsynaptic receptors), although most of the long term depression mechanisms discovered to date suggest an absence of postsynaptic receptors. When detectable, patch clamp recordings showed that the parallel fibre to Purkinje cell contact is usually a weak excitatory synapse (average amplitude 8.4 pA ± 7 pA). Occasionally, stronger inputs could be recorded (~60 pA), only originating from local granule cells (Isope and Barbour, 2002).

1.4.2.1 POSTSYNAPTIC PLASTICITIES

Several plasticities coexist at this synapse, either presynaptically or postsynaptically (Jörntell and Hansel, 2006; Gao et al., 2012), and understanding the rules of induction of long term depression (LTD) or long term potentiation (LTP) mechanisms is of major importance to understand synaptic selection and information processing in the cerebellar cortex (Figure 11).

The first long term plasticity mechanism discovered *in vivo* in the cerebellum was a long term depression (Ito and Kano, 1982). This postsynaptic LTD is an associative plasticity that requires the coactivation of the climbing fibre and parallel fibres, and is expressed at the parallel fibre to Purkinje cell synapse. Initial experiments *in vitro* used non-physiological protocols to depolarise the Purkinje cell, such as current pulses or glutamate puffs, with simultaneous activation of the parallel fibres at low frequency (Sakurai, 1987; Crepel and Jaillard, 1990; Linden et al., 1991; Hartell, 1996; Eilers et al., 1997) (Figure 7A). These protocols were progressively improved to mimic more natural conditions.

The co-activation of climbing fibre and parallel fibre induces a strong LTD at the parallel fibre to Purkinje cell synapse, as predicted in the Marr-Albus-Ito model (Figure 10). This postsynaptic LTD requires a postsynaptic Ca^{2+} signal triggered by both the complex spike and the activation of the perisynaptic metabotropic glutamate receptor $mGluR_1$ by the parallel fibres. The repetitive low frequency stimulation of the parallel fibres can be replaced by more physiological 100 Hz bursts of 8 pulses, leading to similar results (Piochon et al., 2010).

The persistent presence of glutamate in the synaptic cleft during long trains or bursts activates $mGluR_1$, which activates the Phospholipase C (PLC) and produces Inositol triphosphate (IP_3) and Diacylglycerol (DAG). Membrane depolarisation induced by both 2-amino-3-(3-hydroxy-5-methyl-isoxazol-4-yl) propanoic acid receptor (AMPAR) opening and climbing fibre input activates voltage-gated-Ca^{2+}-channels. IP_3 further increases intracellular Ca^{2+} release. Both DAG and high intracellular Ca^{2+} concentration initiate the PKCα pathway. The latter induces the internalisation of AMPAR through a clathrin dependent mechanism (Wang and Linden, 2000; Xia et al., 2000), resulting in smaller EPSCs.

Other pathways can induce postsynaptic LTD. Briefly, a sustained depolarisation of the presynaptic button, such as during a burst, results in Nitric Oxide production through *N*-Methyl-D-aspartate receptors (NMDAR) opening (Casado et al., 2002; Bidoret et al., 2009). NO activates postsynaptic PKG which results in postsynaptic LTD (Lev-Ram et al., 1995, 1997). For the record, other proteins were showed to modulate postsynaptic LTD such as δ2-containing Glutamate receptors, Cannabinoid receptor type 1, Corticotropin-Releasing Factor and possibly short Transient Receptor Potential Channel 3, but they will not be developed here.

Alternatively, postsynaptic LTP can be observed by stimulating the parallel fibres only, more than 300 times at 1 Hz (Lev-Ram et al., 2002; Coesmans et al., 2004) (Figure 11B). In this case, the postsynaptic level of Ca^{2+} is lower than with the co-activation of the climbing fibre. This lower Ca^{2+} signal triggers the Ca^{2+}/calmodulin-activated Protein Phosphatase 2B (PP2B), which release the block of Protein Phosphatase 1 (PP1) by dopamine-and-cAMP-regulated neuronal Phosphoprotein (DARPP32). PP1 action probably results in the integration of new AMPAR at the postsynaptic membrane.

The postsynaptic LTP is often presented as reversing the postsynaptic LTD, acting as a counterpart that prevents the depression of all synapses. A lower Ca^{2+} concentration (or a smaller extent of the Ca^{2+} diffusion) is thought to activate different signalling pathway. The climbing fibre would act as a trigger to perform either LTD or LTP. However, as shown before, several pathways are probably involved in postsynaptic LTD and plasticity regulation might be more complicated. In mice with a global knockout of Ca^{2+}/calmodulin-dependent protein kinase (βCaMKII), LTP and LTD are inverted. These mice are ataxic and display motor learning impairments (van Woerden et al., 2009).

1.4.2.2 PRESYNAPTIC PLASTICITIES

Sustained parallel fibre activation (8 Hz, 120 times) induces a presynaptic LTP (Figure 11C). The induction persists even by blocking the glutamatergic transmission or adding BAPTA in the postsynaptic Purkinje cell. However, removing the extracellular Ca^{2+} prevents the induction of the plasticity. The mechanism requires activation of a PKA-dependent pathway following a presynaptic Ca^{2+} build-up (Salin et al., 1996). Presynaptic LTP is prevented by the activation of the endocannabinoids receptors CB1 (van Beugen et al., 2006), and enhanced by the presence of NO (Jacoby et al., 2001).

Repetitive short bursts in the parallel fibres (50 Hz burst of 5 stimulations, 90 times at 0.2 Hz) induce a short term potentiation too (Goto et al., 2006). However, this form of post tetanic potentiation is not maintained more than 20 minutes and might be different from the presynaptic LTP.

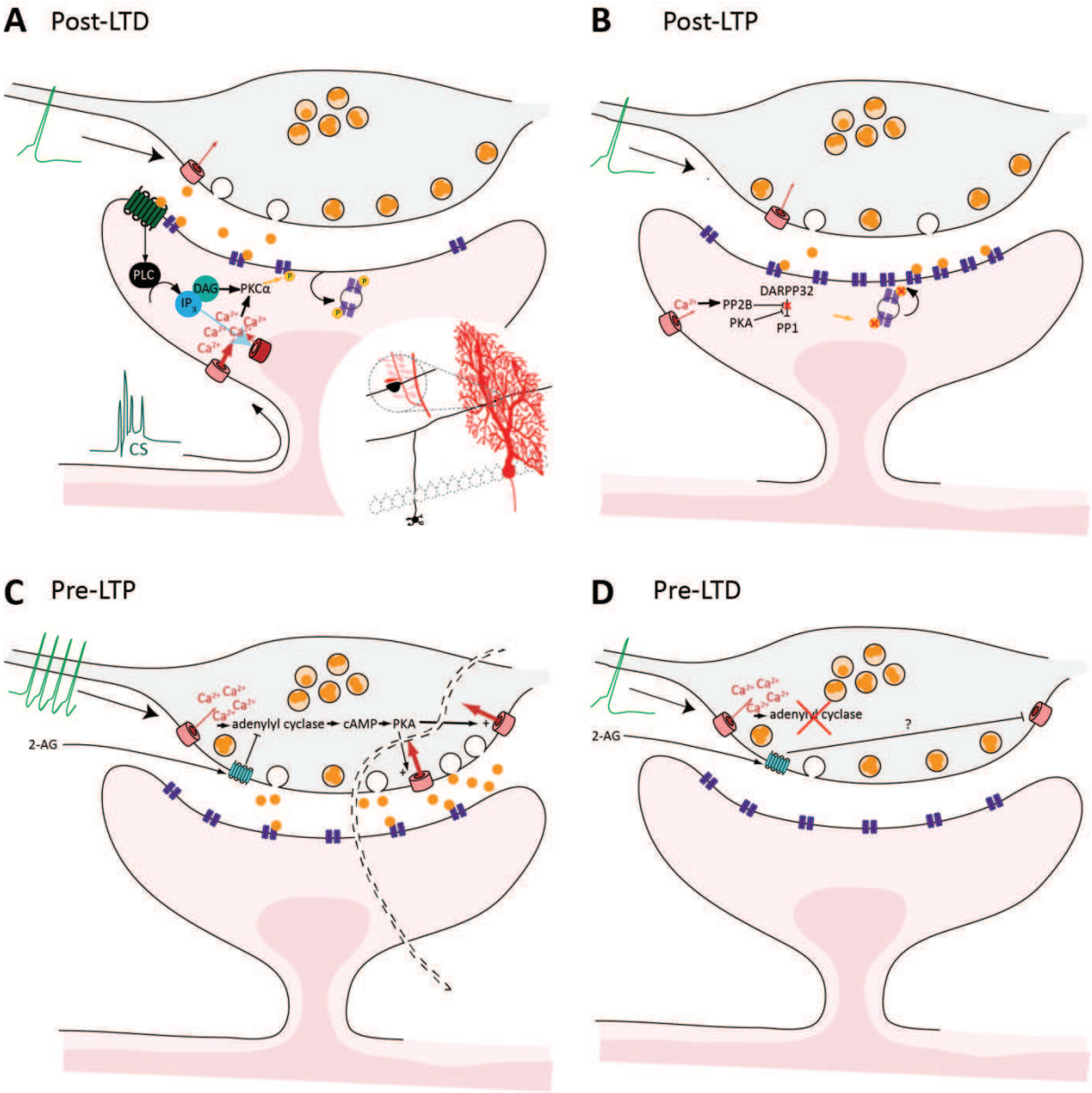

Figure 11 : Plasticities at the parallel fibre to Purkinje cell synapse.

A : Postsynaptic long term depression (LTD) is induced by coincident spiking in the presynaptic parallel fibre and postsynaptic complex spike (CS). Release of glutamate (orange circles) activates postsynaptic AMPA Receptors (AMPAR, purple) and perisynaptic mGluR1 receptors (dark green). Both AMPAR activation and CS depolarisation open voltage gated calcium channels Ca^{2+} (pink ring). mGluR1 activates phospholipase C (PLC), which produces inositol tri-phosphate (IP_3) and diacyglycerol (DAG). IP_3 releases Ca^{2+} from internal stores (red ring). DAG and Ca^{2+} activate protein kinase C alpha (PKCα), which induces AMPAR internalisation. Inset : parallel fibre (black) performs a unique *en passant synapse* on Purkinje cell dendritic spine (red). Other postsynaptic LTD pathways are mentioned in the text.

B : Absence of simultaneous CS and resulting lower intracellular Ca^{2+} concentration activates different signalling pathway. Protein posphatase 2B (PP2B) blocks the inhibition of Dopamine-and-cAMP-regulated neuronal phos-Phoprotein (DARPP-32) onto Protein Phosphatase 1 (PP1). Desinhibited PP1 has phosphatase activity resulting in postsynaptic long term potentiation (LTP).

C : Presynaptic LTP. Sustained presynaptic activation induces Ca^{2+} concentration build-up, which activates a Protein kinase A (PKA) dependent pathway. Protein kinase A (PKA) potentiates Ca^{2+} channels and increases vesicular release. Presynaptic LTP is prevented by activation of endocannabinoid receptor 1 (CB1, cyan).

D : Presynaptic LTD is poorly characterised, but requires PKA pathway blocking.

Recently, a presynaptic form of LTD was described, induced by stimulating the parallel fibres alone at relatively low frequencies (1 to 8 Hz, 120 times) and mediated by NMDAR and endocannabinoids dependent pathways (Qiu and Knöpfel, 2009). In current induction protocols, LTD with such protocol is usually hidden by presynaptic LTP mechanisms and required the use of antagonists to be revealed (Figure 11D).

Finally, to complete the picture a weak form of presynaptic LTD was lately observed (persistent post-tetanic depression), triggered by a unique burst of 10 pulses at 50 Hz, 100 Hz or 200 Hz, with strongest effect at highest frequencies (Bergerot et al., 2013). While the origin of this form of plasticity is still unknown, most of the described mediators of plasticity were tested and do not appear to be involved. An unidentified or a novel retrograde messenger could be implicated.

1.4.2.3 PLASTICITIES INTERPLAY

Various long term plasticities observed at this synapse are difficult to compare, because of the diversity of stimulation protocols, pharmacology and extracellular Ca^{2+} levels. Nonetheless, the existence of these plasticities demonstrates the wide range of theoretical modulations offered by this synapse. It is hard to say if all these mechanisms exist *in vivo* and if they are physiologically relevant. The postsynaptic LTD seems to have a correlate *in vivo* (Ito et al., 1982), but preventing its induction did not systematically provoke motor deficits (van Woerden et al., 2009; Schonewille et al., 2011). The role of the presynaptic LTD is even harder to understand, in the way that the induction protocol requires pharmacological agents. It was recently suggested that all these plasticities coexist and act synergistically, so that impairing one form of plasticity would not necessary affect motor learning (Gao et al., 2012). Even if the plasticities interplay seems complex, observations made so far confirm the function of the parallel fibre to Purkinje cell synapse predicted by the Marr-Albus-Ito model, in which synaptic weights are adjustable under the control of the climbing fibre. Interestingly, other predictions were also confirmed.

1.4.3 GOLGI CELL FUNCTIONS

Ramon y Cajal was already suspecting that the Golgi cell could influence a lot of granule cell by interacting with them in the glomerulus, but the Golgi cell role in cerebellar physiology gained some importance only in the 60's and the 70's with the discovery of their feedback inhibitory role onto granule cells (Eccles et al., 1964). In Marr-Albus-Ito motor learning theory, the granular layer act as a *pattern classification device* (Figure 10). This means that inputs coming from the mossy fibres are separated in distinct beams of parallel fibres. Gain control is of high importance in this model, because the number of patterns that a Purkinje cell can learn is dependent on the number of granule cells activated at the same time. According to the Marr-Albus-Ito model, a too high number of activated mossy fibres will activate too many granule cells and reduce learning abilities of the cerebellum. Golgi cells are activated both by mossy fibres and by granule cells, performing both feedforward and feedback inhibition onto granule cells. As predicted in the model, Golgi cells are able to adjust the gain in the granular layer (Mitchell and Silver, 2003; Hull et al., 2013) through their hyperpolarising role on granule cells. Thus, only the most strongly activated granule cells fire. Golgi

cells have other functions, and notably control temporal aspects mossy fibre inputs through population oscillations (D'Angelo et al., 2001; Kanichay and Silver, 2008; Dugué et al., 2009).

1.4.4 MOLECULAR LAYER INTERNEURONS FUNCTIONS

I suggested previously, on the basis of their morphology, that molecular layer interneurons might be restricted to small local network, and tightly coupled to one or a few Purkinje cells along the parasagittal axis. On a functional point of view, two supplementary arguments can be mentioned.

Few excitatory or inhibitory EPSCs from the parallel fibres are sufficient to impact interneuron discharges (Carter and Regehr, 2002) either by accelerating or delaying the firing. Because functional connection has an important influence on interneuron firing, and ultimately on Purkinje cell discharges (Mittmann et al., 2005), a very precise organisation of the connectivity and a very fine tuning of the synaptic weight at 1: parallel fibres to molecular layer interneuron synapse, 2: molecular layer interneuron to Purkinje cell synapse and 3: molecular layer interneuron to molecular layer interneuron synapse is probably required to perform precise computations (Ekerot and Jörntell, 2001; Jörntell and Ekerot, 2003; Dean et al., 2010).

Finally, molecular layer interneurons are coupled by gap junctions (Mann-Metzer and Yarom, 1999, 2000; Alcami et al., 2012). The coupling index, that is, the fraction of cell depolarisation/hyperpolarisation that is transmitted to a coupled cell is estimated at 0.1 on average, but can reach 0.4 (Mann-Metzer and Yarom, 1999). All coupling experiments were performed in parasagittal slices, but as you can see in Figure $9C_3$ in a horizontal slice, the strict parasagittal coupling of interneurons is striking.

2 SPATIAL ORGANISATION OF THE CEREBELLUM

As presented in the first chapter, the cerebellum appears at a first glance as a homogeneous structure, but since the 60's many evidences have unravelled a fine spatial organisation, both in the anterio-posterior axis and in mediolateral axis. Inputs and outputs are topographically organised, and several cell types such as Purkinje cell and Golgi cells express specific molecular markers. Understanding signal integration in the cerebellar cortex might require taking all these heterogeneities into account.

Several organisational levels were observed in the cerebellar cortex. Each one gives rise to a specific map of the cerebellar cortex, whose precision also depends on the experimental technique used. The nomenclature is complex: zones, microzones, zebrin bands, patches and blebs. They can all describe one aspect of the cerebellar physiology, and will be detailed in the first part of this chapter. Recently, several authors tried to integrate these different maps in a common picture (see the *one map hypothesis* (Apps and Hawkes, 2009)). This review outlined that an important step in the understanding of cerebellar computation is to define the smallest functional unit, i.e. the region of the cerebellar cortex in which all the cells process the same information. This modular unit would be repeated several times in the whole structure in order to process each modality that enters the cerebellum. However, if there are modules, there might also be intermodular communication. In the second part of this chapter, I will summarize the observation describing intramodular and intermodular processing at the microcircuit level, in order to introduce the second article of the manuscript.

2.1 ARCHITECTONIC VARIATIONS

Unlike the somesthesic or motor cortex, no clear cytoarchitectonic segmentation segregates the cerebellar cortex. The only histological variation concerns the distribution of unipolar brush cells in the posterior lobules (Altman and Bayer, 1977). They are considered as internal mossy fibres, since they exert a long-lasting feedforward excitation onto granule cells, amplifying the mossy fibres signal (Mugnaini et al., 2011). The specific role of this cell type in the vestibulocerebellum function remains to be clarified. Besides unipolar brush cells, the other parts of the cerebellum do not appear to display any specific cell types.

In the cerebral cortex, Broadmann areas were initially defined on the base of variations in the thickness of the six different layers. It appears later that these structural variations were correlated with cerebral functions. Although granular and molecular layer thickness can vary between sulci and gyri, it is at least partially due to mechanical constraints of the cortical folding (Braitenberg and Atwood, 1958; Eccles, 1973; Nishiyama and Linden, 2004), and no cerebellar areas could be determined based on this criterion

Myeloarchitecture, that is, the study of density and arrangement of myelinated fibres was also used by Broadmann. Actually, the white matter presents some differences that were later proved to be linked to functional zones (Figure 13A) (Voogd, 1969; Groenewegen and Voogd, 1977).

2.2 ORGANISATION OF THE CLIMBING FIBRE PATHWAY

2.2.1 CLIMBING FIBRE ZONES AND MICROZONES

First anatomical observations that the inferior olive sends its projections to specific regions of the cerebellar cortex were made in the middle of the 20th century, when authors (Szentágothai and Rajkovits, 1959) observed than the lesion of small parts of the inferior olive led to focal climbing fibres degeneration in the cerebellar cortex. Using anatomical study of the myeloarchitecture (Figure 13A) and olivo-cortico-nuclear connections, Voogd defined seven parasagittal zones in the ferret, and later in the cat (Voogd, 1967, 1969) (Figure 12B). Since then, these data were reproduced in the rat (Ruigrok et al., 1992; Sugihara and Shinoda, 2004) and in the mouse (Schonewille et al., 2006; Sugihara and Quy, 2007). A few more subdivisions were recently added, and 12 major parasagittal zones are now identified, each one receiving inputs from a different region of the inferior olive and projecting to a different region of the deep nuclei. Those regions are named from medial to lateral: A, AX, X, B, A2, C1, C2, CX, C3, D1, D0 and D2 zones (Figure 12B).

One single climbing fibre produces five to seven collaterals (Van der Want et al., 1989), each one contacting one single Purkinje cell. These projections follow a strict parasagittal orientation (Figure 12A), and one climbing fibre projects within one zone (Ekerot and Larson, 1979; Trott and Armstrong, 1987; Garwicz et al., 1992; Sugihara et al., 2001), although in some cases, climbing fibres can branch in more than one single zone. For instance, it was shown that some climbing fibres project parasagittally both in C1 and C3 in the paravermis (Voogd et al., 2003). The parasagittal projection of climbing fibres means that a same input, for instance nociceptive inputs from the right hindlimb, is simultaneously processed all along a lobule, and/or across lobules. This suggests that the different lobules share a similar organisation, each one performing a parallel computation based on the same input.

One zone still contains thousands of Purkinje cells. Based on finer neuroanatomical tracings, electrophysiological recordings and Ca^{2+} imaging, each zone could be subdivided in smaller microzones (Armstrong et al., 1974; Courville et al., 1974; Brodal and Kawamura, 1980; Sugihara and Shinoda, 2004; Ozden et al., 2008, 2009; Mukamel et al., 2009) (Figure 12A$_1$, 12A$_2$). Functional recordings initially defined the microzone as a region receiving climbing fibre inputs from the same receptive field (Oscarsson, 1979). The classical subdivision of the inferior olive can be refined to distinguish these smaller units. Izumi Sugihara performed precise injections in the rat inferior olive that labelled only very narrow parasagittal bundles of climbing fibres (Sugihara and Shinoda, 2004)(Figure 12A$_1$, 12A$_2$). They observed a strict organisation in the inferior olive projections and proposed a nomenclature of projecting climbing fibres in 5 groups, each group sharing similar inputs and targeting specific regions of the cerebellum. Since then, a similar organisation was described in the mouse (Quy et al., 2011).

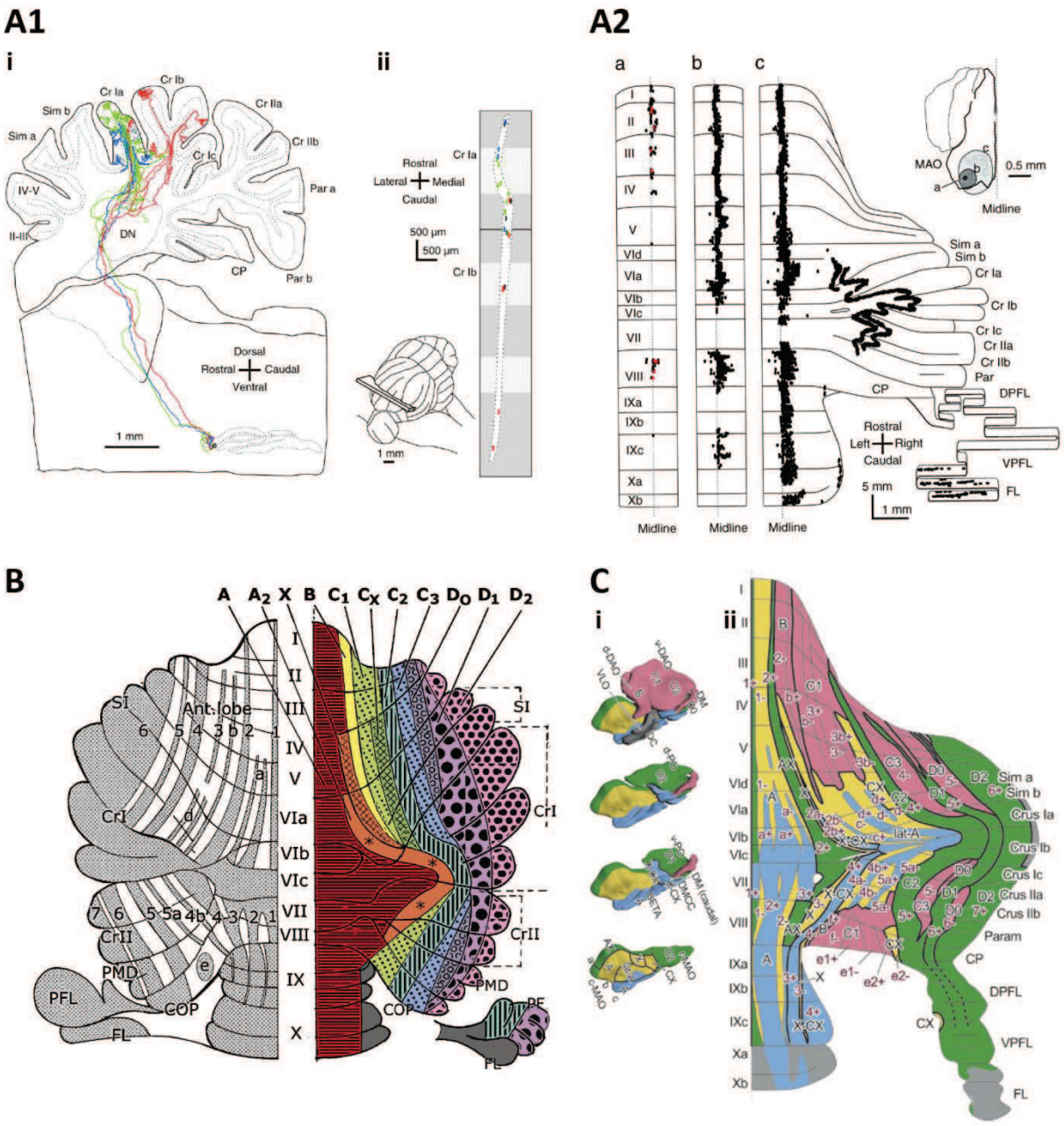

Figure 12 : Organisation of the climbing fibres inputs.

A : Neuronal tracing of climbing fibres. $\mathbf{A_1}$: $\mathbf{A_i}$: Sagittal representation showing neuronal tracing of 3 climbing fibres. Climbing fibres send collaterals in the cerebellar nuclei (DN), and project in one or several lobules in the cerebellar cortex along a parasagittal axis. $\mathbf{A_{ii}}$: Sagittal view from the surface of the cortex in two lobules. Climbing fibres coming from restricted region of the inferior olive project into narrow parasagittal band. $\mathbf{A_2}$: Group data showing increasing dose of injected tracer in the inferior olive (zone a, b and c, see inset) and the corresponding topographical organisation of the climbing fibre projections. Adapted from Sugihara, 2001.

B : Classical cerebellar olivocortical zones (right) and the corresponding zebrin bands (left); adapted from Voogd and Ruigrok, 2004. Left part : numbers indicate aldolase C zebrin bands and other characters refer to hemisphere lobules names. Central part : roman numerals refer to lobule numbers. Right part : Olivocortical zones are indicated on top. Other characters refer to hemisphere lobules names.

C : Sugihara nomenclature for olivocortical projections based on olivary afferences and aldolase C identity of the targets. $\mathbf{C_i}$: Inferior olive is separated in 5 groups (colours). Characters indicate the classical regions of the inferior olive. For abbreviations please refer to figure 21. $\mathbf{C_{ii}}$: Olivary groups are represented in 5 colours. Classical zebrin bands are indicated by numbers. Classical cerebellar olivocortical zones from B are indicated in capital letters. On the left: roman numerals refer to lobule numbers. On the right, other characters refer to hemisphere lobules names. Adapted from Sugihara and Shinoda, 2004.

2.2.2 OLIVO-CORTICO-NUCLEAR LOOPS

Although my project is directly focused on the processing of mossy fibres or climbing fibres inputs within the cerebellum, it is important to keep in mind the organisation of the cerebellar efferences. This point is particularly relevant since it appears that the cerebellum works through closed multi-structure loops.

The inferior olive is topographically organised. Neighbouring neurons are coupled by gap junctions (Llinas et al., 1974) and present membrane oscillations that make them fire simultaneously (Llinás and Yarom, 1986; Khosrovani et al., 2007). Inferior olive neurons project onto Purkinje cells through climbing fibres. Their activation results in synchronised complex spikes in Purkinje cells. Because of the parasagittally organised climbing fibres projections, complex spikes are synchronised in Purkinje cells of one microzone (Welsh et al., 1995). Moreover, as microzones project in a restricted region of the cerebellar nuclei (Sugihara and Shinoda, 2007), cerebellar nuclei neurons can receive simultaneous inhibition from all the Purkinje cells of a same microzone. A pending question was to know if projections from cerebellar nuclei to the inferior olive reach the same neurons than the ones that initially sent the climbing fibres, forming thus a closed loop. In 1969, Voogd described the anatomical zonation in parasagittal stripes of this projection (Voogd, 1969). First functional recordings of a topographically organised olivo-cortico-nuclear network came in 1996 (Ekerot et al., 1979; Garwicz and Ekerot, 1994). Yet, no experiment did simultaneously record the three structures to illustrate the functional existence of the olivo-cortico-nucleo-olivary closed loop (Bengtsson et al., 2011; Blenkinsop and Lang, 2011; Bazzigaluppi et al., 2012). By using optogenetic tools to synchronise Purkinje cells *in vivo*, we demonstrated the first functional existence of such a closed loop. A focal stimulation of Purkinje cells in the cerebellar cortex induced cerebellar nuclei inhibition, followed ~100 ms later by a climbing fibre feedback onto stimulated Purkinje cells. Although we could not manage to record simultaneously the cortex, the cerebellar nuclei and the inferior olive, we used this complex spike feedback as an indicator of the inferior olive firing within the loop, in appendix (Chaumont et al., 2013).

2.3 HISTOCHEMICAL COMPARTMENTATION

The first histochemical heterogeneities in the cerebellar cortex were observed in the 60's (Figure 13B) (Scott, 1963). Scott found that 5'-nucleotidase staining displayed parasagittally oriented bands in the molecular layer. The expression site of this marker was controversial, suggested either in glia (Schoen et al., 1987) or in Purkinje cell dendrites (Marani, 1977). In the following years, some other markers were found in subgroups of Purkinje cells, granule cells, mossy fibres, Golgi cells and unipolar brush cells, as shown below. All these subpopulations, except Golgi cells for now, were shown topographically organised, generally following parasagittal segmentation. However, an important question is to understand how these neuronal subgroups overlap. Does subgroup distribution follow a unique common pattern or do all cell types have their own and independent distribution? In the following part, I will describe a group of biochemical markers of Purkinje cells, the zebrins. Then, I will briefly evoke the histochemical compartmentation of other cerebellar cell types, in relation to zebrin pattern.

2.3.1 ZEBRIN BANDS: A MARKER OF PURKINJE CELLS COMPARTMENTATION

2.3.1.1 ZEBRIN BIOCHEMICAL IDENTITY

After the discovery of the 5'-nucleotidase segmentation in the molecular layer (Figure 13B), other markers sharing similar patterns of distribution were progressively described. They all define parasagittal stripes - or bands - of variable width, that run along several lobules. Because of the striated aspect they give to the cerebellar cortex, they were therefore named *zebrins* by Richard Hawkes and Nicole Leclerc (Hawkes et al., 1985). One of the first marker was labelled by a monoclonal antibody named map155/zebrin II (ZII), which was subsequently identified as aldolase C. Aldolase C/ZII is considered as the prototypical zebrin (Figure 13C_1), displaying seven major positive stripes named P1+ to P7+ from the midline to the hemispheres, interspersed by weaker positive stripes (Figure 13C_2,13C_3) (Hawkes and Herrup, 1995; Sugihara and Shinoda, 2004; Sugihara and Quy, 2007). Except for the possible exception of 5'-nucleotidase, zebrins are expressed only in Purkinje cells.

What are zebrins? The generic name of zebrin is only based on their stripe-shaped cellular distribution within the cerebellar cortex. Zebrins do not constitute a homogeneous class of markers because:

- They have different structures: for example, Heat Shock Protein 25 (Hsp25) is a small protein with chaperone activity while mGluR1b is a metabotropic glutamate receptor.
- They do not share common proteic structural motif or proteic sequence.
- They have different sub-cellular localisation: Excitatory Amino Acid Transporter 4 ($EAAT_4$) is at the membrane whereas PKCδ is in the cytosol.
- They have different developmental expression windows: calbindin, an early-onset zebrin is expressed before P5 but Neurofilament heavy chain (Nfh) - is a late-onset zebrin, expressed only after birth.
- They have different functions: Aldolase C is related to metabolism while PLCγ is involved in intracellular signalling.
- They are not necessarily restricted to the cerebellum ($EAAT_4$ is present in the retina)
- Some of them are not proteins (P-path is a glycolipid).

The prototypical zebrin in the literature is often the Aldolase C/ZII, and many other zebrins share the same pattern (aldolase C, PKCδ, $PLC\beta_3$, $EAAT_4$…) or its opposite pattern (PLCβ4, mGluR1b, neuroplastin…). However at least one other set of mirrored patterns exist, i.e. the Hsp25 versus Nfh pattern.

A closer look reveals subtle differences: some markers split apparently homogeneous ZII bands in smaller units like Purkinje cell protein 2 (pcp2) while some others have more complex overlapping expression (Human Natural Killer 1, dysbindin or neuronal Nitric Oxyde Synathase (nNOS)).

The different zebrins have very different functions, nevertheless, it is likely that they share similar regulating sequences, activating - or inhibiting - the expression of the gene in a subgroup of Purkinje cells. The transcription factors and/or the regulating sequences allowing this cell-specific expression remain to be discovered.

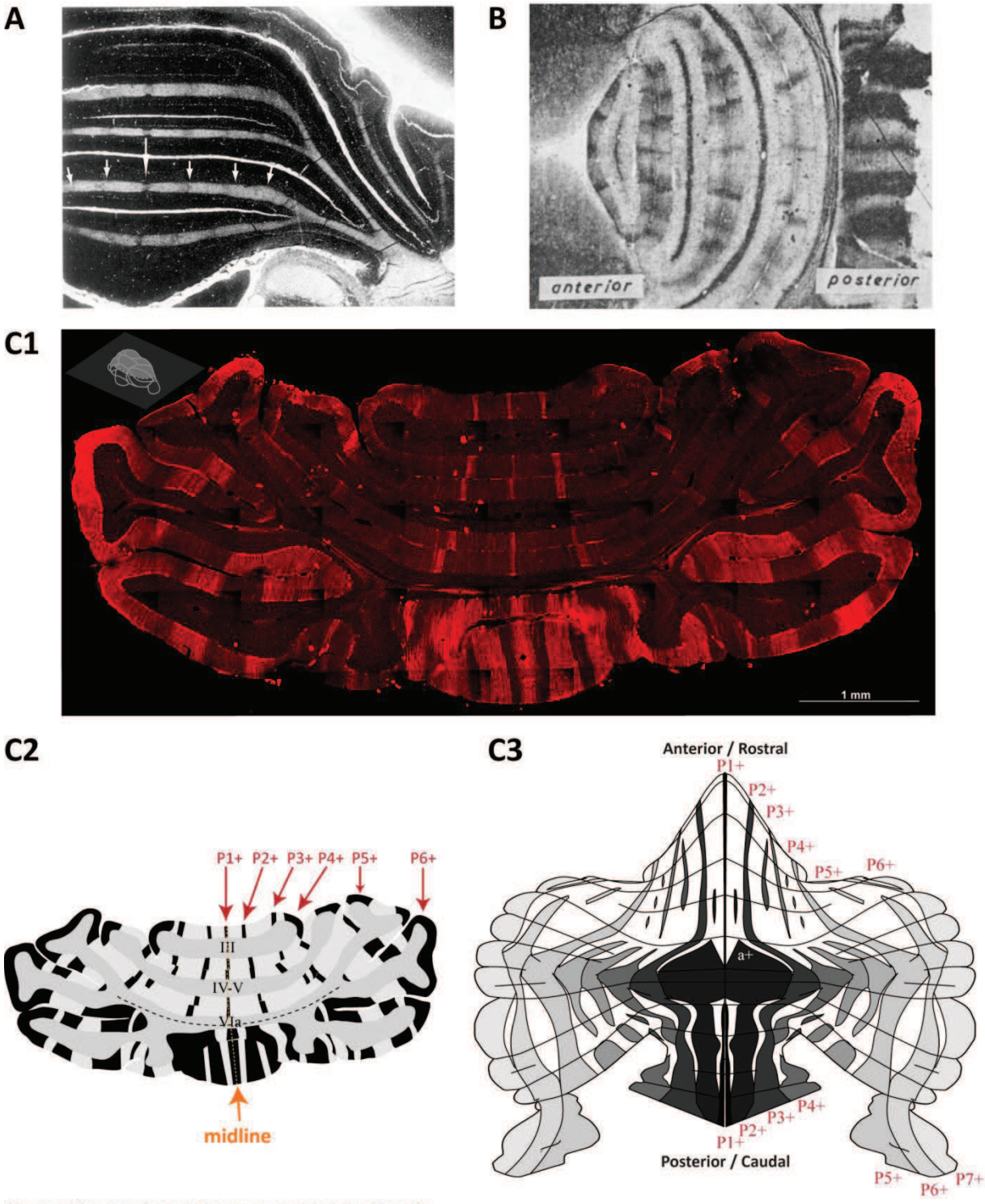

Figure 13 : Myeloarchitecture and Zebrin Bands.

A : Myeloarchitecture of the cerebellum using Häggqvist's staining method. Axons and myelin sheath are labelled differently, revealing variations in axon thickness and myelinisation. Parasagittal organisation of the white matter suggested a compartmentation of the inputs and/or the outputs (white arrows). Adapted from Voogd, 1967.

B : 5'nucleotidase labelling in a 10-week-old mouse. This is the first picture of a parasagittal marker in the cerebellum (Scott, 1963).

C : Aldolase C labelling and zebrin pattern identification. $\mathbf{C_1}$: Aldolase C immunostaining of a horizontal 100 µm slice of the cerebellar cortex (slice position in inset). Aldolase C labelling reveals parasagittal expression pattern of aldolase C (or Zebrin II). Immunostaining and picture by Jean-Luc Dupont. $\mathbf{C_2}$: Vectorised representation of the slice in C_2. Aldolase C bands are symmetrical in regard to the midline (yellow dotted line) and constant between animals. They can be reliably identified. $\mathbf{C_3}$: Zebrin band nomenclature in an unfolded representation of the cerebellar cortex. Scheme adaptated from Sugihara and Quy, 2007 and Sugihara and Shinoda, 2004.

2.3.1.2 DEVELOPPEMENTAL ROLE OF ZEBRINS

One major question that appears when we observe zebrins pattern of expression is their physiological relevance. Are they involved in cerebellar development? In cell migration? In network wiring? And once the network is wired, are they involved in other processes like information processing and plasticities induction? The control of each of these steps could be crucial for the development of the microcircuit.

2.3.1.2.1 EARLY-ONSET ZEBRINS AND LATE-ONSET ZEBRINS

Purkinje cells are generated between E10 and E13 in the mouse, in the roof of the fourth ventricle. They migrate progressively, following a mediolateral gradient, populating first the vermis, and later in the hemispheres (Larouche and Hawkes, 2006). The first heterogeneities in maturating Purkinje cells appear at E15. Both mediolateral and anterioposterior gradients in the expression of a variety of markers is observed. These markers initially form three to four pairs of clusters of Purkinje cells. Hence, they are named *early-onset zebrins*. The first to be discovered was guanosine 3':5'-phosphate-dependent protein kinase (Wassef and Sotelo, 1984). Since then, other early-onset zebrins were observed, such as calbindin or some homeobox genes like En_1, En_2, Pax_2 or Wnt_{17b} (Larouche and Hawkes, 2006). Neurogranin appears to be an exception, since its expression only disappears from Purkinje cells around P20. Most of the early-onset zebrins lose their spatial distribution before P5, either by disappearing from all Purkinje or by becoming homogeneously expressed in all of them. After P5, new zebrin populations, such as aldolase C, form parasagittally oriented stripes (*late onset zebrin).* The cellular interactions leading from clusters to adult stripes are not known, but the dynamic of stripe formation (that is, the correspondence between the embryonic clusters and the adult stripes) from the initial clusters is partially described (Dastjerdi et al., 2012; Fujita et al., 2012).

2.3.1.2.2 ZEBRINS AND CEREBELLAR DEVELOPPEMENT

Are zebrins necessary for the organisational wiring of the cerebellar cortex? Both mossy fibres and climbing fibres contact their targets along parasagittal axis. Mossy fibres organisation is established as soon as E13-14, and some climbing fibre projections already exist at E15 (Grishkat and Eisenman, 1995; Sillitoe et al., 2010). The simultaneity between afferences migration and Purkinje cell cluster formation raises the question to know if afferences organise the Purkinje cell in clusters and stripes, or if Purkinje cells clusters attract migrating mossy and climbing fibres.

Developing mossy fibres contact Purkinje cells before P5 (Mason and Gregory, 1984). When the inner granular layer grows, mossy fibres leave Purkinje cells and contact granule cells and Golgi cells. Somatostatin28$^+$ mossy fibres are a small subset of mossy fibres that target granule cells located below Hsp25$^+$ Purkinje cells. In the weaver mutant mouse, Hsp25$^+$ cells are expressed ectopically. In this mutant, mossy fibres are similarly disorganised, suggesting that Purkinje cell stripe formation precedes the topographic organisation of mossy fibres afferences (Armstrong et al., 2009).

At birth, Purkinje cells are contacted by multiple climbing fibres. After P15, only one climbing fibre per Purkinje cell remains, probably via an activity-dependent mechanism. The precise sequence of

the initial climbing fibre targeting is unknown, but the removal of both the climbing and mossy fibre at E12-E15 does not prevent the formation of the zebrin stripes (Wassef et al., 1990; Sotelo and Chédotal, 2005).

Altogether, these experiments suggest that Purkinje cells are the main organiser of the cerebellar scaffolding, and that this organisation does not depend on the afferences. Cluster dispersion into stripes appears essentially under the control of the Purkinje cells themselves, via adhesion molecules like the α-N-Catenin (Park et al., 2002). Interestingly, it can be noticed that among zebrins, only few guidance proteins were found to date - Eph_{A2}, Eph_{A4}, Eph_{A7} in the chicken, integrin β1 and neuroplastin in the mouse (Murase and Hayashi, 1996; Blanco et al., 2002; Marzban et al., 2003) - , and none of them were shown to directly regulate stripe formation .

2.3.2 HISTOCHEMICAL COMPARTMENTATION OF THE OTHER CORTICAL CELL TYPES

Purkinje cells are not the only cell type to express modular markers. Mossy fibres, granule cells, unipolar brush cells and Golgi cells show organised molecular markers, although less precisely described.

2.3.2.1 MOSSY FIBRES

Only few mossy fibres modular makers are known : cytochrome oxidase (Hess and Voogd, 1986; Leclerc et al., 1990), acetylcholine esterase (Marani, 1977; Boegman et al., 1988), dystrobrevin-associated protein dysbindin (Sillitoe et al., 2003), cocaine-and-amphetamine-regulated-transcript peptide (Reeber and Sillitoe, 2011), somatostatin28 (Armstrong et al., 2009) and Vesicular Glutamate Transporters 1 and 2 ($VGLUT_1$ and $VGLUT_2$) (Gebre et al., 2012) (Figure 14C). For the latter, it is interesting to note that afferences coming from the dorsal column nuclei (gracile nucleus, cuneate nucleus and external cuneate nucleus) heavily express $VGLUT_1$ whereas spinocerebellar mossy fibres preferentially express $VGLUT_2$.

2.3.2.2 GRANULE CELLS

Granule cells express compartmentalised markers too. nNOS (Ahn et al., 1994) is expressed in patches of granule cells in most cerebellar lobules (Figure $14B_1$). However, its expression become almost homogeneous when mossy fibre afferences are removed, suggesting that expression of nNOS reflects compartmentalised mossy fibre expression.

The NR2C-containing-NMDAR are also expressed in topographically organised regions (Karavanova et al., 2007) (Figure $14B_2$), which might have consequences on synaptic plasticity, since NR2C-containing NMDAR have a poor sensitivity to Mg^{2+} blockade and display lower single-channel conductance (D'Angelo et al., 1999; Gall et al., 2005a).

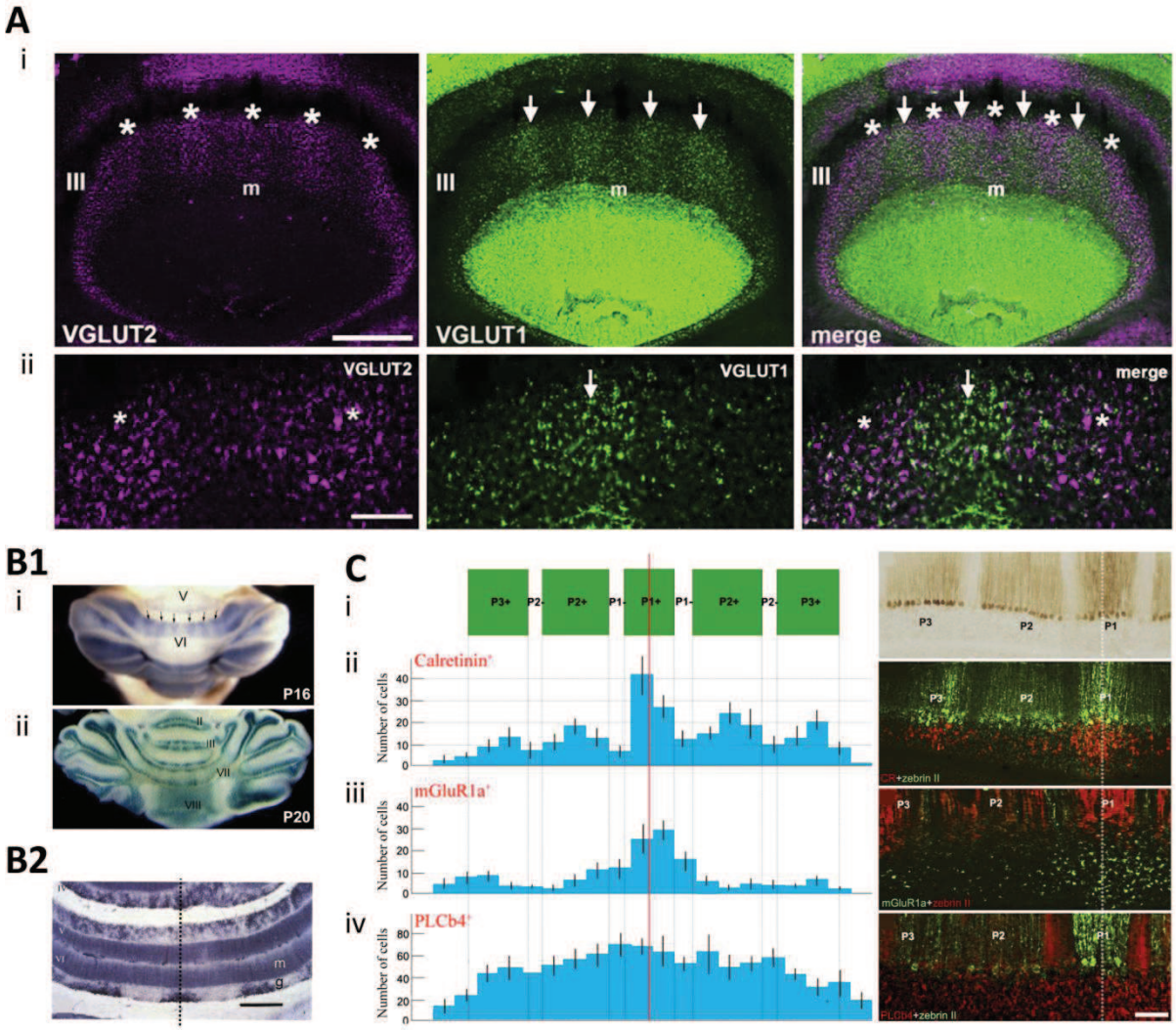

Figure 14 : Other parasagittal markers in the cerebellum

A : Mossy fibres markers. $\mathbf{A}_{i}$: VGLUT2 (left panel, *) and VGLUT1 (middle panel, ↓) staining in the anterior vermis show alternate expression patterns (merge in the right panel). $\mathbf{A}_{ii}$: high magnification images. Adapted from Gebre et al,. 2012.

B : Granule cell markers. $\mathbf{B}_{1}$: β-galactosidase knock in mouse in the NR2C promoter region revealed subpopulation of granule cells in the juvenile mouse (B_{1i} whole cerebellum at P16 ; B_{1ii} horizontal slice at P20). From Karanova et al., 2011. $\mathbf{B}_{2}$: Horizontal slice of adult mouse cerebellum stained with NADPH-diaphorase revealed clusters of expression in granule cells. From Schilling et al., 1994.

C : Unipolar brush cells (UBC) markers. Calretinin⁺ UBC, mGluR1a⁺ UBC and PLCβ4⁺ UBC are three distinct subpopulations. $\mathbf{C}_{i}$: (right panel) immunostaining of aldolase C. $\mathbf{C}_{ii}$ (right panel) : immunostaining of calretinin (red) and aldolase C (green), $\mathbf{C}_{iii}$ (right panel) : immunostaining of mGluR1a (green) and aldolase C (red). $\mathbf{C}_{iv}$ (right panel) : immunostaining of PLCβ4 (red) and aldolase C (green). $\mathbf{C}_{ii}$-$\mathbf{C}_{iv}$ (left panel) : corresponding distributions in regard to aldolase C pattern (C_{i}). At least calretinin+ cells are stricly correlated to aldolase C pattern. Adapted from Chung et al., 2009.

2.3.2.3 UNIPOLAR BRUSH CELLS

Discovered in 1977 (Altman and Bayer, 1977), unipolar brush cells display various proteic profiles, expressing calretinin (Braak and Braak, 1993), $mGluR_{1a}$ and $PLC\beta_4$ (Nunzi et al., 2002; Chung et al., 2009b) or $PLC\beta_4$ without $mGluR_{1a}$ (Chung et al., 2009a). A recent study (Chung et al., 2009c) showed that the medio lateral density of these three subpopulations is not homogeneous (Figure 14C). Calretinin$^+$ population distribution matches with the zebrin II pattern, whereas the two other populations show a different, but symmetrical, distribution not correlated with zebrin patterns. Finally, as for mossy fibres, unipolar brush cells could be split in two populations, one expressing $VGLUT_1$ and the other expressing $VGLUT_2$ (Nunzi et al., 2003). However, the spatial distribution of these two subtypes is not described yet.

2.3.2.4 GOLGI CELLS

Golgi cells are not a homogeneous population, and the different subtypes were described in chapter 1 (Simat et al., 2007) (Figure 8). However, except for a difference on average expression of neurogranin between the vermis and the hemispheres (Singec et al., 2003), no obvious spatial distribution of Golgi cells have been described for the different subtypes. We quantified the spatial distribution of the $GlyT_2^+$ and neurogranin$^+$ subtypes in all cerebellar lobules (see second article).

To my knowledge, no clear indication of spatial histochemical organisation was found for Lugaro cells, basket and stellate cells.

2.4 MOSSY FIBRE AFFERENCES AND FRACTURED SOMATOTOPY

2.4.1 TOPOGRAPHY OF MOSSY FIBRE INPUTS

If climbing fibres and mossy fibres bring highly integrated and complex information, the cerebellum also receives more direct somatosensory information. Some of these are carried out by mossy fibres originating from the spinal cord (Figure 3B). Information is coming from very discrete *receptive fields* (single muscles, small skin regions...), and the distribution of their postsynaptic targets gives precious information on cerebellar organisation. Are this sensory information processed in specific regions, like in the somatosensory cerebral cortex, or are they spread in all cerebellar regions?

2.4.1.1 DECIPHERING THE CEREBELLAR SOMATOTOPIC MAP: EARLY DISCOVERIES

Luciani (1891) and Holmes (1917) showed that a lateral lesion in the cerebellum affects only the ipsilateral side of the body, but Luciani denied the possibility of a somatotopic organisation of the cerebellar cortex. Sherrington, and Loewenthal and Horsley discovered simultaneously in 1897 that focal electrical stimulations affect restricted group of muscles ipsilaterally, but little importance was given to these discoveries during the following years.

In 1904, by comparing more than sixty species, Bolk established the first somatotopic map of the cerebellum. For example, from the particularly big size of the simplex lobule in the giraffe, Bolk deduced that this region might be involved in the control of the neck (Bolk, 1906). In 1910 Edinger and Comolli developed the concept of neo- and paleo-cerebellum (Comolli, 1910; Edinger, 1910). But one of their most important ideas was that precise location in the cerebellar cortex does not necessarily control one given muscle, but rather a specific function. Adrian, in 1943 mapped the proprioceptive and exteroceptive afferences in the anterior lobe, and observed that in this region, a whole homunculus was present (Adrian, 1943). One year after, Snider and Stowell observed 2 other inverted homunculi in each paramedian lobule, in anaesthetized cats (Snider and Stowell, 1944). Although these authors recorded field potential variations, we can suspect that the observations reflected at least partially the mossy fibres activity. However, because of the complex organisation of the cerebellar cortex, it became obvious that any somatotopic map would require separate analysis of mossy fibres inputs, climbing fibre inputs and their effect on Purkinje cell firing.

2.4.1.2 MICROMAPPINGS REVEALED A FRACTURED SOMATOTOPY

In the 70's, the development of electrophysiological recordings allowed Wally Welker's team to show that precise stimulation of tactile receptive fields evoked a restricted activation of granule cells (Shambes et al., 1978b); those regions were named *patches*. A few years later, in 1981, it was shown that primary somatosensory cortex (S1) projection neurons from the neocortex target specific regions of the cerebellar cortex via pontine nuclei (Bower et al., 1981). While recording a local patch of granule cells in the cerebellum, they moved a stimulation electrode in S1, showing a specific pattern of connections between the somatosensory cortical map and the somatosensory cerebellar map. Finally, in 1996, they recorded simultaneously S1 and the cerebellar cortex after whiskers stimulation and demonstrated that cerebellar cortex patches receive both direct short-latency sensory input and indirect long-latency sensory information from S1 (Morissette and Bower, 1996). The hemispheres were extensively mapped in the rat (Shambes et al., 1978a, 1978b; Bower et al., 1981) (Figure 15A_1-15A_3), especially the lobule simplex, crus I, crus II and the paramedian lobule. The vermal part of the lobule IV (Uvula) was also mapped. In each tactile micromapping experiment, the authors found patchy - non-overlapping - responding regions in the granular layer. Another region that was extensively mapped is the paravermal region C3, which corresponds to the receptive fields of the forelimbs (Garwicz et al., 1998a; Ekerot and Jörntell, 2001). Unfortunately, our region of interest, the vermis of lobule III to V (Figure 15A_3) was never mapped. Receptive fields are represented several times throughout the cerebellar cortex, but neighbouring receptive fields are not necessarily represented in neighbouring regions in the cerebellar cortex. Such complex topographical organisation of the inputs is named fractured somatotopy (Figure 15A_1). These micromappings were partially reproducible between animals (Bower and Kassel, 1990) (Figure 15B).

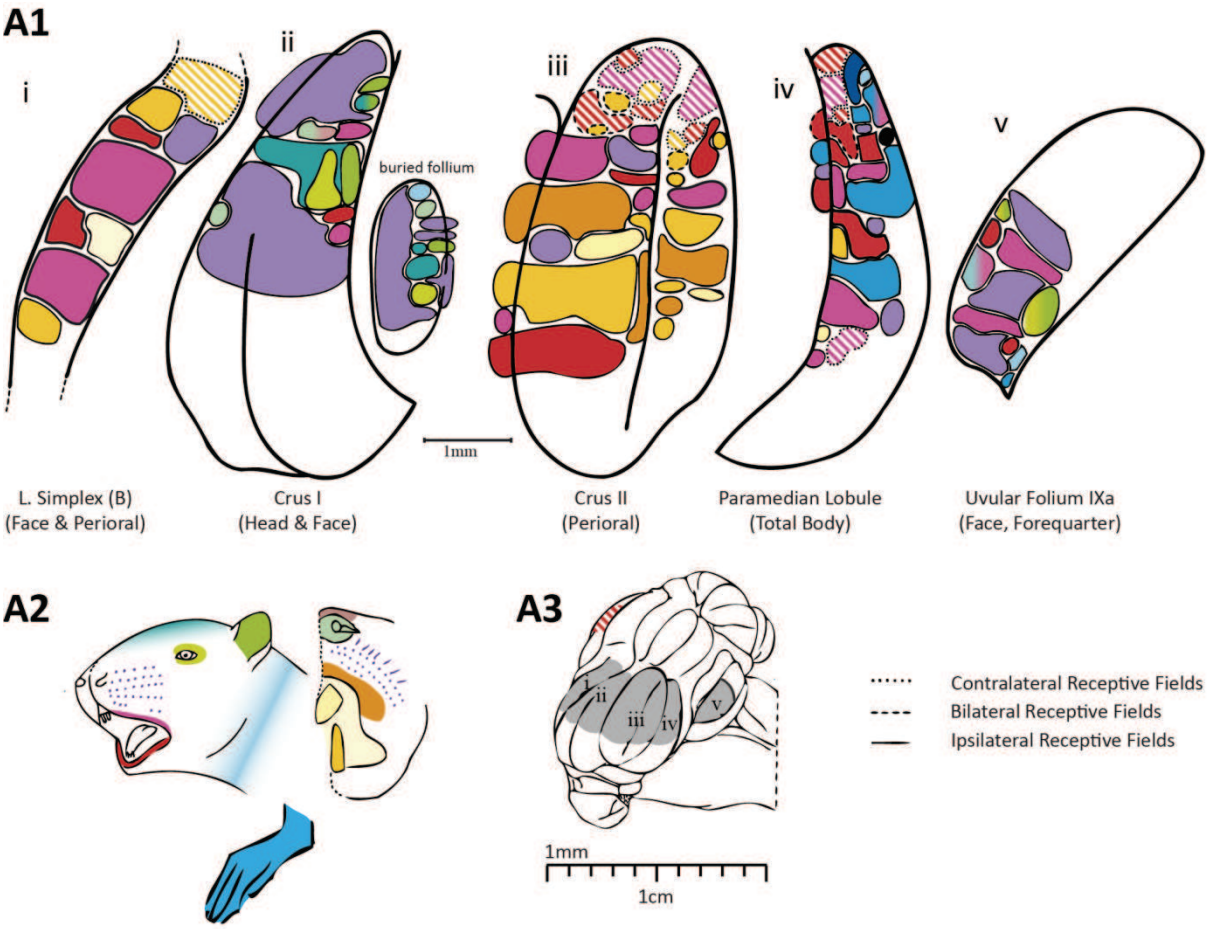

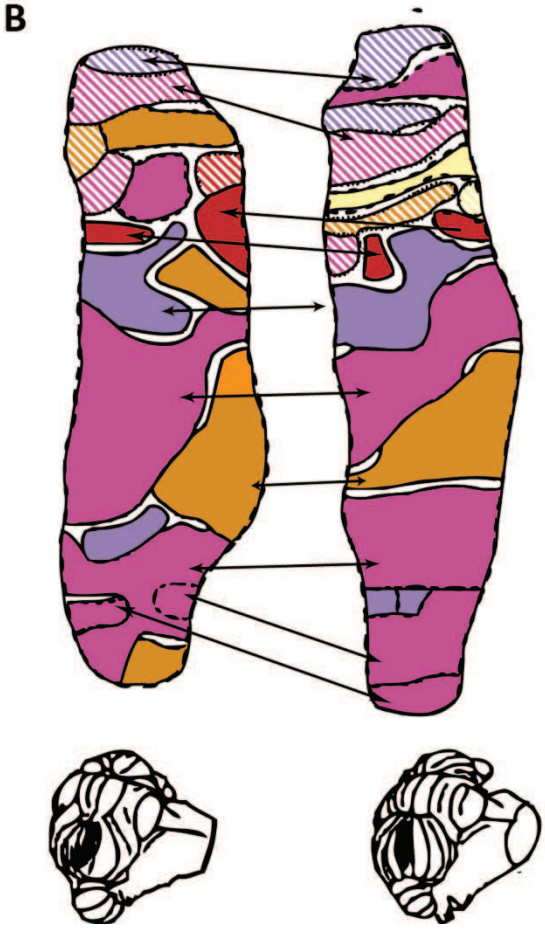

Figure 15 : Fractured somatotopy in the cerebellar cortex.

A : Micromapping of granule cell responses to receptive fields tactile stimulation. $\mathbf{A_1}$ **:** Summarized representation of the micromappings of somesthesic receptive fields in lobule simplex (A_{1i}), Crus I (A_{1ii}), Crus II (A_{1iii}), paramedian lobe (A_{1iv}) and in the vermis of lobule IX (A_{1v}). Patches represent regions in which granular layer responded to somesthesic stimuli. Colours refer to the receptive fields indicated in A_2. Hatched regions indicate regions responsive only to contralateral stimuli. The total body was sometimes partially mapped: in parenthesis: indication of the mapped region for the corresponding lobule. $\mathbf{A_2}$: Delimitation of the receptive fields. $\mathbf{A_3}$: Position of lobules mapped. Hatched region corresponds to our region of interest and was never mapped. Figure adapted from Shambes et al., 1978.

B : Similar fractured somatotopic map between two different rats. Colours correspond to Figure A_2. Hatched region responds to contralateral receptive fields only. Adapted from Bower, 2011.

2.4.1.3 DO MOSSY FIBRES PROJECT AS PATCHES OR STRIPES?

The patchy projections observed in functional mappings were somehow contradictory with the previous tracing studies (Voogd, 1967, 1969; Künzle, 1975). Indeed, when anterograde labelling of various precerebellar nuclei was performed, projections in the cerebellar cortex either display parasagittal bands of almost equal size (in the external cuneate nucleus, gracile nucleus, cuneate nucleus, spinocerebellar tractus or lateral reticular nucleus, Figure 16A_2, 16B_1), or scattered projections (pontine nuclei, see in the hemispheres, Figure 16C_1) (Voogd, 1969; Heckroth and Eisenman, 1988; Ji and Hawkes, 1994). Surprisingly, projections from the lower limbs (spinocerebellar tractus) do not overlap with projections from the upper limbs (Figure 16C_2). This means, at least for the most direct sensory inputs, that the regions of the granular layer processing information from the lower body and from the upper body are separated. The meaning of this segmentation is unknown, but could be compared to the somatotopic maps observed *in vivo*.

Why are the projections in bands, and the functional maps in patches? Mossy fibres functional patches revealed a somehow unexpected organisation in the cerebellum, because they neither follow the climbing fibre/zone/microzone/zebrin parasagittal organisation, nor respect the mediolateral orientation of parallel fibres. One answer could be that neuronal tracing studies showing bands are not precise enough. When single mossy fibres are labelled, they usually branch along the mediolateral axis, projecting in several regions of a same lobule (Figure 16A_2), but also along a parasagittal axis, projecting in several lobules (Figure 16A_1). If we look closer, terminals which apparently form parasagittal bands are actually clustered in very specific lobules that could match with the functional patches (Wu et al., 1999; Shinoda et al., 2000; Pijpers et al., 2006; Quy et al., 2011). More precise mappings, like for the climbing fibres system could be the key to understand the somatotopic organisation of the cerebellar cortex.

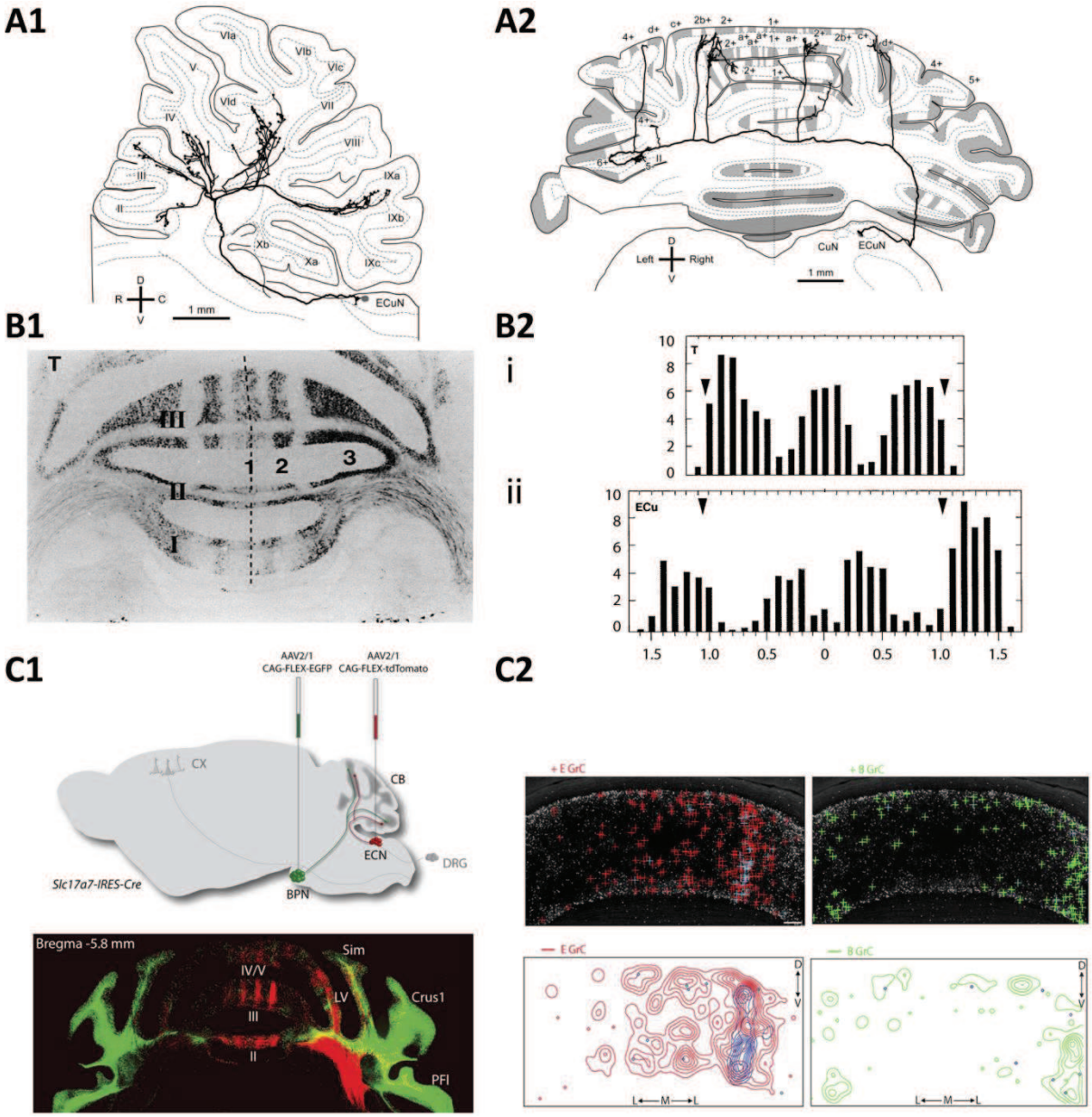

Figure 16 : Organization of the mossy fibres inputs.

A : Single mossy fibre trajectory, adapted from (Quy et al., 2011). $\mathbf{A_1}$: Sagittal representation of the neuronal tracing of a single mossy fibre originating from the external cuneate nucleus. Mossy fibres can send multiple collaterals in several lobules along the parasagittal axis. $\mathbf{A_2}$: Coronal representation of the neuronal tracing of a single mossy fibre originating from the same region of the external cuneate nucleus. Mossy fibres can send multiple collaterals in several cerebellar zones along the mediolateral axis.

B : Labelling of mossy fibres originating from precerebellar nuclei can form parasagittal bands. $\mathbf{B_1}$: Coronal slice of the anterior lobule after injection of wheat germ agglutinin horseradish peroxidase (WGA) in spinal cord thoracic region. Roman numerals indicate lobules, dotted line indicates midline. $\mathbf{B_2}$: Density of the mossy fibre labelling in lobule III following injection of WGA in the thoracic region of the spinal cord ($\mathbf{B_{2i}}$) or in the external cuneate nucleus ($\mathbf{B_{2ii}}$). Black arrows indicate the P2+/P2- zebrin II border. X-axis represents distances from midline in mm. Adapted from Ji and Hawkes, 1994.

C : Mossy fibres display different distribution patterns depending on their origin. $\mathbf{C_1}$: Injection of adeno-associated virus in external cuneate or pontine nuclei. Projections from the external cuneate nucleus displayed band similar to B_{2ii}. Projections from pontine nuclei were mostly located in the paravermis and the hemispheres. $\mathbf{C_2}$: Mossy fibre terminals in lobule III. Upper panels : crosses indicate granule cells contacted by mossy fibre from the external cuneate nucleus (red) or from the pontine nucleus (green). Blue crosses indicate granule cell integrating more than one input from the same nucleus. Lower panels : corresponding density maps. Adapted from Huang et al., 2013.

2.4.2 MATCHING BETWEEN MOSSY FIBRE INPUTS AND CLIMBING FIBRE INPUTS

Even if a full mossy fibres input map doesn't exist, neuronal tracing studies showed that mossy fibres terminals generally branch in regions with similar zebrin identity, and with similar climbing fibre origin (Figure 17A) (Voogd et al., 2003; Pijpers et al., 2006), suggesting that those regions integrate inputs with similar features. The convergence of the two inputs was described in two important studies *in vivo*.

The first one was performed in crus II of the rat cerebellar hemispheres (Brown and Bower, 2001) and consisted in recording complex spike activity (which reflects climbing fibres inputs) and granule cell activity (in the granular layer, which reflects mossy fibres inputs). The authors either recorded several neurons at precise locations while they were stimulating a single skin receptive field (a vibrissae), or recorded a single location in the cerebellar cortex while stimulating different receptive fields of the face.

- The same regions of the cortex presented increased complex spike activity (and thus received climbing fibre inputs) and increased granule cells activity (Figure 17B_1), suggesting that climbing fibres and mossy fibres project to the same locations.
- For a single recording site, the primary receptive field (i.e., the receptive field evoking the strongest response) was the same for both complex spike and granule cells. (Figure 17B_2). It suggests that the primary receptive field is shared between the two inputs, even if one given region integrates information from other secondary receptive fields.
- In that case, another parameter was also quantified (Figure 17B_2, right panel): Purkinje cells within the responding mossy fibre region had an increased simple spike frequency, which could be evoked by both local granule cells through their ascending axon or by distal granule cells through parallel fibres.

A second study observed the convergence of the two inputs in the C3 region in the cat, and obtained similar results concerning climbing fibre receptive fields and mossy fibre receptive field. However, at the Purkinje cell level, activation of local mossy fibres did instead evoke decrease in simple spike firing (Garwicz et al., 1998a; Ekerot and Jörntell, 2001, 2003). Recordings of molecular layer interneurons activity during similar experiments indicated that molecular layer interneurons have also the same receptive field. Decrease in simple spike frequency could thus be explained by feedforward inhibition from local molecular layer interneurons activated by local granule cells. In these experiments local granule cells have essentially an inhibitory effect on local Purkinje cells, through molecular layer interneurons (Ekerot and Jörntell, 2001) (Figure 17C).

Differences in the impact of interneurons between the two sets of experiments might be explained by the animal model, the recorded region, or differences in the balance between excitation (from the ascending axon and the parallel fibres activation) and inhibition (from molecular layer interneurons) which could be due to the distinct surgical procedures (ketamine/xylazine in rats versus decerebration in cats).

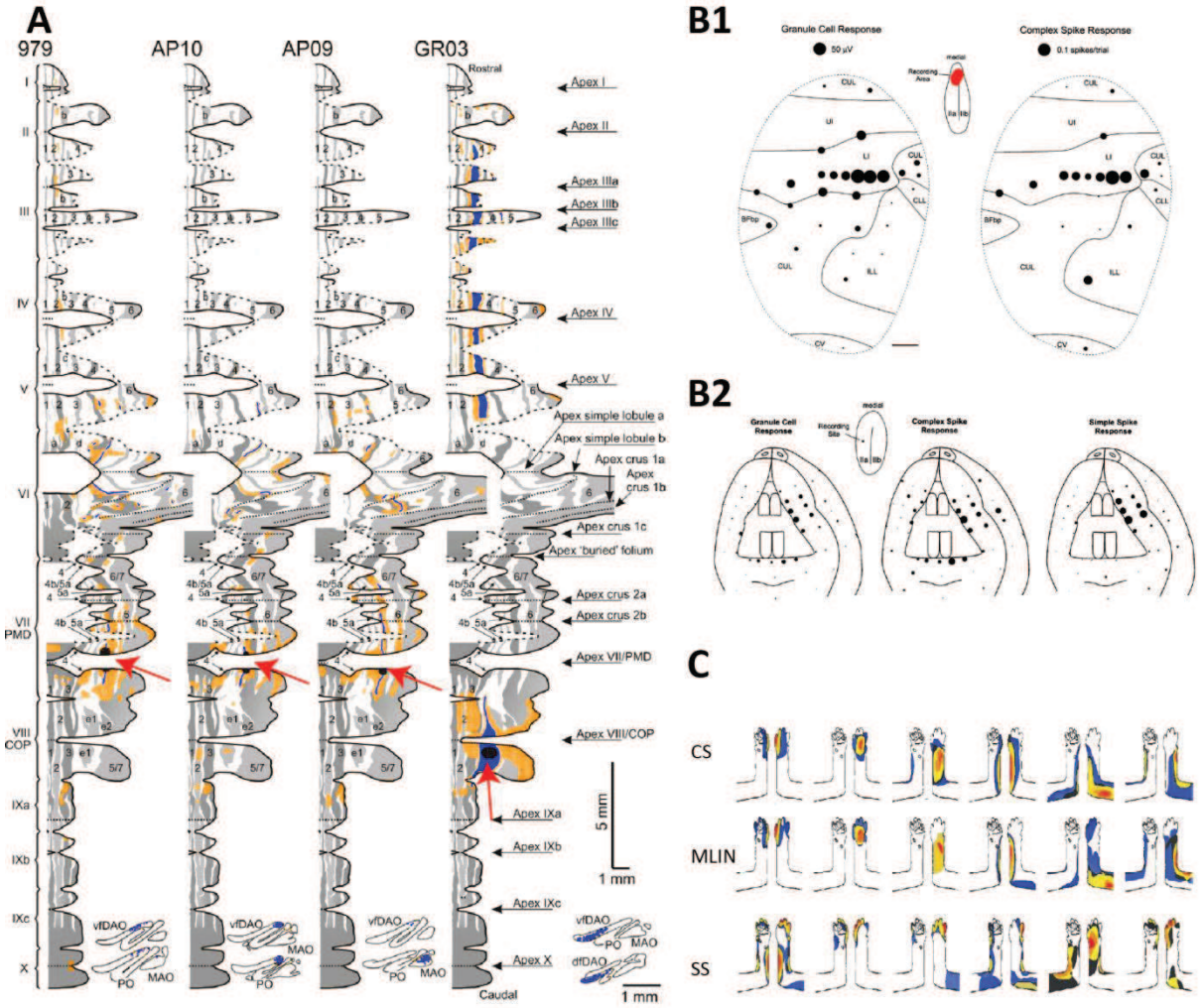

Figure 17 : Mossy fibre and climbing fibre convergence.

A : Neuronal tracing comparing climbing fibres projections and mossy fibres projections in four animals. Scheme represents an unfolded view of the cerebellar cortex, lobules are indicated on the left, sulci and apex are indicated on the right, and zebrin bands are indicated as grey stripes. Climbing fibres (blue) are labelled in the inferior olive (bottom right insets). Injection of retrograde tracer is performed in a cortical region where climbing fibres project (black circle, red arrows). Mossy fibres that sent collaterals in this injected region are retrogradely labelled (orange). This experiment revealed that collaterals of mossy fibres project in similar regions than collateral of climbing fibres (see regions that are different from injection site and contain both orange and blue labelling). Adapted from Pijpers et al., 2006.

B : Micromapping of both climbing fibre and mossy fibre response. $\mathbf{B_1}$: Micromapping of the perioral receptive fields in lobule VII paravermis (recorded area in red). Left panel indicates granule cell response, which corresponds to mossy fibres inputs. Right panel indicates the complex spikes response. Each black circle represent a recorded site. Circle size is proportional to the response amplitude after single receptive filed stimulation. The two systems share the same receptive field in that area. $\mathbf{B_2}$: For a single recording point, mossy fibres (left panel, granule cell responses), and climbing fibre (central panel) are activated by the same receptive fields. Changes in simple spike frequency, which might reflect ascending axon excitatory effect, parallel fibre activation from distal granule cells or changes in molecular layer interneurons activity were evoked by the same receptive fields as local granule cells and complex spikes. Figure from Brown and Bower, 2001.

C : Summary of micromappings in the C3 region of the paravermis, in which complex spikes (CS), molecular layer interneurons (MLIN) or simple spikes (SS) were recorded after stimulation of forelimb receptive fields. Each column indicates a set of experiments in which several cells shared similar receptive fields and were pooled. Colours indicate the degree of similarity between the pooled receptive fields. Red colour indicates a region which was always responding within the group, whereas blue indicates regions responding only in few cases, often at the periphery. CS and MLIN receptive fields were similar, whereas SS receptive fields were distinct (please notice that results differ from B1-B2). Adapted from Ekerot and Jörntell 2003.

2.4.3 FUNCTIONAL RELEVANCE OF FRACTURED SOMATOTOPY

The presence of a fractured somatotopy might reflect a fundamental feature of the cerebellar cortex, which is the ability to coordinate separate modules controlling different functions (i.e. muscles, group of muscles or even more cognitively-related function). This fractured organisation might be optimal to perform task-related learning (Marr, 1969), which requires *a priori* to associate each module with any other module. Parasagittal, repeated and non-overlapping somatosensory inputs from different receptive fields can be associated through the mediolaterally oriented parallel fibres. Parallel fibres cross several functional units, allowing any associative learning between these units. This mesh organisation is probably more economical in term of energy than a system that would necessitate a re-wiring for new associative learnings. It can be noticed that fractured somatotopy is not specific to the cerebellum and was also observed in the primary motor area in the cortex (Gould, 1986; Donoghue et al., 1992; Kaas, 2012). If the cerebellar cortex only associates discrete granule cells patches with small Purkinje cells clusters, and if this association is mediated by the parallel fibres through adjustable synaptic weighting or excitation/inhibition interplay, this feature should be observable *in vitro*. The last part of this chapter will be dedicated to the description of intra- versus intermodular communication mediated by granule cells through their ascending axon and parallel fibres.

2.4.3.1 ANATOMICAL EQUIVALENT OF THE FUNCTIONAL PATCHES

However, before switching to the network scale, I would like to relate an intriguing observation made by Hawkes and colleagues (Hawkes et al., 1997) who used ethanol fixation and paraffin sections. They observed shrunken regions of about 300 µm in the granular layer at reproducible locations, that they called *blebs*. The origin of this experimental observation is unknown, but could be linked to a segregated packing of the axons, or of other granular layer cell types. The blebs size is compatible with the patches described above, and their borders match with zebrin band delimitations. It is possible that blebs are the anatomical correlate of the functional patches. This hypothesis should be verified, and could provide a very convenient tool to localise the inputs after an experiment.

2.5 FROM THE BEAM THE HYPOTHESIS TO THE PATCH HYPOTHESIS

2.5.1 THE BEAM HYPOTHESIS

The first electrophysiological theory of the cerebellar cortex was based on the particular geometrical relationship between parallel fibres and Purkinje cells. The “beam hypothesis” was initially proposed by Valentino Braitenberg and Roger P. Atwood (Braitenberg and Atwood, 1958), and further developed by John Eccles (Eccles et al., 1967). The main idea was that the excitatory parallel fibres activate sequentially all Purkinje cells on their way, inducing a depolarising tidal wave that would ultimately be propagated to the cerebellar nuclei (Figure 18A_1, 18A_2). In this theory, molecular layer interneurons perform an off-beam inhibition flanking the activated beam of parallel fibres, restricting the activated region (Figure 18A_3) (Cohen and Yarom, 2000; Gao et al., 2006; Rokni et al., 2007).

This hypothesis based on the histological organisation of the circuit was convenient to explain timing mechanisms necessary for motor coordination. The slow action potential propagation in the thin unmyelinated parallel fibre would generate a precise temporal sequence of Purkinje cells/Golgi cells/molecular layer interneurons depending on their position. The distance between granule cells and Purkinje cell is thus converted into a timing signal, allowing precise and controlled sequences of movements.

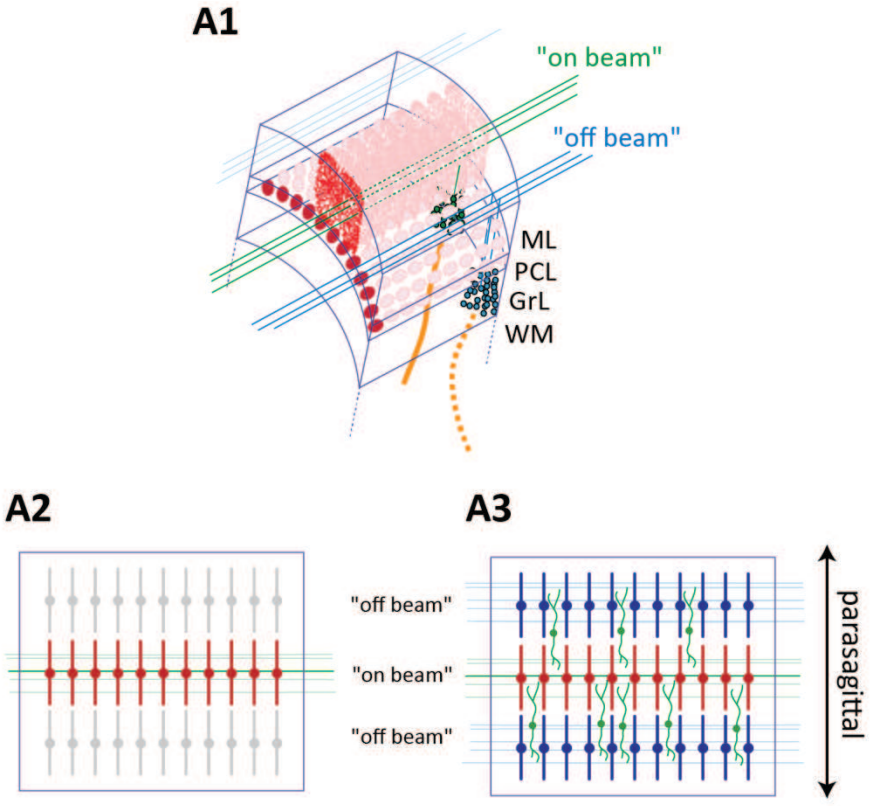

Figure 18 : Beam hypothesis and lateral inhibition.
A_1 : 3D block of cerebellar cortex, similar to Figure 4. Mossy fibres inputs (orange) activate patches of granule cells (blue and green circles represent 2 different patches), which project their axon in the molecular layer as parallel fibres. A patch of granule cells forms a beam of parallel fibres. Purkinje cells (in red) that are activated by a beam of parallel fibres are "on beam". Non-activated Purkinje cells (not represented) are "off beam". ML : molecular layer, PCL : Purkinje cells layer, GrL : granular layer, WM: white matter. **A_2** : Figure A_1, top view. On beam Purkinje cells are activated if parallel fibre to Purkinje cell synapses are not silent. **A_3** : On beam molecular layer interneurons (in green) are also activated. They have larger parasagittal extent for both dendrites and axon, and can inhibit both on beam Purkinje cells and off beam Purkinje cells. Please note that the same interneurons could also be activated by off beam parallel fibres therefore could and inhibit on beam Purkinje cell (not represented).

2.5.2 THE PATCH HYPOTHESIS

Many discoveries excluded this initial view of the cerebellar physiology because depolarising waves could not be observed with physiological stimuli *in vivo*. Instead, authors generally observe patches of activated Purkinje cells located above an activated patch of granule cells, leading to the alternative *patch hypothesis* of the cerebellar functioning already presented (Shambes et al., 1978a, 1978b; Bower et al., 1981; Kassel et al., 1984; Garwicz et al., 1998b; Ekerot and Jörntell, 2001).

The patch hypothesis is based on the observation that *in vivo*, receptive field activation evokes at the same place mossy fibres, granule cells, molecular layer interneuron and Purkinje cells excitation. This columnar activation would resemble cortical column activation in the cortex (Kaas, 2012). However, such organisation would require clarification of the parallel fibres function, since they make numerous synapses on distal Purkinje cells. Several hypotheses could explain the absence of beam activation.

- Parallel fibres do not synapse with all the Purkinje cells. This possibility is however unlikely, based on morphological studies (Napper and Harvey, 1988; Pichitpornchai et al., 1994).
- Synapses are present but silent (Ekerot and Jörntell, 2001; Isope and Barbour, 2002). They could be ineffective for physical reasons (highly filtered for instance), or because they were depressed.
- Excitatory synapses are present and functional, but molecular layer interneurons perform a feedforward inhibition that shunts the depolarisation (Santamaria et al., 2007).
- Another form of input, like monoamines or neuromodulators shunts the effect on the Purkinje cells in specific regions (Libster and Yarom, 2013).

Many of these hypotheses can be addressed *in vivo*, or more easily, *in vitro*.

2.5.2.1 ASCENDING AXON

The anatomical basis of the existence of a different connectivity between local and distal granule cells onto Purkinje cells (or other cell types such as Golgi cells and molecular layer interneurons) is based on the existence of numerous synapses along the ascending branch of the granule cell axon (chapter 1). A disputed question is whether the ascending axon has also specific functional properties, either in term of number of synapses, number of release sites or in release probability.

By using granule cell-Purkinje cell pair recordings *in vitro* in the rat, Philippe Isope and Boris Barbour (Isope and Barbour, 2002) showed that local granule cells have a higher probability to display a functional connection (50% under the dendritic plane, but less that 10% beyond 35 µm) (Figure 19A_1-19A_4). Another study (Sims and Hartell, 2005) estimated that the release probability of local granule cells was higher, and appeared more resistant to LTD compared to parallel fibres. Finally, a recent report using glutamate uncaging showed, on average, strong responses from granule cells (Walter et al., 2009), although these authors insist on the fact that function of ascending axon synapses and parallel fibre synapses are equivalent (Figure 19B). These three experiments suggest that the local ascending axon exert a stronger control onto local Purkinje cells than parallel fibres from distal granule cells.

Another set of experiments addressed the question of the feedforward and lateral inhibition by using glutamate uncaging as described above. In these experiments, local granule cells were purely excitatory (i.e. they do only activate the Purkinje cell located above, without feedforward inhibition) whereas *off beam* granule cells can perform uniformly strong feedforward inhibition, by activating only molecular layer interneurons (Dizon and Khodakhah, 2011). This strong local feedforward inhibition could explain the observation *in vivo* discussed before (Ekerot and Jörntell, 2001) (Figure 17C), in which local granule cells were activated, but Purkinje cells located above were inhibited.

Golgi cells can also be contacted either by the parallel fibres through the apical dendrites and by the ascending axon through basolateral dendrites. A recent study showed that basolateral dendrites are covered by ~400 granule cell contacts (Cesana et al., 2013). Because inputs from the apical dendrites are strongly filtered and represent only 50% of the inputs, this study suggests that activation of Golgi cell by local granule cells implicates feedback inhibition of granule cells within the local patch.

Patch clamp experiments are accurate for addressing connectivity, since it is possible to directly measure the synaptic inputs. However, in mapping experiments, large scale imaging would be the fastest way to map the whole network activity. To further study the connectivity between group of granule cells and Purkinje cells, several imaging studies were performed, either *in vivo* or *in vitro*. However, most of these studies can only display the indirect resultant of excitatory and inhibitory inputs. *In vivo* extracellular recordings present similar problems than imaging studies: simple spike firing in Purkinje cells is only the resultant of intrinsic firing and its modulation by inhibitory and excitatory inputs.

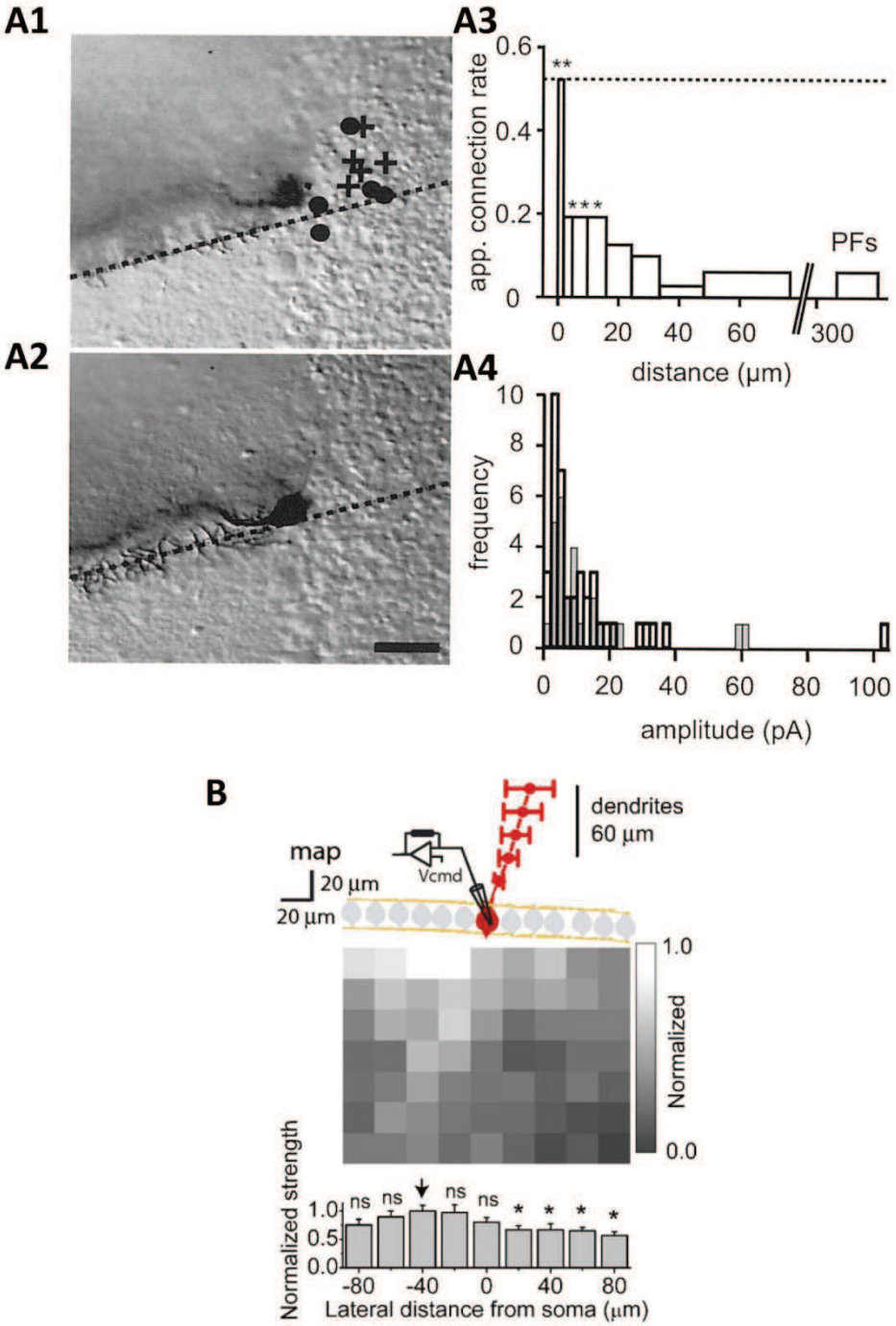

Figure 19 : Functional discrepancies between local and distal granule cells.

A : Granule cell - Purkinje cell pair recordings (Isope and Barbour, 2002). Purkinje cells are recorded in whole cell patch clamp and granule cells in loose cell patch clamp. Inhibition was blocked. $\mathbf{A_1}$ and $\mathbf{A_2}$: Picture of a recorded Purkinje cell at two different levels. Dotted line indicates the dendritic plane of the Purkinje cell. Crosses indicate unconnected granule cell, circle indicates connected granule cell. $\mathbf{A_3}$: Probability of connection between a granule cell and a Purkinje cell, in function of the distance from dendritic plane. $\mathbf{A_4}$: distribution of average synaptic weights between pairs.

B : Glutamate uncaging experiments in adult rats (Walter et al., 2009). Focal laser spots are evoked at controlled coordinates. Laser spots release caged glutamate, which activates the local granule cells. Purkinje cells (red) are recorded in whole cell patch clamp. Inhibition is blocked. Top pannel : Average map. Each square represents a stimulation point. The whole granular layer is mapped, and the map represents normalised average response (scale bar on the right). Bottom pannel : Responses are then re-averaged by columns and re-normalised (middle panel). Local granule cells present a stronger connection which could be due to higher synaptic weights or more connected cells.

2.5.2.2 CA^{2+} AND VOLTAGE IMAGING

Ca^{2+} imaging allows the visualization of the activation in several cells simultaneously. Unfortunately, individual granule cell to Purkinje cell connections cannot be mapped, since most of the Ca^{2+} signal is induced by complex spike depolarisation. Ca^{2+} imaging studies essentially helped to describe the climbing fibre inputs (Mukamel et al., 2009; Ozden et al., 2009) rather than the mossy fibre-parallel fibre-Purkinje cell pathway activation. However, a recent study performed successful Ca^{2+} imaging of compound parallel fibre activity (Cramer et al., 2013). In this study, the authors observed beam-like response in crus I after electrical stimulation of the limbs (Figure 20A), whereas they observed patch-like response in crus II following vibrissae stimulation. They also electrophysiologically confirmed that Purkinje cells along the beam were activated. Their findings support the beam hypothesis, but also show important variability in information processing depending on the recorded region.

Voltage-sensitive dyes were used in the late 90's in an isolated cerebellum preparation. The authors observed a beam-like activation of the cerebellar cortex when using direct electrical stimulation of the parallel fibres (Cohen and Yarom, 1998) (Figure $20B_1$). In the same study, stimulation of the white matter, and thus of mossy fibres (and climbing fibres) evoked patch-like responses (Figure $20B_2$). The authors concluded that a single patch of granule cells was not sufficient to activate Purkinje cells along parallel fibres beam. However, the exact origin of the voltage signal detected was not precisely determined, and the authors suggested that they could rely on Ca^{2+} spikes in the Purkinje cell dendrites, that would be only triggered by the strongest inputs.

2.5.2.3 AUTOFLUORESCENCE IMAGING

Flavoproteins autofluorescence the can be used to detect the synaptic activity in neurons. Ca^{2+} uptake and extrusion, as well as the activation of intracellular pathways (for instance by metabotropic receptors) require energy. Changes in energetic metabolism can be seen as variations of the autofluorescence of flavoproteins. This signal was used to detect the activation of the mossy fibre-granule cell-Purkinje cell pathway (Reinert et al., 2004). In Timothy Ebner's group studies, the direct electrical activation of parallel fibres results in beam activation of the Purkinje cells, flanked by *off beam* inhibition due to molecular layer lateral inhibition (Reinert et al., 2004; Gao et al., 2006). When physiological stimulation of the vibrissae were performed, the same cortical region displays patch-like response (Gao et al., 2006). However, they showed in recent experiments that the size of the autofluorescent signal responding region had a increased surface when inhibition was blocked (which prevents lateral inhibition by molecular layer interneurons, and granule cells feedback and feedforward inhibition by Golgi cells, (Figure $20C_1$)), and could be transformed into a beam-like response by blocking $EAAT_4$ (Figure $20C_2$) (Cramer et al., 2013). These experiments showed that inhibitory interneurons (molecular layer interneurons and Golgi cells) shunt excitation by both feedforward inhibition within the beam, and lateral inhibition in flanking regions, and that molecular markers such as $EAAT_4$ tightly control the excitability of Purkinje cells in the network. Yet, autofluorescence might not be precise enough to detect fine connection properties between granule cell and Purkinje cells. Although autofluorescent signal can usually be seen 100 ms to 1s after the stimulus, in their experiments the response is only expressed 20 to 25 seconds later, and might reflect complex mechanisms such as plasticity induction.

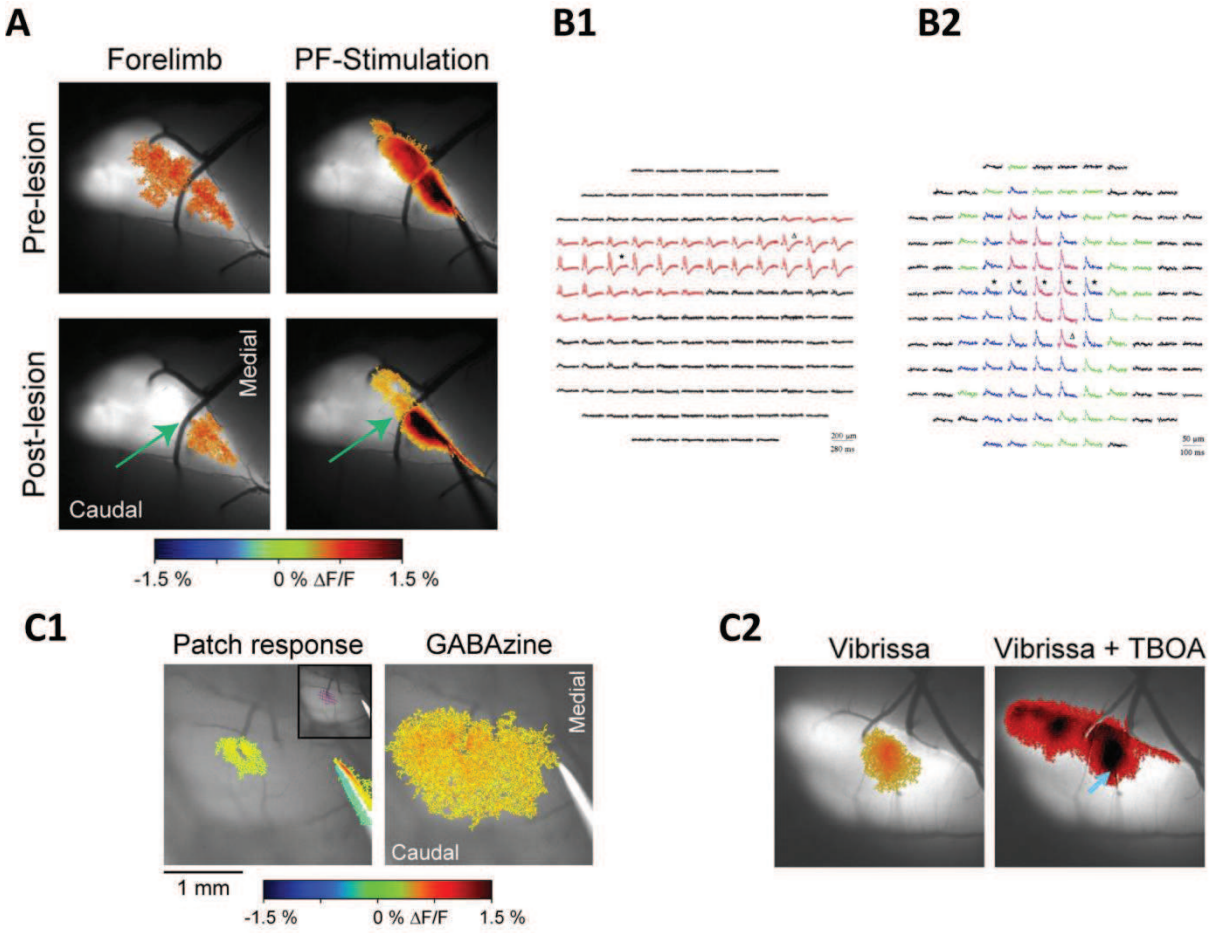

Figure 20 : Large scale imaging of patch-like and beam-like activity in the cerebellar cortex.
A : Ca^{2+} imaging of the cerebellar cortex after electrical stimulation of forelimb (left panels) or direct electrical stimulation of a beam of parallel fibres (right panel). After electrolytic lesions of the molecular layer (green arrow), beam-like activity is prevented. From Cramer et al., 2013.
B : Voltage dye imaging in isolated cerebellum. Figure represents the cerebellar cortex surface. Variation in signal indicates changes in membrane potential in parallel fibres, interneurons and Purkinje cells. $\mathbf{B_1}$: Direct electrical stimulation of parallel fibres with a train evoked a beam of activity. $\mathbf{B_2}$: Stimulation of mossy fibres evoked a patch of activity. From Cohen and Yarom, 1998.
C : Autofluorescence imaging in the cerebellar cortex. $\mathbf{C_1}$: Patch like response to vibrissae stimulation in crus II (left panel) is considerably increased when inhibition is blocked by bath application of gabazine, a blocker of $GABA_A$ receptors (right panel). $\mathbf{C_2}$: Patch like response to vibrissae stimulation in Crus II (left panel) is turned into a beam-like response when excitatory amino acid transporters (EAATs, including $EAAT_4$) are blocked by TBOA (right panel). From Cramer et al., 2013.

To conclude, intermodular connection between patches/microzones/zebrin is possible, based on anatomical, *in vitro* and *in vivo* studies. The variety of results obtained between studies suggests that cerebellar regions might not be homogeneous, and that experimental conditions strongly affect the precision of the mappings. An exhaustive map of the connections in an identified region could help to link together all these results, and this is the main subject of the second article of this manuscript. A precise description of the inputs and outputs in our region of interest can be found in introduction to the second article. This section will be very technical, but illustrates the degree of precision of cerebellar organisation (Figure 30 and introduction of the second article).

3 HIGH FREQUENCY TRANSMISSION IN THE CEREBELLUM: SHORT TERM PLASTICITIES AND TEMPORAL CODING

As we saw in the previous parts, cerebellum is involved in sensory-motor processing. Inputs are coming from various origins, some of them carrying direct sensory inputs, some others coding more integrated sensory information, while a third population carry information from the cerebral cortex. All these inputs project to precise cerebellar regions to be either locally processed or integrated with inputs from other regions. All these tasks are performed in a few milliseconds to adjust movement in almost real time, requiring an extremely precise temporal processing. As we will see in this chapter, the cerebellum works at very high rates and high frequency coding is conserved throughout all processing steps. But high frequency processing require specific adaptations for accurate signal transmission, and at that time scales, short term plasticities are major compounds of signal processing. In a second time, I will describe the short term plasticity dynamics occurring at the parallel fibre to Purkinje cell synapse, which is the synapse I studied in my first article.

3.1 TEMPORAL ORGANISATION OF HIGH FREQUENCY CEREBELLAR INPUTS

One convenient way to understand signal processing is to describe how the incoming information is encoded, and how input affects output. The most abundant inputs to the Purkinje cells are actually the parallel fibres inputs. Since the only output of the cerebellar cortex is encoded by the Purkinje cell discharges, it is likely that the final effect of the mossy fibres-granule cells-Purkinje cells pathways is to modulate the Purkinje cell firing

3.1.1 FIRING PATTERNS IN THE MOSSY FIBRE → GRANULE CELL → PURKINJE CELL PATHWAY

3.1.1.1 PRECEREBELLAR NUCLEI AND MOSSY FIBRES FIRING

Mossy fibres originate from different precerebellar nuclei, which process different modalities. Mossy fibre discharge profiles are likely to be heterogeneous. For instance tactile stimulation induces bursts while proprioceptive information is transmitted at lower frequencies (Bengtsson and Jörntell, 2009). External cuneate nucleus neurons and lateral reticular nucleus neurons were extensively studied, because they carry tactile information from the digits, paw and forearm, and can both be physiologically activated by tactile stimulation (Figure 21A). Nearly equivalent electrical stimulation are often used, as they are temporally more precise (Bengtsson and Jörntell, 2009). Skin stimulation rapidly evokes firing in the precerebellar nuclei (only 5 ms after stimulus in external cuneate neurons and 10 ms later in the lateral reticular nucleus neurons). External cuneate neurons fire with fast bursts that can reach 1000 Hz (Figure 21B). This initial high frequency bursting phase is usually followed by other spikes at lower frequencies.

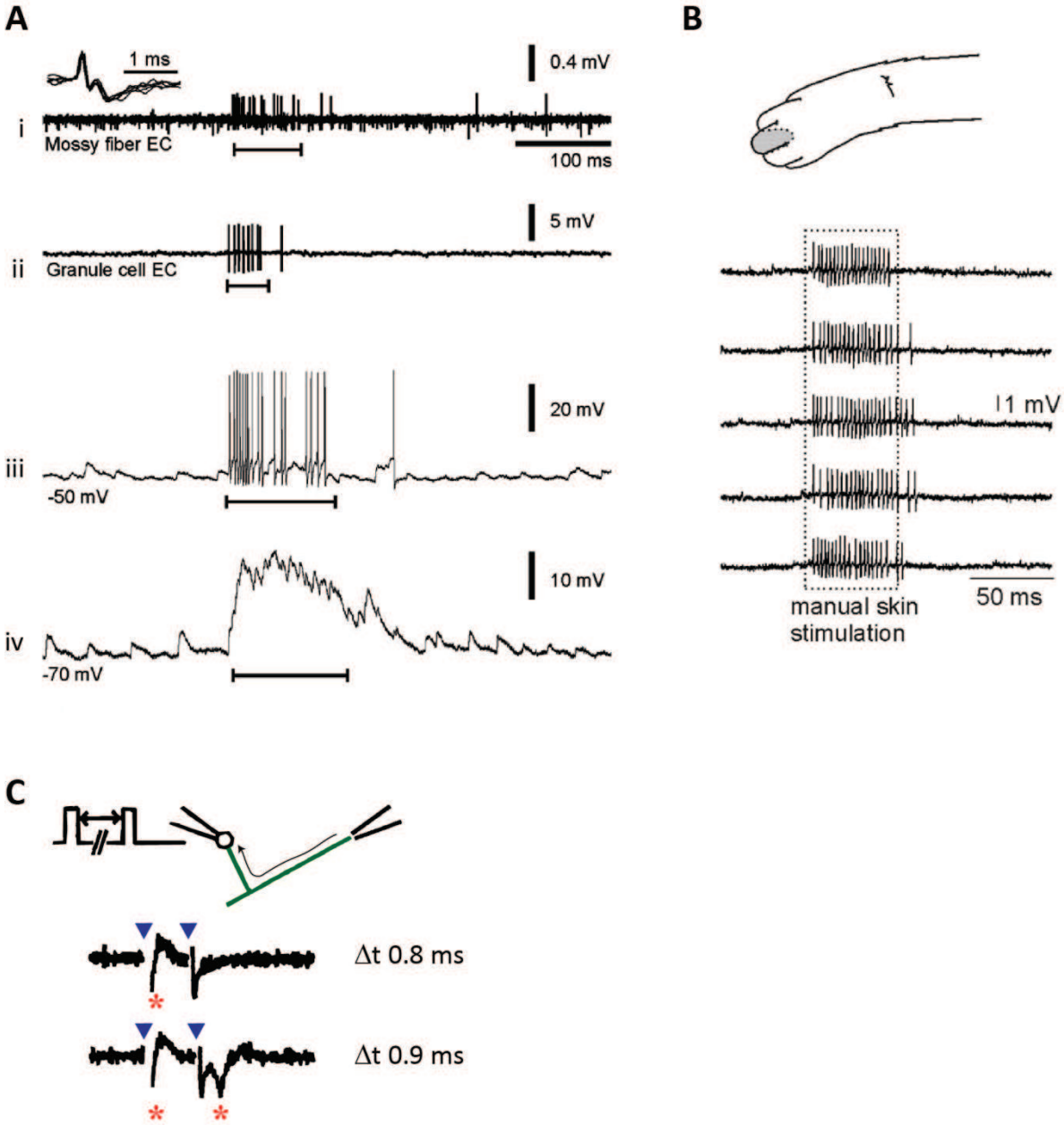

Figure 21 : High frequency transmission in the mossy fibre pathway.

A : Manual cutaneous stimulation of the forelimb in decerebrated cat (capped bar). $\mathbf{A}_{i}$: 5 ms after stimulation high frequency bursts are recorded in external cuneate nucleus mossy fibres terminals. $\mathbf{A}_{ii}$: In response to mossy fibre input, granule cell evokes high frequency burst. Extracellular recording. $\mathbf{A}_{iii}$: Same as A_{ii}, in intracellular recording with no current injection. $\mathbf{A}_{iv}$: Same as A_{iii}, with current injection to prevent firing. Mossy fibres high frequency bursts of EPSPs can be recorded in the absence of stimulus; both synaptic noise and spontaneous firing are very low.

B : Bursting profile of granule cells responses to manual skin stimulation (forelimb shaded area, top panel).

A and B are from Jörntell and Ekerot, 2006.

C : Paired stimulations of parallel fibre (green), evoking antidromic action potential (red asterisk), recorded with loose-cell patch clamp at cell soma, at 37°C. Two stimulations at 1250Hz failed to evoke two action potentials. Two stimulations at 1100 Hz were successfully transmitted across the whole axon. Adapted from Isope and Barbour, 2002.

3.1.1.2 SHORT TERM PLASTICITIES AT THE MOSSY FIBRE TO GRANULE CELL SYNAPSE

Mossy fibre to granule cell synapse is located within the glomerulus. The synaptic transmission is mediated essentially by AMPA conductances, with an important contribution of the glutamate spillover coming from the other extra synaptic sites within the glomerulus (DiGregorio et al., 2002). NMDAR also contribute to the charge transfer, particularly in the adult and in the case of a sustained activation at low frequency like in the vestibulocerebellum (Silver et al., 1992; Schwartz et al., 2012).

Since there is no filtering in granule cells, recorded EPSCs are very fast (10%-90% rise time between 0.19 ms (DiGregorio et al., 2002) and 0.43 ms (Cathala et al., 2003)). Upon repetitive stimulation, synaptic transmission is depressed with a paired-pulse ratio of 0,43 at 100 Hz. Short half-width and strong depression of the EPSCs also come from a strong desensitization of the postsynaptic AMPAR (Xu-Friedman and Regehr, 2003). After a strong initial depression, the neurotransmitter release reaches a plateau, and can be sustained for a very long period at high frequency, up to 300 Hz (Saviane and Silver, 2006).

3.1.1.3 GRANULE CELL FIRING

3.1.1.3.1 MULTIMODAL/UNIMODAL INTEGRATION

Granule cells express the extrasynaptic α6-containing $GABA_A$ Receptor ($GABA_AR_{\alpha6}$), which has ten folds higher affinity than classical α1-containing $GABA_AR$ (Ducić et al., 1995). Because of the high $GABA_AR\alpha6$ affinity, granule cells are very sensitive to GABA spillover within the glomerulus. The permanent spontaneous spiking activity of Golgi cells maintain granule cells in a hyperpolarised, around -71mV, (Brickley et al., 1996; Rossi and Hamann, 1998), and limit granule cell firing in response to single mossy fibre inputs. However, one single mossy fibre input is probably not sufficient to induce an action potential in granule cells, and it was suggested that all four granule cell dendrites have to be activated simultaneously (Chadderton et al., 2004; Jörntell and Ekerot, 2006). However, some authors suggested that at high frequencies, one single mossy fibre could activate a granule cell (Rancz et al., 2007). In both cases, granule cell firing requires temporal summation of the EPSCs. Since AMPA currents have very fast kinetic, mossy fibre inputs should fire in near synchrony.

There is a debate whether granule cell integrates multimodal or unimodal inputs. Multimodal integration would allow the granule cell to perform *pattern discrimination* or *recoding,* by firing only when a specific set of mossy fibres are co-activated. Unimodal integration would rather turn the granule cell into a noise filter, selecting only the strongest sensory inputs. Experiments suggest that both situations can exist, but a recent tracing study, showing that granule cells have rarely all their four dendrites occupied by mossy fibres from the same origin, emphasized the existence of multimodal integration (Huang et al., 2013)

3.1.1.3.2 HIGH FREQUENCY DISCHARGES

The input/output curve showed that granule cells can fire at high frequencies, up to 250 Hz, with low accommodation (Chadderton et al., 2004), transmitting reliably high frequency bursts coming from mossy fibres.

In Fredrik Bengtsson experiment *in vivo* (Bengtsson and Jörntell, 2009) electrical stimulation of the skin evokes bursts of action potentials in the granule cell with a latency of 6.5 ms, that is only 1.5 ms after the external cuneate neurons firing, a delay in accordance with the synaptic conduction between the two structures (Figure 21A, 21B). These burst are transmitted along the granule cell axon and finally reach presynaptic buttons.

More generally, burst coding in the central nervous system are often found in sensory systems (Krahe and Gabbiani, 2004), and the possible role of burst firing in the cerebellum will be addressed in the general discussion.

3.1.1.3.3 AXONAL CONDUCTION DURING HIGH FREQUENCY BURSTS

In the classical view of neurotransmission, each spike evoked at the soma triggers the release of neurotransmitter at presynaptic terminals in an all-or-none manner. This model is challenged by experiments showing that axon may play an essential role in neurotransmission by modifying the properties of spike propagation along the axon during high frequency burst (Debanne, 2004). Most of the examples below were demonstrated in invertebrates or other brain structures, and their existence in the cerebellar cortex remains to be demonstrated. However, they illustrate the complexity of neuronal computation that may occur during a burst.

First of all, it is interesting to note that the highest rates recorded approach the limit of the absolute refractory period of an action potential in the granule cells, which is about 0.9 ms in the parallel fibre (Isope and Barbour, 2002) (Figure 21C). Typically, high frequency rates can induce spike transmission failures, particularly at branching points - the T of the granule cell axon could be one of the weaknesses - or when the axon diameter varies, which is the case at each *en passant* synapse (Grossman et al., 1979). However, recording granule cell soma while evoking backpropagated action potential showed that failures are rare in parallel fibres (Isope and Barbour, 2002). Some other mechanisms can induce a conduction block, like an insufficient repolarisation (Krnjevic and Miledi, 1959) or an excessive hyperpolarisation induced for instance by BK channels (Zhang and Jackson, 1993). In the parallel fibres, the activation of axonal $GABA_AR$ produces an axonal depolarisation due to high intracellular Cl^- concentration, increasing the axonal excitability and even promoting orthodromic action potential initiation at the soma (Pugh and Jahr, 2011).

It was recently proposed that action potential could be considered as an analog-digital signal rather than purely analog. The concept is based on several observations that showed a modification in the shape of the action potential (Debanne et al., 2013). Two major mechanisms should be considered:

In the hippocampus, it was demonstrated that repetitive discharges tends to increase the width of the action potential, and thus the amount of Ca^{2+} entering into presynaptic terminals (Geiger and Jonas, 2000). In that case, the shape of the action potential was directly dependent of the firing context. The position of the action potential within the burst affects its impact on the synapse. This kind of mechanisms could theoretically occur in the cerebellar cortex because, as stated before, high frequency bursts are a common feature.

A second aspect of analog-digital signalling considers the membrane potential when the action potential is emitted, which can be modified by subthreshold synaptic activity. It was suggested that these subthreshold depolarisations could be passively propagated along the axon. Depending on the

axonal space constant, this depolarisation can reach the most proximal synapses (which are very close to the soma in the granule cell ascending axon) and increase Ca^{2+} influx, hence increasing the release of neurotransmitter. The depolarisation preceding the spike can modify the width of the action potential by inactivating specific K^{+} conductances, increasing consequently Ca^{2+} influx. These mechanisms were not demonstrated in the mossy fibre-granule cell-Purkinje cell pathway, but an increased GABA release following a depolarising pre-pulse at the molecular layer interneurons to Purkinje cells synapse can occur (Bouhours et al., 2011).

3.2 MODULATION OF PURKINJE CELL DISCHARGE

The Purkinje cell is the sole output of the cerebellar cortex, converging towards cerebellar nuclei neurons. Modification of Purkinje cell spiking regularity induces ataxia (Walter et al., 2006; De Zeeuw et al., 2011). Unravelling Purkinje cells firing control is a keystone in the understanding of cerebellar physiology. To understand how information is processed, we need to integrate both the effects of excitatory and inhibitory inputs on Purkinje cell firing, and how neighbouring Purkinje cells are correlated.

Although my project does not directly address the Purkinje cell discharge regulation, any changes in the synaptic integration at the parallel fibre to Purkinje cell synapse will ultimately modulate the Purkinje cell firing, and consequently, the cerebellar output. These modulations will be briefly presented in this section.

Figure 22 : Simple spikes and complex spikes in Purkinje cells.
A_1 : Extracellular recording of Purkinje cell spontanous firing in mouse under urethane anaesthesia. Black trace indicates simple spikes, red indicates a complex spike. **A_2** : Magnification of trace in A_1. Same legend as A_1. Traces from Joseph Chaumont.

3.2.1 DISCHARGE PATTERNS

Purkinje cells have complex electrophysiological properties (De Zeeuw et al., 2011). They elicit two types of action potential: the complex spike, associated with the climbing fibre input, and the simple spike (Figure 22A). Purkinje cells can also display several types of firing patterns, and it is thus important to present these different profiles before developing the effect of the parallel fibre to Purkinje cell neurotransmission on Purkinje cell discharge.

3.2.1.1 SIMPLE SPIKES AND PACEMAKER ACTIVITY

Simple spikes are classical Na^+ spikes generated at the level of the axonal initial segment (Figure 22A). Since dendrites Na^+ channels are poorly expressed in dendrites, the electrotonic depolarisation is transmitted in the dendrites through passive conductances and does not reach the dendritic spines. Purkinje cells have a pacemaker activity (Figure $22A_1$). Simple spikes are evoked spontaneously at a frequency of 20 to 60 Hz, but can reach a maximal firing frequency around 250 Hz in the case of strong depolarisations by climbing fibres or parallel fibres (Shin et al., 2007; De Zeeuw et al., 2011; Chaumont et al., 2013). The cell is autorythmic even in the absence of any presynaptic inputs (Häusser and Clark, 1997), although the regularity of the pattern is modulated by excitatory and inhibitory inputs (Llinás and Sugimori, 1980; Raman and Bean, 1999). In the rat, mean firing rate is similar (45.5 Hz). *In vitro* experiments show comparable firing frequencies, but the much lower level of activity in the network tends to increase the regularity of the discharge. The cell has a pacemaker activity.

3.2.1.2 COMPLEX SPIKES AND CA^{2+} INFLUX

Complex spikes are evoked after the massive depolarisation induced by a climbing fibre input. This type of action potential is unique in the central nervous system. The Ca^{2+} dendritic spikes might activate Ca^{2+}-dependent K^+ conductances present in the Purkinje cell dendrites, such as BK and SK channels, which can modulate the simple spike activity. This massive Ca^{2+} input is also involved in plasticity mechanisms.

In vivo recordings performed as early as 1956 (Granit and Phillips, 1956) showed that the Purkinje cell can be silent. Purkinje cells have two stable states. The upstate is characterised by the autorythmic activity of the Purkinje cell, while the downstate is a depolarised state in which the Purkinje cell autorythmic activity is interrupted due to inactivation of voltage dependent Na^+ channels (Loewenstein et al., 2005). The climbing fibre was proposed as a toggle switch, controlling Purkinje cell transitions between the up- and the downstate, but the physiological relevance of the downstate remains in question, as it is more often observed *in vitro*, in anaesthetised or decerebrated animals (Schonewille et al., 2006).

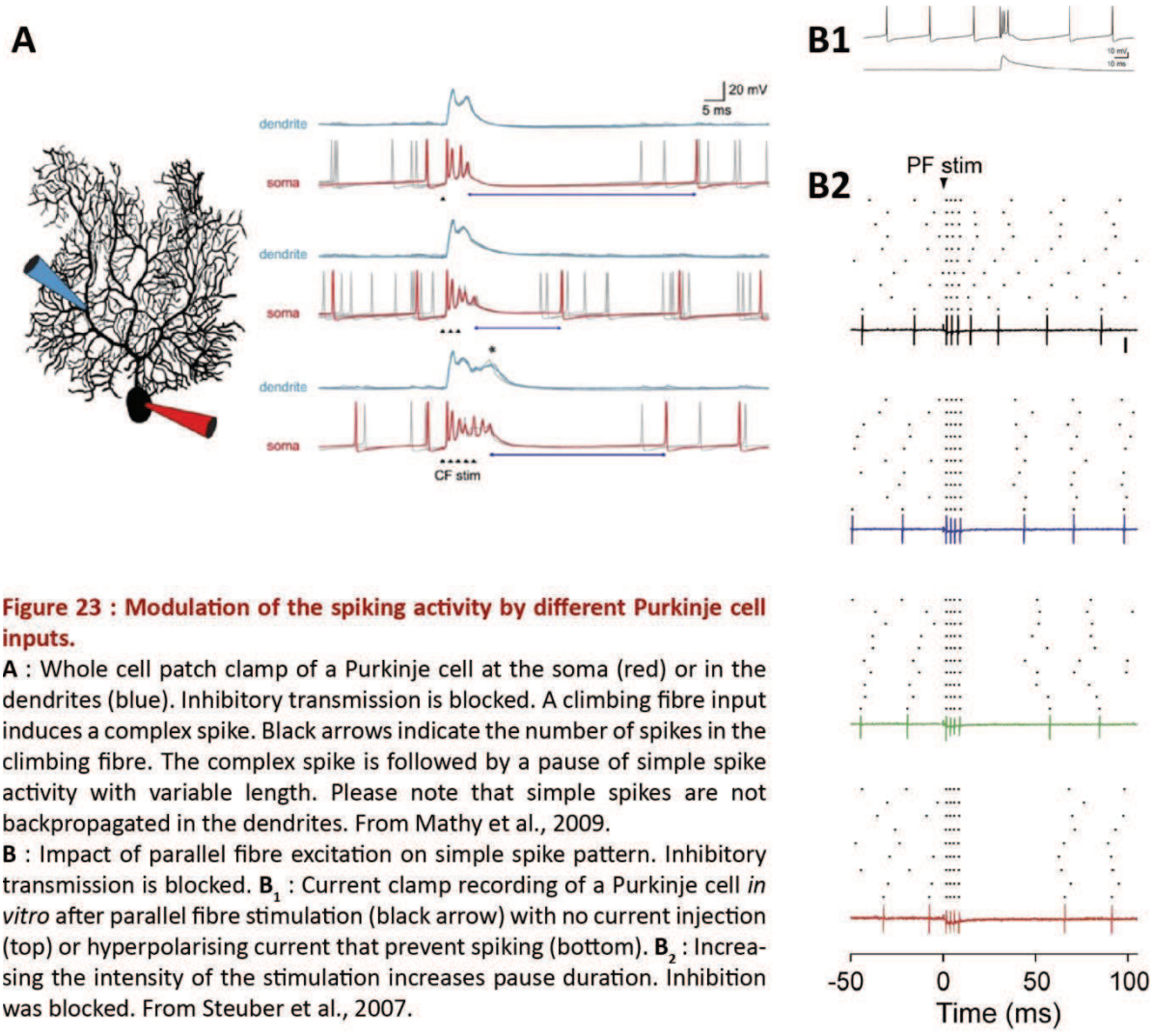

Figure 23 : Modulation of the spiking activity by different Purkinje cell inputs.

A : Whole cell patch clamp of a Purkinje cell at the soma (red) or in the dendrites (blue). Inhibitory transmission is blocked. A climbing fibre input induces a complex spike. Black arrows indicate the number of spikes in the climbing fibre. The complex spike is followed by a pause of simple spike activity with variable length. Please note that simple spikes are not backpropagated in the dendrites. From Mathy et al., 2009.

B : Impact of parallel fibre excitation on simple spike pattern. Inhibitory transmission is blocked. $\mathbf{B_1}$: Current clamp recording of a Purkinje cell *in vitro* after parallel fibre stimulation (black arrow) with no current injection (top) or hyperpolarising current that prevent spiking (bottom). $\mathbf{B_2}$: Increasing the intensity of the stimulation increases pause duration. Inhibition was blocked. From Steuber et al., 2007.

3.2.1.3 MODULATION OF PURKINJE CELL FIRING BY SYNAPTIC INPUTS

In vivo, in both anaesthetised and awake animals, Purkinje cell firing is modulated by excitatory and inhibitory inputs. Short pauses in Purkinje cell firing (a few tens to a few hundreds of milliseconds) can also occur during the upstate of Purkinje cells (Figure 23A, $23B_1$, $23B_2$).

Molecular layer interneurons and parallel fibres either subtly modulate the Purkinje cell firing or induce pauses. Hyperpolarisation induced by GABA release from the molecular layer interneurons can directly delay the next action potential initiation, or induce a short pause (Häusser and Clark, 1997; Mittmann and Häusser, 2007; Steuber et al., 2007). The limit between a delayed action potential and a pause is not clear, and might be simply due to the input strength. An excitatory burst from the parallel fibres depolarises the cell in a first time, which increases Purkinje cell firing frequency (if the effect is not counteract by feedforward inhibition). Excitatory inputs can be followed by a pause (Walter and Khodakhah, 2006; Mittmann and Häusser, 2007) (Figure $23B_1$, $23B_2$), likely to be driven by SK and BK conductances (McKay et al., 2007).

Pauses are often evoked by the massive depolarisation by the climbing fibre, which activates Ca^{2+}-activated K^+ channels such as SK, BK and IKCa channels. The after-hyperpolarisation induced by these channels can switch the cell between upstate and downstate but in most cases it induces short pauses in Purkinje cell discharge (Llinás and Sugimori, 1980; Stuart and Häusser, 1994; Mittmann and Häusser, 2007; Mathy et al., 2009; Engbers et al., 2012).

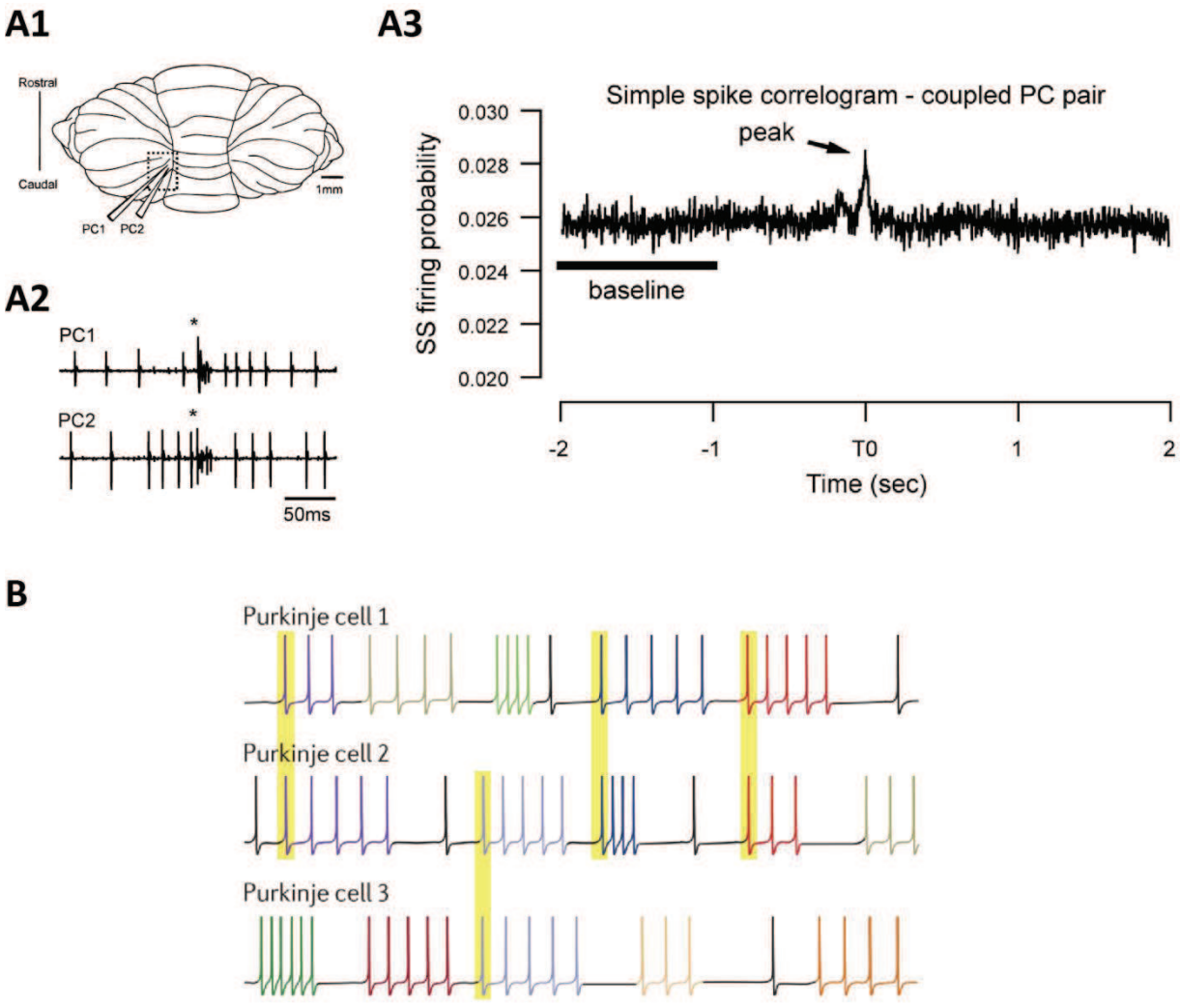

Figure 24 : Spiking activity in Purkinje cell and bistability.
A : Simple spike synchrony *in vivo* between pairs of Purkinje cells. $\mathbf{A_1}$: location of the recordings in medial Crus II, paramedian lobule and the copular pyramidis. $\mathbf{A_2}$: Example of traces with both simple spikes and complex spikes (asterisk).
$\mathbf{A_3}$: cross-correlogram of spontaneous simple spike activity from the same purkinje cell pair. Correlation was weak, but significantly higher than in distal pairs. From Wise et al., 2010.
B : Purkinje cells display motif of firing. In average, Purkinje cells firing is poorly correlated between cells, but patterns onset is strongly correlated between neighbouring cells. From de Zeeuw et al., 2011.

3.2.2 PURKINJE CELLS SYNCHRONY

Since Purkinje cell within a microzone send highly converging projections onto cerebellar nuclei, it is important to take into account the synchrony between neighbouring cells to understand cerebellar output. In this part, I will briefly address the question of the synchrony between neighbouring Purkinje cells, with particular interest in differences between *on beam* synchrony and *off beam* synchrony. Indeed, *on beam* Purkinje cells might be modulated by similar parallel fibre inputs, whereas *off beam* Purkinje cells cannot.

3.2.2.1 SIMPLE SPIKES SYNCHRONY DURING A BEHAVIOURAL TASK

Simple spikes represent more than 90% of the spiking activity, and thus of the inhibition performed on cerebellar nuclei neurons. Determining the mechanisms controlling synchrony between different Purkinje cells is a major issue to understand cerebellar output. As both pauses and regular spiking are modulated by the mossy fibre-parallel fibre input, and since Purkinje cells along a beam can receive similar inputs, it is important to know if *on beam* Purkinje cells are more correlated to each other than *off beam* Purkinje cells.

When recording simple spike activity in pairs of neurons *in vivo* (Figure 24A_1, 24A_2), short period of synchrony of one or two spikes can occur (Heck et al., 2007; Wise et al., 2010) (Figure 24A_3). This synchrony is not mediated by complex spikes since synchrony occurs in the absence of complex spikes in 75% of the cases. Consequently, the synchrony can either remains *on beam* as suggested by Heck (Heck et al., 2007), or occurs in different beams and microzones, *off beam*, as proposed by Wise (Wise et al., 2010) (Figure 22A).

In Detlef Heck experiments, extracellular recordings of Purkinje cells on awake animals showed that Purkinje cells were mostly desynchronised. However, during reaching tasks, Purkinje cells located *on beam* show slight synchrony during a short period (one or two action potentials) while *off beam* Purkinje cells showed no synchrony at all. The authors suggest that the high initial synchrony between cells reflects the fact that those cells were involved in the same multi-joint/multi-muscle task, whatever the microzone they belong to. In this interpretation, the synchrony essentially points out the coordination of Purkinje cell subsets. As no more synchrony occurs after the first spike, the authors suggested that the following discharge might code other parameters such as muscle tension. Nevertheless, these experiments demonstrated that Purkinje cells is synchrony is under the control of mossy fibre inputs, a role previously attributed to complex spike activity.

3.2.2.2 SYNCHRONY OF THE SIMPLE SPIKE PATTERNS

The identification of regular patterns between Purkinje cells is a quite complicated point, because no major and obvious synchrony is visible at first sight. Do Purkinje cell populations only encode the onset of sensory event as suggested by the low simple spike synchrony?

Tactile stimulation of receptive fields induces short bursts in granule cells tightly time-locked with the stimulus onset. However joint ankle manipulation can evoke more sustained synaptic activity (Jörntell and Ekerot, 2006). Similarly, experiments performed in the vestibulocerebellum showed that EPSCs frequency in Purkinje cells correlates with the animal's direction and velocity during vestibular stimulation using body rotation (Arenz et al., 2008). In these long-lasting stimuli, it is likely that the firing pattern of Purkinje cell also contains information after the onset.

Shin et al. used the coefficient of variation of the interspike interval between three adjacent spikes (CV_2), as a marker of pattern regularity (Shin et al., 2007). During simple spike firing, Purkinje cell present periods of higher regularity, termed regular spiking patterns. These simple spike patterns last up to hundreds of milliseconds (Figure 24B). They also observed that neighbouring Purkinje cells, although not synchronous, can display synchronous occurrence of the regular spiking patterns (i.e., the patterns in two cells start simultaneously, but then have different firing frequencies). Complex spike occurrences had little effect on simple spikes patterns and the authors made the hypothesis that patterns are likely to be under the control of parallel fibres excitatory inputs and molecular layer interneurons inhibition. Moreover, synchrony between patterns of neighbouring cells was increased during tactile stimulation, which is carried by the mossy fibres - granule cells - Purkinje cells pathway.

3.3 SHORT TERM PLASTICITIES AT THE GRANULE CELLS TO PURKINJE CELLS SYNAPSE DURING HIGH FREQUENCY BURSTS

As we saw in the previous section, pauses, synchrony and firing patterns in Purkinje cells are often correlated with the mossy fibre input, which can be mediated by both the ascending axon of granule cells and the parallel fibres. Inputs patterns on Purkinje cell modulate the cerebellar output, particularly in the case of bursts and trains, in which EPSCs are potentiated by short term plasticities. In my first article, I studied short term plasticities at the parallel fibre to Purkinje cell synapse in order to describe synaptic integration during high frequency bursts. The presynaptic function of Ca^{2+} in vesicular release, short term facilitation and refilling is described in this section.

3.3.1 PRESYNAPTIC CA^{2+} AND VESICULAR RELEASE

3.3.1.1 CA^{2+} CHANNELS SUBTYPES

When an action potential enters a synaptic terminal (or, in the case of the parallel fibres, passes through an *en passant* synapse), the membrane depolarisation activates voltage gated Ca^{2+} channels (Figure $25A_1$). In the parallel fibre to Purkinje cell presynaptic element, the Ca^{2+} channels involved in vesicular release are the N-type ($Ca_v2.2$), P/Q-type ($Ca_v2.1$). L- and T-type channels are not present in the presynaptic button (Figure 25B). Blocking P/Q-type channels with ω-agatoxin-IVA prevents 50% of the Ca^{2+} influx, and 90% of the vesicular release (Figure $25B_1$), whereas blocking N-type with ω-conotoxin-GVIA prevents only 30% of the Ca^{2+} influx and 50% of the vesicular release (Figure $25B_2$) (Hillyard et al., 1992; Mintz et al., 1995). This result indicates first a synergic action of both channel types in neurotransmitter release, but also that P/Q-type Ca^{2+} channels are more effective at

triggering release. R-type ($Ca_v2.3$) channels are also present at the synapse and mostly involved in presynaptic long term potentiation (Myoga and Regehr, 2011).

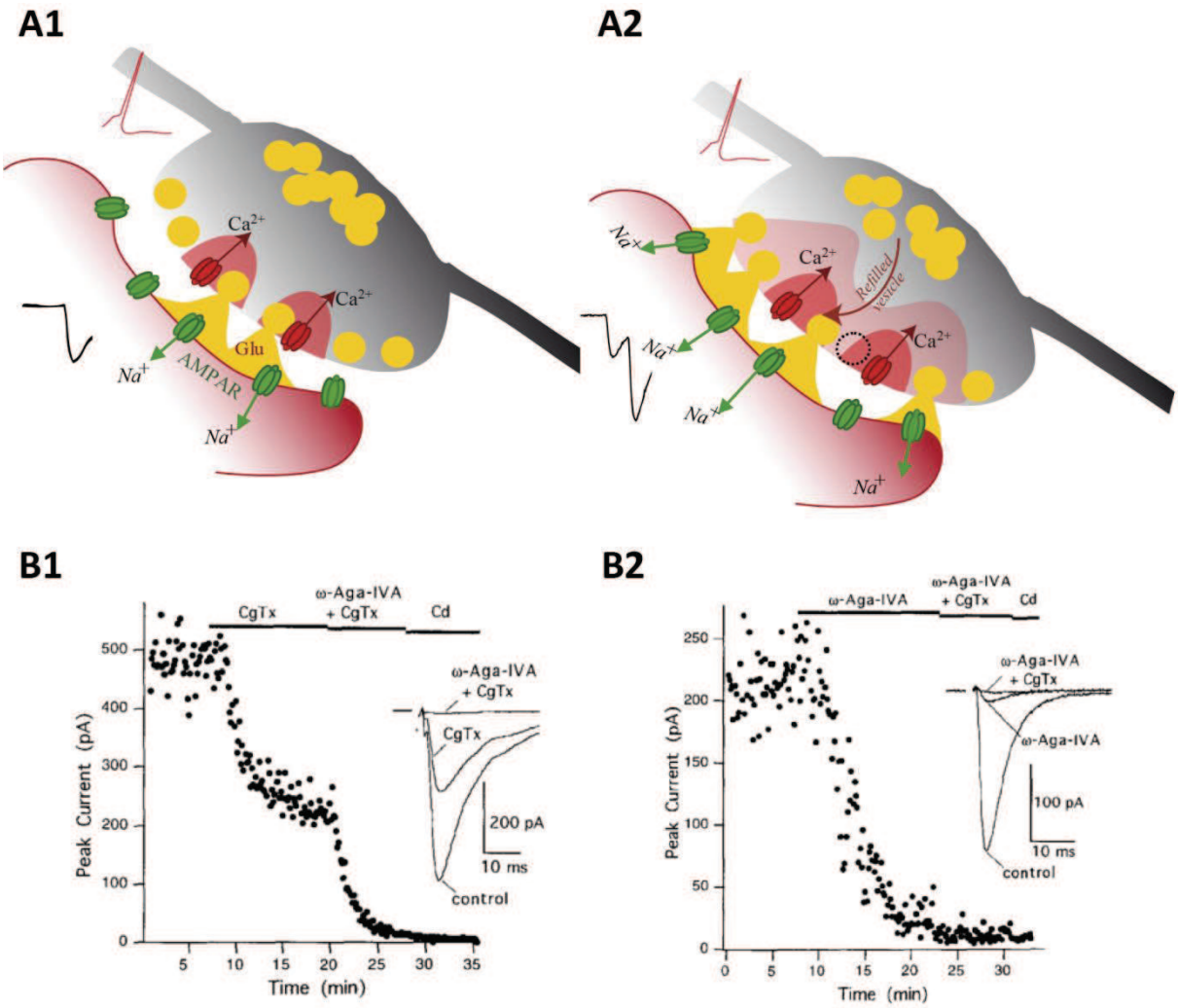

Figure 25 : Presynaptic Ca^{2+} controls neurotransmitter release.

A : Classical model of presynaptic short term facilitation. $\mathbf{A_1}$: An action potential (red trace, upper left) depolarises the presynaptic button, which opens voltage-gated Ca^{2+} channels (red barrels). Ca^{2+} influx forms a nanodomain in which high Ca^{2+} concentration triggers vesicle (yellow circles) fusion with the plasma membrane, and neurotransmitter release in the synaptic cleft. Released glutamate induces AMPAR activation and Na^+ influx, which can be detected as an EPSC. $\mathbf{A_2}$: In the classical view, the initial Ca^{2+} domain extends progressively. On the other hand Ca^{2+} uptake and Ca^{2+} buffers limit Ca^{2+} diffusion. If a second action potential depolarises the presynaptic button shortly after, a second Ca^{2+} influx sums with the previous triggering more vesicular release, resulting in an increased EPSC. Sites where a vesicle was previously released (dotted circle) can be reloaded with new vesicles.
B : Amplitude of evoked EPSCs during bath application of ω-conotoxin-GVIA (N-type Ca^{2+} channels blocker), ω-agatoxin-IVA (P/Q-type Ca^{2+} channels blocker) or Cd^{2+} (blocks all voltage gated calcium channels). From Mintz et al., 1995. $\mathbf{B_1}$: ω-conotoxin-GVIA prevents 50% of neurotransmitter release. Supplementary ω-agatoxin-IVA application blocks 95% of EPSCs, and transmission is completely prevented by Cd^{2+}. $\mathbf{B_2}$: ω-agatoxin-IVA prevents 90% of neurotransmitter release, and ω-conotoxin-GVIA does not block further transmitter release.

3.3.1.2 CA^{2+} MICRO- AND NANO-DOMAIN

Ca^{2+} channels positioned within the active zone are more or less tightly coupled with the vesicles docked at the plasma membrane. The number of channels per vesicle and their proximity can vary between synapses, regulating the amplitude and the extent of the Ca^{2+} influx (Bucurenciu et al., 2008; Eggermann et al., 2012). After Ca^{2+} channel opening, Ca^{2+} enters the presynaptic terminal and activates several sensors before being captured by the endogenous buffers (Figure25A_1). In the parallel fibre button, common buffers such as calbindin are not present. It is likely that the buffering capacities are mediated essentially by the calretinin (Bastianelli, 2003; Gall et al., 2005b; Schmidt et al., 2013). The high Ca^{2+} concentration around the Ca^{2+} channels is called micro- or nano-domain, depending on its extent (more than 100 nm against less than 100nm respectively). In the parallel fibre button P/Q Ca^{2+} channels were estimated to be located between 20 and 30 nm from the fusion site, identifying nanodomain coupling (Schmidt et al., 2013).

If 1: the vesicle in proximity of a Ca^{2+} channels is ready to be released i.e. the proteins necessary for the membrane fusion are available, 2: the vesicle is close enough to the membrane, 3: if the Ca^{2+} transient activates Ca^{2+} sensors, then the vesicle membrane fuses with the plasma membrane through an active process, and release its content of neurotransmitter. The Ca^{2+} is then buffered and progressively extruded by the Ca^{2+} pump (Regehr, 1997), until the free Ca^{2+} concentration reach its initial value. This step can take tens of milliseconds. In a single presynaptic button at the parallel fibre to Purkinje cell, the Ca^{2+} dye signal decay was estimated between 25 to 55 ms (Brenowitz and Regehr, 2007) but the real decay of free Ca^{2+} is probably much faster (Bornschein et al., 2013).

3.3.2 SHORT TERM FACILITATION AND SHORT TERM DEPRESSION

During repetitive firing, a repeated Ca^{2+} influx enters the presynaptic button (Figure 25A_2, 26A_1, 26A_2). If the residual Ca^{2+} due to the previous Ca^{2+} influx persists in the presynaptic button, the new input of Ca^{2+} adds up to the residual Ca^{2+}. The direct consequence is a higher Ca^{2+} concentration than with a single action potential (Figure25A_2, 26A). At the parallel fibre to Purkinje cell synapse, Ca^{2+} was shown to sum linearly, even at high frequency (more than 300 Hz) and for long trains (more than 12 times), in a single button (Mintz et al., 1995; Brenowitz and Regehr, 2007) (Figure 26A_2, 26A_3, 26A_4), which induces an increase of the amplitude of the second EPSC (*paired-pulse facilitation*). This effect is robust between synapses, although there can be individual variations (Atluri and Regehr, 1996; Isope and Barbour, 2002; Sims and Hartell, 2005), see first article.

Release probability is proportional to the Ca^{2+} concentration (Katz and Miledi, 1968) and it is usually thought that facilitation is linked to low initial release probability. If the release probability is low, only a very small fraction of the readily releasable pool (RRP) is released at the first action potential. Release probability increases as the intracellular Ca^{2+} increases, inducing a larger release at the second action potential (Figure 25A, and see first article).

Conversely, if the initial release probability is high, most of the release-ready vesicles can be released at the first action potential and when the second action potential occurs, only a few remaining vesicles are available. Hence, the second EPSC has smaller amplitude (paired-pulse depression).

Finally, vesicles do not have exactly the same proteic equipment. The exact number of regulatory proteins can vary (Ting et al., 2007), and their activity can be regulated, for instance by phosphatases and kinases (Lonart et al., 2003; Simsek-Duran et al., 2004). Besides the proteins that are necessary for vesicle fusion, Ca^{2+} Channels can be regulated too (Brown et al., 2004), which might ultimately affect the final Ca^{2+} concentration in the nanodomain. Thus, the probability of release of a given vesicle, which is ultimately a measure of the efficiency of the vesicular fusion, can fluctuate. Several of the proteins involved in vesicular release are Ca^{2+} dependent (Burgoyne, 2007; Eggermann et al., 2012). It is possible that the initial Ca^{2+} transient acts as a toggle button for some more reluctant sites, that could be recruited, during a train for instance (Doussau et al., 2010).

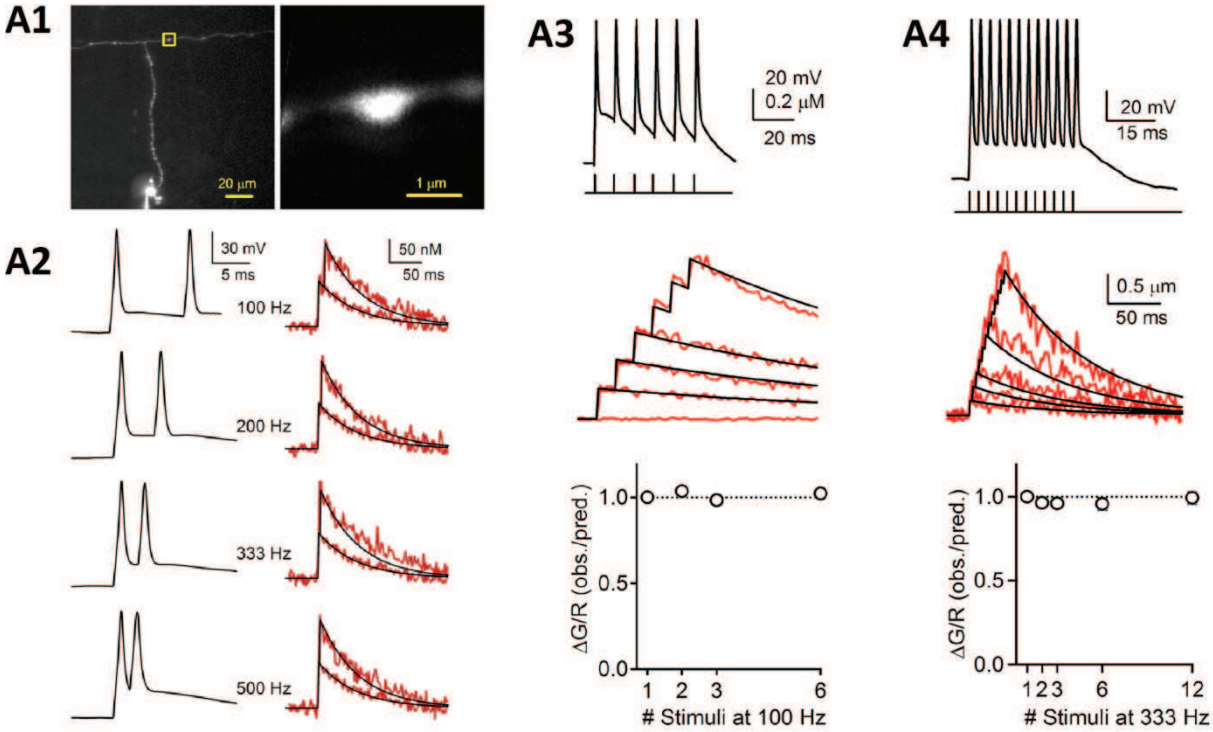

Figure 26 : Calcium transients during high frequency bursts.
A : Ca^{2+} imaging in a single presynaptic parallel fibre button. $\mathbf{A_1}$: single granule cell filled with Alexa 594 fluorescent dye (left panel). Higher magnification of a presynaptic button (right panel). $\mathbf{A_2}$: Pairs of action potentials are evoked in granule cell at 4 different frequencies (left panel. From top to bottom: 100Hz, 200Hz, 333Hz and 500Hz), while Fluo-5F Ca^{2+} dye imaging is performed in a single presynaptic button (right panel). Individual Ca^{2+} transients can be isolated and summed linearly at all frequencies. $\mathbf{A_3}$: 100Hz train of 6 pulses (top) showed that all Ca^{2+} transients sum linearly (middle), without saturation of Ca^{2+} buffers. Bottom panel indicates the ratio between the recorded response and theoretical linear sum of the Ca^{2+} transients. $\mathbf{A_4}$: same as A_3, but at 333Hz. From Brenowitz and Regehr, 2007.

3.3.3 VESICLE REFILLING

During the two action potentials, sites that previously released a vesicle can be refilled. The nomenclature in the literature can be confusing, as this process is alternatively termed *site reloading*, *site refilling* or *site replenishment*. This must not be mixed up with the process in which vesicles are refilled/reloaded/replenished with neurotransmitters. If the site refilling is extremely fast, then even a synapse with moderate or high release probability can facilitate. A very fast site refilling was demonstrated at the mossy fibre to granule cell synapse, using specific proteic equipment such as bassoon (Hallermann et al., 2010; Hallermann and Silver, 2013).

At the parallel fibre to Purkinje cell synapse, the initial release probability was first estimated at 5% (Dittman et al., 2000; Foster et al., 2005), although higher values were then proposed (Isope and Barbour, 2002; Sims and Hartell, 2005). The refilling kinetics on the other hand were never quantified, even if a recent estimate at the parallel fibre to stellate cell synapse suggested a very fast replenishment of the sites (15 ms to 20 ms) (Crowley et al., 2007).

Release probability, number of release sites and site refilling rate are estimated in the first paper of this manuscript (Valera et al., 2012), and a mechanistic hypothesis of neurotransmitter release at this synapse is proposed. In order to finely describe the parameters of the vesicular release at the parallel fibre to Purkinje cell synapse, we used the variance-mean analysis. The conditions of use, and the nomenclature related to this technique will be briefly introduced in a supplementary introduction before the first article of this manuscript.

3.4 A FEW PRECISONS ON THE ACUTE SLICE MODEL

For practical reasons, most *in vitro* studies - including mine - usually focus either on the input-output function of the cerebellar cortex, or on the input-output function of the cerebellar nuclei. The use of these “isolated” models is very convenient because it allows an easier and finer study of the different cell types. *In vitro* studies take advantage of a better control of drugs application, patch clamp recordings, Ca^{2+} imaging etc.... All those precious tools allow us to progressively unravel the fine communication mechanisms between the cells. However, extrapolation of the results to *in vivo* model requires to perform *in vitro* experiment as physiological as possible, otherwise, failing that, we should be careful with conclusions. In slices, the natural inputs as well as some cellular processes are cut, the neuromodulators are partially washed, and the network activity is deeply affected. Nevertheless, it is possible to take advantage of some of these effects, for example to study synaptic transmission at individual synapses, or to map the network as we did. *In vitro* studies benefit in these two cases of a lower background activity, allowing a more precise characterisation of the considered parameters.

4 ARTICLE I

4.1 SUPPLEMENTARY INTRODUCTION TO VARIANCE-MEAN ANALYSIS

When a postsynaptic current is recorded experimentally, the current size is defined by the number of activated postsynaptic receptors, which also depends on the quantity of presynaptically released neurotransmitter. In the example below, we will consider an excitatory synapse in which transmission is only controlled by the effect of glutamate on postsynaptic AMPA receptors. This situation, which is a simplification of the *in vivo* processes, however represents the major part of the neurotransmission at most excitatory synapses. Understanding the main parameters describing excitatory transmission can be performed using the *variance-mean-analysis* or its more complex, but more realistic version, the *multiple-probability fluctuation analysis* (MPFA).

Variance mean analysis was first introduced by Katz and Miledi (Katz and Miledi, 1972). In the 70's the vesicular release was thought to result from statistical collisional events between neurotransmitter vesicles and plasma membrane, in the presynaptic terminal. The authors tried to use small "noise" fluctuations in the postsynaptic evoked currents to unravel mechanisms underlying neurotransmitter release.

Variance mean analysis methods were further developed to allow graphical determination of the statistical parameters describing ionotropic channels opening (Sigworth, 1980) or quantum size of evoked EPSCs (Simonneau et al., 1980). It was only in late 90's that precise graphical description of the relationship between variance and recorded current has been used (Traynelis et al., 1993; Silver et al., 1996; Humeau et al., 2001a, 2001b, 2002). Since then, it was used in many structures of the central nervous system (Branco and Staras, 2009), and progressively refined, like the recent development of MPFA (Silver et al., 1998; Reid and Clements, 1999; Clements and Silver, 2000; Silver, 2003).

4.1.1 THE QUANTAL PARAMETERS N, P AND Q

Many parameters explain and modulate the size of the postsynaptic current. Two molecules of glutamate are necessary to activate a postsynaptic AMPAR. So the size of the current is defined by:

1. The glutamate content of each vesicle
2. The number of postsynaptic receptors
3. The time during which the glutamate is active in the synaptic cleft, which takes into account release duration, uptake efficiency and a few other modulating parameters.

An initial approximation is to assume that postsynaptic receptors density facing the release sites is homogeneous, and that glutamate binding duration is also homogeneous. We can temporary postulate that each time a vesicle of glutamate is released, wherever it is released, it induces the same postsynaptic current. The postsynaptic current evoked by the release of single vesicle content at a single synapse is the *quantum*, named $\boldsymbol{Q}$ (Figure 27A$_2$).

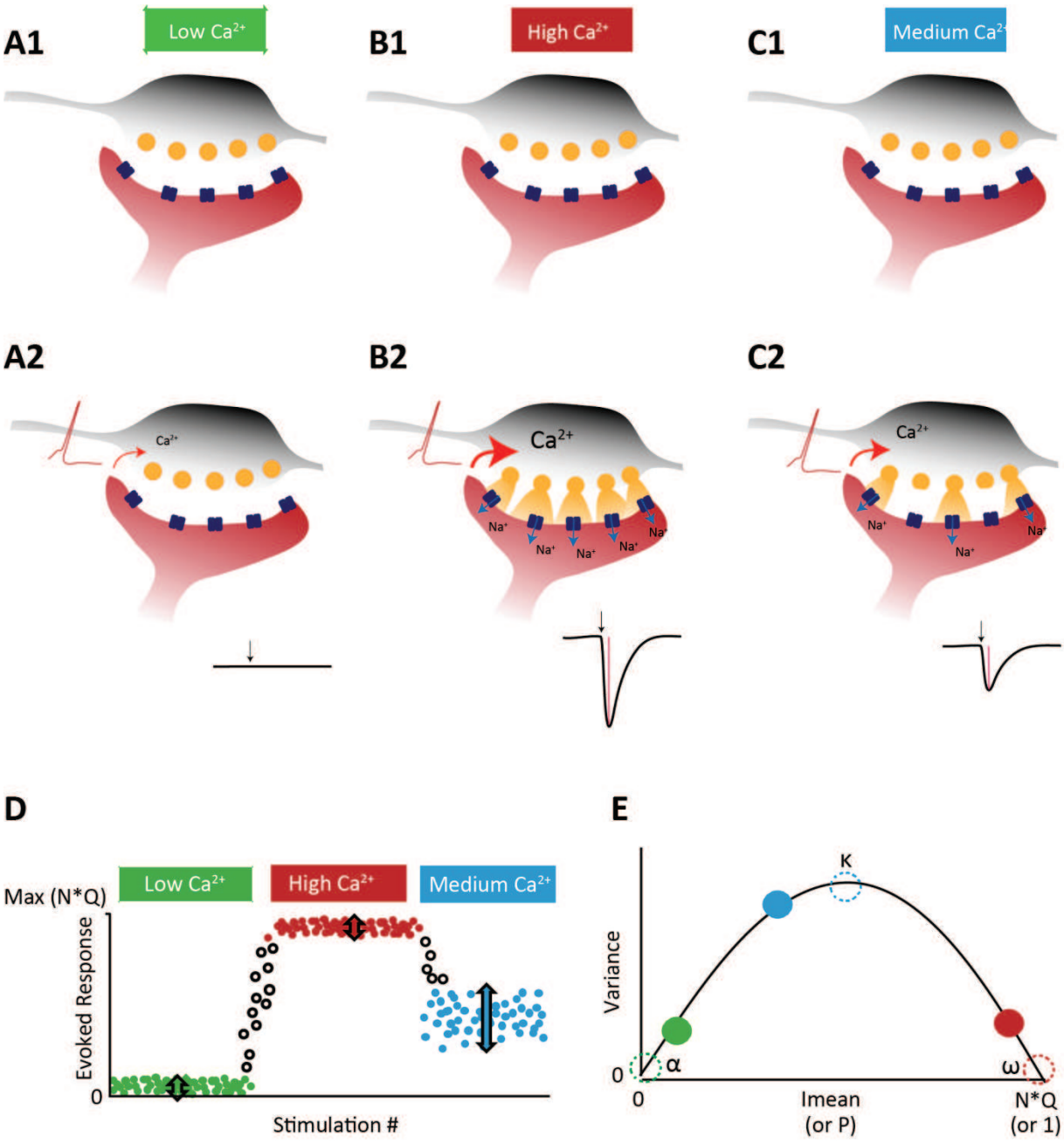

Figure 27 : Release is dependent on extracellular Ca^{2+} concentration.

A to C : **1** : Initial condition; **2** : First action potential (red) evokes the opening of Ca^{2+} channels, Ca^{2+} influx (red arrow). Ca^{2+} induces vesicular fusion and glutamate release (yellow). Each released vesicle activates the facing AMPA receptors (dark blue), evoking a postsynaptic Na^{+} (blue arrow) influx which can be recorded as an excitatory postsynaptic current (EPSC, inset, black arrow indicates action potential arrival).

A : Low Ca^{2+} (near 0 mM).

B : High Ca^{2+} (for instance 6 mM)

C : Medium Ca^{2+} (for instance 2.5 mM).

D : EPSCs amplitude plot in the three different Ca^{2+} conditions represented in A, B and C. EPSC amplitude is comprised between 0 and N*Q. Thick arrows indicate the variance for each condition.

E : Mean Variance versus Mean amplitude plot in the three Ca^{2+} conditions presented in D. X-axis can be expressed in release probability (P). Theoretical values : at 0 Ca^{2+}, Imean = 0 pA and release probability = 0 (point α; green dotted circle). At high Ca^{2+}, Imean = N*Q, and release probability = 1 (point ω; red dotted circle). Maximal variance is reached for P=0.5 (point κ; blue dotted circle). Greek letters are used in text.

The number of vesicles that could theoretically be released at one given time has an upper limit corresponding to the total number of docked and release-ready vesicles. The total amount of release-ready vesicles forms the RRP. A site which is considered as release-ready has all the proteic equipment necessary to perform vesicle fusion, and is named *release site*. To induce detectable postsynaptic current, postsynaptic receptors must face the release site, otherwise the site is silent.

In our nomenclature, the parameter $\boldsymbol{N}$ takes into account the total number of docked and release-ready vesicles with postsynaptic AMPAR. It can be noted that in the literature, the term N often refers to the number of morphologically docked vesicle, whereas our definition describes functionally competent vesicles. Thus, if we release all the release-ready vesicles at once, at all the sites, the maximal recorded postsynaptic current is $\boldsymbol{A_{max} = N \cdot Q}$ (Figure 27B$_2$)

However, all the readily releasable vesicles are not necessary released, and usually, only a fraction of them fuses with the membrane. This observation, performed at the population level is actually the result of a probabilistic event occurring at each individual site. At each release site, a vesicle has a given probability to release glutamate termed Pr_{site} (Figure 27E). The average Pr_{site} of all the release sites is therefore termed $\boldsymbol{P}$.

The probabilistic aspect of vesicular release was introduced in the early 50's (Fatt and Katz, 1952; Del Castillo and Katz, 1954; Boyd and Martin, 1956a, 1956b). Poisson distribution of the miniature events suggested that neurotransmitter release was described by binomial statistics. Assuming that each vesicular release is independent, the average current $\boldsymbol{\bar{A}}$ is:

$$\boldsymbol{\bar{A} = N \cdot P \cdot Q}$$

As the release is a stochastic mechanism, the exact number of released quanta can vary around that mean value, which can be quantified using the variance *Var*. In binomial statistics:

$$Var = N \cdot P \cdot (1 - P)$$

Experimentally, as the measured current is always scaled by the size of the quantum Q, we measure:

$$\boldsymbol{Var = N \cdot P \cdot (1 - P) \cdot Q^2}$$

On average, in one given experimental condition and for one population of neurons, there should be one average value of the variance, described by a function $Var = f(A)$.

The release probability was shown to vary with extracellular Ca^{2+} concentration (Katz and Miledi, 1968). 0 mM of extracellular Ca^{2+} should prevent the vesicular fusion ($P = 0$), and a few mM of Ca^{2+} should rise at maximum the release probability to a ceiling value of $P = 1$.

In the Figure 27A, 27B and 27C, three examples are represented. In the first case (Figure 27A); the extracellular Ca^{2+} concentration is low. The vesicular release is Ca^{2+} dependent, and thus, at 0 mM of extracellular Ca^{2+} each trial results in no release: $\bar{A} = N \cdot 0 \cdot Q$. Consequently, the variance is 0. This is the point *α* (Figure 27 E).

In a second step (Figure 27B), we applied a very high extracellular Ca^{2+} concentration. At maximal Ca^{2+}, P = 1 and release-ready vesicles fuse. The measured current is maximal and $\bar{A} = N \cdot 1 \cdot Q$. If the experimenter wait long enough, that is the time necessary for all previously released vesicles to

be replaced by a new release-ready vesicle, another stimulation will result again in a complete release. Consequently, this point has a null variance too, but a maximal $\bar{A}$ value (see point *ω*).

All the intermediate extracellular Ca^{2+} concentration result in a number of released quanta that is between 0 and N (Figure 27C), with a mean value proportional to the Ca^{2+} influx. At each trial, the recorded current fluctuates around $\bar{A}$ (Figure 27D). The higher variance is reached for $P = 0.5$; see point κ (Figure 27E).

4.1.2 ANALYTIC METHOD

The advantage of the Variance mean analysis is to allow simple repetitive measurements of an average response to give information about single release sites parameters.

However, in order to discriminate N, P and Q, it is necessary to vary one of these parameters, while the others remain fixed. The most convenient tool to play with is the extracellular Ca^{2+} concentration, because this will lead to changes in Ca^{2+} influx, and thus in the release probability at each site (P_{site}) (Katz and Miledi, 1968).

$$Var = N \cdot P\,(1 - P) \cdot Q^2$$

$$Var = Q^2 \cdot N \cdot P - Q^2 \cdot N \cdot P^2$$

$$Var = Q^2 \cdot N \cdot\ P - \frac{Q^2 \cdot N^2 \cdot P^2}{N}$$

$$\boldsymbol{Var = 0 + Q \cdot \bar{A} - \frac{\bar{A}^2}{N}}$$

Var = 0+Q·$\bar{A}$-$\frac{\bar{A}^2}{N}$ is of the form: $f(x) = a + bx + c^2$, which describes a parabola in which

$a = 0$ 0 is theoretical (any systematic bias in measurement, like signal noise, can be detected here as a constant offset that can be subtracted)

$b = Q$ The initial slope gives Q, the value of the quantum

$c = -\frac{1}{N}$ Thus $1/c$ gives N the total number of sites

Any variation of the other quantal parameters has a specific mathematical and therefore graphical signature (Figure 27E, 28A). Changes in N, Q and P affect parabola shape, as illustrated in Figure 28B.

4.1.3 MULTPLE PROBABILITY FLUCTUATION ANALYSIS

Simple binomial statistics oversimplify vesicular release mechanisms. Indeed, as stated before, it is highly unlikely that released vesicle content induces the exact same postsynaptic current each time. The release probability can vary at one given site between trials, or between release sites in a single synapse or, in the case of composed EPSCs, between sites in different synapses.

These variation can be taken into account as a coefficient of variation of the quantum (CV_Q) (Silver et al., 1998; Reid and Clements, 1999; Silver, 2003). This total variability can be further split into intrasite variability CV_{QI} (the quantum changes between trials at a given site) and intersite variability CV_{QII} (the quantum varies across sites). Moreover, the release probability between sites can vary, as it was shown for instance at the climbing fibre to Purkinje cell synapse (Foster et al., 2005). Variation in release probability is taken into account with a parameter termed CV_P.

4.1.3.1 INTRASITE VARIABILITY (CV_{QI})

There are multiple factors leading to change in the quantum size between trials:

- asynchronous transmitter release
- receptor activation fluctuation due to variation in the amount of released transmitter
- stochastic gating of channels

When several vesicles are released, the variance of each sites sums linearly. Thus, CV_{QI} can be observed as a linear function located under the parabola (Figure 28C, orange line) which is maximized at $= 1$.

4.1.3.2 INTERSITE VARIABILITY (CV_{QII})

Various release sites can also present differences, mostly due to:

- variation in the number of Ca^{2+} channels, Ca^{2+} sensors or other proteic equipment
- variation in the coupling between Ca^{2+} channels and Ca^{2+} sensors
- variation in cleft geometry or glutamate uptake
- electronic distance from the soma (and related space clamp issues)

It is likely that these differences are amplified if more than one synapse is concerned. The effect of this source of variance is a second parabola that sums with the initial parabola resulting from a simple binomial law (Figure 28C, dotted orange line). Thus the effect is maximal at $P = 0.5$, but negligible when $P = 0$ or $P = 1$.

4.1.3.3 RELEASE PROBABILITY VARIABILITY

Heterogeneities in Ca^{2+} influx between release sites can be observed when the numbers of Ca^{2+} channels, the type of Ca^{2+} channels or the sensitivity of Ca^{2+} sensors vary. As release probability is dependent on Ca^{2+} concentration, a supplementary source of fluctuation can be added. In the MPFA model, fluctuation in P (CV_P) can be modelled using families of beta functions (Silver, 2003). It can be easily expressed through a factor alpha. If alpha is high, the parabola shape is not affected, but if alpha is low, parabola shape is strongly affected at high Ca^{2+} concentrations (Silver, 2003).

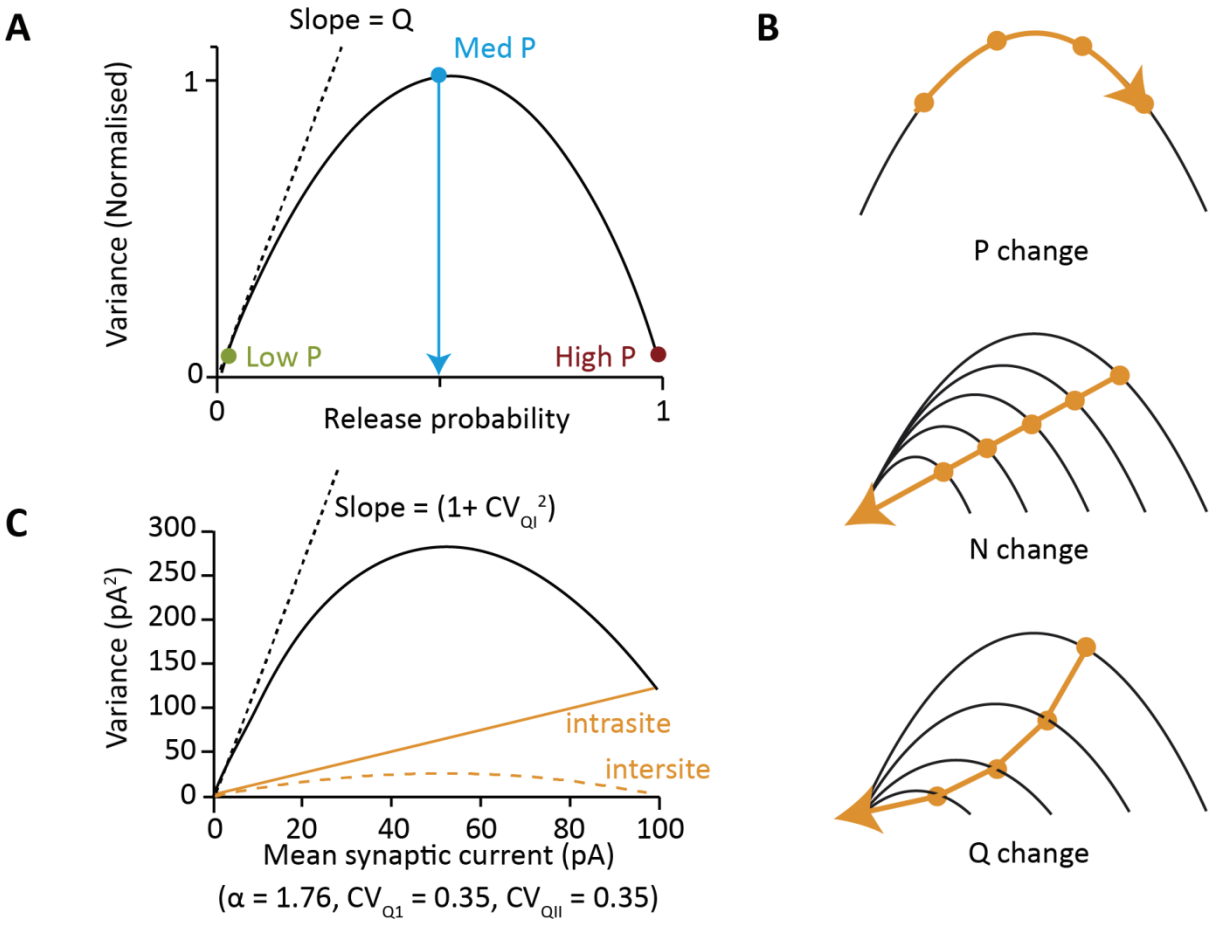

Figure 28 : Binomial and multiple probability fluctuation analysis.
A : In the simple binomial model, the mean variance versus mean amplitude plot is a parabola. Before normalisation, the initial slope of the parabola indicates the quantum Q. If the amplitude is normalised to maximal amplitude, the x-coordinate at one Ca^{2+} concentration gives the mean release probability.
B : Graphical representation of the variations of P, N or Q. P change does not modify parabola shape. N change induces a homothetic scaling of the parabola. Q change affects parabola shape as it changes the initial slope. Please not that both N and Q changes reduce the maximal extent of the parabola, since Amax = N*Q.
C : Multiple probability fluctuation analysis, adapted from (Clements and Silver, 2000). The parabola in A is affected by two supplementary sources of variance. Final parabola results of the sum of all variances. Intersite variance (orange dotted line) results from different release probability between all the release sites. Intersite variance is described by a parabola. Intrasite variance (orange line) results from variability within each release site. Thus, intrasite variability increases as the number of recruited sites increases.

4.1.3.4 MPFA QUANTAL PARAMETERS

The CV_{QI} cannot be obtained easily from the fit and must be estimated from separated experiments. For instance adding Sr^{2+} in the bath induces an asynchronous release that can be used to estimate the total CV_Q, but not the intersite or intrasite contribution to the CV_Q . Typically, in other systems in which the value was estimated, the value was estimated between 0.2 and 0.4. In most cases, CV_Q do not affect much the parabola shape or the parameters quantification. CV_P can be estimated using FM1-43 to identify single vesicles between release sites (Murthy et al., 1997; Clements and Silver, 2000). In some cases, binomial statistics are sufficient to describe vesicular release (Humeau et al., 2001b, 2002). Precise demonstration can be found in (Silver, 2003).

Compared to the simple unimodal model, taking into account CV_Q gives:

$$\boldsymbol{Var = \left[Q \cdot \bar{A} - \frac{\bar{A}^2}{N}\right] \cdot \left(1 + CV_{QII}^2\right) + Q \cdot \bar{A} \cdot CV_{QI}^2}$$

In that case, the slope of the parabola is $\cdot\ (1 + CV_{\mathrm{QI}}{}^2)$, the parabola maximum is shifted to $\frac{(1 + CV_{\mathrm{QI}}{}^2)}{2}$ and the second foot of the parabola never cross again the x-axis (Figure 28C).

If we further take into account CV_P, we obtain:

$$\boldsymbol{Var = \left[Q \cdot \bar{A} - \frac{\bar{A}^2}{N} \cdot (1 + CV_P^2)\right] \cdot \left(1 + CV_{QII}^2\right) + Q \cdot \bar{A} \cdot CV_{QI}^2}$$

In our article we performed both simple binomial model and MPFA, but we only observed subtle differences.

4.2 PRESENTATION OF THE FIRST ARTICLE

In 2002, Philippe Isope and Boris Barbour described the properties of the unitary granule cell to Purkinje cell connection (Isope and Barbour, 2002). Purkinje cells were recorded using whole cell patch clamp, while individual granule cell were stimulated using loose-cell attached patch clamp. Surprisingly, when a granule cell was functionally connected to a Purkinje cell, very few failures in neurotransmitter release were observed (the estimated probability of synaptic failure, i.e. the probability that no vesicle releases neurotransmitter at the synapse was 0.1). This value was in contradiction with previous reports that estimated a very low release probability (about 5%) and an unreliable synaptic transmission (Dittman et al., 2000). Actually, estimating the release probability is complicated to achieve in pair recordings, as connection probability is low, average synaptic weight is very low (~8 pA) and failures are difficult to identify. Moreover, long and stable recordings with changes in extracellular Ca^{2+} concentration are difficult to achieve.

During my PhD, my work was initially to study the short term plasticities at this synapse. The aim was to understand how the information is transmitted across all the frequency range of granule cell firing, and particularly at very high frequencies. Thus, I performed whole cell patch clamp of Purkinje cell, while stimulating distal granule cell soma using triple pulses at various frequencies. We were surprised by one specific result: the synapse was facilitating at all frequencies between the first and the second pulses, but then, there were no more facilitation (compare Figure 3C and 3D in the article). Since facilitation is thought to reflect release probability, does that mean that maximal release probability is reached as soon the second spike is evoked, independently on the frequency?

To answer that, and several others unanswered questions from Philippe Isope and Boris Barbour study, (Isope and Barbour, 2002), we used several approaches to characterise: the initial release probability at various extracellular Ca^{2+} concentrations, the number of release sites, the quantum size, the refilling rate and the precise facilitation curve. This project is now continued by Frédéric Doussau, who found more direct evidences supporting our data. Some of them are presented as supplementary results.

4.3 ADAPTATION OF GRANULE CELL TO PURKINJE CELL SYNAPSES TO HIGH-FREQUENCY TRANSMISSION

Cellular/Molecular

Adaptation of Granule Cell to Purkinje Cell Synapses to High-Frequency Transmission

Antoine M. Valera,[1,2] Frédéric Doussau,[1,2] Bernard Poulain,[1,2] Boris Barbour,[3,4,5] and Philippe Isope[1,2]

[1]Institut des Neurosciences Cellulaires et Intégratives, Centre National de la Recherche Scientifique, Unité Propre de Recherche 3212, Strasbourg, F-67084 France, [2]Université de Strasbourg, Strasbourg, F-67084 France, [3]Ecole Normale Supérieure, Institut de Biologie de l'Ecole Normale Supérieure, Paris, F-75005 France, [4]Centre National de la Recherche Scientifique, Unité Mixte de Recherche 8197, Paris, F-75005 France, and [5]Inserm, Unité 1024, Paris, F-75005 France

The mossy fiber (MF)–granule cell (GC) pathway conveys multiple modalities of information to the cerebellar cortex, converging on Purkinje cells (PC), the sole output of the cerebellar cortex. Recent *in vivo* experiments have shown that activity in GCs varies from tonic firing at a few hertz to phasic bursts >500 Hz. However, the responses of parallel fiber (PF)–PC synapses to this wide range of input frequencies are unknown, and there is controversy regarding several frequency-related parameters of transmission at this synapse. We performed recordings of unitary synapses and combined variance–mean analysis with a carefully adapted extracellular stimulation method in young and adult rats. We show that, although the probability of release at individual sites is low at physiological calcium concentration, PF–PC synapses release one or more vesicles with a probability of 0.44 at 1.5 mM $[Ca_{2+}]_e$. Paired-pulse facilitation was observed over a wide range of frequencies; it renders burst inputs particularly effective and reproducible. These properties are primarily independent of synaptic weight and age. Furthermore, we show that the PF–PC synapse is able to sustain transmission at very high frequencies for tens of stimuli, as a result of accelerated vesicle replenishment and an apparent recruitment of release site vesicles, which appears to be a central mechanism of paired-pulse facilitation at this synapse. These properties ensure that PF–PC synapses possess a dynamic range enabling the temporal code of MF inputs to be transmitted reliably to the PC.

Introduction

The very abundant granule cell (GC)–Purkinje cell (PC) synapses are believed to be the storage site for much of the information that is acquired during motor learning and then used during the execution of coordinated movements. Synaptic plasticity at this connection, in part controlled by the activity of climbing fibers, has been studied extensively: the synapse exhibits at least postsynaptic LTD and LTP (Hansel et al., 2001; Lev-Ram et al., 2002; Coesmans et al., 2004; Ito, 2006), as well as a form of presynaptic LTP (Salin et al., 1996). These plasticities are thought to result in the broad range of synaptic weights observed in paired recordings from the adult and also to generate the large majority of synapses that have been deduced to be silent (Ekerot and Jörntell, 2001; Isope and Barbour, 2002; Brunel et al., 2004).

Recent studies have highlighted the ability of GCs to discharge action potentials over an extraordinarily wide range of frequencies, up to 1 kHz (Chadderton et al., 2004; Jörntell and Ekerot, 2006; Rancz et al., 2007; Arenz et al., 2008). Moreover, burst firing appears to play a critical role in the rules governing the induction of synaptic plasticity (Jörntell and Ekerot, 2002; Brown et al., 2003; Bidoret et al., 2009). At a synaptic level, however, the corresponding properties of GC–PC synaptic transmission are unclear. It is unknown, for instance, whether the synapse can sustain such high rates of transmission. There is also some uncertainty in the literature regarding the release probability and the paired-pulse ratio (PPR), with apparently different results being obtained depending on the precise stimulation and recording conditions (Perkel et al., 1990; Atluri and Regehr, 1996; Isope and Barbour, 2002).

We therefore set out to investigate several interrelated properties of this key cerebellar synapse, focusing particularly on frequency-related parameters, such as the release probability and the PPR. We used recordings of unitary synapses and compared them with responses to a carefully designed extracellular stimulation method, enabling us to obtain equivalent results with both techniques. We find that, despite a release probability greater than reported previously, the parallel fiber (PF)–PC synapse is able to facilitate over short bursts and sustain transmission at very high frequencies.

Materials and Methods

Slice preparation. All experimental procedures conform to national and National Institutes of Health guidelines on animal experimentation. Slices were prepared from young and adult male Wistar rats (young, P17–P21; adult, 2–3 months, 250–450 g). The short time window for

Received June 22, 2011; revised Nov. 22, 2011; accepted Dec. 24, 2011.

Author contributions: B.P. and P.I. designed research; A.M.V., B.B., and P.I. performed research; A.M.V., F.D., B.B., and P.I. analyzed data; A.M.V., B.P., B.B., and P.I. wrote the paper.

This work was supported by the Centre National pour la Recherche Scientifique, Ecole Normale Supérieure, Université de Strasbourg, Ministère de la Recherche, Agence Nationale pour la Recherche Grants ANR-09-MNPS-038, ANR-2010-JCJC-1403-1, and ANR-08-SYSC-005. We thank Jean-Luc Rodeau and Jean de Barry for helpful discussions and Sophie Reibel-Foisset for technical assistance (Animal Care Center, IFR37, Strasbourg).

Correspondence should be addressed to Dr. Philippe Isope, Institut des Neurosciences Cellulaires et Intégratives, CNRS, Université de Strasbourg, 5 rue Blaise Pascal, 67084, Strasbourg, France. E-mail: philippe.isope@inci-cnrs.unistra.fr.

DOI:10.1523/JNEUROSCI.3175-11.2012

 0270-6474/12/323267-14$15.00/0

young animals was chosen to minimize the impact of developmental variation on the studied parameters. Methods for adult slices preparation and paired recordings have been described previously (Isope and Barbour, 2002). The (similar) methods detailed below are those used for the young animals. Rats were anesthetized by inhalation of isoflurane. Animals were killed by decapitation, and the cerebellum was dissected out and placed in a cold ACSF (4°C) bubbled with carbogen (95% O_2, 5% CO_2) containing the following (in mM): 120 NaCl, 3 KCl, 26 $NaHCO_3$, 1.25 NaH_2PO_4, 2.5 $CaCl_2$, 2 $MgCl_2$, 10 glucose, 0.00005 minocyclin (Sigma-Aldrich). Transverse slices (330-μm-thick) were prepared (Microm HM 650V; Microm) in potassium-based medium containing the following (in mM): 130 K-gluconate, 14.6 KCl, 2 EGTA, 20 HEPES, 25 glucose, 0.00005 minocyclin, and 0.05 D-AP-5 (Dugué et al., 2005). After cutting, slices were soaked a few seconds in a sucrose-based medium at 34°C containing the following (in mM): 230 sucrose, 2.5 KCl, 26 $NaHCO_3$, 1.25 NaH_2PO_4, 25 glucose, 0.8 $CaCl_2$, 8 $MgCl_2$, 0.00005 minocyclin, and 0.05 D-APV. Slices were maintained in a water bath at 34°C in bubbled ACSF. Experiments were done at 34°C (in young and at 32°C in adult animals) using the same bubbled ACSF containing 100 μM picrotoxin to block all inhibitory transmission. In experiments using extracellular stimulations, NMDA, adenosine, CB_1, and $GABA_B$ receptors were blocked to limit modulation of EPSC amplitude by stimulation-dependent activation of these receptors; respectively, the following antagonists were added (in mM): 0.001 AM251 (*N*-(Piperidin-1-yl)-5-(4-iodophenyl)-1-(2,4-dichlorophenyl)-4-methyl-1*H*-pyrazole-3-carboxamide), 0.05 D-AP5 (D-(−)-2-Amino-5-phosphonopentanoic acid), 0.0005 DPCPX (8-cyclopentyl-1,3-dipropylxanthine), and 0.001 CGP52432 (3-[[(3,4-dichlorophenyl)-methyl]amino]propyl] (diethoxymethyl)phosphinic acid). JNJ16259685 (3,4-dihydro-2*H*-pyrano[2,3]β-quinolin-7-yl)(*cis*-4-methoxycyclohexyl) methanone) (mGluR1 receptor antagonist) was also added at 0.002 mM for 100 Hz trains. Drugs were obtained from Tocris Bioscience or Ascent Scientific.

Recordings. In young rats (P17–P21), whole-cell patch-clamp recordings in voltage-clamp mode were obtained using 3–4 MΩ pipettes with a Multiclamp 700 amplifier (Molecular Devices), and optimal series resistance (R_s) compensation (80% of 5–10 MΩ, typically) was applied. R_s was monitored in all experiments, and cells were held at −60 mV. The pipette internal solution contained the following (in mM): 135 $KMeSO_4$, 6 NaCl, 10 HEPES, 4 MgATP, and 0.4 Na_2GTP, with pH adjusted to 7.3 with KOH (osmolarity to 300 mOsm). Voltages were not corrected for the liquid junction potential, which was calculated to be 9 mV (i.e., the real membrane potential was 9 mV more hyperpolarized than reported). We accepted recordings for which the inward current at −60 mV did not exceed 1 nA. No correlation between PPR and leak current (Spearman's rank order test for PPR at 50 Hz, $p > 0.05$, $n = 55$) was observed. Synaptic currents in PCs were low-pass filtered at 2 kHz and then sampled at 20–50 kHz.

For paired recordings, loose cell-attached stimulation and recording of GCs was performed using a purpose-built amplifier as described previously (Barbour and Isope, 2000). Only GCs in which an action potential could be distinguished clearly and elicited reliably were analyzed. Only connections in which postsynaptic responses and presynaptic action potentials had the same threshold were retained. Stimulation was adjusted to be just suprathreshold so as to minimize the probability of stimulating other nearby GCs or axons. To calculate the mean EPSCs, we averaged together all sweeps in which GC excitation was successful.

Repetitive extracellular GC stimulation was effected by stimulating in the GC layer with a 16-site iridium microelectrode array (type "A" probe; NeuroNexus Technologies) combined with an ISO-STIM 01D (NPI Electronic), allowing us to make bipolar stimulations between arbitrary pairs of sites. Stimulation intensity was adjusted to evoke an initial current of ~100 pA (110 ± 61 pA; $n = 60$). The low intensity and short duration of the stimulation (6 ± 3 V for 70 μs, $n = 60$) minimized the duration of the artifact. No correlation was observed between stimulation intensity and PPR (PPR at 50 Hz, Spearman's rank order test, $\rho = 0.16$, $p = 0.31$, $n = 41$) or between EPSC1 (*A*1) and PPR (PPR at 50 Hz, Spearman's rank order test, $\rho = -0.13$, $p = 0.42$, $n = 41$). By stimulating in the deeper regions of the GC layer, we minimized PF recruitment that might occur when stimulating near the molecular layer. The extracellular stimulating electrodes were systematically placed laterally to the PC (in the direction of the PFs) and at a sufficient distance to ensure that only parallel and not ascending axon synapses were activated. This placement also facilitated avoidance of antidromic activation of the PC and stimulation of the climbing fiber.

Definitions. It will be important below to distinguish clearly three different definitions of release probability and related parameters. We first consider the quantal definition of a release site, which is a associated with the release of zero or one quantum or vesicle. We term the probability of this event Pr_{site} and the complementary failure probability Pf_{site}. A connection between a GC and a PC is likely to comprise several such sites, whose number we denote *n*. The combined probability of at least one vesicle being released at a connection is defined as Pr_{syn}, whereas the complementary failure probability (release of no vesicles at a connection) is termed Pf_{syn}:

$$Pf_{syn} = (Pf_{site})^n = (1 - Pr_{site})^n$$

Finally, *N*, *P*, *Q* are reserved for the mean–variance analysis of compound synaptic responses evoked by extracellular stimulation described below.

Analysis of recordings from pairs of neurons. Data acquisition was performed using pClamp10 (Molecular Devices). Analysis was performed in the Igor graphing and analysis environment (Wavemetrics), using Synaptix (B.B.), SpAcAn (Guillaume Dugué, Instituto Gulbenkian de Ciencia, Lisbon, Portugal), and macros developed in house (A.M.V. and P.I.). Response amplitudes of individual EPSCs were measured automatically as follows: (1) after smoothing of the raw trace, the procedure found the minimum of the trace in a 5 ms time window after the stimulus onset; and (2) the peak was estimated by averaging 20 points centered on the minimum and subtracting the baseline value. Noise measurements were obtained by applying exactly the same procedure to portions of traces that contained no evoked responses. We define *A*1, *A*2, and *A*3 as the evoked EPSC amplitude resulting from the first, second, and third stimuli:

$$\mathrm{PPR}^{A2}_{A1} = \frac{\text{mean } A2}{\text{mean } A1};\ \mathrm{PPR}^{A3}_{A2} = \frac{\text{mean } A3}{\text{mean } A2}$$

For frequencies >50 Hz, *A*2 and *A*3 were corrected for the residual current of the preceding EPSC by fitting the preceding EPSC decay phase with a single exponential and subtracting its value at the time point of the EPSC peak being measured. Above 200 Hz, only the peak of the burst response was measured (see Results). In a few pairs, the amplitude histograms of evoked EPSCs and the noise histogram did not overlap, and failures could then be identified unequivocally ($n = 7$ pairs). However, in all other paired recordings, the low signal-to-noise ratio (SNR) precluded direct identification of failures and obliged us to use more indirect methods for estimating this parameter. Our overall approach was to compare amplitude histograms with measurements of noise to estimate the proportion of failures (Pf_{syn}) in a given paired recording (Isope and Barbour, 2002). Once the EPSC amplitude and noise histograms had been obtained, Pf_{syn} was estimated by scaling part of the noise distribution to fit the corresponding range of the EPSC amplitude distribution. We chose to scale the noise histogram to the EPSC amplitude histogram for values greater than zero (EPSCs having negative amplitudes by convention; for additional illustration, see Isope and Barbour, 2002, their Figs. 4, 5). This analysis was performed for all pairs recorded ($n = 18$). This procedure overestimates the proportion of failures when the SNR is low. Therefore, although it is not accurate under all conditions, the estimate does represent a reliable lower bound on the failure proportion. This is useful in the present context because we shall seek below to establish that the Pr_{syn} is higher than previously estimated.

Extracellular stimulation protocols and analysis. Acquisition of data was performed using the WinWCP 4.2.x freeware (John Dempster, Strathclyde Institute of Pharmacy and Biomedical Sciences, University of Strathclyde, UK). For PPR analysis, three stimuli were systematically applied at various frequencies distributed randomly throughout the protocol and repeated at a rate of 0.1–0.14 Hz. All measurements were made on averages of 20 traces. Because high-frequency stimuli were used, the residual decay of *A*1 contaminated *A*2 (see Fig. 3*B*). For frequencies ≤100 Hz, *A*2 was calculated as described above by subtracting the extrap-

olated exponential fit of the preceding EPSC. The fitting function was calculated between 2 ms after the peak and the following artifact. For frequencies ≥200 Hz, *A*1, *A*2, and *A*3 could not be discriminated. Mean *A*1 was then the average of traces with a single stimulus. Mean *A*2 was given by (average double-stimulus response − mean *A*1) and mean *A*3 by (average triple-stimulus response) − (average double-stimulus response). When measuring individual EPSCs at the second stimulus (*A*2), residual current from *A*1 could not be estimated by a simple exponential fit because of noise. We then used the mean decay time constant from averaged EPSCs to correct amplitudes of individual EPSCs. In trains of 30 stimuli, individual amplitudes were determined as follows: (1) each $EPSC_n$ of the averaged train was fitted using a biexponential function; and (2) these fits were then used as templates to fit individual EPSCs in each train and used to estimate residual current during the subsequent response.

Variance of the mean EPSC at the first stimulation (mean *A*1) was calculated from at least 100 individual traces. Traces were analyzed only if series resistance fluctuations were <15%. Because a slight linear rundown was sometimes observed during recordings, spurious variance was subtracted by using a linear fit of the time course of *A*1.

Variance–mean analysis. Variance–mean analysis was developed and described in detail in previous studies (Silver et al., 1998; Reid and Clements, 1999; Clements and Silver, 2000; Humeau et al., 2001, 2002, 2007; Clements, 2003; Silver, 2003; Saviane and Silver, 2007; Doussau et al., 2010). Because of the long stable recordings required for these analyses, they were applied to recordings in which compound GC responses were elicited in PCs by extracellular stimulation in the GC layer. The responses therefore comprised multiple synaptic connections. As a first approach to analyzing these data, we applied a simple binomial model to the responses. This represents the stimulated synapses as an ensemble of N independent release sites with a release probability P, and quantal size Q.

This simple model assumes that P and Q are uniform; because this is an unlikely physiological situation, the influence of possible heterogeneity was also taken into account (see below). It should be noted that N is a functional parameter and release statistics will only reflect sites that are able to release vesicles. Thus, N does not take into account long-lasting silent sites. In practical terms, only sites containing a readily-releasable vesicle (i.e., docked and fully primed) would contribute to the observed N (Humeau et al., 2001, 2002, 2007). Individual responses are assumed to sum linearly (a significant approximation in the presence of multivesicular release). By the independence of the sites, their means and variances also sum linearly. According to a simple binomial model, the mean of the response ($\bar{A}$) is given by

$$\bar{A} = N \cdot Pr_{site} \cdot Q,$$

with fluctuations of the responses around the mean having variance,

$$\text{var} = N \cdot Pr_{site} \cdot (1 - Pr_{site}) \cdot Q^2.$$

When only P is modified (by changing $[Ca^{2+}]_e$), var = $f(\bar{A})$ is a parabola:

$$\text{var} = Q \cdot \bar{A} - \frac{\bar{A}^2}{N} \quad (1)$$

This can be used to estimate Pr_{site}, because $Pr_{site} = 0.5$ at the peak of the parabola and 1 at the greater root of the parabola:

$$Pr_{site} = \frac{\bar{A}}{N \cdot Q} \quad (2)$$

The initial slope of the parabola provides an estimate of the weighted average of Q and the greater root of the parabola gives ($N \cdot Q$). Neither Pr_{site} nor Q is likely to be uniform in practice. We have shown previously that synaptic weights can vary widely without evidence of correlated changes in release probability, which could imply strong variation of Q (Isope and Barbour, 2002). Variation of Q in a multisite binomial model will preserve the parabolic shape of the variance–mean relation, but the apparent Q will be weighted toward the larger individual values of Q. Variation in Pr_{site} causes departure from the parabolic form. For this reason, we applied multiple-probability fluctuation analysis (MPFA) (Clements and Silver, 2000; Silver, 2003), which explicitly models nonuniform Pr_{site} values and also incorporates intersite and intrasite sources of variance in the quantal size Q (Clements, 1991; Clements and Silver, 2000; Silver, 2003). Using this analysis, quantal parameters were estimated by fitting the variance (var) of the mean amplitude ($\bar{A}$) at different Pr_{site} (by changing $[Ca^{2+}]_e$) in each individual experiment by a simplified multinomial:

$$\text{var} = \left[Q \cdot \bar{A} - \frac{Q \cdot \bar{A}^2 \cdot (1 + \alpha)}{\bar{A} + N \cdot Q \cdot \alpha} \right] \cdot (1 + CV_{QII}^2) + Q \cdot \bar{A} \cdot CV_{QI}^2 \quad (3)$$

were CV_{QI} and CV_{QII} are the coefficients of variation (CV) of the intrasite and intersite quantum variability, and α is a family of β distributions that mimics dispersion of Pr_{site} (Silver, 2003). Because CV_{QI} and CV_{QII} could not be evaluated separately, we made an estimation of the total quantum variability (CV_Q) by recording quantal events in ACSF in which Ca^{2+} was replaced by 5 mM Sr^{2+} (see Results). Therefore, we fixed CV_{QI} and CV_{QII} at different values such that

$$CV_Q^2 = CV_{QI}^2 + CV_{QII}^2$$

Fits of the var = $f(\bar{A})$ plots were weighted by the theoretical error of the variance (σ_{sample}) for n observations (i.e., n EPSCs):

$$\sigma_{sample} = \sqrt{\frac{1}{n}\left[\mu_4 - \frac{n-3}{n-1} \mu_2^2 \right]} \quad (4)$$

where μ_2 and μ_4 are the second and fourth central population moments, respectively; h statistics were used to estimate these parameters (Silver, 2003). The dispersion in release probability was estimated as follows:

$$CV_{Pr_{site}} = \sqrt{\frac{1 - Pr_{site}}{Pr_{site} + \alpha}} \quad (5)$$

If the number of releasable vesicles in a given experimental condition is not fixed, this can cause an increase of EPSC variance without changing the mean, tending to lead to an overestimation of N.

Simple model of PPR. Let $N1$ and $P1$ represent the number of functional release sites and their release probability at the first stimulus, whereas $N2$ and $P2$ represent the analogous values at the second stimulus. At the first stimulus, $P1 \cdot N1$ vesicles are released, leaving $(1 - P1) \cdot N1$ sites filled with a release-ready vesicle. In the time interval between stimuli 1 and 2, a fraction (R) of the sites emptied at stimulus 1 is resupplied with release-ready vesicles; their number is $R \cdot (P1 \cdot N1)$. Thus, at the second stimulus, the number of sites with a releasable vesicle is $N2 = (1 - P1) \cdot N1 + R \cdot (P1 \cdot N1)$. Accordingly, if the quantal size does not change between the stimuli 1 and 2,

$$PPR_{\frac{A2}{A1}} = \frac{[(1 - P1) \cdot N1 + R \cdot P1 \cdot N1] \cdot P2}{P1 \cdot N1}$$

which can be rearranged to

$$PPR_{\frac{A2}{A1}} = \frac{[1 - P1 + R \cdot P1] \cdot P2}{P1}$$

Thus, the values of PPR depend on the rate of vesicle replenishment. If no replenishment occurs between the two stimuli, PPR reaches its minimal theoretical value:

$$PPR_{\frac{A2}{A1}} = \frac{(1 - P1) \cdot P2}{P1}$$

In contrast, if complete replenishment occurs, PPR reaches a maximum theoretical value:

$$PPR_{\frac{A2}{A1}} = \frac{P2}{P1}$$

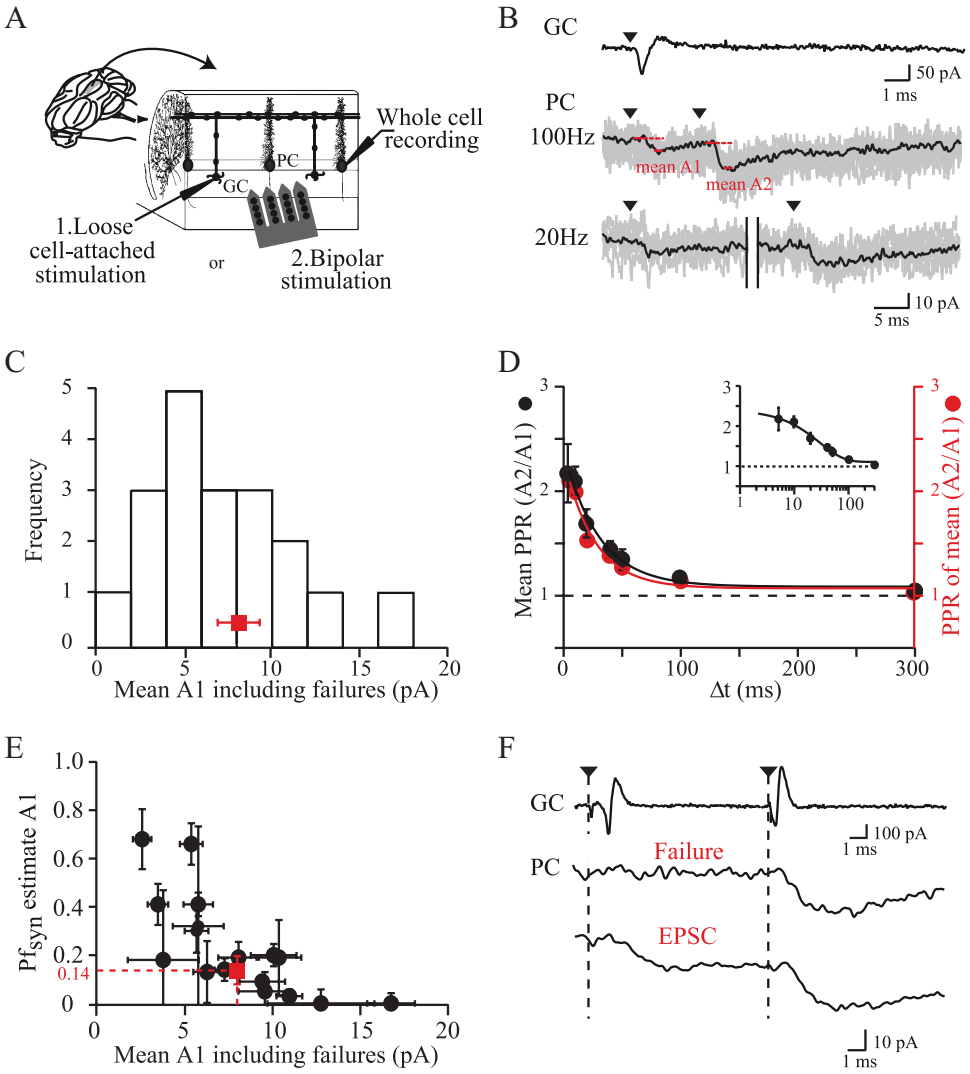

Figure 1. Properties of unitary GC–PC synapses in young rats (P17–P21). ***A***, Diagram showing the typical orientation of cell pairs recorded in this study and the positioning of extracellular stimulation. PCs were whole-cell clamped near the surface of transverse cerebellar slices. GCs were stimulated and recorded in loose cell-attached mode or stimulated using bipolar stimulations. ***B***, Typical GC–PC paired recording. The GC action potential was evoked and recorded as a capacitive current in loose-cell attached mode. The stimulus artifact (black triangle) has been subtracted. Evoked EPSCs were recorded in a connected PC at varying frequencies. Gray, Individual traces; black, averaged traces; red, mean *A*1 and *A*2. ***C***, Histogram of the mean EPSC amplitudes including failures at the first stimulation (mean *A*1) for all pairs ($n = 18$). Red, Average EPSC amplitude. ***D***, Left axis, Average PPR as a function of interstimulus interval fitted by a single exponential (solid line, $\tau = 29.4 \pm 8.49$ ms). Inset, Same data but with a logarithmic *x*-axis. Right axis and red, PPR calculated as (mean *A*2 of all pairs)/(mean *A*1 of all pairs). ***E***, Distribution of estimated failure probabilities plotted as a function of mean *A*1 with their bootstrap SE estimates (error bars). ***F***, Comparison of mean *A*2 when failures of release occurred at the first stimulus (middle trace) and when failures of release were excluded (bottom trace) at 100 Hz for one connection. The action potentials in the presynaptic GC stimulated and recorded in the loose-cell attached mode are shown in the top trace.

We also considered the situation during which the number N of release sites increases between the two stimuli. Therefore, the PPR may be given by

$$\mathrm{PPR}_{\frac{A2}{A1}} = \frac{[(1 - P1 + (R \cdot P1)) \cdot N1 + N\mathrm{extra}] \cdot P2}{P1 \cdot N1}$$

where *N*extra is the number of extrasites with a releasable vesicle at stimulus 2 that were reluctant at stimulus 1. In such a case, even if P1 = P2 = 1 and no refilling occurs, PPR can theoretically reach values >1 (i.e., $\frac{R \cdot N1 + N\mathrm{extra}}{N1} > 1$).

Statistics. Unless stated, means are reported with SDs, whereas error bars in figures represent SEMs, except in Figures 1*E*, 2*A*, 4C_1, and 5. Unless stated, statistical tests were the nonparametric Mann–Whitney *U* and Spearman's rank order tests. On several occasions, we applied the nonparametric "bootstrap" method (Efron and Tibshirani, 1993) for estimating the standard error of complex parameters, in particular the probability of failure (see Figs. 1, 3). Briefly, traces were selected randomly, with replacement, from those initially analyzed, until an equal number was accumulated. The original analysis was then simply reapplied to this replicate data set and "bootstrap replicates" of the desired parameter produced. Repetition of this procedure 10,000 times generated sufficient replicates to estimate the SE of the parameter replicates. Despite the apparent circularity of reusing the sample data, the theory underpinning bootstrap methods has demonstrated that the SE obtained will be a good approximation to that of the underlying population.

Results

PF-PC connections

We recorded unitary GC–PC synaptic responses at near-physiological temperature in transverse slices prepared from young rats (Fig. 1; P17–P21, 2.5 mM $[Ca^{2+}]_e$; 34°C) or adult rats (Fig. 2; 2 mM $[Ca^{2+}]_e$; 32°C). PCs were whole-cell clamped at −60 mV via a somatic patch pipette and the EPSCs were elicited by stimulating GCs. Combined loose cell-attached stimulation and recording (Barbour and Isope, 2000; Isope and Barbour,

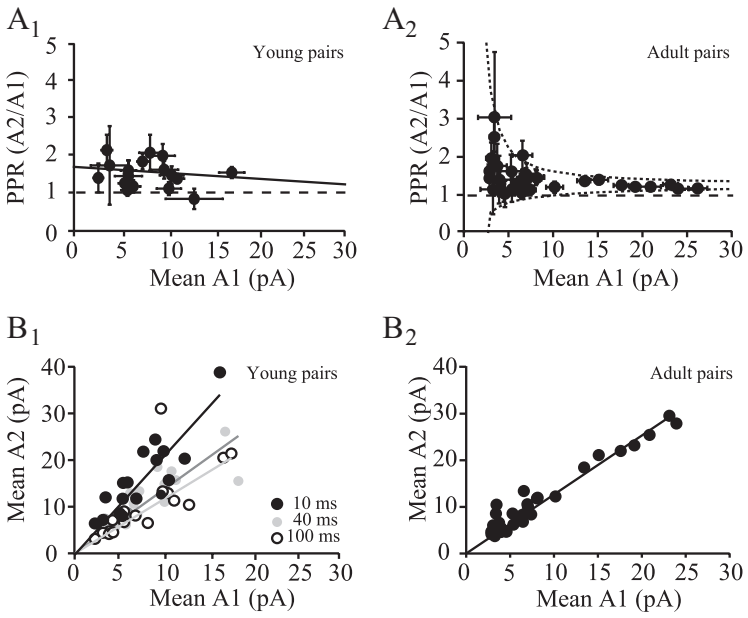

Figure 2. PPR at unitary GC–PC connections in young and adult rats. ***A1***, Plot of all PPRs against mean *A*1 including failures at 25 Hz for GC–PC connections in young rats. Error bars are bootstrap estimates of the SE of the mean *A*1 (*x*-axis). For the ratios (*y*-axis), error bars were calculated using the following formula: $SE_{A2/A1} \approx (A2/A1).\mathrm{sqrt}.((SE_{A1}/A1)^2 + (SE_{A1}/A2)^2)$. ***A2***, Same plot for adult connections. Dashed lines represent the 5th and 95th percentiles of the distribution of ratios of two Gaussian distributions, whose means are in the ratio (*A*2/*A*1) = 1.25, of which the lesser amplitude (*A*1) is given on the *x*-axis of the plot. The SDs of the Gaussians are the mean SE of the amplitude measurements (1 pA). Note that adult pairs were recorded at 2 mM $[Ca^{2+}]$ and young pairs at 2.5 mM $[Ca^{2+}]$. ***B1***, Plot of mean *A*2 including failures against mean *A*1 including failures for all individual connections and linear fit (solid line) for three different frequencies of stimulation (100, 25, and 10 Hz). ***B2***, Same plot for adult pairs at 25 Hz.

2002) was applied to GCs. Paired- or triple-pulse stimulations at varying frequencies were applied. An example of a paired recording in a young rat (Fig. 1*B*) shows the action potential recorded in the GC as a capacitive current and several EPSCs recorded in the PC. Identification of connected GCs was performed by eye and confirmed by offline averaging of individual traces. For each connection, we calculated the mean amplitude of EPSCs elicited by each stimulus (mean *A*1 and mean *A*2; Fig. 1*B*) including failures (which often could not be identified). $PPR_{A2/A1}$ was then given by (mean *A*2)/(mean *A*1) as suggested by Kim and Alger (2001). In all, 18 GC-PC pairs with detectable responses were obtained. The mean amplitude of the first EPSC was 8.1 ± 4.1 pA ($n = 18$; Fig. 1*C*) in young rats.

Modest paired-pulse facilitation and low failure probability at unitary synapses

For each individual unitary connection, the $PPR_{A2/A1}$ was determined for a wide range of frequencies (0.3–200 Hz; Fig. 1*D*) and plotted against interstimulus interval (Δt). In all but one pair recorded, only facilitation was observed. In 16 of 18 pairs, the time course of facilitation could be fitted by a single exponential. Figure 1*D*, in which PPRs were averaged ($n = 18$; $PPR_{A2/A1}$ at 50 Hz = 1.7 ± 0.14, $PPR_{A2/A1}$ at 100 Hz = 2.1 ± 0.15; τ = 29.4 ± 8.49 ms; $[Ca^{2+}]_e$ = 2.5 mM), shows that facilitation is modest and decays more quickly than reported previously using compound stimulation in the molecular layer (Atluri and Regehr, 1996; Foster et al., 2005). Because averaging PPR across pairs gives the same importance to small, noisy connections as to strong connections, we also averaged the mean amplitude from all pairs and then plotted the ratio of these means as a function of interstimulus interval. Very similar values of PPR and time course of facilitation were obtained ($PPR_{A2/A1}$ at 50 Hz = 1.54, $PPR_{A2/A1}$ at 100 Hz = 1.99; τ_{fit} = 25.3 ± 8.7 ms, $n = 18$; Fig. 1*D*), suggesting that the modest PPR did not result from a bias toward small connections. The PPR appeared not to depend on the level of the PF connection in the molecular layer, because PPR was not correlated with the EPSC decay time constant (Spearman's rank order test, $\rho = -0.28$, $p = 0.25$, $n = 18$), which is a reasonable proxy for distance from the PC layer (Roth and Häusser, 2001).

Because the PPR is generally assumed to reflect the release probability, we then set out to quantify this parameter. Because paired GC–PC recordings do not allow the long protocols required for extensive direct characterization of Pr_{site} (Silver et al., 1998, 2003; Oleskevich et al., 2000; Humeau et al., 2002), we sought to determine the probability of failures of transmission, Pf_{syn} (see definitions in Materials and Methods). We first used the approach of Isope and Barbour (2002), based on the comparison of the histogram of EPSC amplitudes and that of the noise. Pf_{syn} at 2.5 mM $[Ca^{2+}]_e$ was obtained by scaling the two amplitude histograms (mean Pf_{syn} at $A1 = 0.14 \pm 0.15$; $n = 18$). Note that here we refer to the global failures of transmission at the GC-PC connection; these require a failure of vesicle fusion at each release site of the connection. Figure 1*E* shows a scatter plot of the failure probability estimates against mean *A*1. Reproducing this analysis for the second response (*A*2) at 25 Hz showed a significant decrease in Pf_{syn} at the second stimulus (mean $Pf_{syn\ A2} = 0.05 \pm 0.09$; $n = 9$, $p < 0.01$, Wilcoxon's paired rank test), leading to an absence of failures in five pairs. It should be noted that this method overestimates Pf_{syn} when EPSC amplitude and noise histogram overlap (Isope and Barbour, 2002). The actual composite Pf_{syn} is thus certainly equal to or lower than 0.14 at 2.5 mM $[Ca^{2+}]_e$. This value of Pf_{syn} allows us to make a first estimate of the release probability at an individual site, by combination with the estimate of seven to eight docked vesicles at the PF–PC synapse reported by Xu-Friedman et al. (2001). Thus, $Pf_{syn} = (1 - Pr_{site})^n$ where $n = 7$ or 8, which yields $Pr_{site} = 0.22–0.24$.

We tested the possibility that desensitization of postsynaptic receptors could reduce PPR. We choose a sample of paired recordings in which the amplitude histogram did not overlap with that of the noise, allowing successes of transmission to be discriminated unequivocally from failures (Saviane and Silver, 2006). Although this method might appear biased by the selection of stronger connections, the putative involvement of desensitization at the second stimulus would presumably tend to be overestimated. At 100 Hz, we compared the average amplitude of the second EPSC when a failure occurred at the first stimulus with the average EPSC when release of vesicles was observed at the first stimulation (Fig. 1*F*). Remarkably, no difference in the amplitudes of the EPSCs elicited by the second stimulus was detected between the two conditions (mean *A*2 when there were failures at the first stimulation = 12.8 ± 2.4 pA; mean *A*2 when there were successes at the first stimulation = 12.9 ± 1.6 pA; $n = 7$ cells, Wilcoxon's paired rank test, $p = 0.93$). This suggests that neither postsynaptic desensitization nor depletion of vesicles play a significant role under these conditions.

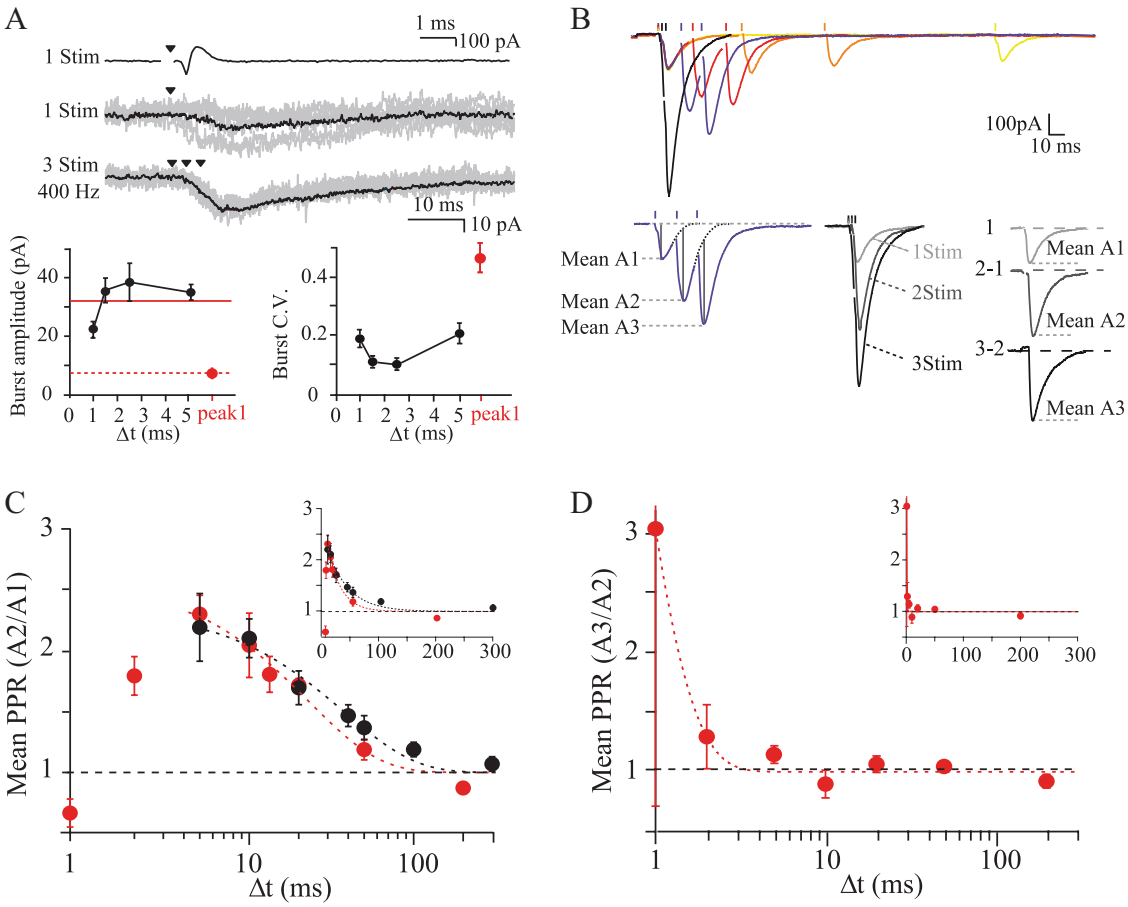

Figure 3. High fidelity of synaptic transmission during high-frequency bursts. ***A***, Increased reliability of GC–PC transmission during high-frequency bursts of stimuli. Top, Example of GC–PC paired recordings for one stimulus and three stimuli at 400 Hz. Solid dark line, Their averages. Bottom left, Amplitude of summated EPSCs against interstimulus interval. Bottom right, CV against interstimulus interval. Red, Mean *A*1. ***B***, Extracellular triplet stimulation in the GC layer. Top, Examples of traces with intra-triplet frequencies ranging from 5 to 500 Hz. Bottom left, EPSC decays were fitted with a single exponential (dotted line), and the amplitudes of EPSCs were measured after correction for residual amplitude of the preceding EPSC. Bottom right, At frequencies >100 Hz, EPSC amplitudes were extracted from average responses to single, double, and triple stimuli. ***C***, Red, Mean $PPR_{A2/A1}$ as a function of interstimulus interval using extracellular stimulation (with a logarithmic *x*-axis). Black, Mean $PPR_{A2/A1}$ in paired recordings (same as Fig. 1). Inset, Same data with a linear axis. ***D***, Mean $PPR_{A3/A2}$ as a function of interstimulus interval with a logarithmic *x*-axis. Inset, Same data with a linear axis.

Variability of paired-pulse facilitation at unitary connections

Paired GC-PC recordings allowed us to study the variability of PPR between unitary connections. Thus, at 25 Hz, $PPR_{A2/A1}$ ranged from 0.8 to 2.1. Plotting PPR against mean EPSC amplitude for all pairs recorded in young rats (Fig. 2A_1) and in adult rats (Fig. 2A_2; dataset described by Isope and Barbour, 2002) appeared to show a tendency for PPR to increase with decreasing EPSC amplitude. Similar trends have been interpreted as reflecting a decreasing Pr_{syn} with amplitude (Markram et al., 1997). However, the effect of the low SNR of the small connections must be taken into account. In general, any ratio with a small, noisy denominator can show great variation. This can be understood by considering the ratio of two Gaussians; the resulting Cauchy distribution has neither mean nor SD because sometimes a division by zero occurs. The effect of the small noisy denominator is apparent in the broad spread of PPR values at small *A*1. This spread can plausibly be explained as the result of a noisy ratio with a fixed underlying PPR, as shown by the 5th and 95th percentiles of the simulated distribution of the ratio of two Gaussians whose means were in the ratio 1.25 and whose SDs were the (approximate) SE (1 pA) of the mean amplitude (Fig. 2A_2). Thus, in adult rats, all connections may share similar values of paired-pulse facilitation (~1.25 in adult pairs at 25 Hz and 2 mM $[Ca^{2+}]_e$). We then plotted mean *A*2 versus mean *A*1 for all connections (Fig. 2*B*), because this representation does not suffer from the same sensitivity to noise as does a ratio with a small and noisy denominator (Kim and Alger, 2001). The plot could be well fitted by a line, the slope of which gave the PPR. Determination of PPR by averaging all *A*1 and *A*2 (Fig. 1*D*) or by fitting *A*2 versus *A*1 of all connections with a single line (Fig. 2*B*) give very similar $PPR_{A2/A1}$ values for all frequencies tested in both young rats (Fig. 2B_1, $PPR_{10\ ms} = 2.06 \pm 0.12$, $PPR_{40\ ms} = 1.35 \pm 0.01$, $PPR_{100\ ms} = 1.15 \pm 0.05$; 2.5 mM $[Ca^{2+}]_e$) and adult rats (Fig. 2B_2; $PPR_{40\ ms} = 1.26 \pm 0.05$; 2 mM $[Ca^{2+}]_e$). These findings demonstrate that PPR at the PF-to-PC synapse is a parameter that depends on the frequency of stimulation but appears to be independent of synaptic weight.

High fidelity of synaptic transmission at unitary synapses during high-frequency bursts

Because *in vivo* experiments have shown that GCs can fire at very high frequency (Chadderton et al., 2004; Jörntell and Ekerot, 2006; Rancz et al., 2007; Arenz et al., 2008), we applied short bursts of three stimuli at higher frequencies (up to 1 kHz; Fig. 3*A*) to investigate the behavior of the synaptic response at these frequencies. Separation of EPSCs was not possible >200 Hz, so we

measured the amplitude and CV of the compound EPSC. As shown in Figure 3*A*, bursts of action potentials led to a fourfold increase in the compound response, a fourfold decrease in CV and a corresponding fourfold increase in the SNR (SNR_{peak1} = 2.2 vs $SNR_{400\ Hz}$ = 10, where SNR = mean/SD), showing that release of vesicles was sustained to the third stimulus. At 1 kHz, the modest enhancement in burst amplitude and the higher CV than at lower frequencies suggested that action potential initiation failed in a few trials because of the refractory period, which is ~1 ms under these conditions (Isope and Barbour, 2002).

We conclude the following from our unitary synapses: (1) the GC–PC connection shows a low probability of failure of transmission; (2) the synapse nevertheless facilitates; and (3) high-frequency bursts of action potentials elicit strong, reliable responses. To understand the mechanisms underlying these phenomena, we then studied more systematically the properties of the GC–PC synapse.

GC layer stimulation reproduces the PPR of unitary connections

Unfortunately, paired recordings between GCs and PCs do not allow extensive characterization of synaptic parameters, such as the probability of release and the rate of vesicle replenishment, because high-frequency stimulation in the loose cell-attached configuration frequently led to breakdown of the GC membrane. For this reason, we used extracellular stimulation using iridium multi-electrode arrays placed deep in the granular layer (see Materials and Methods and Fig. 1*A*). GC stimulation should generate a more diffuse pattern of active PFs than stimulation in the molecular layer. The use of the metal electrode arrays enabled balanced and low-voltage bipolar stimulation, reducing the artifact and accelerating recovery between stimuli. The deep position in the GC layer prevented inadvertent stimulation of PFs. We applied up to three stimuli at high frequencies. For frequencies up to 100 Hz, EPSC amplitudes were corrected for the residual current from the preceding current (Fig. 3*B*; see Materials and Methods), whereas above 100 Hz, the mean *A*1, *A*2, and *A*3 were estimated using a three-step protocol in which sequences of one, two, and three stimuli were applied. The mean *A*2 and *A*3 were then estimated by subtraction (Fig. 3*B*; see Materials and Methods). No significant differences were observed between PPR values from unitary connections and those obtained using GC layer stimulation (Fig. 3*C*; nonlinear regression analysis test, $p = 0.11$). For intervals of 5 ms and greater, $PPR_{A2/A1}$ decreased exponentially with interval; the values obtained were lower than most published values over the whole frequency range (Matsukawa et al., 2003; Foster et al., 2005). Furthermore, as observed in paired recordings, for all these frequencies, the facilitation of the response induced by the first stimulus was maintained from the second to the third stimulus (Fig. 3*D*). $PPR_{A3/A2}$ and $PPR_{A2/A1}$ at the shortest intervals, 1 and 2 ms, deviated from the extrapolated curves fitting the data for longer intervals. The reciprocal decrease of $PPR_{A2/A1}$ and increase of $PPR_{A3/A2}$ suggested that the deviations were caused by failures of excitation. Some stimuli could plausibly have fallen into at least the relative refractory period at these intervals (measurement of the refractory period in GCs under similar conditions found values ~1 ms; Isope and Barbour, 2002).

The combination of a significant release probability (see the above estimate Pr_{site} = 0.22–0.24) and paired-pulse facilitation might be expected to lead to rapid exhaustion of the readily-releasable pool (RRP). If we assume a slow rate of vesicle replenishment (Pyle et al., 2000) at 2.5 mM $[Ca^{2+}]_e$ and an initial $Pr_{site} = 0.22$, 22% vesicles in the RRP would be released at the first stimulus and 78% remain available. Given a $PPR_{A2/A1}$ = 2.3 at 200 Hz (Fig. 3*C*), 51% of quanta would be released at the second stimulus. After two stimuli, only a fraction 100-51-22 = 27% of vesicles of the initial RRP would remain for a third response, which should therefore be severely depressed (predicted $PPR_{A3/A2}$, 27/51 = 0.5). This prediction was, however, not verified, because $PPR_{A3/A2} = 1.13$, indicating that $1.13 \times 51 = 58\%$ of the initial RRP was again released (Fig. 3*D*). This implies that a number of vesicles equivalent to 31% of the initial pool were recruited, docked, and fully primed to be ready for release in 10 ms. This calculation clearly indicates that the observed PPR values obtained at 2.5 mM $[Ca^{2+}]_e$ during triplet stimulation at high frequency cannot be explained simply by an increase of a uniform Pr_{site} at the time of stimuli 2 and 3.

Three scenarios could explain the increase in the number of vesicles released during short bursts of three action potentials: (1) initial release probability at individual release sites was lower than estimated; (2) the apparent number of active release sites (*N*) increased during the interstimulus interval or reluctant sites are recruited; and (3) a high rate of fusion site replenishment with release-ready vesicles compensates for vesicles released. We shall first explore in detail the initial release probability.

Determination of release probability at the PF-to-PC connection

The determination of release probability of individual release sites, Pr_{site}, by the identification of quantal peaks in synaptic amplitude histograms was precluded by the small size of the quantal event and its variability compared with the level of noise (Clements, 1991; Larkman et al., 1991). We therefore used protocols modifying initial Pr_{site}. Varying extracellular $[Ca^{2+}]_e$ dramatically altered *A*1 (Fig. 4*A*) as expected if initial Pr_{site} varied. For example, in the experiment in Figure 4*A*, *A*1 ranged from 2.5 pA at 1.5 mM $[Ca^{2+}]_e$ to 277 pA at 4 mM $[Ca^{2+}]_e$ (mean *A*1 = 17.3 pA at 1.5 mM $[Ca^{2+}]_e$; mean *A*1 = 171.4 pA at 4 mM $[Ca^{2+}]_e$; n = 9). The relation between mean *A*1 and $[Ca^{2+}]_e$ could be well fitted by a sigmoid function (Fig. $4A_2$) as shown previously at many connections (Augustine and Neher, 1992; Mintz et al., 1995; Foster et al., 2005). If we assume that the plateau of fits represents the maximal release probability and not saturation of postsynaptic receptors (see below), we can interpret the EPSC amplitude relative to the plateau as being approximately proportional to the release probability. Thus, based on the sigmoid fit, average Pr_{site} would be close to 0.7 at 4 mM $[Ca^{2+}]_e$ (Fig. $4A_2$; Pr_{site} = 0.2 at 2.5 mM $[Ca^{2+}]_e$; Pr_{site} = 0.08 at 1.5 mM $[Ca^{2+}]_e$). The possible influence of postsynaptic receptor saturation was examined by performing a set of experiments using the low-affinity competitive antagonist γ-D-glutamylglycine (γDGG) (4 mM) to relieve AMPA receptor saturation. Application of γDGG (4 mM) reduced EPSC amplitudes by 94.1% at 2.5 mM $[Ca^{2+}]_e$ (control: mean *A*1 = 518.9 ± 306.5 pA; γDGG: mean *A*1 = 32.3 ± 28.5 pA, n = 5 cells). $[Ca^{2+}]_e$ was then varied from 1.5 to 6 mM, and mean EPSC amplitudes were measured at the steady state. Figure $4A_2$ (red dots) shows that the normalized relation EPSC = $f([Ca^{2+}]_e)$ in γDGG is close to that observed in control conditions (Pr_{site} = 0.1 ± 0.04 at 1.5 mM $[Ca^{2+}]_e$; Pr_{site} = 0.26 ± 0.17 at 2.5 mM $[Ca^{2+}]_e$; Pr_{site} = 0.57 ± 0.09 at 4 mM $[Ca^{2+}]_e$, n = 5). Assuming that the effect of γDGG is at least partially competitive with the synaptic glutamate transient (i.e., that some γDGG unbinds before the glutamate transient decays), these data suggest that AMPA receptor saturation did not influence our results at concentrations up to 4 mM $[Ca^{2+}]_e$. We note, however, that a

competitive antagonist would be expected to deform the curve of *A*1 versus $[Ca^{2+}]_e$ by inhibiting more strongly the smaller EPSCs, which are presumably produced by a lower glutamate concentration. This does not appear to have occurred. An absence of multivesicular release could provide an explanation, but this would contradict our and others' estimates of $n = 7$ releasable vesicles at this synapse. It also seems unlikely that γDGG is entirely uncompetitive given its widespread use as a competitive antagonist, although slow kinetics of glutamate unbinding from the receptors combined with rapid dilution of released glutamate might conceivably prevent the γDGG from competing effectively.

The release probability of 0.25 and the maximum response estimated to correspond to seven releasable vesicles can be interpreted to give information about AMPA receptor occupancy. The AMPA receptor occupancy resulting from the release of a single vesicle is unlikely to exceed 100/7 = 14%. This is significantly lower than that estimated at the mossy fiber–GC synapse (DiGregorio et al., 2007), possibly reflecting differences in synapse geometry or receptor properties, but agrees closely with modeling of diffusion and receptor activation at small synapses (Barbour, 2001).

Plotting mean $PPR_{A2/A1}$ against $[Ca^{2+}]_e$ (Fig. 4B_1) highlights the strong correlation between PPR and initial Pr_{site} at the first stimulus. Interestingly, when the time courses of the PPR were plotted at all calcium concentrations, they could be fitted by single exponentials having very similar time constants whose mean was 22.6 ± 2.7 ms (Fig. 4B_2; respectively, $\tau = 20.4$, 25.3, 19.3, and 25.2 ms at 1.5, 2.5, 3, and 4 mM $[Ca^{2+}]_e$). The time course of paired-pulse facilitation was therefore relatively independent of calcium concentration.

To obtain an independent estimate of Pr_{site}, we analyzed the synaptic amplitude fluctuations of compound EPSCs (*A*1) evoked by extracellular stimulation in the GC layer at different $[Ca^{2+}]_e$ (see Materials and Methods). The variance of *A*1 was then determined and plotted against the corresponding mean *A*1 at different $[Ca^{2+}]_e$ ($n = 9$; Fig. 4C_1). The var = *f*(mean *A*1) relationships were well fitted by parabolae (Eq. 1), as expected for a variation in Pr_{site}. From the individual parabolae obtained in each experiment, we determined *Q* and *N* (mean *Q* = 10.8 ± 3.9 pA, mean $N = 72 \pm 64$, $n = 9$). According to Equation 2, $Pr_{site} = 0.26 \pm 0.15$ ($n = 9$) at 2.5 mM $[Ca^{2+}]_e$ in agreement with previous results (Sims and

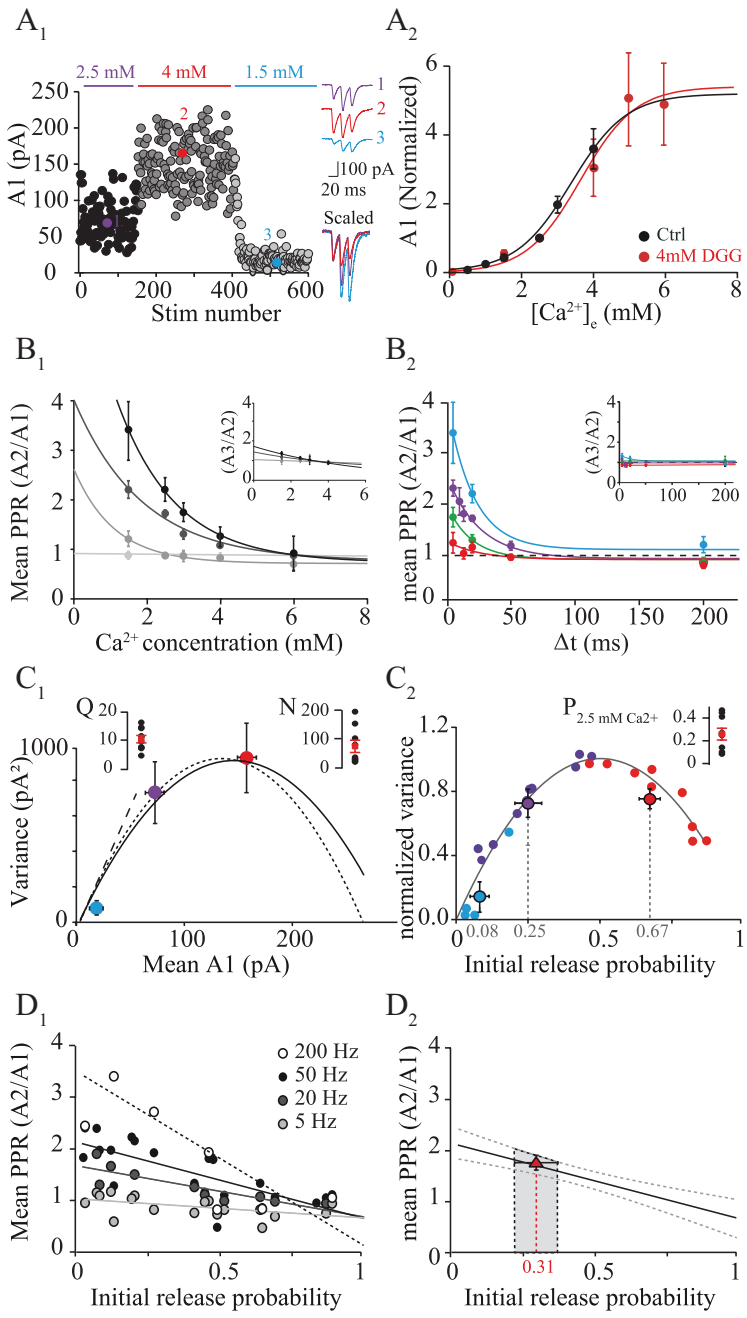

Figure 4. Estimation of initial Pr_{site} at GC–PC synapses. ***A1***, Time course of *A*1 as $[Ca^{2+}]_e$ was varied: 2.5, 4, and 1.5 mM. Insets at right, Averages of 10 traces at 2.5, 4, and 1.5 mM $[Ca^{2+}]_e$. Numbers refer to the time points identified in the time course. ***A2***, Average of mean *A*1 for all experiments as a function of $[Ca^{2+}]_e$, normalized to the value at 2.5 mM $[Ca^{2+}]_e$, in control conditions (black circles; $n = 9$) and in the presence of γDGG (red circles; $n = 5$) fitted by a sigmoid using the following formula: base + max/(1 + exp(($[Ca^{2+}]_{half} - [Ca^{2+}]_e$)/rate))). In control conditions, base = 0.02, max = 5.17, $[Ca^{2+}]_{half} = 3.38$, rate = 0.76; in γDGG, base = 0, max = 5.28, $[Ca^{2+}]_{half} = 3.64$, rate = 0.77. ***B1***, Mean $PPR_{A2/A1}$ at different interstimulus intervals (from black line to light gray line: 5, 20, 200, and 2000 ms), as a function of $[Ca^{2+}]_e$ ($n = 10$) fitted by a single exponential. Inset, Same plot for mean $PPR_{A3/A2}$. ***B2***, Mean $PPR_{A2/A1}$ as a function of interstimulus interval at 1.5 mM (blue, $n = 4$), 2.5 mM (purple, $n = 10$), 3 mM (green, $n = 4$), and 4 mM (red, $n = 9$) $[Ca^{2+}]_e$ fitted by a single exponential. Inset, Same plot for mean $PPR_{A3/A2}$. ***C1***, Variance–mean analysis: example of variance of *A*1 at 1.5, 2.5, and 4 mM $[Ca^{2+}]_e$ for one experiment plotted against mean *A*1 (same cell as in ***A1***) and same color code as in ***C1***. Each experiment was fitted by a parabola using a binomial model (dotted line) or a multinomial model with $CV_I = 0.2$ and $CV_{II} = 0.34$ (solid line). Error bars are an evaluation of the theoretical error of the sample variance (σ_{sample}) for *n* observations. Inset, Individual values of *Q* and *N* ($n = 9$) obtained using the multinomial model. ***C2***, Parabolae for all cells ($n = 9$ cells) normalized at the maximum variance (var_{max}) and maximum amplitude ($N \cdot Q$). Color-filled circles represent the mean variance of *A*1 for all experiments and the corresponding initial Pr_{site} for 1.5 mM (blue, $Pr_{site} = 0.08 \pm 0.08$), 2.5 mM (purple, $Pr_{site} = 0.25 \pm 0.16$), and 4 mM (red, $Pr_{site} = 0.67 \pm 0.17$) $[Ca^{2+}]_e$. Inset, Individual values of Pr_{site} at 2.5 mM Ca^{2+} ($n = 9$). ***D1***, $PPR_{A2/A1}$ of each experiment as a function of initial Pr_{site} estimated in Figure 4*C2* and fitted by a line ($n = 9$ cells) at 5, 20, 50, and 200 Hz. ***D2***, Initial Pr_{site} of GC–PC paired recordings estimated by comparison of their PPR with the data in ***D1***. The estimated Pr_{site} was 0.31 ± 0.26 (red triangle) at 2.5 mM $[Ca^{2+}]_e$.

Table 1. Estimated Pr_{site} using different methods

$[Ca^{2+}]_e$ (mM)	Control	γDGG	Binomial	MPFA ($CV_I = 0.4$, $CV_{II} = 0.4$)	MPFA ($CV_I = 0.2$, $CV_{II} = 0.34$)
1.5	0.08 ± 0.04	0.1 ± 0.04	0.08 ± 0.08	0.07 ± 0.08	0.08 ± 0.08
2.5	0.2	0.26 ± 0.17	0.26 ± 0.15	0.24 ± 0.15	0.25 ± 0.16
4	0.7 ± 0.41	0.57 ± 0.09	0.71 ± 0.14	0.65 ± 0.18	0.67 ± 0.17

Pr_{site} were estimated directly from the $A1 = f([Ca^{2+}]_e)$ relationship in control conditions (first column) and during perfusion of 4 mM γDGG (second column) or from variance–mean plots fitted by a simple binomial model (third column) or a multinomial model (fourth and fifth columns).

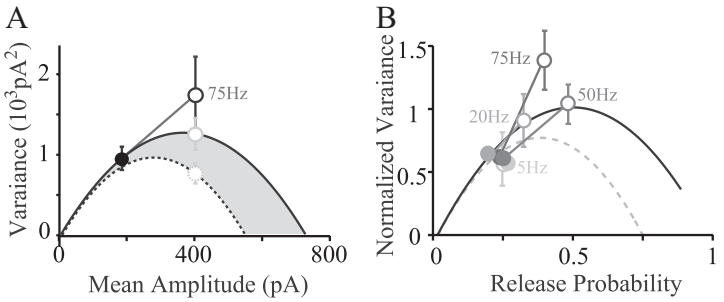

Figure 5. Additional release sites during high-frequency triplet stimulation. ***A***, Example of variance–mean analysis of *A*1 (filled black circle) and *A*2 (open black circle) for one experiment at 75 Hz and 2.5 mM $[Ca^{2+}]_e$. Error bars are σ_{sample} (see Results). Errors of the variance calculated by the bootstrap method were similar ($\sigma_{A2} = 484$ pA^2 vs $\sigma_{sample\ A2} = 403$ pA^2). The parabola was estimated from variance of *A*1 at 1.5, 2.5, and 4 mM $[Ca^{2+}]_e$. Dashed line is the simulated parabola expected if no replenishment of vesicles occurred between *A*1 and *A*2 ($N \cdot P$ vesicles released between *A*1 and *A*2). Open light gray circles, Corresponding points of same mean amplitude on simulated parabolae. ***B***, Averaged variance–mean analysis for *A*2 at increasing frequencies (5–75 Hz, open circles) superimposed on the average parabola of normalized variance–mean analysis for *A*1 (solid line and filled circles). Dashed line is the averaged simulated parabola expected if no replenishment of vesicles occurred between *A*1 and *A*2.

Hartell, 2005). The value of *Q* is also in agreement with the estimate deduced from the amplitudes of asynchronous individual (i.e., monoquantal) events when EPSCs recorded in PCs were evoked after replacement of extracellular Ca^{2+} ions by 5 mM Sr^{2+} (median = 11.5 pA; mean = 13.1 ± 6.3; $n = 1007$ mEPSCs from 6 cells). However, it should be noted that both of these quantal estimates may suffer from error. Detection of mEPSCs is subject to a threshold, and it is likely that some mEPSCs fall below it. The mean of the detected mEPSCs will therefore tend to overestimate the true amplitude. Conversely, the simple binomial model overestimates *Q*, too, in the way that it does not take into account the quantum variability (see below), overestimating *Q* by a factor $(1 + CV_Q^2)$ (Silver, 2003).

Because the simple binomial model does not take into account non-uniformity of Pr_{site} and *Q*, we also analyzed our data using MPFA (Silver, 2003). Quantal parameters were extracted by fitting the var = *f*(mean *A*1) relationships obtained from each experiment with a multinomial (Eq. 3) weighted by the theoretical error of the sample variance for *n* observations (i.e., *n* EPSCs; Fig. 4C_1; see Materials and Methods). The compound CV_Q (i.e., intrasite and intersite variability) was estimated from the amplitudes of asynchronous individual events recorded in 5 mM Sr^{2+}. The value $CV_Q = 0.4$ was similar to those reported for other excitatory synapses (Silver et al., 1998, 2003; Bekkers and Clements, 1999). Because it was not possible to estimate the coefficients of variation of the intrasite (CV_{QI}) and intersite (CV_{QII}) quantal variability, we tested several scenarios that all gave similar estimates of Pr_{site} (Table 1). For the rest of the study, we used $CV_{QI} = 0.2$ (Silver et al., 1996) and thus $CV_{QII} = 0.34$ (see Materials and Methods). Overall, the parameter α introduced in Equation 3 to mimic dispersion of Pr_{site} was found to be scattered (median = 2.11), suggesting that variability in Pr_{site} between the different synaptic release sites was not strongly modified when Pr_{site} was modified. We also estimated the non-uniformity of Pr_{site}: mean CV of $Pr_{site} = 0.47 \pm 0.43$ ($n = 9$). To pool the variance–mean data obtained from multiple experiments, individual plots were normalized by their peak variance (var_{max}) and by $A1_{max}$ given by NQ (Fig. 4C_2; Doussau et al., 2010). Figure 4C_2 shows a summary of the data fitted with the MPFA method and then normalized as explained. In Figure 4C_2, the mean values were $Pr_{site} = 0.08 \pm 0.08$ at $[Ca^{2+}]_e = 1.5$ mM, $Pr_{site} = 0.25 \pm 0.16$ at $[Ca^{2+}]_e = 2.5$ mM and $Pr_{site} = 0.67 \pm 0.17$ at $[Ca^{2+}]_e = 4$ mM. The Pr_{site} values at 1.5, 2.5, and 4 mM $[Ca^{2+}]_e$ from the four different methods used were summarized in Table 1. They all gave very similar results.

The relation between $PPR_{A2/A1}$ and Pr_{site} was constructed from experiments in which the PPR was determined and the Pr_{site} was obtained from a variance–mean analysis (Fig. 4D_1). A linear relationship between $PPR_{A2/A1}$ and Pr_{site} could be established for each frequency of stimulation: for instance, at 50 Hz, $PPR_{A2/A1} = 2.12–1.48\ Pr_{site}$. As already suggested by Figure 3 *C* and *D*, for all frequencies of stimulation PPR > 1, even for $Pr_{site} > 0.5$. The maximum theoretical values of PPR (see model of PPR in Materials and Methods) occur when $Pr_{site} = 1$ at the second stimulus ($P2 = 1$) and thus $PPR_{max} = 1/P1$ ($P1$ corresponding to Pr_{site} at the first stimulus). We found that, at 200 Hz, when $P1 = 0.25$, $PPR_{A2/A1} = 2.8$ (Fig. 4D_1), which is below the theoretical maximum of 4 (i.e., $1/P1 = 1/0.25$). However, when $P1 = 0.65$, $PPR_{A2/A1} = 1.5$ which corresponds to the maximum theoretical value (i.e., $1/0.65 = 1.54$; Fig. 4D_1), suggesting that all release sites were replenished between the two stimuli (in 5 ms). Note that, at 200 Hz, receptor desensitization cannot be excluded and the observed PPR may even underestimate the number of vesicles released. Such a high rate of reloading of individual empty sites would be in the range of the fastest rates reported (Dittman et al., 2000; Crowley et al., 2007). An alternative possibility is that release sites that were nonfunctional (or reluctant) at the first stimulus could contribute to exocytosis at the second stimulus. This hypothesis will be tested below.

Using the calibration relation of Figure 4D_1 between PPR and Pr_{site}, we then estimated that the average Pr_{site} at individual GC-PC connections was 0.31 ± 0.4 at 2.5 mM $[Ca^{2+}]_e$ (Fig. 4D_2). Having obtained several independent estimates that were all consistent with a Pr_{site} of 0.24, we could then combine this value with the estimated Pf_{syn} (0.14) obtained from the stronger connections among the paired recordings (Fig. 1*E*) to estimate the average number of release sites, *n*, at a single GC-PC connection. According to a binomial model, $n = \log(Pf_{syn})/\log(1 - Pr_{site})$, which gives $n = 6.8$ release sites, a number close to the number of docked vesicles reported at this synapse (Xu-Friedman et al., 2001).

Additional release sites during high-frequency triplet stimulation

The combination of a release probability of ~0.24 and paired-pulse facilitation might be expected to lead to rapid exhaustion of the RRP (see above). We therefore investigated whether recruitment of additional release sites (i.e., an increase in the number of functional release sites, *N*) could explain the strongly facilitated

second and third responses (Fig. 4*B*). We used variance–mean plots, which allow a graphical determination of modifications of the binomial parameters *N*, *P*, or *Q* (see Materials and Methods; Clements and Silver, 2000; Humeau et al., 2001). The respective means and variances of the amplitudes of the first (*A*1) and second (*A*2) EPSCs at 2.5 mM $[Ca^{2+}]_e$ were calculated at 5, 20, 50, and 75 Hz (Fig. 5) in five experiments. These were fitted by either Equation 1 (Fig. 5) or Equation 3 (data not shown). Whereas the individual (var_{A1}, mean *A*1) points should fall on the parabola by construction, this is not necessarily the case for the points (var_{A2}, mean *A*2) from the second stimulus. If no change in *Q* occurred, the (var_{A2}, mean *A*2) points should fall on a $var_{A2} = f$(mean *A*2) relationship with the same initial slope (*Q* unchanged) but with a different *N*2, which determines the greater root of the parabola. *N*2 represents the number of release sites at which a vesicle ready for release was available at the time of *A*2. Two extreme situations can arise depending on the rate of vesicle replenishment. If no replenishment occurred between stimuli, then $N2 = N1 \cdot (1 - P1)$; if replenishment were complete, however, $N2 = N1$ (see model in Materials and Methods). Thus, if no extra sites (*N*extra) are recruited between *A*1 and *A*2, the (var_{A2}, mean *A*2) points should fall between the parabolae, corresponding to these two extremes (Fig. 5*A*, gray area). Conversely, if extra sites are recruited between stimuli, the extent of the var $= f$(mean *A*2) relationships may be larger than those determined for *A*1. In this case, its extent would be determined by the number of sites not used at *A*1 (i.e., at which a vesicle remains) + the number of emptied sites replenished between *A*1 and *A*2 + *N*extra sites (see model in Materials and Methods). If *N*extra is greater than the number of nonreplenished sites after *A*1 (var_{A2}, mean *A*2), points may lie above the parabolae for *A*1. Note that the increase in amplitude of *A*2 may combine alterations in *N* and of Pr_{site} (as a result of residual calcium). Because release is probabilistic, *N*2 will vary, and this additional variance may obscure the reduction expected from the vesicle depletion resulting from the first release.

We observed that, up to 50 Hz, although ~25% of the sites would have been emptied at the first stimulus ($Pr_{site} = 0.25$ at 2.5 mM $[Ca^{2+}]_e$), the points for *A*1 and *A*2 both lay on the same parabola (Fig. 5*B*). This suggests that, during the corresponding interstimulus interval, sites emptied at *A*1 have been fully replenished or recruitment of *N*extra sites had compensated those not replenished at the time of *A*2. However, at 75 Hz, *A*2 points clearly deviated from the reference parabola toward higher values (Fig. 5*A*,*B*). To evaluate whether the observed deviations were significant, we calculated the theoretical error of the sample variance (σ_{sample}; Eq. 4) for *A*2 and compared it with the error of the sample variance deduced for the reference relationship at the corresponding mean amplitude (Fig. 5*A*; error bars are σ_{sample}). In four of five experiments, the increase in variance was found to be significant (Student's *t* test, $p < 0.01$). Calculating the error in variance using the bootstrap method (see Materials and Methods) gave the same results (see legend of Fig. 5*A*). Note that, for the statistical comparison, we compared var_{A2} with the estimated variance of the reference parabola, which implied $N2 = N1$, a full replenishment of emptied sites between the two stimuli. Because complete recovery was unlikely, we therefore underestimated the differences in variance at *A*2 and *A*1 of the number of sites not replenished between the two stimuli. If we make the assumption that a frequency-dependent increase of *Q* is unlikely, the points obtained at 75 Hz indicate a significant increase in *N* between the first and second stimuli. By varying *N* in the reference $var_{A1} = f$(mean *A*1) relationship, we estimated the increase in apparent *N* to be between 1.6-fold and 2.2-fold with full replenishment of emptied sites and between 2.1-fold and 2.7-fold without replenishment.

We further investigated this deviation from the reference $var_{A1} = f$(mean *A*1) relationship during high-frequency trains (30 stimuli at 100 Hz; Fig. 6*A*; see Materials and Methods). We verified that EPSC amplitudes were stable across successive trains. The variance (var_{An}) for each stimulus number (An) in the train was calculated and plotted against the corresponding mean amplitude (mean An; Fig. 6*A*). These data were then compared with a reference $var_{A1} = f$(mean *A*1) relationship constructed as a parabola from the observed (var_{A1}, mean *A*1) point and an estimate of *Q* obtained from evoked mEPSCs in the presence of strontium (Fig. 6*A*; Saviane and Silver, 2006). As reported above in the triplet stimulation protocol (Fig. 5), the (var_{An}, mean An) points for the second and third stimuli deviated from the reference parabola, but the variance of the following responses converged toward that of the first response. These findings show that the increased variances of *A*2 and *A*3 and their deviation from the predicted parabola were attributable to an increase in *N*, the number of readily-releasable vesicles, which then declined again as the train continued. It seems likely that the numbers of avail-

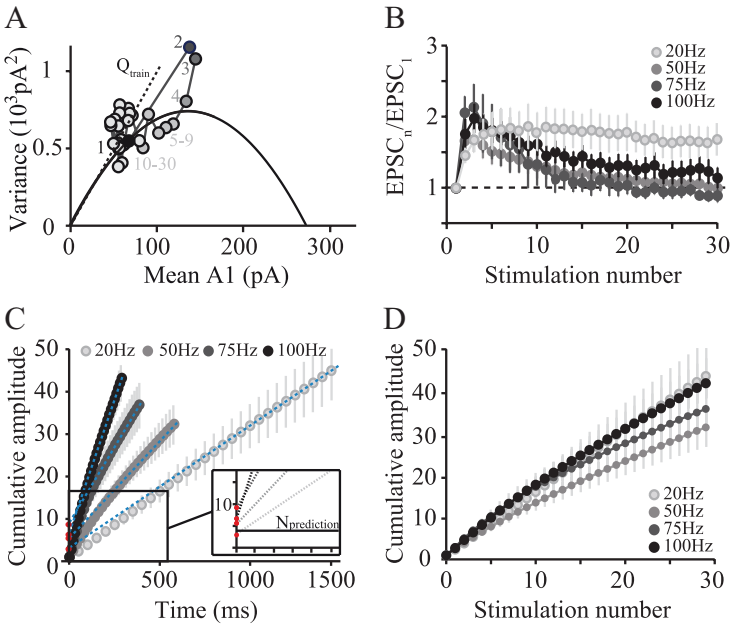

Figure 6. Sustained GC–PC synaptic transmission during trains of stimuli. ***A***, Variance–mean analysis at each stimulus number in 100 Hz trains (numbers identify stimulus number) superimposed on the initial parabola having an initial slope of $Q = 10.8$ pA and based on the variance of the first stimulus (*A*1). ***B***, Average of $EPSC_n/EPSC_1$ ratios in trains at 100, 75, 50, and 20 Hz as a function of stimulus number ($n = 6$). ***C***, Cumulative plot of EPSC amplitudes (normalized to *A*1) during trains at 100, 75, 50, and 20 Hz. Dotted blue line, Linear fit of the steady-state region of the cumulative plot. Red dots, *y*-Axis intercepts of the fits indicating the estimation of *N* (RRP). Inset, Detail of the data within the black rectangle; solid line, prediction of *y*-axis intercept if *N* were constant ($N = 1/P_{release}$). ***D***, Same cumulative plots against stimulus number.

able vesicles varied stochastically in the steady-state phase of the response to trains; such variation may have increased the variance beyond that expected for a small fixed value of *N*.

Ultrafast replenishment during high-frequency activity

Previous studies have shown that fast vesicle replenishment can occur at PF synapses (Crowley et al., 2007). The rate of this process is calcium dependent at climbing fiber synapses on PCs (Dittman and Regehr, 1998), and this has been extrapolated to models of transmission at PF synapses (Dittman et al., 2000). We therefore investigated the rate of replenishment of emptied site with release-ready vesicles during trains of stimuli at different frequencies. As can be seen in Figure 6*B*, responses first increased in amplitude before slowly decaying back to a level comparable with the first response, the exception being 20 Hz trains, during which facilitation was maintained throughout. These data offer several insights. First, the initial large responses presumably reflect emptying of the RRP of vesicles. Second, because the steady-state amplitude is smaller than the largest responses observed, it seems likely that release site replenishment is the limiting process during the late portion of the trains. To quantify these two aspects of the release process, we calculated the cumulative EPSC amplitude for each experiment, normalized by the first response (Fig. 6*C*). A line was fitted to the steady-state region of the plot and extrapolated to time 0. This intercept gives an estimate of the size of the initial RRP (or *N*) if Pr_{site} during trains is maximal (Schneggenburger et al., 2002). The ratio of the amplitude of the first EPSC in the train to the RRP size is also an estimate of the initial release probability. Finally, the slope of the asymptotic fitted line can be used to calculate the relative rate of release site replenishment (Schneggenburger et al., 1999, 2002). Our results are reported after normalization to *A*1 in each experiment. Figure 6*C* shows that both the slope of the linear fits and the size of the initial RRP (*N*) increased at higher frequencies of stimulation. At 20, 50, 75, and 100 Hz, the $r \cdot t + N$ functions, with t in milliseconds, were respectively, $0.028 \cdot t + 3.23$, $0.046 \cdot t + 5.72$, $0.07 \cdot t + 9.66$, and $0.12 \cdot t + 7.19$. The greater slope of the steady-state region at high frequency indicated accelerated replenishment, increasing fourfold (from 0.028 to 0.12 per millisecond) between 20 and 100 Hz. Interestingly, at higher frequencies, the replenishment rate appeared to be approximately proportional to the rate of release, because similar amplitude time courses with respect to stimulus number were observed at different frequencies (Fig. 6*D*).

Surprisingly, we also observed that the apparent size of the RRP (given by the intercept of the back-extrapolated fit of the linear portion of cumulative plot with *y*-axis) increased with stimulation frequency and thus that the ratio $A1/RRP_{frequency}$ (which is an estimate of Pr_{site} at the time of first stimulus) decreased. RRP/*A*1 in the cumulative plots gives a value close to 4, at low frequencies consistent with the estimate of $Pr_{site} = 0.25$, with higher values (~8) occurring with higher frequencies. Thus, estimated RRP and therefore *N* increased approximately twofold between 20 and 100 Hz (Fig. 6*C*), confirming the deduction made using mean–variance analysis.

Because at 100 Hz the An were ~1.25 times amplitude of *A*1 (Fig. 6*B*), the rate of replenishment was $\sim 1.25 \cdot n$ sites $\cdot Pr_{site} = 1.25 \cdot 6.8 \cdot 0.25 = \sim 2$ vesicles in 10 ms. We assume that facilitation by residual calcium reaches high levels in the steady-state phase of the trains. If true, each stimulus will release all release-ready vesicles. If replenishment is described by a simple exponential time course, the number of replenished sites $= n(1 - \exp(-t/\tau))$, and we can calculate the time constant (during 100 Hz trains) from $\tau = -10$ ms$/\ln(1 - 2/n)$. Depending on whether we take $n = \sim 7$ (the estimate for control conditions) or $n = \sim 14$ (i.e., assuming that n doubles because of the recruitment of sites), we obtain $\tau = 30$ or 65 ms.

Discussion

Our experiments enable us to quantify at least approximately several parameters of transmission at the GC–PC synapse. We shall first describe its operation at 2.5 mM $[Ca2^+]_e$ and 34°C, conditions chosen to facilitate comparison with previous work, before evaluating the physiological implications of our findings.

Modest PPR

We found modest paired-pulse facilitation (Figs. 1, 3, 4) that decayed with a single exponential of 25–30 ms. These properties were identical in paired recordings and in the experiments using extracellular stimulation; in the latter, we also showed that the decay of facilitation was quite insensitive to the extracellular calcium concentration. These properties differ significantly from those of some previous studies (Atluri and Regehr, 1996; but see Foster et al., 2005; Sims and Hartell, 2005), which reported higher PPR values with a slower, calcium-dependent decay. The reasons for these differences remain unclear. The use of molecular layer stimulation in most previous studies may contribute, as we have reported previously higher PPR values with this method (Isope and Barbour, 2002), but this difference is not systematic (Sims and Hartell, 2005). A strong gradient of PPR with respect to stimulation position in the molecular layer has been reported (Foster et al., 2005), but the absence of any correlation between PPR and EPSC decay time constant in our paired recordings suggests they were not subject to such a positional gradient, because EPSCs of synapses higher in the molecular layer tend to display longer time constants (Roth and Häusser, 2001). In the paired recordings, no evidence was obtained that either PPR or release probability was correlated with EPSC amplitude, once the effects of noise on the analyses were taken into account (Fig. 2; see simulation in the study of Isope and Barbour, 2002, their Fig. 5). We note that the present recordings were obtained with extracellular stimulation lateral to the PC at distances precluding activation of ascending axons or local GCs. The low PPR we obtain can therefore not be attributed to differential properties of ascending axon inputs (Sims and Hartell, 2006); this confirms our previous results in the adult rat (Isope and Barbour, 2002).

Release probability

The PPR is widely reported to be related to the release probability, a finding we confirm with the linear relation reported here (Fig. 4). Because we found a lower PPR than in previous reports, we expected to obtain correspondingly higher estimates of release probability, which we measured through multiple experimental approaches. Activated from the resting state, the synapse displayed a low failure probability (failure to release any vesicles, Pf_{syn}), estimated by histogram analysis of the paired recordings to be 15% or less. The dependence of EPSC amplitude (elicited by extracellular stimulation in the GC layer) on the extracellular calcium concentration indicated that the control probability of release (Pr_{site}) was ~0.25 of the maximum; the insensitivity of this relation to the low-affinity AMPA receptor antagonist γDGG suggested that receptor saturation did not affect this determination (assuming, however, that the antagonist was at least partially competitive during transmission at this synapse). Combining the Pf_{syn} from paired recordings with the estimated Pr_{site} yielded an estimate of the RRP of ~7 vesicles, which is in perfect agreement with an electron microscopic count of the number of docked

vesicles at this synapse (Xu-Friedman et al., 2001). This estimated release probability was corroborated by using variance–mean analysis of compound EPSCs, which provided an almost identical value of Pr_{site} (0.25). Use of the more sophisticated MPFA yielded similar values to the simple binomial analysis (Table 1) but suggested that release probability might be quite heterogeneous ($CV_{Pr} = 0.47$). Because neither the release probability estimates nor the PPRs from the paired recordings displayed significant variation in excess of that expected from the action of noise in the analyses, it is likely that the heterogeneity of release probability is between release sites of individual synapses rather than between synapses. Such intrasynaptic heterogeneity provides a plausible mechanism for the apparent recruitment of release sites we observe (see below). Compared under similar experimental conditions ($[Ca^{2+}]_e$ and temperature), the Pr_{site} we have determined is thus several fold greater than previous estimates ($Pr_{site} = 0.08$ and $Pr_{syn} = 0.44$ at 1.5 mM $[Ca^{2+}]_e$ in our study; $Pr_{site} = 0.02$ and $Pr_{syn} = 0.13$ in the study of Foster et al., 2005).

Recruitment of release sites

Two strands of evidence suggest that the apparent number of release sites—equivalent to the number of releasable vesicles—can increase during high-frequency stimulation. The first is the deviation of the second and the third responses from the reference variance–mean parabola, which is most simply explained by a variation in *N*. The second is the estimate of the RRP derived from the cumulative EPSC amplitude plots during the trains. In both cases, the apparent number of release sites increases approximately twofold. The size of the apparent recruitment (twofold at 75 Hz, equivalent to an interval of ~13 ms) and its frequency dependence (apparent at 75 Hz but not 50 Hz), coupled with the simple exponential kinetics of paired-pulse facilitation, strongly suggest that the recruitment is an integral, indeed dominant, aspect of the facilitation mechanism. Non-uniformity of release probability across sites at a synapse could explain this phenomenon. We propose that only high-release-probability sites respond effectively to the first stimulus but that facilitatory mechanisms—for instance, binding of residual calcium to the release machinery—at low-probability sites then enables them to respond to the second stimulus. The non-uniformity of release probabilities could reflect distance of the release sites from calcium channels. The kinetics and calcium independence of the PPR would be consistent with a mechanism as simple as binding of calcium to a single site. It is unclear whether the putative low-probability sites can be recruited at the first stimulus when calcium is raised or whether their recruitment always necessitates a conditioning pulse, as has been reported at the calyx of Held (Sakaba and Neher, 2001; Neher, 2006). If a conditioning pulse is required, the conversion of reluctant vesicles into active ones must occur rapidly but not instantaneously, thus affecting the time course of the PPR at the smaller interpulse intervals. However, the time course of PPR displayed remarkably simple kinetics except at the very short intervals in which spike propagation failure can also occur.

Fast vesicle replenishment

Our results indicate that vesicle replenishment becomes limiting during trains at frequencies higher than ~20 Hz (at 2.5 mM $[Ca^{2+}]_e$), because EPSC amplitudes decrease below their maximum, whereas facilitatory residual calcium would be expected to increase toward a plateau (Fig. 6*B*). This enables us to estimate the rate of replenishment. We find that the rate increases with the frequency of stimulation, reaching the equivalent of one control EPSC, corresponding to approximately two vesicles per stimulus at 100 Hz or one vesicle in 5 ms. We also calculated a replenishment time constant of 30 or 65 ms (depending on the assumed number of release sites in operation) at 100 Hz; this may be compared with the one vesicle per 20 ms reported for the GC–interneuron synapse (Crowley et al., 2007). Recruitment of release sites during trains may enhance the process of supplying vesicles to the active zone. The fact that similarly sized EPSCs can be maintained as the frequency of trains increases (Fig. 6*B*) suggests that the rate of replenishment adapts to compensate for the increased release. One possible mechanism for this observation could be calcium-dependent recovery from depression. This process has been clearly demonstrated at the climbing fiber–PC connection, in which a rapid, calcium-dependent phase of recovery from paired-pulse depression is observed (Dittman and Regehr, 1998). The process has also been suggested to operate at PF–PC synapses on the basis of modeling of responses to trains (Dittman et al., 2000), although no direct evidence of a time-dependent recovery phase exists for this connection.

After a period of inactivity, vesicle supply mechanisms will have equilibrated and may be able to furnish initial rates of replenishment exceeding those occurring in the steady state, when supply gradients have been established. Such enhanced initial replenishment could help explain the apparent absence of depressing mechanisms in the paired recordings, in which the responses to a second stimulus were independent of whether the first stimulus triggered release of a vesicle or not (Fig. 1). Both vesicle depletion and receptor desensitization would normally reduce the response to the second stimulus if there was release at the first, but no such effect was observed, suggesting that neither mechanism was significant. However, when a release occurred, >25% of vesicles would have been released (failures were excluded in this case); these were therefore presumably essentially replenished in 10 ms.

Although it is possible that accelerated replenishment might underlie the early increase in the number of releasable vesicles during high-frequency stimulation, for this to be the only mechanism would require an extremely fast, maybe unrealistically fast, process, and its activity-dependent regulation would also need to allow a twofold "overshoot" of the control response that nevertheless decays away rapidly. We believe that it is unlikely that this combination of properties would be satisfied and therefore favor separate mechanisms for the apparent recruitment/facilitation and for replenishment.

Physiological implications

GCs are able to discharge action potentials at frequencies exceeding 1 kHz *in vivo* (Chadderton et al., 2004; Jörntell and Ekerot, 2006; Rancz et al., 2007; Arenz et al., 2008), but it was not known how such high rates were transmitted to the postsynaptic PC. We show that, at both low (20 Hz) and high (up to 700 Hz) rates of stimulation, the transmission facilitates and can be maintained during long trains (Figs. 3, 6) at 2.5 mM $[Ca^{2+}]_e$. The postsynaptic response to a burst is therefore much stronger and less variable than that to a single action potential or that predicted from simple summation of single action potential responses. For example, three action potentials at 400 Hz elicit a compound EPSC fourfold greater than that after a single action potential; the CV is similarly reduced fourfold (Fig. 3*A*).

Several of our experiments, including high-frequency stimulations, were performed at 2.5 mM $[Ca^{2+}]_e$, to facilitate comparisons with previous literature. How might our results be extrapolated to a more physiological free calcium concentration ~1.5 mM $[Ca^{2+}]_e$ (Silver and Erecińska, 1990; see also Rancz et

al., 2007)? We measured the release probability directly at this concentration and found a value of 0.08 per site (Pr_{site}), translating to 0.44 for release of at least one vesicle at a synapse (Pr_{syn}). Frequency-dependent facilitation is stronger at the lower calcium concentration (Fig. 4). We furthermore expect that recruitment of release sites and acceleration of vesicle replenishment will enable even higher frequencies of activity to be transmitted with high fidelity at the lower extracellular calcium concentration. Our experiments on pairs from the young and the adult suggest that the basic synaptic properties are essentially preserved between the two developmental stages.

In summary, our results show how the GC–PC is particularly well adapted to transfer high-frequency activity from GCs to PCs, thereby preserving the high dynamic range of the mossy fiber/GC system.

References

Arenz A, Silver RA, Schaefer AT, Margrie TW (2008) The contribution of single synapses to sensory representation in vivo. Science 321:977–980.

Atluri PP, Regehr WG (1996) Determinants of the time course of facilitation at the granule cell to Purkinje cell synapse. J Neurosci 16:5661–5671.

Augustine GJ, Neher E (1992) Calcium requirements for secretion in bovine chromaffin cells. J Physiol 450:247–271.

Barbour B (2001) An evaluation of synapse independence. J Neurosci 21:7969–7984.

Barbour B, Isope P (2000) Combining loose cell-attached stimulation and recording. J Neurosci Methods 103:199–208.

Bekkers JM, Clements JD (1999) Quantal amplitude and quantal variance of strontium-induced asynchronous EPSCs in rat dentate granule neurons. J Physiol 516:227–248.

Bidoret C, Ayon A, Barbour B, Casado M (2009) Presynaptic NR2A-containing NMDA receptors implement a high-pass filter synaptic plasticity rule. Proc Natl Acad Sci USA 106:14126–14131.

Brown SP, Brenowitz SD, Regehr WG (2003) Brief presynaptic bursts evoke synapse-specific retrograde inhibition mediated by endogenous cannabinoids. Nat Neurosci 6:1048–1057.

Brunel N, Hakim V, Isope P, Nadal JP, Barbour B (2004) Optimal information storage and the distribution of synaptic weights: perception versus Purkinje cell. Neuron 43:745–757.

Chadderton P, Margrie TW, Häusser M (2004) Integration of quanta in cerebellar granule cells during sensory processing. Nature 428:856–860.

Clements J (1991) Quantal synaptic transmission? Nature 353:396.

Clements JD (2003) Variance–mean analysis: a simple and reliable approach for investigating synaptic transmission and modulation. J Neurosci Methods 130:115–125.

Clements JD, Silver RA (2000) Unveiling synaptic plasticity: a new graphical and analytical approach. Trends Neurosci 23:105–113.

Coesmans M, Weber JT, De Zeeuw CI, Hansel C (2004) Bidirectional parallel fiber plasticity in the cerebellum under climbing fiber control. Neuron 44:691–700.

Crowley JJ, Carter AG, Regehr WG (2007) Fast vesicle replenishment and rapid recovery from desensitization at a single synaptic release site. J Neurosci 27:5448–5460.

DiGregorio DA, Rothman JS, Nielsen TA, Silver RA (2007) Desensitization properties of AMPA receptors at the cerebellar mossy fiber granule cell synapse. J Neurosci 27:8344–8357.

Dittman JS, Regehr WG (1998) Calcium dependence and recovery kinetics of presynaptic depression at the climbing fiber to Purkinje cell synapse. J Neurosci 18:6147–6162.

Dittman JS, Kreitzer AC, Regehr WG (2000) Interplay between facilitation, depression, and residual calcium at three presynaptic terminals. J Neurosci 20:1374–1385.

Doussau F, Humeau Y, Benfenati F, Poulain B (2010) A novel form of presynaptic plasticity based on the fast reactivation of release sites switched off during low-frequency depression. J Neurosci 30:16679–16691.

Dugué GP, Dumoulin A, Triller A, Dieudonné S (2005) Target-dependent use of co-released inhibitory transmitters at central synapses. J Neurosci 25:6490–6498.

Efron B, Tibshirani R (1993) An introduction to the bootstrap. London: Chapman and Hall.

Ekerot CF, Jörntell H (2001) Parallel fibre receptive fields of Purkinje cells and interneurons are climbing fibre-specific. Eur J Neurosci 13:1303-1310.

Foster KA, Crowley JJ, Regehr WG (2005) The influence of multivesicular release and postsynaptic receptor saturation on transmission at granule cell to Purkinje cell synapses. J Neurosci 25:11655–11665.

Hansel C, Linden DJ, D'Angelo E (2001) Beyond parallel fiber LTD: the diversity of synaptic and non-synaptic plasticity in the cerebellum. Nat Neurosci 4:467–475.

Humeau Y, Vitale N, Chasserot-Golaz S, Dupont JL, Du G, Frohman MA, Bader MF, Poulain B (2001) A role for phospholipase D1 in neurotransmitter release. Proc Natl Acad Sci USA 98:15300–15305.

Humeau Y, Popoff MR, Kojima H, Doussau F, Poulain B (2002) Rac GTPase plays an essential role in exocytosis by controlling the fusion competence of release sites. J Neurosci 22:7968–7981.

Humeau Y, Doussau F, Popoff MR, Benfenati F, Poulain B (2007) Fast changes in the functional status of release sites during short-term plasticity: involvement of a frequency-dependent bypass of Rac at *Aplysia* synapses. J Physiol 583:983–1004.

Isope P, Barbour B (2002) Properties of unitary granule cell→Purkinje cell synapses in adult rat cerebellar slices. J Neurosci 22:9668–9678.

Ito M (2006) Cerebellar circuitry as a neuronal machine. Prog Neurobiol 78:272–303.

Jörntell H, Ekerot CF (2002) Reciprocal bidirectional plasticity of parallel fiber receptive fields in cerebellar Purkinje cells and their afferent interneurons. Neuron 34:797–806.

Jörntell H, Ekerot CF (2006) Properties of somatosensory synaptic integration in cerebellar granule cells *in vivo*. J Neurosci 26:11786–11797.

Kim J, Alger BE (2001) Random response fluctuations lead to spurious paired-pulse facilitation. J Neurosci 21:9608–9618.

Larkman A, Stratford K, Jack J (1991) Quantal analysis of excitatory synaptic action and depression in hippocampal slices. Nature 350:344–347.

Lev-Ram V, Wong ST, Storm DR, Tsien RY (2002) A new form of cerebellar long-term potentiation is postsynaptic and depends on nitric oxide but not cAMP. Proc Natl Acad Sci USA 99:8389–8393.

Markram H, Lübke J, Frotscher M, Roth A, Sakmann B (1997) Physiology and anatomy of synaptic connections between thick tufted pyramidal neurones in the developing rat neocortex. J Physiol 500:409–440.

Matsukawa H, Wolf AM, Matsushita S, Joho RH, Knöpfel T (2003) Motor dysfunction and altered synaptic transmission at the parallel fiber-Purkinje cell synapse in mice lacking potassium channels Kv3.1 and Kv3.3. J Neurosci 23:7677–7684.

Mintz IM, Sabatini BL, Regehr WG (1995) Calcium control of transmitter release at a cerebellar synapse. Neuron 15:675–688.

Neher E (2006) A comparison between exocytic control mechanisms in adrenal chromaffin cells and a glutamatergic synapse. Pflugers Arch 453:261–268.

Oleskevich S, Clements J, Walmsley B (2000) Release probability modulates short-term plasticity at a rat giant terminal. J Physiol 524:513–523.

Perkel DJ, Hestrin S, Sah P, Nicoll RA (1990) Excitatory synaptic currents in Purkinje cells. Proc Biol Sci 241:116–121.

Pyle JL, Kavalali ET, Piedras-Rentería ES, Tsien RW (2000) Rapid reuse of readily releasable pool vesicles at hippocampal synapses. Neuron 28:221–231.

Rancz EA, Ishikawa T, Duguid I, Chadderton P, Mahon S, Häusser M (2007) High-fidelity transmission of sensory information by single cerebellar mossy fibre boutons. Nature 450:1245–1248.

Reid CA, Clements JD (1999) Postsynaptic expression of long-term potentiation in the rat dentate gyrus demonstrated by variance–mean analysis. J Physiol 518:121–130.

Roth A, Häusser M (2001) Compartmental models of rat cerebellar Purkinje cells based on simultaneous somatic and dendritic patch-clamp recordings. J Physiol 535:445–472.

Sakaba T, Neher E (2001) Quantitative relationship between transmitter release and calcium current at the calyx of held synapse. J Neurosci 21:462–476.

Salin PA, Malenka RC, Nicoll RA (1996) Cyclic AMP mediates a presynaptic form of LTP at cerebellar parallel fiber synapses. Neuron 16:797–803.

Saviane C, Silver RA (2006) Fast vesicle reloading and a large pool sustain high bandwidth transmission at a central synapse. Nature 439:983–987.

Saviane C, Silver RA (2007) Estimation of quantal parameters with

multiple-probability fluctuation analysis. Methods Mol Biol 403:303–317.

Schneggenburger R, Meyer AC, Neher E (1999) Released fraction and total size of a pool of immediately available transmitter quanta at a calyx synapse. Neuron 23:399–409.

Schneggenburger R, Sakaba T, Neher E (2002) Vesicle pools and short-term synaptic depression: lessons from a large synapse. Trends Neurosci 25:206–212.

Silver IA, Erecińska M (1990) Intracellular and extracellular changes of $[Ca^{2+}]$ in hypoxia and ischemia in rat brain in vivo. J Gen Physiol 95:837–866.

Silver RA (2003) Estimation of nonuniform quantal parameters with multiple-probability fluctuation analysis: theory, application and limitations. J Neurosci Methods 130:127–141.

Silver RA, Cull-Candy SG, Takahashi T (1996) Non-NMDA glutamate receptor occupancy and open probability at a rat cerebellar synapse with single and multiple release sites. J Physiol 494:231–250.

Silver RA, Momiyama A, Cull-Candy SG (1998) Locus of frequency-dependent depression identified with multiple-probability fluctuation analysis at rat climbing fibre-Purkinje cell synapses. J Physiol 510:881–902.

Silver RA, Lubke J, Sakmann B, Feldmeyer D (2003) High-probability uniquantal transmission at excitatory synapses in barrel cortex. Science 302:1981–1984.

Sims RE, Hartell NA (2005) Differences in transmission properties and susceptibility to long-term depression reveal functional specialization of ascending axon and parallel fiber synapses to Purkinje cells. J Neurosci 25:3246–3257.

Sims RE, Hartell NA (2006) Differential susceptibility to synaptic plasticity reveals a functional specialization of ascending axon and parallel fiber synapses to cerebellar Purkinje cells. J Neurosci 26:5153–5159.

Xu-Friedman MA, Harris KM, Regehr WG (2001) Three-dimensional comparison of ultrastructural characteristics at depressing and facilitating synapses onto cerebellar Purkinje cells. J Neurosci 21:6666–6672.

4.4 SUPPLEMENTARY RESULTS

Visualizing the existence of a reluctant pool is challenging, particularly if the vesicles share similar properties with the vesicles of the RRP (same quantum size, activation of identical postsynaptic receptors etc…). In this first article it was suggested that reluctant pool could be recruited as soon as the second EPSC during paired or triplet pulses, and at frequency higher than 50 Hz (but probably not or very weakly at 20Hz, and not at all at 5Hz).

The aim of this supplementary result is to show a more direct illustration of the existence of reluctant vesicles at the parallel fibre to Purkinje cell synapse.

Frédéric Doussau used a low frequency depression (LFD) protocol previously used in the aplysia to silent either the RRP only or both the RRP and the reluctant pool. Low frequency stimulation induces presynaptic plasticities that can silent specific vesicle release sites. In the invertebrate, it was shown that the mechanism is PKA and synapsin-dependent (Doussau et al., 2010), however LFD was never investigated at the parallel fibre to Purkinje cell synapse. Frédéric Doussau found that when other forms of plasticities are blocked, LFD can be observed at parallel fibre to Purkinje cell synapses (Figure $29A_1$, $29A_2$).

He used this tool to silence the RRP (which is recruited with single pulses), in order to study the properties of the reluctant vesicle pool (which is recruited only during high frequency bursts and trains).

4.4.1 SUPPLEMENTARY METHODS

All methods are similar to (Valera et al., 2012), except that animals were P18 to P25 C57BL/6 or CD1 mice and that stimulation was performed in the molecular layer 200 µm to 500µm laterally to the dendritic tree of Purkinje cells with monopolar borosilicate electrodes.

Initial baseline can be recorded by using stimulations at 0.033 Hz (10 stimulations). Low frequency depression was induced by performing 300 pulses at 2Hz (Δt=500ms, Figure $29B_1$ left and middle panel). 500ms after the 300^{th} pulse, a train of 50 stimuli at 100Hz was performed (test train; Figure $29B_1$ right panel).

We addressed the properties of the reluctant pool. Although the exact characteristics of the reluctant pool are not known, we assumed that the reluctant pool could be affected by LFD too as soon as it was involved in the LFD protocol.

In a second protocol, low frequency depression was induced by performing 100 triplet of pulses instead of single pulses (total = 300 pulses in both cases). We performed 3 set of experiments using 3 different frequencies of triplets, (Figure $29B_2$). A test train of 50 stimuli at 100Hz was performed 500ms after the 300^{th} pulse to see if the reluctant pool was affected by this LFD protocol (Figure $29B_2$ right panel).

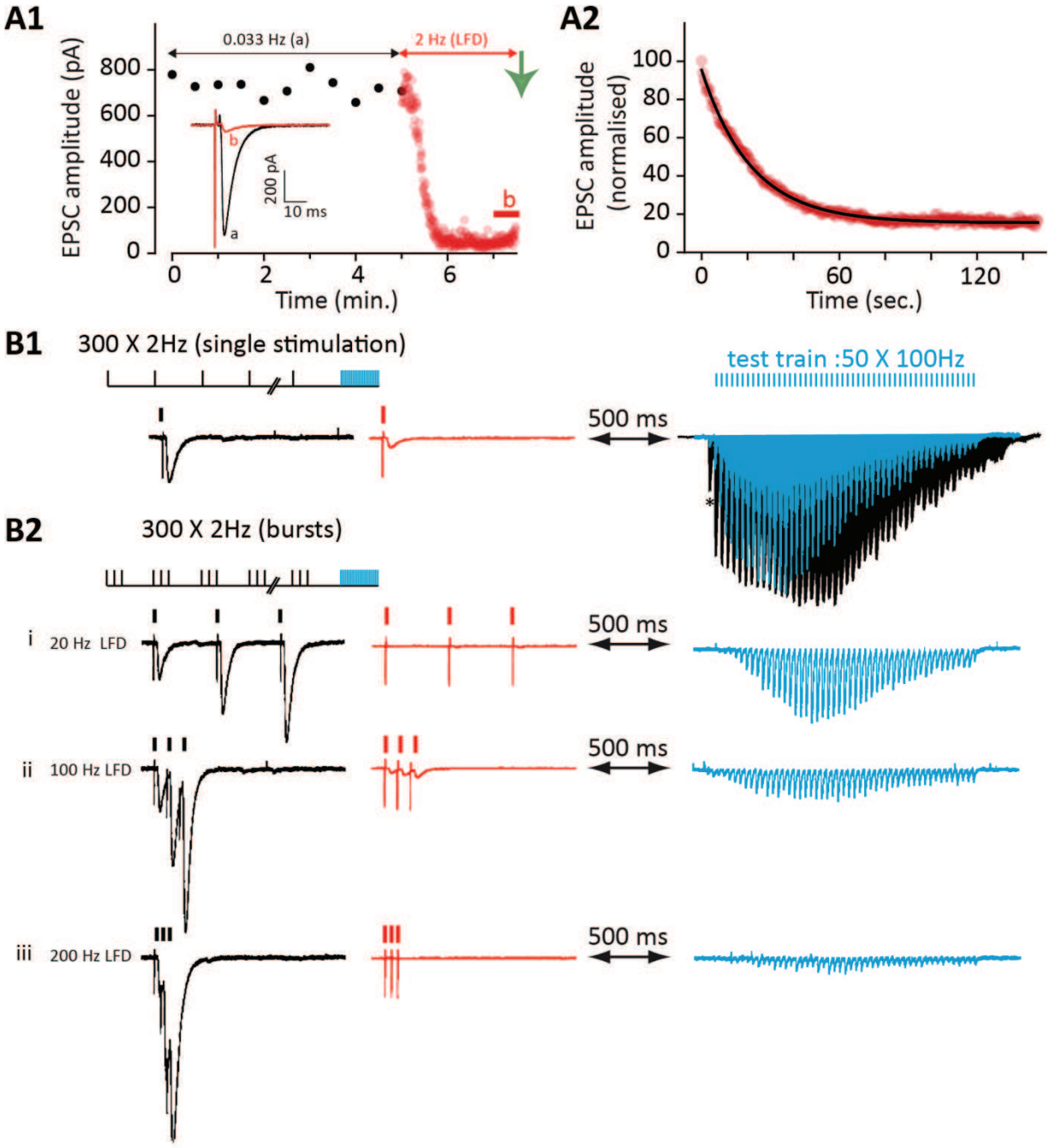

Figure 29 : Supplementary results. Two distinct low frequency depression protocols silence either basal release pool or both basal and reluctant release pool.

A : Low frequency depression protocol (LFD). $\mathbf{A_1}$: EPSCs are recorded in whole cell patch clamped Purkinje cells while parallel fibres are stimulated. Pharmacology is similar to (Valera et al., 2012). Baseline (black circles) consist in 7 stimulations at 0.033 Hz. LFD protocol consist in 300 stimulations at 2Hz (Dt = 500ms; red circles). Stimulations can be either single pulse (see B_1), or triple pulses (see B_2, triple pulses at 20 Hz, 100 Hz or 200 Hz). LFD protocol is followed 500ms after the last by 50 pulses at 100 Hz to verify is vesicular release can still occur. Inset represent the average EPSC during baseline (a, black trace) and during the last 15 EPSC (b, red trace). $\mathbf{A_2}$: EPSCs size follow exponential decay during LFD protocol; t = 21.7 s; steady state = 15.46% of initial EPSC.

$\mathbf{B_1}$: Blue trace is the post-LFD test train. Black trace is a pre-LFD control train. After single pulse LFD, initial EPSC (black trace, left panel) is reduced by 85% (red trace, middle panel), but 100 Hz train of 50 pulses can still recruit reluctant sites (blue trace, right panel. Please note that recruitement of reluctant sites starts only at the second pulse, and might be complete arounf the 7th-8th pulse). $\mathbf{B_{2i}}$-$\mathbf{B_{2iii}}$: Similar protocol with bursts instead of single pulses, at 20Hz (B_{2i}), 100 Hz (B_{2ii}), 200 Hz (B_{2iii}). Left, middle and right panels as in B_1. Recruitement of reluctant sites is weaker, beacause some of the reluctant sites were silenced during LFD protocol. At 200 Hz, final test train could not recruit more vesicles because all reluctant vesicles were silenced during LFD.

4.4.2 SUPPLEMENTARY RESULTS

When only the RRP was inactivated through LFD, a high frequency burst could recruit supplementary (reluctant) vesicles (Figure 29B_1 right panel). Compared to control train (red trace), the first event of the test train is strongly depressed, but neurotransmitter release can be observed after the second stimuli. These results suggest that vesicular release is still possible, but only for frequencies trains. The fact that the synapse was depressed could be due to pool depletion. However the same protocol at higher frequency do not induce LFD, although the number of released vesicle is superior, demonstrating that LFD is an active silencing mechanism.

When a stimulation protocol that is known to recruit reluctant pool was used for the LFD induction - i.e., single pulses were replaced by triple pulses at 20 Hz, 100 Hz and 200 Hz, repeated every 500ms. According to (Valera et al., 2012), 100Hz triplet should strongly recruit the reluctant vesicles - , we hypothesised that both the RRP and the reluctant sites will be affected by LFD. Indeed when LFD was induced at intermediate frequency (20 Hz, Figure 29B_{2i}), some vesicles could still be released during a train, although vesicular release occurs only after 3-4 pulses only. It suggests that some vesicles of the reluctant pool were not available anymore. When LFD was induced at higher frequency (200 Hz, Figure 29B_{2iii}), no more vesicular release occurred during the test train, although the total amount of vesicles released during depression protocol was similar (for instance paired-pulse ratio $EPSC_3/EPSC_1$ at 100 Hz = 3.52; paired-pulse ratio $EPSC_3/EPSC_1$ at 200 Hz = 3.6, and cumulative plot was similar in both cases)

These results suggest that vesicles recruited during the test train following LFD belong to a distinct pool that was not silenced by the LFD protocols with single pulses or low frequencies, but that was silenced at 200Hz. These results are consistent with our article, in which we suggest that only the RRP is used at low frequencies, whereas during bursts, reluctant vesicles can be recruited. Higher frequencies recruit more vesicles, and paired-pulse facilitation probably reflects the use of reluctant vesicles between $EPSC_1$ and $EPSC_2$, and thus corresponding to an increase in N.

5 ARTICLE II

5.1 PRESENTATION OF THE SECOND ARTICLE

When Heloïse Cruveiller, a previous PhD student, started her thesis project in 2007, she performed preliminary experiments in which Golgi cells located close to a zebrin border were recorded. She performed stimulations in the granular layer, using glass electrodes, to see if granule cells within the same zebrin band were more strongly connected than granule cells located outside the band. These experiments were complicated to achieve, as moving precisely the stimulation pipette was difficult.

In 2012, we decided to reproduce these initial results, by improving the stimulation technique. We used a glutamate uncaging stimulation system which allowed us to simultaneously record a Golgi cell and stimulate granule cells at precise software-controlled coordinates. Our initial working hypothesis was that zebrin borders were defining functional modules in the cerebellum. Even though this initial hypothesis was not exact, we used zebrin bands as precise markers to accurately locate the recorded Golgi cell and the stimulated granule cells. I further spent more than one year to program a software allowing automated analysis of the mappings. Now, this software is functional and allows us to perform very fast analyses.

After mapping the Golgi cell input patterns, we decided to study the organisation of the granular cell connections to other cell types of the cerebellar cortex, that is, Purkinje cells and molecular layer interneurons. Fortunately, those cell types showed particularly interesting input patterns.

Those results are presented in this second article, which is not in its definitive form.

5.2 FUNCTIONAL PRECISIONS ABOUT OUR REGION OF INTEREST

5.2.1 MEDIOLATERAL AND ANTEROPOSTERIOR POSITION OF THE RECORDINGS

During my PhD, all the recordings were performed using horizontal slices, essentially in lobules III to VII. Occasionally, I could record cells in the lobule II or VIII, but lobule VIII was always avoided because of the possible presence of unipolar brush cells that could complicate the analyses. More precisely, all the recordings performed in the first article were in the whole range of the cerebellar vermis (between P4+ zebrin bands on each side), even though the precise location was never recorded. For the second article, the precise location of the cell was known, and all the recordings were performed in lobules III or IV, between the two P2+ bands. This region is actually restricted, measuring 700 µm in width at most.

Recording such a narrow region minimizes possible biological variability. However, we must keep in mind that, since this region is dedicated of the processing of spinocerebellar information, the observed mechanisms might present specificities.

5.2.2 INPUTS AND OUTPUTS IN OUR REGION OF INTEREST

All the description below is summarized in Figure 30. Numerous abbreviations are used only in this section and in figure 30, and are listed here:

AICG : Anterior interstitial cell group
AIN : Anterior interposed nucleus
c-MAO : caudal part of the medial accessory olive
DC : Dorsal cap of Kooy
d-DAO : dorsal fold of the dorsal accessory olive
DLH : Dorsolateral hump (of the AIN)
DLP : Dorsolateral protuberance (of the FN)
DM : Dorsomedial subnucleus of the principal olive
DMC : Dorsomedial crest (of the AIN)
DN : Dentate (lateral) nucleus
FN : Fastigial (medial) nucleus
ICG : Interstitial cell group
IO : Inferior Olive
LVN : Lateral vestibular nucleus
PIN : Posterior interposed nucleus
r-MAO : rostral part of the medial accessory olive
SVN : Superior vestibular nucleus
v-DAO : ventral fold of the dorsal accessory olive
VL : ventral leaf of the principal olive

For other cerebellar regions, information can be found in (Sugihara, 2011).

5.2.2.1 OLIVO-CORTICAL PROJECTIONS

Based on neuronal tracings performed in the rat (Sugihara and Shinoda, 2004), our region of interest receives olivary inputs from:

- The caudal-and-intermediate parts of the subnucleus *a* of the caudal-MAO (for the most medial part of the cortex, i.e. zebrin bands P1+, P1- and P2+).
- The dorsal-DAO for the more external zebrin bands (P2-, b+, P3+).

- The ventral DAO for the b- zebrin band, but this region is often out of our experimental range.

Based on tracing experiments and zebrin identity (Sugihara and Shinoda, 2004; Sugihara, 2011), Sugihara grouped the P1+ and P2+ bands inside the group I projections (Figure 30, green regions), that is, information from the Inferior olive essentially under mesodiencephal (cerebral) control. However, inside this group, the region of the inferior olive projecting to P1+ and P2+ in the anterior lobules are in the subnucleus *a* which process also spinal inputs. a+ is in the group IIa (blue regions), receiving vestibular inputs. P1- is in the group III (yellow regions), receiving Somatosensory, vestibular and mesodiencephalic inputs. Finally P2-, b+ and b- are in the group IV (red/pink regions) receiving only somatosensory inputs.

5.2.2.2 CORRESPONDING CORTICO-NUCLEAR PROJECTIONS

- P1+ projects to the ventral Fastigial Nucleus (medial part).
- The first half of P1- projects to the rostrodorsal part of the Fastigial Nucleus (medially).
- The second half of P1- (equivalent to a- when the a+ band is present) projects to the rostrodorsal part of the Fastigial Nucleus (laterally).
- The first half of P2+ projects to the ventral Fastigial Nucleus (lateral part).
- The second half of P2+ projects to the ventral ICG (ventral part)
- P2- projects to the LVN and to the AICG, except for the most medial region in Lobule IV (Zone CX) which project to the to the rostrodorsal part of the Fastigial Nucleus (laterally).
- b+ projects to the LVN and to the AICG
- b- projects to the AIN

As we can see, regions that share similar zebrin identity (for example P1-) can project to different cerebellar nuclei. As each cerebellar nucleus finally project to different regions of the brain or of the medulla, it means that Purkinje cells receiving similar olivary inputs will spread the signal to different targets.

5.2.2.3 CORRESPONDING OLIVARY INPUTS

- The ventral part of the subnucleus a of the c-MAO (P1+, P2+) receives inputs from the ICG (and the ventral part of the MN), but also from the spinal cord (Matsushita et al., 1991; Sugihara and Shinoda, 2007; Sugihara, 2011).
- The dorsal-DAO receives information from the spinal cord. Inputs are mostly proprioceptive (Berkley and Hand, 1978; Gellman et al., 1983)

We can identify the anatomical basis of the olivo-cortico-nucleo-olivary loop. Thus, signal that starts from the caudal part of the subnucleus *a* of the caudal MAO, projects to P1+, which in turn projects to the ventral fastigial nucleus (medial part), finally projecting back to the ventral part of the subnucleus a of the c-MAO (and probably to other targets).

For more details, please see the recent review by Izumi Sugihara (Sugihara, 2011). More generally, the aldolase C positive bands apparently receive cerebral, tectal, vestibular and visual inputs,

whereas aldolase C negative bands receive somatosensory inputs (Sugihara and Shinoda, 2004). However, those rules might not apply everywhere.

Alternatively, it is possible to use Voogd and Ruigrok nomenclature (Voogd and Ruigrok, 2004). Briefly, P1+ is in the region A, P1- in the region A1, P2+ in the region AX, P2- is essentially in the region X, except in lobule IV when a new region CX appears at the proximal part of P2-. B+ corresponds to the region B and b- corresponds to C1.

5.2.2.4 CORRESPONDING MOSSY FIBRES INPUTS

Among the projections to the anterior vermis, in lobules III and IV mossy fibres carry sensory information from the forelimbs through the external cuneate nucleus, the cuneate nucleus and the gracile nucleus (Gerrits et al., 1985; Akintunde and Eisenman, 1994; Ji and Hawkes, 1994), but also from the parvocellular region of the lateral reticular nucleus, which carry more integrated sensorimotor information (Wu et al., 1999).

Inputs from the hindlimbs arrive through the spinocereballar tractus, forming a complementary pattern of projection (Ji and Hawkes, 1994; Gebre et al., 2012).

Pontine projections seem weak in this region (Brodal and Bjaalie, 1992; Huang et al., 2013), except in a small parasagittal band that could be b+ (but not properly identified in Huang experiments).

We unfortunately lack precise somatosensory mappings of the receptive fields in the anterior vermis, such as those performed in the C3 region or in the hemispheres (Bower et al., 1981; Jörntell et al., 1996; Garwicz et al., 1998b).

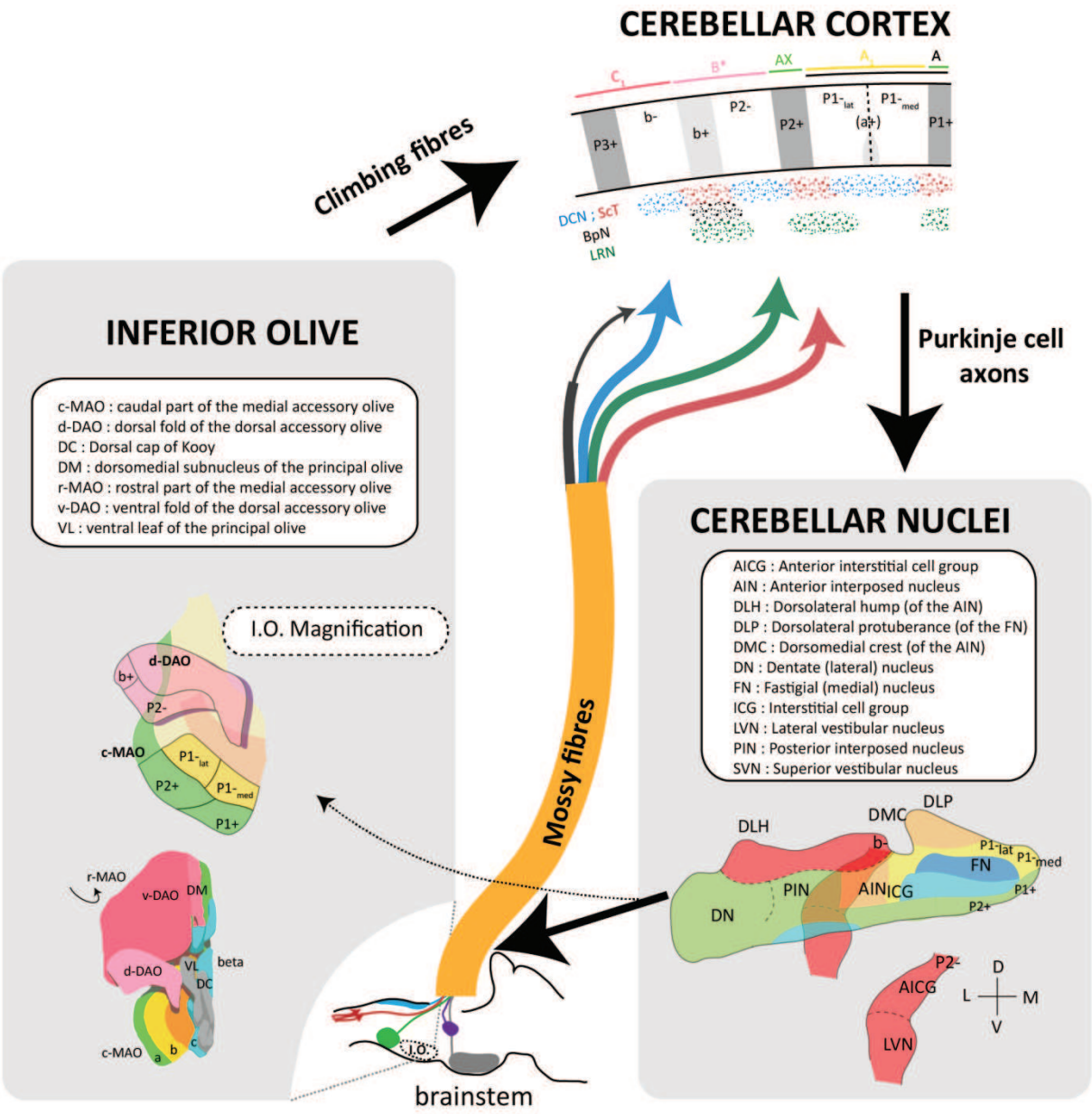

Figure 30 : Inputs and outputs in the anterior cerebellar vermis. Composite Figure.
References are in the legend. Summary table can be found in Sugihara, 2011.
Inferior Olive (I.O. left), Cerebellar Cortex (Top) and cerebellar nuclei form a closed loop. Projections between these 3 structures and cerebellar output from the cerebellar nuclei are indicated with black arrows. In all structures, the regions targeting or receiving information from cortical zebrin bands are indicated.
Mossy fibres (orange) inputs are originating from various precerebellar nuclei and terminate in parasagittal bands in cerebellar cortex granular layer. DCN : Dorsal column nuclei (External cuneate, cuneate and gracile nucleus); ScT : Spinocerebellar tractus. DCN and ScT from Ji and Hawkes, 1994; BpN : Pontine nuclei (Huang et al., 2013); LRN: Lateral reticular nucleus (Wu et al., 1999) (for more details, refer to Figure 3).
Inferior Olive is topographically organised. Bottom part, whole inferior olive. Colours represent olivary groups in Sugihara nomenclature; see Sugihara and Shinoda, 2004. Same colour code for cerebellar nuclei.
Cerebellar cortex. Zones A, A1, AX, B and C1 are indicated on top. B*: In intermediate lobule IV, zone X appears between zone AX and B. In posterior part of lobule IV, zone A2 appears between Zone X and AX (Voogd and Ruigrok, 2004). Zebrin names use Hawkes nomenclature. a+ is only present is intermediate lobule IV.
Cerebellar nuclei nomenclature is from Sugihara and Shinoda, 2007.

5.3 CEREBELLAR MODULES ARE COORDINATED BY GRANULE CELL INPUTS

CEREBELLAR MICROZONES ARE COORDINATED BY GRANULE CELL INPUTS

Valera M Antoine, Binda Francesca, Pawlowski Sophie, Dupont Jean-Luc, Casella Jean-François, Cruveiller Héloise, Rothstein Jeffrey, Poulain Bernard and Isope Philippe.

(1) Institut des Neurosciences Cellulaires et Intégratives, CNRS UPR 3212, Université de Strasbourg, France

(2) Brain Science Institute, Johns Hopkins University, School of Medicine, Baltimore, USA

First paragraph

Information processing underlying motor coordination is supported by a highly organized modular organization of the cerebellum[1–5]. Although uniform, the cerebellar cortex is segregated in a wealth of individual modules characterized by the congruence of the two main inputs of the cerebellum, the mossy and the climbing fibres, onto Purkinje cells[6–11]. Those biochemically segregated parasagittal strips of Purkinje cells receive and integrate information from one specific part of the body[12]. Purkinje cells that belong to the same module converge to restricted areas of cerebellar nuclei that send back the cerebellar computation to the cerebral cortex, the brainstem or the spinal cord depending on the origin of incoming information[13,14]. A negative feedback from cerebellar nuclei to the inferior olive, the source of the climbing fibres, closes this olivo-cortico-nuclear loop that control cerebellar-dependent motor learning[15,16]. Granule cells, the relay between mossy fibres and Purkinje cells, send a long axon, the parallel fibres, that cross many modules; however whether they play a role in module coordination is still unknown[2]. Here we show that the cerebellar cortical modules are selectively associated by the parallel fibres. Indeed, Purkinje cells belonging to a given module are preferentially connected by local granule cells and by one or several groups of distant granule cells in a stereotyped manner that is highly conserved between animals, associating identified modules. Surprisingly, molecular interneurons display a reciprocal pattern of granular cell inputs. Furthermore, we found that the distribution of the different types of Golgi cells match with module boundaries. Our results demonstrate that modules, identified by their mossy fibre inputs, are linked together by the functional synaptic organization of their granule cell inputs on the different cell types of the cerebellar cortex. We anticipate our study to be a starting point for the description of the identity card of individual modules of the cerebellar cortex. Unravelling the map of the coordinated parasagittal stripes will help to determine the precise role of individual modules and provide key information in order to understand the rules governing cerebellar dependent motor coordination.

Number of words: 337

Main text

Cerebellar modules were identified by the topographical organization of the climbing fibre inputs on Purkinje cells (PC), followed by the demonstration that mossy fibres (MFs) input originated from the

same body part often match climbing fibre receptive fields[6–11]. Also, biochemical markers expressed specifically in PCs, called zebrins, define parasagittal bands that share some common boundaries with individual modules or microzones[9,12,17–19]. MFs project on cerebellar granule cells (GCs) that send long bifurcating axons, the parallel fibres, which perpendicularly contact thousands of PCs and potentially activate beams of PCs (i.e. 'the beam hypothesis')[1,20,21] belonging to several modules. Paradoxically, several studies showed that PCs are excited only by small subsets of GCs most often localized below the PCs[7,11,18,22–26]. These results led to the hypothesis that local granule cells provide the major input to PCs via the ascending part of their axon and that most of the granule cell to Purkinje cell synapses are silent. Ultimately, this suggests that information processing is restricted to the incoming column and that cerebellar nuclei or downstream structure will combine the computation performed by the cerebellar cortex. Nevertheless, recent studies have suggested that the restricted receptive field of PCs could result from the feedforward inhibition exerted by molecular interneurons and that PCs are excited by widespread GCs in a given lobule[21,27]. These findings would suggest that PCs integrate and compute information arising from many modules in the same lobule via the parallel fibres.

In order to address the functional synaptic organization of granule cell inputs on PCs, Golgi cells (GoCs) and interneurons (MLIs) of the cerebellar cortex, we combined laser-scanning photostimulation of RuBi-glutamate[28] that enables the systematic mapping of synaptic connections and whole-cell patch-clamp of postsynaptic cells on acute cerebellar slices. We choose to restrict our study to the vermal portion of lobule III and IV (Fig 1), a region in which individual modules could be identified by a combination of the zebrin band pattern and by specific MF inputs (spinocerebellar and cuneocerebellar inputs)[17]. AAV9-GFP viruses were stereotaxically injected *in vivo* in the external nucleus that relay cutaneous and proprioceptive inputs from the forelimb. MFs projections were then traced in the cerebellar cortex and compared to the zebrin band pattern (Fig 1B, C), allowing us to draw boundaries of putative modules that we called arbitrarily M_I to M_V. This framework was used to 3D reconstruct and positioned each recorded cell. Also, we found that the profile of expression of two proteins specifically expressed in GoCs (neurogranin, NeuG and glycine transporter type 2, Glyt2; see methods) defined several groups of GoCs. Combining double immunohistochemical staining against AldolaseC (a zebrin II marker)[30] and NeuG on a transgenic mice carrying eGFP under Glyt2 transporter, we demonstrated that the distribution of these GoC subtypes followed similar modular organisation rules than MF projections in lobule III and IV (Fig 1D; see methods), indicating that individual module might have a specific repertoire of GoC subtypes.

Transgenic mice carrying eGFP under EAAT4 promoter[29] allowed us to visualized zebrin band patterning (Zebrin II; Fig 1A) on transverse acute slices and record cells at a given position in the lobule (see methods). We first recorded individual or pairs of PCs in $P1^+$, $P1^-$ and $P2^+$ zebrin bands and systematically uncaged RuBi glutamate on each side of the PC (grid extension was -332 µm to 332 µm from the soma; Fig 2A). Uncaging efficiency was assessed by recording individual GCs. Glutamate reliably elicited burst of action potentials in GCs (19.6 ± 6.6 spikes at the centre of the spot, N=7; see methods), attesting that even unlikely[31], low probability connection will be unmasked. The total synaptic charge evoked by glutamate uncaging was used to account for the synaptic weight elicited by GCs from each location in the grid. In order to decrease the stochastic bias when determining spatial maps and because projections from MFs were evenly distributed in the depth of the granule cell layer (Fig 1B), each complete map was performed several times (5.1 ± 2.3 N=89). The charge of the noise was also calculated and Z-score representations were built for each cell recorded (Fig 2A,

B). Strikingly, we observed that distant GC hotspots of highly connected regions were always found. The robustness of the observed patterns were tested by recording pairs of neighbouring PCs and by quantifying the grid point by point correlation between the two patterns (Fig 2C). Indeed, a strong correlation was found between charge patterns for paired PCs (Pearson coefficient r = 0.74 ± 0.14, N=9 pairs, 5 animals), although no correlation between distant PCs was seen.

These spatial patterns of synaptic charge were highly reproducible from PC to PC at the same location, but more importantly from animal to animal (N=49 PCs, N = 18 animals, Fig 3A). For example, PCs from different animals but recorded in module M_I systematically displayed hotspots of connection locally and in module M_{III} (Fig3A). We then asked whether this synaptic charge was reproduced when PC were recorded in different modules (from M_I to M_{III}). Individual charge pattern were binarized (see methods) and a sliding average of 3 consecutive PCs was performed between P1+ and P2+ (Fig 3B; N=46 patterns ; 18 animals). We then identified several stereotyped patterns of synaptic connections (Fig 3B, C) that depend on the position of the recorded PC. For example, the 22 PCs located in M_I are highly connected by local GCs and by GCs from ipsilateral and contralateral M_{III}. However, the 8 PCs GC located in M_{III} display a strong synaptic link with ipsi and contralateral M_{II}. Interestingly, M_I PCs are mainly excited by modules carrying the same modality of MF inputs, i.e hindlimb proprioceptive projections from the Clarke column (Fig 3C). It should be noted that in both median patterns, synaptic connections in the troughs are observed at such very low rate that in individual mapping absence of connection at some location systematically occurred. Nevertheless, those group of GCs are connected to PCs belonging to other modules (Fig 3B). Therefore, our results demonstrate that module M_I receiving projections from the hindlimb have experienced plasticity that led to the selection of GC inputs from another module receiving the same projections. Interestingly, other modules can display very different spatial GC to PC synaptic organization leading to other rules of coordination with neighbouring modules (Fig 3C). This features explain the regular averaged spatial maps observed when all mapping from any modules are aligned on PC soma[32] (Supplementary Figure 3).

When then address the spatial maps displayed at the two other synaptic connections of the cerebellar cortex, the GC to Molecular interneuron (MLI) and the GC to Golgi cell (GoC) synapses. MLIs were whole cell clamped (N = 7 cells) and the map of GC inputs (the number of synaptic events were counted instead of the total synaptic charge, see methods; Fig 4A) was also found unevenly distributed, with several hotspots of connections. Interestingly, in the group belonging to module M_I, median patterns of GC inputs on MLIs were reciprocal to PCs patterns in $P1^-$ band, suggesting that M_I PCs are activated by MFs - via GCs - targeting the module M_{III}, whereas they are inhibited - via MLIs - by MFs projecting to module M_{II}. 3D reconstruction of MLIs showed that dye coupling was frequent and parasagittally organized as expected from the orientation of their dendritic tree (Fig 4B; when coupled, average coupling 5.4 ± 2.3 cells; N=16/27 dye coupled cells) indicating that the spatial profile of PC inhibition will be conserved. We finally addressed the organization of GC synaptic inputs onto the GoCs using transverse slices of EAAT4-Glyt2-eGFP mice (see methods). Surprisingly, we found that the pattern of GC inputs onto GoCs was similar for all location mapped in any module and that the majority of the GC excitatory synaptic inputs (81% of total inputs) are made by local GCs (Fig 4C*i*,C*ii*) as recently suggested[33]. Based on Z-score charge patterns and 3D reconstruction of GoC, the extension of the responding zone was 240 µm, which matches with the extension of the GoC axonal plexus (214 ± 30µm N=10; Fig 4 C*iii*). Therefore, unlike GC inputs on PCs, these findings demonstrate

that excitatory inputs on Golgi cells are restricted to the local module confirming that Golgi cells implement an inhibitory feedback circuit in the granule cell layer[33].

Our data revealed that the synaptic organization of GC inputs on cell types of the cerebellar cortex in lobule III and IV is stereotyped among animals and depends on the identity of the cortical modules (Fig 4E), suggesting that they are actively combined and coordinated in order to process the information further to the cerebellar nuclei. These computational principles favour synchronization of Purkinje cells in specific modules, allowing a better readout of the information by nuclear cells[34]. We then demonstrated that cerebellar cortical modules are selectively associated by parallel fibres, indicating that climbing fibre dependent synaptic plasticities have built this particular synaptic organization. Interestingly, since this organization is conserved among animals, further studies identifying the identity of the associated modules would tell us which behavioural task is stored in this cortical area.

number of words: 1528

References

1. Thach, W. T., Goodkin, H. P. & Keating, J. G. The cerebellum and the adaptive coordination of movement. *Annu. Rev. Neurosci.* **15,** 403–442 (1992).

2. Apps, R. & Garwicz, M. Anatomical and physiological foundations of cerebellar information processing. *Nat. Rev. Neurosci.* **6,** 297–311 (2005).

3. Ruigrok, T. J. H. Ins and outs of cerebellar modules. *Cerebellum* **10,** 464–74 (2011).

4. Glickstein, M., Sultan, F. & Voogd, J. Functional localization in the cerebellum. *Cortex.* **47,** 59–80 (2011).

5. Oscarsson, O. Functional units of the cerebellum - sagittal zones and microzones. *Trends Neurosci.* 143–145 (1979).

6. Ito, M. *The Cerebellum and Neural Control*. (Raven Press, 1984).

7. Brown, I. E. & Bower, J. M. Congruence of mossy fiber and climbing fiber tactile projections in the lateral hemispheres of the rat cerebellum. *J. Comp. Neurol.* **429,** 59–70 (2001).

8. Voogd, J., Pardoe, J., Ruigrok, T. J. H. & Apps, R. The distribution of climbing and mossy fiber collateral branches from the copula pyramidis and the paramedian lobule: congruence of climbing fiber cortical zones and the pattern of zebrin banding within the rat cerebellum. *J. Neurosci.* **23,** 4645–56 (2003).

9. Pijpers, A., Apps, R., Pardoe, J., Voogd, J. & Ruigrok, T. J. H. Precise spatial relationships between mossy fibers and climbing fibers in rat cerebellar cortical zones. *J. Neurosci.* **26,** 12067 (2006).

10. Bengtsson, F., Ekerot, C.-F. & Jörntell, H. In vivo analysis of inhibitory synaptic inputs and rebounds in deep cerebellar nuclear neurons. *PLoS One* **6,** e18822 (2011).

11. Garwicz, M., Jorntell, H. & Ekerot, C. F. Cutaneous receptive fields and topography of mossy fibres and climbing fibres projecting to cat cerebellar C3 zone. *J. Physiol.* **512 (Pt 1,** 277–293 (1998).

12. Apps, R. & Hawkes, R. Cerebellar cortical organization: a one-map hypothesis. *Nat. Rev. Neurosci.* **10,** 670–81 (2009).

13. Voogd, J. & Glickstein, M. The anatomy of the cerebellum. *Trends Neurosci.* **21,** 370–5 (1998).

14. Buisseret-Delmas, C. & Angaut, P. The cerebellar olivo-corticonuclear connections in the rat. *Prog. Neurobiol.* **40,** 63–87 (1993).

15. Welsh, J. P., Lang, E. J., Suglhara, I. & Llinás, R. Dynamic organization of motor control within the olivocerebellar system. *Nature* **374,** 453–7 (1995).

16. Welsh, J. P. & Llinás, R. Some organizing principles for the control of movement based on olivocerebellar physiology. *Prog. Brain Res.* **114,** 449–61 (1997).

17. Ji, Z. & Hawkes, R. Topography of Purkinje cell compartments and mossy fiber terminal fields in lobules II and III of the rat cerebellar cortex: spinocerebellar and cuneocerebellar projections. *Neuroscience* **61,** 935–54 (1994).

18. Hallem, J. S. *et al.* Spatial correspondence between tactile projection patterns and the distribution of the antigenic Purkinje cell markers anti-zebrin I and anti-zebrin II in the cerebellar folium crus IIA of the rat. *Neuroscience* **93,** 1083–94 (1999).

19. Pijpers, A., Voogd, J. & Ruigrok, T. J. H. Topography of olivo-cortico-nuclear modules in the intermediate cerebellum of the rat. *J. Comp. Neurol.* **492,** 193–213 (2005).

20. Heck, D. H., Thach, W. T. & Keating, J. G. On-beam synchrony in the cerebellum as the mechanism for the timing and coordination of movement. *Proc. Natl. Acad. Sci. U. S. A.* **104,** 7658–63 (2007).

21. Cramer, S. W., Gao, W., Chen, G. & Ebner, T. J. Reevaluation of the beam and radial hypotheses of parallel fiber action in the cerebellar cortex. *J. Neurosci.* **33,** 11412–24 (2013).

22. Cohen, D. & Yarom, Y. Patches of synchronized activity in the cerebellar cortex evoked by mossy-fiber stimulation: questioning the role of parallel fibers. *Proc. Natl. Acad. Sci. U. S. A.* **95,** 15032–15036 (1998).

23. Isope, P. & Barbour, B. Properties of unitary granule cell-->Purkinje cell synapses in adult rat cerebellar slices. *J. Neurosci.* **22,** 9668–78 (2002).

24. Lu, H., Hartmann, M. J. & Bower, J. M. Correlations between purkinje cell single-unit activity and simultaneously recorded field potentials in the immediately underlying granule cell layer. *J. Neurophysiol.* **94,** 1849–60 (2005).

25. Ekerot, C. F. & Jörntell, H. Parallel fibre receptive fields of Purkinje cells and interneurons are climbing fibre-specific. *Eur. J. Neurosci.* **13,** 1303–1310 (2001).

26. Jörntell, H. & Ekerot, C.-F. Reciprocal bidirectional plasticity of parallel fiber receptive fields in cerebellar Purkinje cells and their afferent interneurons. *Neuron* **34,** 797–806 (2002).

27. Santamaria, F., Tripp, P. G. & Bower, J. M. Feedforward inhibition controls the spread of granule cell-induced Purkinje cell activity in the cerebellar cortex. *J. Neurophysiol.* **97,** 248–63 (2007).

28. Fino, E. *et al.* RuBi-Glutamate: Two-Photon and Visible-Light Photoactivation of Neurons and Dendritic spines. *Front. Neural Circuits* **3,** 2 (2009).

29. Gincel, D. *et al.* Analysis of cerebellar Purkinje cells using EAAT4 glutamate transporter promoter reporter in mice generated via bacterial artificial chromosome-mediated transgenesis. *Exp. Neurol.* **203,** 205–12 (2007).

30. Ahn, A. H., Dziennis, S., Hawkes, R. & Herrup, K. The cloning of zebrin II reveals its identity with aldolase C. *Development* **120,** 2081–90 (1994).

31. Valera, A. M., Doussau, F., Poulain, B., Barbour, B. & Isope, P. Adaptation of Granule Cell to Purkinje Cell Synapses to High-Frequency Transmission. *J. Neurosci.* **32,** 3267–3280 (2012).

32. Walter, J. T., Dizon, M.-J. & Khodakhah, K. The functional equivalence of ascending and parallel fiber inputs in cerebellar computation. *J. Neurosci.* **29,** 8462–73 (2009).

33. Cesana, E. *et al.* Granule cell ascending axon excitatory synapses onto Golgi cells implement a potent feedback circuit in the cerebellar granular layer. *J. Neurosci.* **33,** 12430–46 (2013).

34. Person, A. L. & Raman, I. M. Purkinje neuron synchrony elicits time-locked spiking in the cerebellar nuclei. *Nature* **481,** 502–5 (2012).

Supplementary Information

Slice preparation

All experimental procedures conform to national and NIH guidelines on animal experimentation. Slices were prepared from P17 to P90 CD1 mice. EAAT4-GFP (gift from Jeffrey D. Rothstein) and $GlyT_2$-GFP (gift from Hanns Ulrich Zeilhofer) strain of mice were bred together , allowing us to visualize zebrin bands and Golgi cells during the experiment,). $EAAT_4$-$GlyT_2$-GFP mice were anaesthetized by inhalation of isoflurane. Animals were killed by decapitation, the cerebellum was dissected out and placed in a cold ACSF (4°C) bubbled with carbogen (95% O_2, 5% CO_2), containing in mM: NaCl 120; KCl 3; $NaHCO_3$ 26; NaH_2PO_4 1.25; $CaCl_2$ 2.5; $MgCl_2$ 2. Glucose 10, Minocyclin 0.00005 (Sigma-Aldrich). 300 µm-thick tranverse slices were prepared (Microm HM 650V, Microm) in potassium-based medium, containing in mM: K-gluconate 130; KCl 14.6; EGTA 2; HEPES 20; Glucose 25; minocyclin 0.00005, D-AP5 0.05. After cutting, slices were soaked a few seconds in a sucrose-based medium at 34°C, containing in mM: Sucrose 230; KCl 2.5; $NaHCO_3$ 26; NaH_2PO_4 1.25; Glucose 25; $CaCl_2$ 0.8; $MgCl_2$ 8; minocyclin 0.00005. Slices were maintained in a water bath at 34°C in bubbled ACSF. Experiments were done at 34°C using the same bubbled ACSF. We blocked inhibitory transmission and NMDA, Adenosine, CB1, $GABA_B$ and mGluR1 receptors to limit modulation of EPSC amplitude by stimulation-dependent activation of these receptors; respectively, the following antagonists were added (in mM): Picrotoxin 0.1, Strychnine 0.001, D-AP5 0.05, DPCPX 0.0005, AM251 0.001, CGP52432 0.001 and JNJ16259685 0.002. Drugs were obtained from Tocris-Cookson or Ascent Scientific. For all uncaging experiments, we applied 100 µM RuBi glutamate (Ascent Scientific).

Errors in mapping due to slice angle were estimated by taking advantage of the expression of GFP in Lugaro cells in EAAT4-Glyt2-GFP mice(Supplementary Figure 2C). Lugaro cells express $GlyT_2$ in their axon, which runs parallel to the parallel fibers. We estimated the angle of 10 Lugaro cell axon spanning 10 slicesand obtained an average angle of 0.85 ± 0.82°, and no slice had more than 2° angle in average. Moreover, the fact that we systematically recorded distal inputs in Purkinje cells confirms that slices were not tilted.

Recordings

Whole-cell patch-clamp recordings in voltage clamp mode were obtained using 3-4 MΩ pipettes for Purkinje cells, 6-8 MΩ pipettes for Golgi cells and 10 MΩ pipettes for molecular layer interneurons, using a Multiclamp 700 amplifier (Molecular Devices, Sunnyvale, USA). Optimal series resistance (R_s) compensation (80% to 90% typically) was applied. R_s was monitored in all experiments and cells were hold at -60 mV. The pipette internal solution contained (in mM): $CsMeSO_4$ 135; NaCl 6, HEPES 10; MgATP 4; Na_2GTP 0.4. For cell reconstruction, we added (in $mg.ml^{-1}$): biocytin 1 and neurobiotin 1. pH was adjusted to 7.3 with KOH and osmolarity to 300 mOsm. Voltages were not corrected for the liquid junction potential, which was calculated to be 9 mV (i.e. the real membrane potential was 9 mV more hyperpolarized than reported). We accepted recordings for which the inward current at -60 mV did not exceed 1 nA for Purkinje cells and 250 pA for other cells. Synaptic currents in Purkinje cells were low-pass filtered at 2 kHz, and then sampled at 20 kHz-50 kHz. All recorded cells were located in the lobules III or IV.

Extracellular stimulation protocols

Acquisition of data was performed using the WinWCP 4.2.x freeware (John Dempster, SIPBS, University of Strathclyde, UK). Glutamate uncaging was performed using the point scan system of Fluoview FV300 confocal microscope fibre-coupled to a blue light diode pump solid state laser (DPSS,

473 nm, CrystaLaser, USA). Pulses of 20ms duration at 30mW were used throughout the experiments.

Diffusion of uncaged RuBi-glutamate during laser stimulations was estimated by recording Purkinje cells in the horizontal plane and uncaging glutamate on the parasagittally oriented dendrites with short resolution steps (20 µm). Action potentials in the network were blocked with TTX (1 µm). Direct stimulation of glutamate receptors with RuBi-glutamate uncaging on Purkinje cell dendrites gives an upper bound of the stimulation spot size. Half width was 33.0 ± 1.8 µm (supplementary Figure 1A). Granule cells have short dendrites, which could increase the real stimulated region size. We estimated this extent by recording granule cells while uncaging glutamate with 10 µm steps. We estimated both the range of glutamate diffusion in the granular layer (by recording direct stimulation of glutamate receptors in whole cell patch clamp, supplementary Figure $1B_1$) and the range of activated granule cells (by recording evoked action potentials in cell-attached patch clamp, supplementary Figure $1B_1$). Half width of direct stimulation was 59.6 ± 2.1 µm. Half-width of evoked action potentials was 45.5 ± 10.9 µm. The average number of evoked action potentials was 19.6 ± 6.6, but only occurs when the cell is at the center of the spot. This value overestimates the average number of spikes evoked by RuBi-glutamate uncaging. Finally, we estimated the impact of the focus plane on granule cell responses. We performed stimulation of granule cells while recording a connected Purkinje cell, and changed the focus with 10 µm steps. Average recorded currents were constant in the granular layer, suggesting that for a given coordinate the stimulation was constant at all focus planes (supplementary Figure 1C).

Mappings were performed by doing point-scan stimulation at controlled positions. Stimulation coordinates were controlled with the Fluoview embedded controller (PAPP). In each experiment, the recorded cell was placed at the center of the field, with the slice oriented so that the Purkinje cell layer follows the X-axis. Stimulation were performed up to 332µm on each sides of the recorded cell, with 41.5 µm steps, and by performing 2 to 5 lines at various depth of the granular layer. The upper line was always just under the Purkinje cell line. The number of consecutive lines was adjusted depending on the depth of the granular layer.

Time interval between uncaging spot was 3.5 s of neighboring regions to ensure independence of the site. Stimulation of neighboring sites (distance = 41.5µm) do not affect the amplitude of a connected region (supplementary Figure 2B). One single site was never stimulated faster at more than 0.008 Hz. At 0.01Hz, repeated stimulation showed no change in EPSC charge. Change in amplitude was +2.7 ± 2.6% $events^{-1}$ (supplementary Figure 2A). Measures were performed using homemade routines written in python.

Analyses

Since mappings were performed in regions in which zebrin band width can slightly change, we systematically normalized the cell position by the average size of the zebrin bands in lobules III and IV zebrin. The P1+/P1- border was used as the origin. Average P1+ width was 48.5 µm, average P1- width was 275.6 µm, average P2+ width was 64.6 µm and average P2- width was 445.2 µm (N = 89). It can be noted that regions close to the midline (such as our module M_I) are poorly affected by distortion, since they are not affected by changes in band size.

Since evoked currents and background noise were different between cells,, we corrected this bias by using the Z–Score of EPSC charge. Background noise was calculated at all recording points with similar parameters (same baseline, same measurement range but located at the end of the recorded trace). Evoked currents charge was then divided by the standard deviation of the background noise. In Golgi cells, stimulations close to the soma evoked direct stimulation of the basolateral dendrites, which tends to overestimate EPSCs charge. We thus performed a preliminary median filtering which removed direct current. Spontaneous events were not affected by the filtering, indicating that we did not mask small distal inputs. Since we could discriminate individual EPSCs in molecular layer interneurons, we calculated the Z-Score of the total number of EPSCs elicited by ..

A Z-Score above 3.09 corresponds to a P-value of 0.001 and was considered as a significant connection. Hence, the Binarized representation in the spatial map was built by assigning a value of 1 to Z-score value above 3.09 at a given location, and 0 for Z-score below 3.09. Thus, this representation directly addresses the question of the existence or not of connected granule cells.

For group data, patterns from several cells were pooled using their normalized representations. A smoothing average was performed with a window size corresponding to our uncaging step size (41.5 µm), and a smoothing window of 10.375 µm (1/4 of the step size). Different values of binning gave similar results.

Immunostaining and image processing

At the end of the experiment, a picture of the mapped field is taken, using GFP fluorescence.All slices were fixed in 4% paraformaldehyde after the experiment. Immunohistochemistry was performed using aldolase C polyclonal antibody to confirm zebrin band positions. Biocytin/neurobiotin filled cells were visualized with strepatavidin alexa fluor conjugate (555 nm). Slices were mounted in prolong Gold. Each experimental slice was then reconstructed using confocal microscopy. Confocal images and image from the initial experiment were then aligned, allowing to position accurately the zebrin bands and to confirm the lobule. Alignments between experimental images and confocal images show no shrinkage of the slice in the mediolateral axis, and GFP signal could be perfectly aligned. Golgi cells were reconstructed with the free software Vaa3d.

Statistics.

Means are reported with standard deviations, while error bars in figures represent SEMs,. Unless stated, statistical tests were the non-parametric Mann-Whitney-U and Spearman rank order tests. Correlations were calculated using Pearson coefficient.

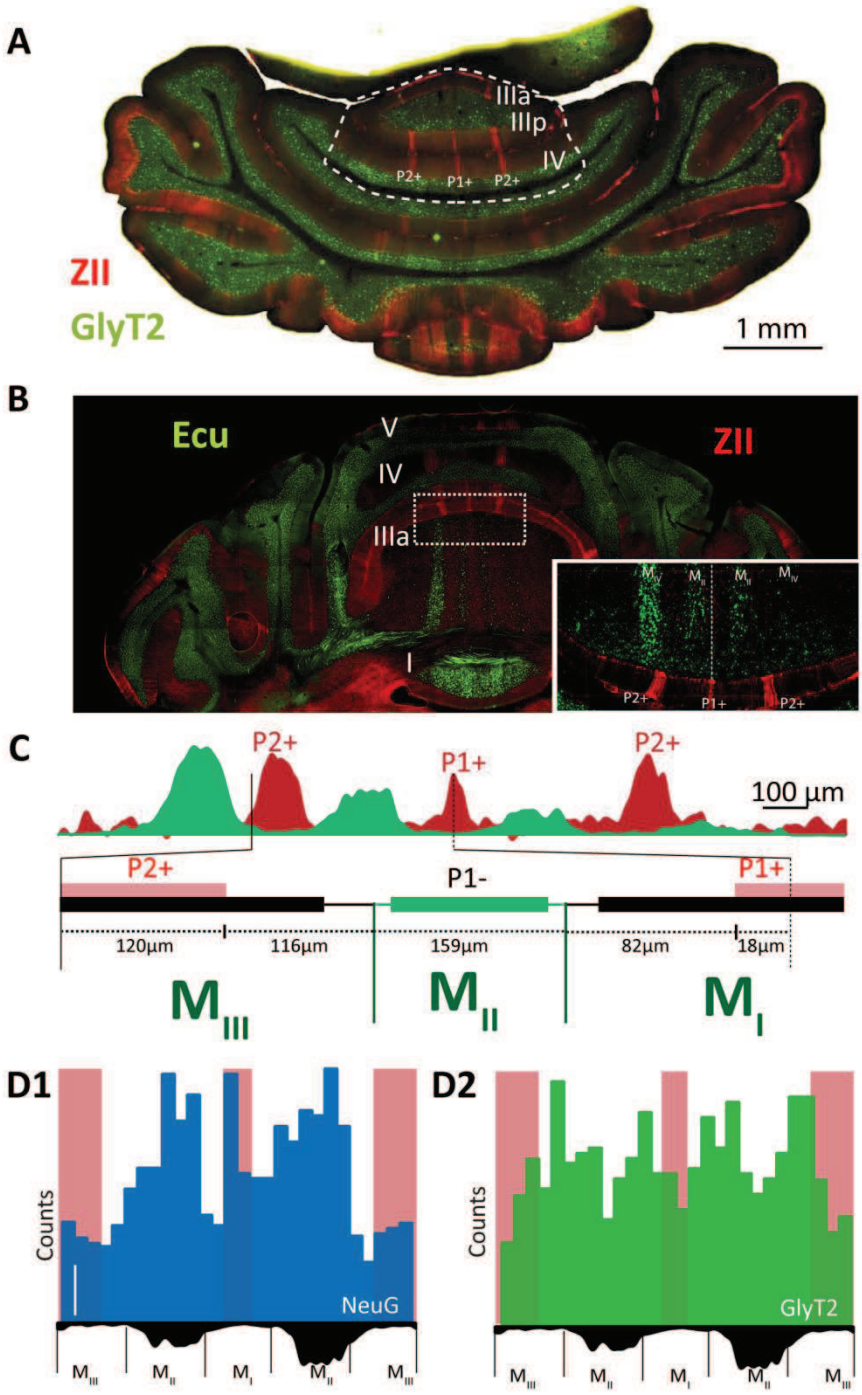

Figure 1. Description of the cerebellar modules in the medial part of lobule III and IV.

A: Anti-zebrin II (Aldolase C, red) labelling on a cerebellar slice of a Glyt$_2$-eGFP transgenic mice in which Golgi cells are labelled (green). Dashed lines represent the region studied and targeted lobules are numbered.

B: Green, mossy fibre projections from external cuneate identified by AAV9-GFP fluorescence. Red, anti-zebrin II staining. Inset, zoom into the region of interest identified by the dashed rectangle.

C: Intensity plot profiles from the dashed area in B highlighting relationships between zebrin band patterning and mossy fibre projections from the external cuneate nucleus in lobule III and IV. Inset below identifies the mean extension in µm of individual modules defined by mossy fibre boundaries (M_I to M_{III}).

D: Distribution of Golgi cell soma in lobule III and IV between P1+ and P2+ from two Golgi cell subtypes, neurogranin (NeuG in blue) and Glycine transporter type 2 (Glyt2 in green). Note matching boundaries with mossy fibres inputs.

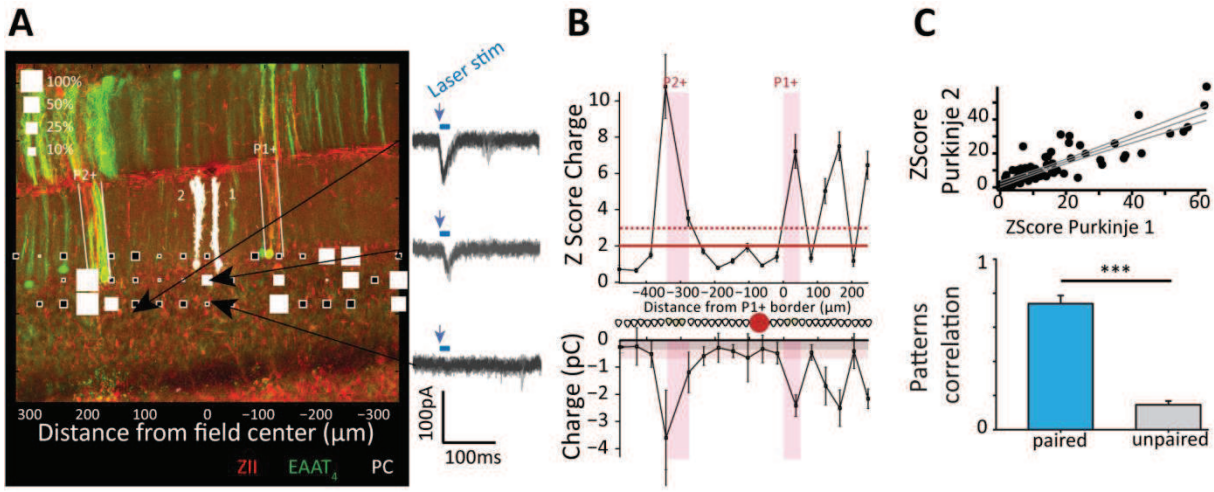

Figure 2. Patterns of granule cell inputs on Purkinje cells elicited by RuBi glutamate uncaging are heterogenous.
A: Left panel, reconstruction of one individual experiment. Purkinje cells (white) are whole cell clamped on acute slices from EAAT4-GFP mice (green). Post-hoc counterstaining with anti-zebrin II refine zebrin band boundaries (red). White square size illustrates the charge of the EPSCs elicited by uncaging at each location. Right panel, superimposed EPSCs recorded at identified location. Blue bar, uncaging flash (20 ms)
B: Mean charge (lower plot) and Z-score (upper plot; compared to the background noise current, see methods) of the maximum EPSC charge recorded in each column of the photostimulated grid field. The position of the Purkinje cell in P1- band is identified by the red plain circle. Red line illustrates the level of the background noise. Values above the dashed red line are higly significant (Zscore > 3.09; see methods).
C: Upper panel, correlation of Z-score values between pairs of Purkinje cells at each column location (n = 9 pairs). Lower panel, histogram of the mean pearson coefficient of individual correlation between pairs of Purkinje cells compared to non-paired Purkinje cells. Values ± SEM.

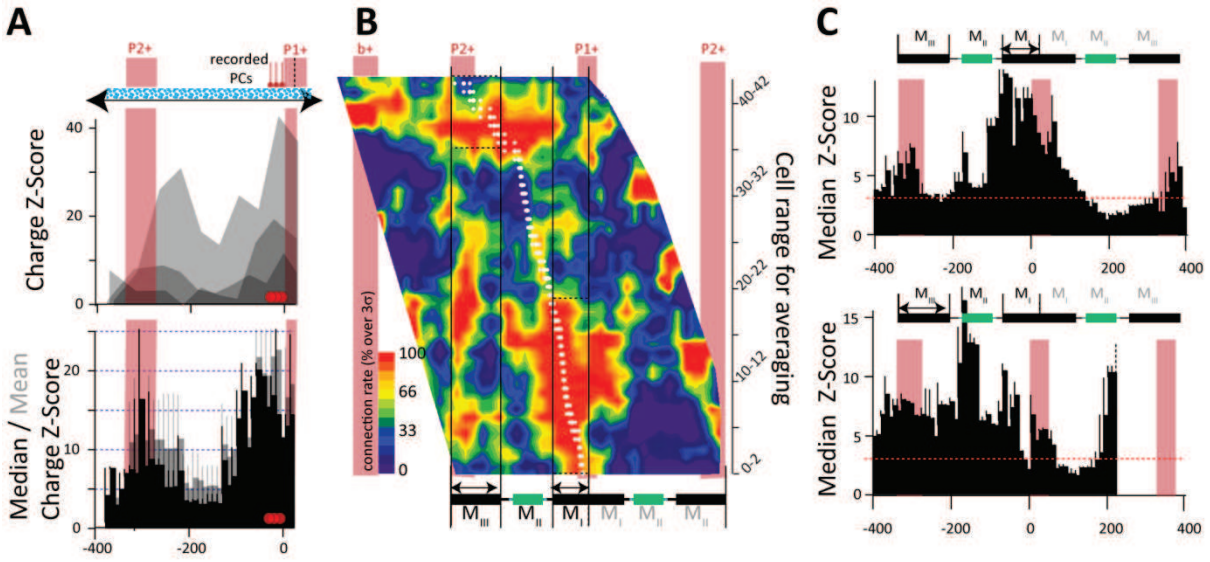

Figure 3. Patterns of granule cell inputs in Purkinje cells are stereotyped and conserved between animals.

A: Upper panel, superimposed Z-score pattern of the mean EPSC charge for 3 different Purkinje cells recorded at the same location in different animals (grey shaded plain curves). Lower panel, averaged mean charge (grey histogram) and median mean charge for the same 3 Z-score patterns. Zebrin bands illustrated in red. Red circles, Purkinje cells positions.

B: Spatial map of the rate of connection between granule cells and Purkinje cells for Purkinje cells located at each position of the photostimulated area. Each horizontal line is a mean pattern for 3 consecutive cells. The full map is built by sliding average with an increment of one cell (n= 49 cells, N = 18 animals). Patterns were binarized before averaging (see methods). Zebrin bands illustrated in red. Anatomical modules identified in Fig 1 are represented below (black and green rectangles, from M_I to M_{II}) bilaterally.

C: Median pattern of Z-score of the EPSC charge for Purkinje cells located in M_I (n = 22 cells) and M_{III} (n = 8 cells).

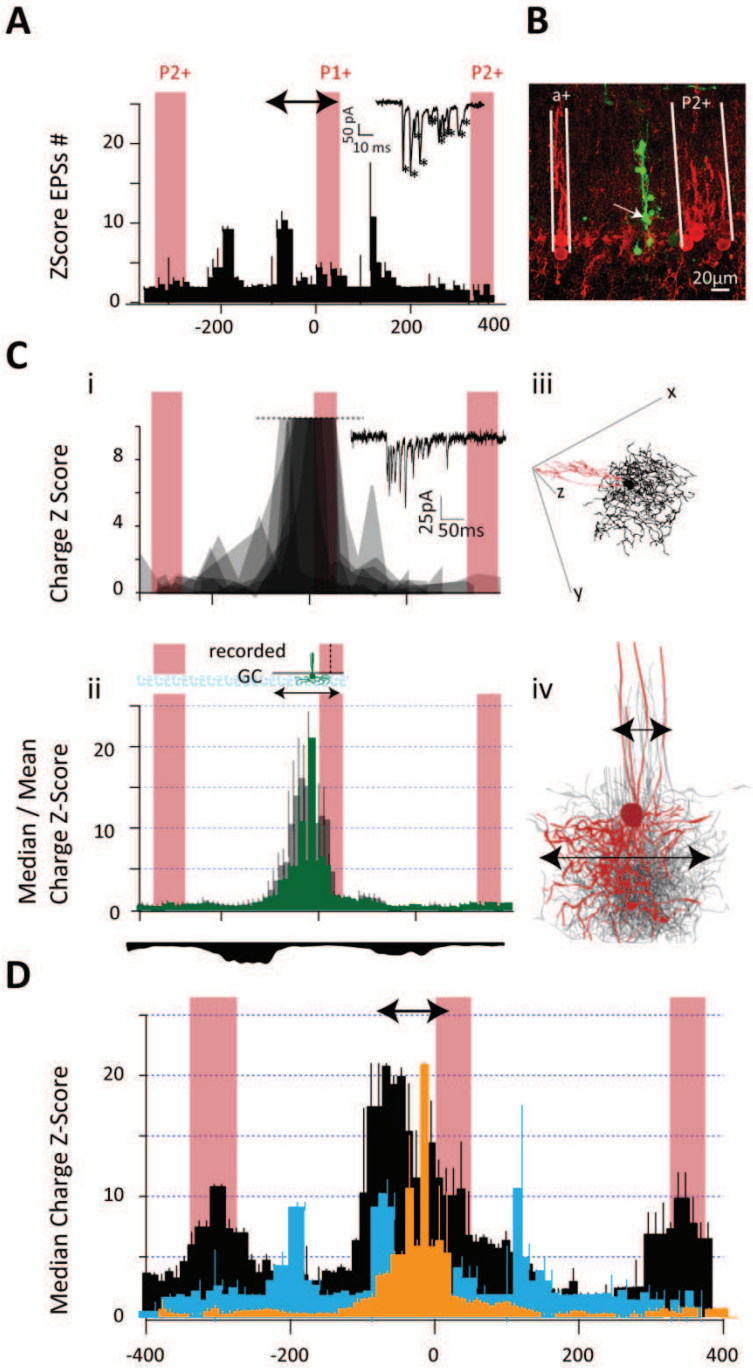

Figure 4. Patterns of granule cell inputs in molecular interneurons and Golgi cells.

A: Mean pattern of Z-scores of the number of synaptic events induced by glutamate uncaging (see methods) in molecular interneurons located in MI (n= 7 cells). Inset, example of recorded EPSCs in an interneuron.

B: reconstruction of the interneuron and dye coupled cells following recordings.

C: i, superimposed Z-score patterns of the mean EPSC charge for 9 different Golgi cells recorded in MI in different animals (grey shaded plain curves). Inset, example of recorded EPSCs in a Golgi cell. ii, median pattern of Z-score of the EPSC charge for Golgi cells located in MI. iii, upper panel, 3D reconstruction of one Golgi cell. Lower panel, superimposition of the 8 Golgi cells reconstructed illustrating the extension of the axonal plexus (see text).

D: Superimposed median charge Z-score for all cell types recorded in MI, Purkinje cells (black), molecular interneurons (blue) and Golgi cells (orange).

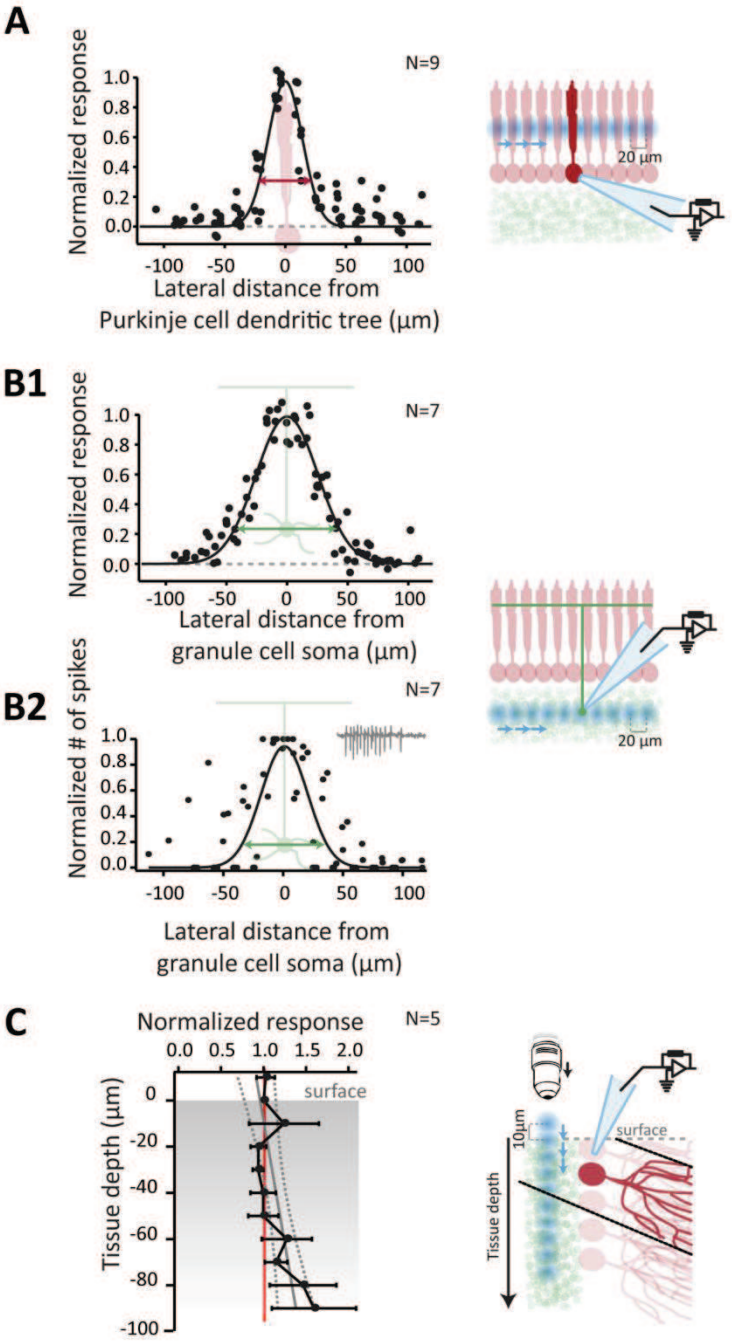

Supplementary Figure 1. Glutamate uncaging resolution

A: Diffusion of RuBi-Glutamate was estimated by performing stimulations across the flat dendritic tree of Purkinje cells. Step between stimulations is 20µm. Action potentials are blocked with TTX, and only direct stimulation of the dendrites is recorded

B: Granule cell dendrites can decrease the resolution of the system, as they can be stimulated a few tens of micron from their soma. We estimated the range of activation of granule cells by performing experiment similar to A, but with granule cell recording. **B2:** Activation of granule cells do systematically evoke action potentials. We performed an experiment similar to B, but granule cell was recorded in cell attached patch clamp.

C: Mapping are not dependent on the focus plane, and the depth of the focus plane did not affect the size of the recorded current when the region was connected. Dotted line indicate the region in which granule cells can be connected to the recorded Purkinje cell. Granule cells located deeper are off-beam. Scaling was exagerated for illustration purpose, Purkinje cell dendritic tree is about 200µm.

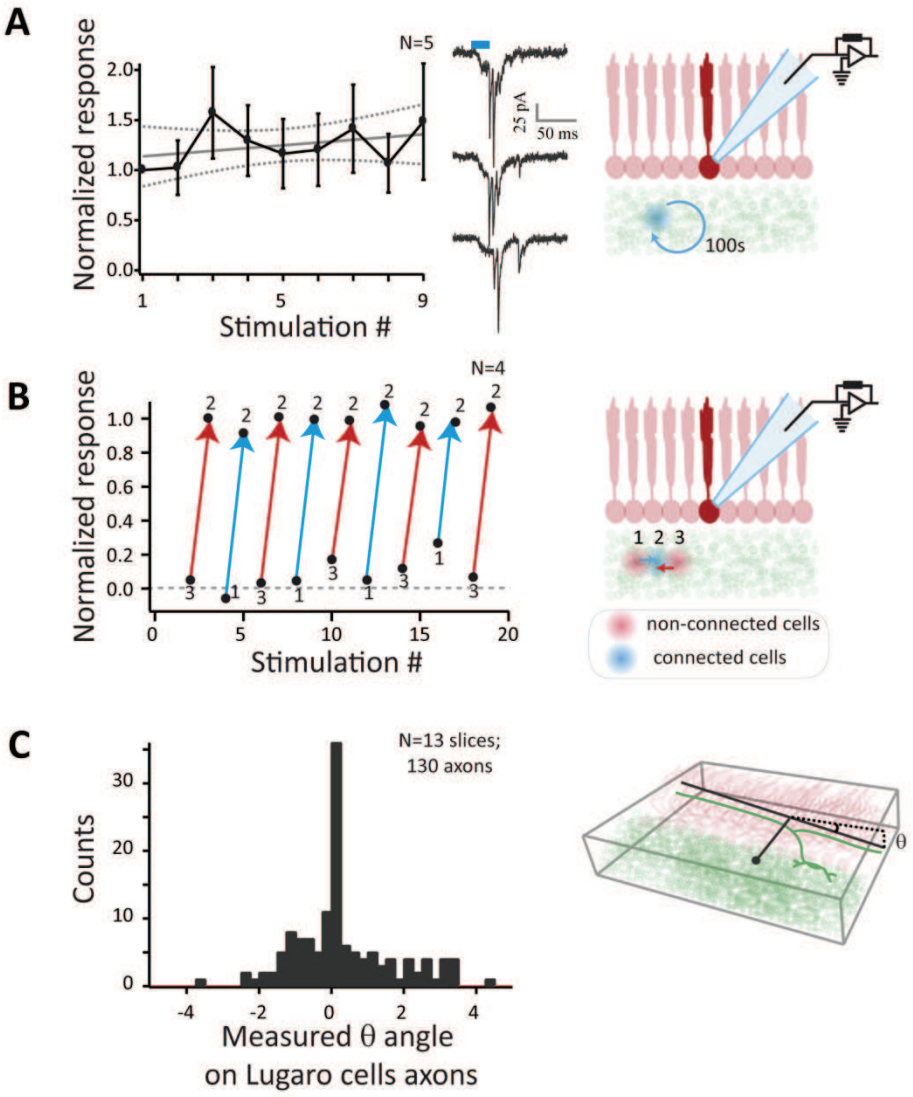

Supplementary Figure 2. Independence of the sites, reproducibility of the stimulations, absence of slice tilt

A: Stimulation repeated at a same location every 100s (0.01Hz) show reproducible patterns. Middle panel: Trace exemple recorded in Golgi cell

B: Stimulation of adjacent sites does not influence the reponses. The two red sites (sites 1 and 3) were not connected to the recorded Purkinje cell (red cell with patch pipette), and were surrounding a connected region (blue site, site 2). Stimulating site 1 then site 2 (blue arrow) gives similar responses than stimulating site 3 then site 2 (red arrow). Δt = 3s between 2 sites.

C: Slices are not tilted. In $GlyT_2$+ mice, Lugaro cell express GFP and it is possible to follow their axon along the mediolateral plane. To estimate slice angle, we measured 10 axons of Lugaro cell that were crossing the 660µm in each slice. Measurments are based on Z-stack of confocal images (with steps of 1µm).

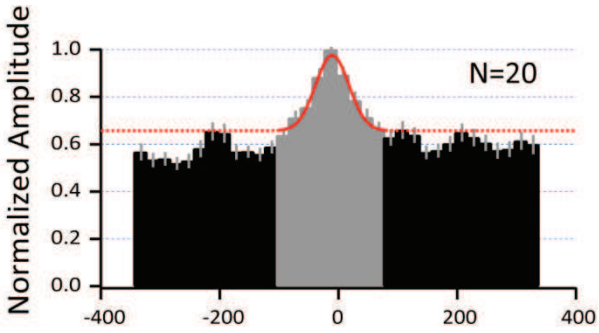

Supplementary Figure 3. Granule cell to Purkinje cell connection without taking into account cell position.
20 cells of our data set, located every ~15µm between P1+ and P2+ were averaged using methods previously descibed in other studies: Cells are centered, mean amplitude of each bin is measured. The pattern of each cell is normalised to its maximum. patterns are averaged and normalised. This figure indicates than even is a region as restricted as P1-, the absence of positional information still mask the spatial organisation of the inputs.
Grey region corresponds to the range mapped in the adult mouse in previous studies, and red gaussian fit correspond to the fit obtained when extrapolating fit from grey region.

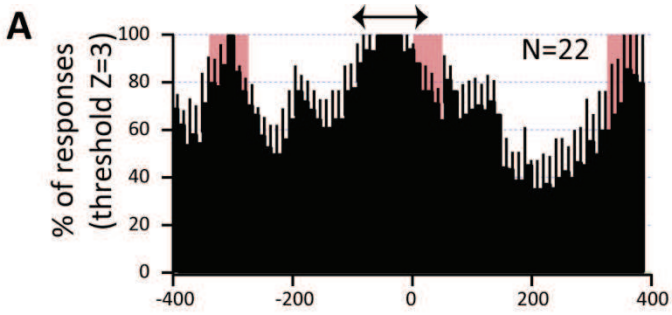

Supplementary Figure 4. Group data for zone M_I
Histogram of the binnarized responses of the cells located in M_I (black arrow). This histogram is a group data of cells located in M_I from the Figure 3B. For each cell pattern, bin with Z-Score of charge > 3.09 = 1, and cells with no or very small connections (Z-Score <3.09) = 0. Granule cells located in M_{III} ipsi and contralaterally present systematic strong connections (100% ipsilaterally, 83% contralaterally), whereas inputs from M_{II} represent only 53% of the strong inputs ipsilaterally and 37% contralaterally.

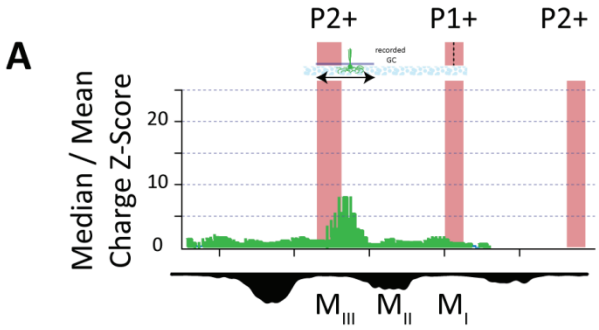

Supplementary Figure 5. GlyT$_2$ Golgi cells in M$_{III}$ also present only local inputs

A: Granule cells input pattern of 7 GlyT$_2$ Golgi cell located in M$_{III}$ were mapped. Cells presented only local inputs such as GlyT2 located in M$_I$. Other information are similar to Figures 4Ci and 4Cii

6 DISCUSSION

6.1 HETEROGENEOUS SYNAPTIC ORGANISATION OF GRANULE CELL INPUTS

6.1.1 PURKINJE CELLS ARE EXCITED BY SPECIFIC HOTSPOTS OF GRANULE CELLS

Our mapping showed the first stereotyped and reproducible organisation of the synaptic connections between granule cells and their postsynaptic targets (Purkinje cells, molecular layer interneurons and Golgi cells). Accurate positioning of recorded cells and stimulated granule cells were achieved by using transgenic mice expressing GFP under $EAAT_4$ promoter, a protein that has a zebrin II-like pattern of expression. Purkinje cells, molecular layer interneurons or Golgi cells located in similar location on the cerebellar cortex (same zebrin band, same lobule) were recorded while granule cells were photostimulated via glutamate uncaging, at controlled locations. Cells were filled with biocytine and further reconstructed.

Our study showed that the probability of connection does not decay progressively as suggested in previous *in vitro* experiments (Isope and Barbour, 2002; Sims and Hartell, 2005; Walter et al., 2009), but is rather spatially organised. Besides the fact that most granule cells are not connected to the recorded cell, as previously showed by several studies, the connected granule cells are grouped in specific locations in the granular layer, forming hotspots. These results might have been missed in previous study for several reasons.

First, experiments using stimulation in the molecular layer are complicated to interpret since it is not possible to know the position of the soma of activated parallel fibres. Distal stimulation in the molecular layer can activate a parallel fibre belonging to a local granule cell through backpropagated action potential.

Second, the slowly decaying probability of connection often recorded (Isope and Barbour, 2002; Sims and Hartell, 2005; Walter et al., 2009) is likely to be due to heterogeneous population averaging, and can be reproduced in our own set of data if we do not take into account the position of the recorded cell (see supplementary figure in the second article). In Purkinje cells, local granule cell inputs were observed in most experiments, and generally evoked the strongest response. However, distal inputs could be of similar strength, and in some rare cases, even stronger. In molecular layer interneurons, the strength of local and distal inputs was similar.

In our experiments, connection patterns were reproducible between animals, although there was interindividual variability. Strongly connected and non-connected regions for a given set of recorded cells were generally located at similar locations between experiments. Stereotyped input patterns could be observed for Purkinje cells, molecular layer interneurons and Golgi cells. The results are summarised in the Figure 31. In Purkinje cells, pair recordings showed that the correlation of granule cells input patterns was stronger when two neighbouring cells were recorded than when the cells were at the same location but in different animals. Similar uncaging experiments were performed to describe input patterns in Golgi cells and in molecular layer interneurons. Strikingly, molecular layer interneurons had a responding pattern distinct to Purkinje cells input pattern, except for the local

granule cells that target both Purkinje cells and molecular layer interneurons. Alternatively, $GlyT_2^+$ Golgi cells were mostly activated by local inputs.

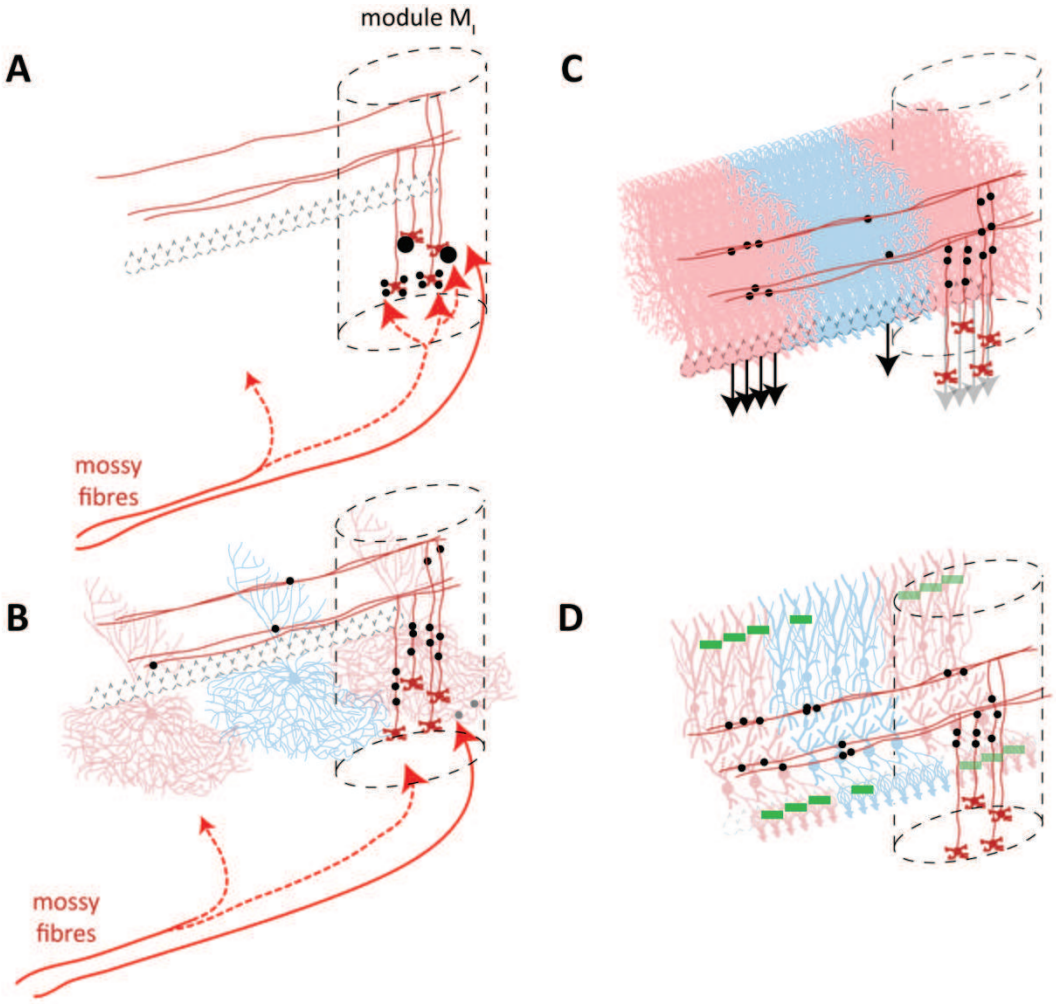

Figure 31 : Summary of mapping experiments.
Black circles represent excitatory synapses. Dotted barrel represents a module (M_I), delimited by shared mossy fibre inputs.
A : Mossy fibres originating from specific mossy fibre inputs (for instance: spinocerebellar tractus) activates specific patches of granules cells, defining a module. Mossy fibres can branch and send collaterals (dotted arrow) in several modules. Granule cells are activated both by simultaneous inputs from different mossy fibres (pattern classification; small black circles on each dendrites), or by high frequency bursts (high pass filter; Big black circle).
B : Intramodular granule cells (red) strongly activate local Golgi cells on their basolateral or apical dendrites, through granule cell ascending axon or proximal parallel fibres, inducing feedback inhibition within the module. Distal Golgi cells can be weakly activated by parallel fibres. Mossy fibres can also directly activate Golgi cells (grey circles) inducing feedforward inhibition onto intramodular granule cells.
C : Granule cells strongly activate local Purkinje cells through ascending axon and proximal parallel fibres, and distal Purkinje cells through parallel fibres. Activation of distal parallel fibres can occur both in regions receiving similar mossy fibres inputs (red Purkinje cells), and in regions integrating different modalities. Connected regions can be smaller than a module. Connected Purkinje cells firing is thus modulated (black and grey arrows).
D : Parallel fibres activate local molecular layer interneurons within module through ascending axon and proximal parallel fibres, and distal molecular layer interneurons through parallel fibres. Molecular layer interneurons perform only local inhibition onto Purkinje cells (green -) and other molecular layer interneurons (not represented). At one location, parallel fibres activate either Purkinje cells or molecular layer interneurons, but not both.

6.1.2 HYPOTHESIS ON THE ORIGIN OF CONNECTED HOTSPOTS

The heterogeneous pattern of connectivity contrasts with the morphological studies showing that parallel fibres contact on average 54% of the Purkinje cells they cross (Harvey and Napper, 1991; Pichitpornchai et al., 1994). Two interpretations are possible:

1. The density of the synapses is actually not homogeneous, and the regions which are not/poorly connected lack synapses.
2. The density is constant, but the regions not/poorly connected contain more silent synapses.

The first hypothesis would involve a developmental process that could select some regions rather than others. Due to parasagittal organisation of Purkinje cell markers, climbing fibres and mossy fibres afferences, this hypothesis cannot be excluded. A mechanism dependent on the histochemical or zebrin identity of the Purkinje cell could serve as a selection signal, as some zebrins such as cadherins are adhesion molecules (Redies et al., 2011) and others such as BEN are guidance proteins (Chédotal et al., 1996). Alternatively, an activity-dependent mechanism is still possible. After birth, Purkinje cells are multi-innervated by several climbing fibres. Around P15, only one climbing fibre per Purkinje cell remains, through mechanisms that involve synaptic activity and Ca^{2+} signalling (Kakizawa et al., 2000). Similar processes could select specific sets of parallel fibres. However, this *wiring* selection would be in contradiction with most of the current models of cerebellar cortex physiology, in which parallel fibres can perform associative learning by linking a granule cell with any Purkinje cell on its path. To address this hypothesis, one solution could be to count varicosity density throughout cerebellar cortical modules, knowing labelled granule cell position, which would indicate if presynaptic button are present.

The second explanation would assume that the connection density is homogeneous, but that further selection mechanisms would silent synapses belonging to granule cells from specific regions. This silencing mechanism is easy to explain in regards to plasticities already described (Gao et al., 2012). In the Marr-Albus-Ito model, the coincident activation of the climbing fibre and the parallel fibres synapse leads to the silencing of the latter through long term depression. Based on the observation that the mapping profiles are similar across animals for an analogous Purkinje cell, but more correlated for neighbouring Purkinje cells in a same animal, we hypothesised that the mapping profile is likely to be due to the animal history. This hypothesis is supported by experiments in which a strong stimulation of the parallel fibres in vivo induces modification of the receptive fields activating Purkinje cells (Jörntell and Ekerot, 2002).

6.1.3 NEIGHBOURING CELLS SHARE INPUT PATTERNS

In our paired recordings, Purkinje cells belong to the same parallel fibres beam and share a fraction of their parallel fibre inputs (Heck et al., 2007; Wise et al., 2010). Microzones, defined by climbing fibres inputs, are a few hundreds of micrometers width (although the size is likely to vary between cerebellar regions). The distance between Purkinje cells in a pair is usually less than 40 µm and it is likely that recorded Purkinje cells belong to the same microzone and share climbing fibre inputs originating from the same olivary region. Since neighbouring Purkinje cells should have similar parallel fibre and climbing fibre inputs, plasticities induction might be similar in both cell (and thus

synaptic weights); neighbouring cells would share a similar "learning history". Indeed, when patching neighbouring cells, we always saw highly correlated patterns.

On the other hand, Purkinje cells in different microzones have often different biochemical markers, i.e., they belong to different zebrin band. Thus, we would expect to see different connection patterns while patching two cells on both side of a zebrin border. This experiment has not been performed yet and would be particularly interesting to do.

To verify if patterns of connectivity are due to associative motor learning, (see 2nd article), another approach would be to record cells in an immature cortex. If the motor learning in the cerebellum is performed through LTP and LTD mechanisms, it would be interesting to observe the granule cell input maps before learning has occurred. Are all the regions homogeneously connected? Are they initially all silent?

6.1.4 SHARED PATTERNS BETWEEN ANIMALS

Climbing fibre and mossy fibre inputs are conserved between animals. The fact that granule cell to Purkinje cell connection patterns also share similarities between animals is more intriguing. Because these patterns are due to motor learning performed during the life of the animal, and because they are conserved between animals, it means that the connected regions have behavioural reasons to be preferentially connected from one animal to the other. In the anterior vermis, inputs mostly carry information from the limbs and from the trunk. Based on the alternative patterns between spinocerebellar inputs and external cuneate inputs, it is conceivable that some regions process information from the hindlimbs while other regions process information from the forelimbs. Unfortunately, in the absence of a more precise mapping of the sensory inputs, it is hard to say precisely which receptive field activates the different patches of granule cells.

A recent study addressed the question of the organisation of Purkinje cells projections (Ruigrok et al., 2008). Transynaptic retrograde tracings using rabies viruses showed that specific muscles like the tibialis anterior or the gastrocnemius muscles (two antagonist ankle joint muscles) are contacted by specific groups of Purkinje cells after only a few relays. For instance, the tibialis anterior is the indirect target of Purkinje cells located in B+ ipislaterally and P1-$_{lateral}$ ipislateraly, whereas the gastrocnemius muscle is the indirect target of Purkinje cells located in B+ ipislaterally and P1-$_{lateral}$ contralaterally. By comparison, the flexor digitorum muscle (controlling digits movements in the forelimbs) is the indirect target of Purkinje cells located essentially in the paravermis, but also in P2- and P1-$_{median}$ both ipsi- and contra-laterally. Later in the infection, more Purkinje cells are labelled, but the labelling remains restricted to negative bands. The key point in these experiments is that specific sets of Purkinje cells (which might correspond to the climbing fibre microzone - a hypothesis that was not tested) send their output onto specific muscles, from one animal to the other. However, some groups of Purkinje cells ultimately project to more than one muscle (see ipsilateral B+ in the example above). This experiment illustrates the complex organisation of the cerebellar output, with regions controlling probably complex set of muscles in order to evoke synergistic movements in response to specific sensory contexts (Apps and Garwicz, 2005).

Association can be performed at the input stage of the cerebellum by the mossy fibres to granule cell synapses, as predicted by David Marr and James Albus (Marr, 1969; Albus, 1971), and observed experimentally (Jörntell and Ekerot, 2006; Dean et al., 2010; Huang et al., 2013). It is conceivable that for one given set of Purkinje controlling a muscle or a set of muscles, some connected patches of granule cells belong to regions processing pure sensory information (for instance direct somatosensory information only from mossy fibres from the external cuneate), while other patches of granule cells would carry information from several origins, such as somesthetic and cortical information (for instance, mossy fibres from external cuneate nucleus and pontine nucleus)

If the association between patches of granule cells and specific Purkinje cells is the consequence of learning, it would not be surprising to find some regions more often connected, because muscles synergies associate specific sets of muscles, such as specific sets of agonist and antagonist muscles. Some movements are performed by all animals, independently of the animal history, such as walking, rearing or withdrawal movements. The reproducible patterns we observed might be due to the association of trunk and limbs muscles in such common tasks. An interesting experiment would be to see how the patterns are affected when animal movements are restricted from birth.

6.1.5 THE MOLECULAR LAYER INTERNEURONS DISTINCT PATTERN

Molecular layer interneurons receive only very discrete inputs. In our experiments, granule cell inputs were found from few regions compared to inputs onto Purkinje cells. The very discrete organisation of the inputs is in accordance with previous studies, estimating the number of functional synapses at $\sim 3\%$, the others being silent (Ekerot and Jörntell, 2001; Jörntell and Ekerot, 2002, 2003). The fact that less granule cells contact molecular layer interneurons compared to Purkinje cell can be easily explained by the restricted number of parallel fibres that cross the molecular layer interneuron dendritic tree.

Since a single parallel fibre can drive the firing of a molecular layer interneuron (Carter and Regehr, 2002; Brenowitz and Regehr, 2007), and that inhibitory postsynaptic currents induced by single molecular layer interneurons can strongly shape the Purkinje cell firing (Häusser and Clark, 1997; Mittmann et al., 2005), the restricted number of functional synapses might indicate that individual molecular layer interneuron are highly task-specific. This idea can be further strengthened by the synergistic plasticities occurring in the cerebellar cortex. Indeed, induction of LTD at the parallel fibre to Purkinje cell synapses induces simultaneously LTP at the parallel fibre to molecular layer interneuron synapses. Conversely, induction of LTP at the parallel fibre to Purkinje cell synapses induces simultaneously LTD at the parallel fibre to molecular layer interneuron synapses (Bell et al., 1997; Han et al., 2000; Jörntell and Ekerot, 2002; Coesmans et al., 2004; Gao et al., 2012). Thus, the same teaching signal potentiates excitation or inhibition through a set of parallel fibres, but not both.

It would be interesting to see if neighbouring molecular layer interneurons in the same animal share the same level of correlation in granule cells input maps than Purkinje cells (see 2nd article), as they integrate the same climbing fibre inputs but, different beams of parallel fibres as opposed to Purkinje cells. However, this smaller sampling of the whole molecular layer, compared to Purkinje cells, could be compensated by their strong gap junction coupling (Mann-Metzer and Yarom, 1999). Since plasticities are under the control of the climbing fibre input, it is not surprising to see opposite

patterns between excitatory patches of granule cells and “inhibitory” patches of granule cells onto Purkinje cells (i.e. activating molecular layer interneurons which inhibit only Purkinje cells close to their soma, because of their parasagittal extent).

Our observations that molecular layer interneurons can be stimulated by local granule cells are in accordance with previous *in vivo* recordings (Ekerot and Jörntell, 2001). However, in our experiments, strong activation was often evoked by distal patches of granule cells too. Yet, mossy fibres carrying similar information can branch in several parasagittal regions of the cerebellar cortex through their numerous collaterals, so distal granule cells could actually process information from the same receptive field. As the experiments *in vivo* were performed in different regions, comparisons with existing observation might be difficult.

6.2 GOLGI CELLS ARE LOCAL INTERNEURONS

6.2.1 FUNCTION OF THE APICAL DENDRITES

It was initially proposed that the basolateral dendrites are activated by local granule cells, hence modulating the gain within the network, whereas the apical dendrites were able to detect the global level of excitation in the network through the parallel fibres (Marr, 1969), but this dichotomy was never confirmed.

In our experiments, we could not detect strong EPSCs evoked by distal granule cells contacting the apical dendrites through parallel fibres, whereas local granule cells evoked very strong EPSCs in a 100µm range around the soma. As apical dendrites extend more than 600µm parasagittally, there is still a chance that we have missed a fraction of the inputs. This possibility is however unlikely to explain the lack of distal inputs, since Purkinje cells and molecular layer interneurons which have a similar orientation could be easily activated by distal granule cells. An alternative explanation is that Golgi cells apical dendrites have different functions.

Golgi cells are coupled by connexin36 gap junction, which synchronize their activity in the beta range (Courtemanche et al., 2002; D’Angelo and De Zeeuw, 2009; Dugué et al., 2009) in the absence of inputs, essentially through hyperpolarisation (Dugué et al., 2009). Gap junction are mostly located in the lower part of the apical dendrite (Vervaeke et al., 2010). High electrical filtering by apical dendrites weakens the impact of parallel fibres on the Golgi cell soma (Dieudonne, 1998; Vervaeke et al., 2012), but models suggest that the current flowing between gap junction of coupled Golgi cells could drive the firing if multiple Golgi cells are activated at the same time. Thus, it was suggested that Golgi cells apical dendrites could contribute to spatial averaging of the excitatory inputs in the cerebellar cortex.

80% of the Golgi cells express also mGluR2 in the apical dendrites (Simat et al., 2007). When activated by glutamate, $mGluR_2$ induce cell hyperpolarisation by activating G-protein inwardly-rectifying potassium channels (GIRK) (Watanabe and Nakanishi, 2003) and BK channels (Hull et al., 2013). In this second study, the authors showed that after activation of mGluR2 receptors on apical dendrites, hyperpolarisation first reduces the spontaneous firing rate of Golgi cells. In a second time,

a $CaMK_{II}$-dependent pathway is activated, which results in a persistent increase in spontaneous firing rate lasting more than 30 min, and thus of the tonic inhibition onto granule cells. Hence, a sustained activation of the apical dendrites could ultimately lead to stronger inhibition of granule cells. This effect could be important for specific sensory adaptation, where permanent sensory stimuli (for instance: the wind on hair receptors, the water during a swimming task, or the contact of the sole against the floor…) would induce an unnecessary background noise that would prevent the treatment of more significant information.

Together with our mapping experiments, and the recent confirmation of the granule cell to Golgi cell synapse on basolateral dendrites (Cesana et al., 2013), all these experiments suggest that Golgi cell intra-modular local inputs contact the basolateral dendrites and have probably a very distinct function compared to extra-modular inputs carried by parallel fibres.

6.2.2 FUNCTIONAL RELEVANCE OF GOLGI CELLS SUBPOPULATIONS

A second unanswered question is the functional signification of two different Golgi cell subpopulations, one purely GABAergic whereas the other is both GABAergic and glycinergic ($GlyT_2^+$ Golgi cells). The distribution of $GlyT_2^+$ cells is correlated with the mossy fibre inputs, so that spinocerebellar inputs might preferentially activate $GlyT_2^+$cells.

In the neocortex, inhibitory interneurons of specific subtypes are electrically coupled and forms discrete network modules (Gibson et al., 1999). As Golgi cells are coupled by gap junctions, it would be interesting to know if different subtypes form different subpopulations that could be restricted within specific cerebellar modules or specific types of sensory inputs. This hypothesis could be tested both *in vitro* and *in vivo*, but might first require a better anatomical understanding of the Golgi cell subpopulations connectivity.

6.3 HIGH FREQUENCY BURSTS ALLOW RELIABLE INFORMATION TRANSFER

In the first article of this manuscript, we saw that the parallel fibre to Purkinje cell synapse is able to sustain very high frequency release during high frequency stimulations. Previous estimates of release probability at the parallel fibre to Purkinje cell synapse suggested a very low value, around 5% (Dittman et al., 2000; Foster et al., 2005), and that synaptic transmission by single parallel fibres was unreliable. Using several experimental approaches, we found that in physiological condition, the release probability is probably over 15%, with a number of release-ready vesicles compatible with previous ultrastructural observations (Xu-Friedman et al., 2001). The initial probability of successful transmission - i.e. the probability for at least one vesicle to be released - is around 0.6, and is likely to approach 1 in case of short bursts. We found, using variance mean analysis, that this efficient transmission is possible because a reluctant pool can be recruited during high frequency bursts, increasing the number of available vesicles. As illustrated in supplementary results, we found further evidences of the functional relevance of this reluctant pool. Moreover, we found ultra fast vesicle sites refilling kinetics, which allow synapses to sustain long trains. Altogether, these results suggest that information in the mossy fibre pathway is not low-pass filtered by an unreliable

neurotransmission in the last step of the cerebellar cortical processing, but is rather accurately transmitted.

6.3.1 RELUCTANT VESICLES ALLOW RELIABLE TRANSMISSION AT THE PARALLEL FIBER TO PURKINJE CELL SYNAPSE

Several arguments could justify the existence of a reliable transmission at this synapse.

First, granule cells have no - or very low - spontaneous firing (Jörntell and Ekerot, 2006). Granule cell discharges is tightly controlled in the granular layer, by the requirement for coincident inputs to reach the threshold for action potential (granule cells fire only if their 4-5 dendrites are simultaneously activated, or if high frequency burst occurs (Jörntell and Ekerot, 2006; Rancz et al., 2007)) and by tonic inhibition performed by Golgi cells. Thus, any firing in granule cells might indicate a significant message. As a first filtering is performed in the granular layer, it might not be necessary to have a second noise filtering at the parallel fibre to Purkinje cell synapse. Moreover, as most of the synapses are silent, because of synaptic selection mechanisms, remaining sites might be particularly efficient to transmit the signal, as they were tightly selected. Finally, if one of the aim of parallel fibres is to transmit the onset of the stimulus (Heck et al., 2007), at least for some modalities, then the onset of the burst must be transmitted reliably, and initial release probability should not be too low.

Although moderately efficient in the case of a unique EPSC (~60% of chance to transmit the signal, if Ca^{2+} concentration is only 1.5 mM (Silver and Erecińska, 1990; Rancz et al., 2007)), transmission becomes very reliable when a burst is evoked. In the case of tactile information, the average instantaneous frequency is over 500 Hz (Jörntell and Ekerot, 2006), a frequency at which EPSCs facilitation is close to a factor of 2 and temporal summation is maximised in the dendritic spine, in which no dendritic filtering occurs. The existence of a reluctant pool which can be recruited only during high frequency bursts might be a synaptic adaptation emphasising synaptic transmission at single synapses. Although the mechanisms leading to low frequency depression at such synapse are not known (see supplementary results), the recent results of Frédéric Doussau showed that reluctant vesicles can be quickly recruited, in 2-3 pulses only, and that they significantly contribute to neurotransmission during bursts. Both the variance mean analysis and the more direct demonstration presented in supplementary results suggest that reluctant can increase basal release by a factor of two.

At the soma, integration rules might be different. Slow kinetics of EPSCs due to dendritic filtering suggests that Purkinje cells could be temporal integrators. High frequency bursts or simultaneous inputs from different dendritic spines both result in strong temporal summation, modulating Purkinje cell firing (Roth and Häusser, 2001).

6.3.2 FAST VESICLE REPLENISHMENT ALLOWS SUSTAINED TRANSMISSION OF THE SIGNAL

In vivo recordings showed that granule cells do not only code the onset of the stimulus (Heck et al., 2007; Bengtsson and Jörntell, 2009), but also the velocity of body movements (Arenz et al., 2009), or the intensity of joint movements (Jörntell and Ekerot, 2006). Both vestibular mossy fibres and proprioceptive mossy fibres can carry sustained stimuli. Our discovery that fast vesicle replenishment allows sustained release was also observed at the mossy fibre to granule cell synapse, and indicates that the whole mossy fibre pathways can transmit sustained trains of information (Saviane and Silver, 2006). An important point would be to know how long can be the granule cell firing sustained (Arenz et al., 2009). Moreover, even short-bursting somatosensory mossy fibres could be sustainably activated. We can imagine situations in which tactile stimulus is repeated at fast rate, like perhaps in a fast typing task or maybe during the detection of textures by skin touch. If continuous sensory information comes from the same receptive field, it is possible that sustained neurotransmitter release might be a common feature in the mossy fibre pathway, whatever the type of input.

In several other structures of the central nervous system performing fast and sustained release, specific proteic equipment was demonstrated (Matthews and Fuchs, 2010; Hallermann and Silver, 2013). At the mossy fibre to granule cell synapse, bassoon is a protein of the active zone involved in sustained vesicular release. Bassoon knockout mice display higher depression and slower vesicle reloading during sustained trains, whereas basal transmission is unaffected (Hallermann et al., 2010). Although its role was not investigated yet, the existence of bassoon at both the parallel fibre to Purkinje cell synapse and parallel fibre to molecular layer interneurons synapse suggest that this protein might be involved in the sustained transmission (Richter et al., 1999). It would be interesting to see if a conditional knockout mice lacking bassoon in parallel fibres would have impairments in learning or in sensorimotor tasks.

6.3.3 *ON BEAM* BURSTS INFLUENCE THE CEREBELLAR OUTPUT

Purkinje cells from a given microzone project onto same cerebellar nuclei neurons. Cerebellar nuclei neurons are spontaneously active at high frequency, between 50 and 90 Hz (Bengtsson et al., 2011; Blenkinsop and Lang, 2011; Person and Raman, 2012a). Although the number of converging Purkinje cells onto cerebellar nuclei is not clear, between 860 (Palkovits et al., 1977) and 34 (Person and Raman, 2012b), it was recently showed using dynamic clamp that if as few as 5% of the converging cells were synchronised, Purkinje cells could drive the cerebellar nuclei output (Person and Raman, 2012a). Our recordings suggest that neighbouring Purkinje cells share similar inputs. Neighbouring Purkinje cells are not only connected by the same granule cell hotspots, but the relative synaptic weights of each hotspot is similar in both cells. Thus, when granule cells fire, they are likely to induce a similar depolarisation in neighbouring Purkinje cells within the beam. Since neighbouring Purkinje cells have synchronised firing because of their recurrent collaterals (de Solages et al., 2008), similar inputs, exciting synchronised cells, might induce a synchronised firing of both cells. These shared inputs might ultimately potentiate the effect of Purkinje cells within the same microzone and the same beam onto cerebellar nuclei neuron firing. It can be noted that high frequency bursts could optimise the impact of only a few parallel fibres on Purkinje cell firing. Thus, the sudden activation of

only a few tens of connected granule cells, which is in the range of the connected hotspot we recorded, could drive Purkinje cell firing.

6.3.4 BURSTS AND PLASTICITY INDUCTIONS; RELEVANCE OF THE PURKINJE CELL PROTEIC PROFILE

Finally, cerebellar organisation might be strongly dependent on its histochemical compartmentation. Purkinje cells express a large diversity of markers along parasagittal bands. These zebrin bands might actually influence synaptic input processing, since some of these markers are linked to neurotransmission ($mGluR1_b$, $EAAT_4$, $GABA_AR_{b2}$), kinase signalling ($PLC\beta_4$, $PLC\beta_3$, PKCδ), or Ca^{2+} signalling (neuronal calcium sensor 1, neurogranin).

ZII^+ bands express $mgluR1_b$ isoform, which has less potency to activate the downstream phospholipases than the $mGluR1_a$ isoform. Using autofluorescence, Ebner's team showed that high frequency bursts of action potentials in the parallel fibres activate only $mGluR1_a$ positives Purkinje cells. This long-lasting activity in autofluorescence is blocked by mGluR1 antagonists, and is thought to reflect long term potentiation (Wang et al., 2011).

Similarly, $EAAT_4$ promotes glutamate uptake in the synaptic cleft. Thus, in synapses with $EAAT_4^+$ Purkinje cells, the activation of ionotropic and metabotropic receptors will be reduced compared to synapses with $EAAT_4^-$ Purkinje cells. Blocking EAATs during vibrissae stimulation that normally evokes single patch response revealed multiple patches of activation multiple, suggesting that these regions were only weakly activated because of glutamate uptake (Cramer et al., 2013).

Although we do not know if compensatory mechanisms can counteract the lack of one isoform, it is likely that identity of the postsynaptic cell can control crucial parameters such as plasticity induction or duration of the EPSCs. Because patterns are distributed along parasagittal zebrin bands, it would mean that this differential processing of similar inputs is module-specific, and that each module would express a specific "proteic identity card", giving to that module specific sensibility to particular input patterns. However the physiological consequence of such molecular profiles is difficult to interpret since plasticity interplay and transmission modulation are not fully described yet.

Finally, it can be noted that histochemical compartmentation of other cell types might also modulate information processing. For example, as illustrated in Figure 14B, some granule cells can express NR2C, apparently under zebrin II negative bands only. As NR2C-NMDAR have lower sensitivity to Mg^{2+} block (Dingledine et al., 1999) and prolonged activation time course (Cathala et al., 2000), and that NMDA component has a strong impact on spillover mediated excitation of granule cells in the glomerulus (DiGregorio et al., 2002), it might indicate differential processing of information related to Purkinje cell zebrin pattern, such as a lower sensitivity to glutamate spillover in NR2C negative granule cells. For instance, it was recently showed that low frequency transmission (50Hz) at the mossy fibre to granule cell synapse is sustained through NR2C subunit activation (Schwartz et al., 2012). Would that mean that low frequency inputs are filtered in NR2C-negative granule cells, or that *in vivo*, the input patterns are intrinsically different, and that differential NMDAR expression is a compensation to normalise granule cell firing patterns in the entire cerebellar cortex? The question remains open.

6.4 CONCLUSION AND FUTURE DIRECTIONS

Besides the experiments already mentioned above, I would like to suggest some extra experiments that, in my opinion, would be very interesting to perform in a near future.

Concerning high frequency transmission, I think that the next step to understand the temporal processing in the mossy fibre pathway should be to decipher the molecular mechanisms regulating short term plasticities during high frequency bursts. The Ca^{2+} kinetics of these plasticities were already studied, but the control of the different vesicle pools has not been investigated yet. Moreover, we should take advantage of what is already know in other models such as aplysia or at the Calyx of Held, in which similar mechanisms were observed. On a more physiological point of view, it is important to understand how bursts drive Purkinje cell firing, and how the molecular layer inhibitory interneurons can modulate excitation. Once the short term plasticities will be accurately described, the interplay between excitation and inhibition will be easier to interpret.

An important question in cerebellar processing is to understand the function of molecular layer interneurons. For instance, does one parallel fibre activate a Purkinje cell and perform feedforward inhibition onto the same cell? Or does feedforward inhibition recorded *in vitro* using compound stimulation only due to the activation of unrelated bundles of axons, some of them performing excitation, some of them performing inhibition? These questions could be addressed by performing either pair recordings, or by adapting our mapping experiments to study both inhibition and excitation. The latter experiment is actually, I think, the most important of my list in term of cerebellar physiology, because it might solve several unanswered question at the same time, about both spatial and temporal aspect of the signal processing, and would maybe give precious information for computational models.

On a more integrated scale, to properly understand our region of interest, we would need an accurate mapping of sensory inputs and of Purkinje cell outputs. This mapping could be performed *in vivo*, or by using tracing studies. Accurate identification of the Purkinje cells controlling different groups of muscles could indicate what the real influence range of a Purkinje cell is: one single muscle? A pair of agonist and antagonist muscles? A whole set of agonist or antagonist muscles, involved in specific synergistic movements such as those involved in withdrawal reflexes? Perhaps considering single Purkinje cells as primary motor neurons is a mistake, and cerebellar units are probably composed of cell populations.

7 REFERENCES

– A –

Adrian E (1935) Discharge frequencies in the cerebral and cerebellar cortex. J Physiol 83:32–33.

Adrian E (1943) Afferent areas in the cerebellum connected with the limbs. Brain 66:289–315.

Ahn a H, Dziennis S, Hawkes R, Herrup K (1994) The cloning of zebrin II reveals its identity with aldolase C. Development 120:2081–2090.

Akintunde a, Eisenman LM (1994) External cuneocerebellar projection and Purkinje cell zebrin II bands: a direct comparison of parasagittal banding in the mouse cerebellum. J Chem Neuroanat 7:75–86.

Albus J (1971) A theory of cerebellar function. Math Biosci 10:25–61.

Alcami P, Franconville R, Llano I, Marty A (2012) Measuring the firing rate of high-resistance neurons with cell-attached recording. J Neurosci 32:3118–3130.

Altman J, Bayer SA (1977) Time of origin and distribution of a new cell type in the rat cerebellar cortex. Exp Brain Res 29:265–274.

Apps R, Garwicz M (2005) Anatomical and physiological foundations of cerebellar information processing. Nat Rev Neurosci 6:297–311.

Apps R, Hawkes R (2009) Cerebellar cortical organization: a one-map hypothesis. Nat Rev Neurosci 10:670–681.

Arenz A, Bracey EF, Margrie TW (2009) Sensory representations in cerebellar granule cells. Curr Opin Neurobiol 19:445–451.

Arenz A, Silver RA, Schaefer AT, Margrie TW (2008) The contribution of single synapses to sensory representation in vivo. Science 321:977–980.

Armstrong CL, Chung S-H, Armstrong JN, Hochgeschwender U, Jeong Y-G, Hawkes R (2009) A novel somatostatin-immunoreactive mossy fiber pathway associated with Hsp25-immunoreactive purkinje cell stripes in the mouse cerebellum. J Comp Neurol 517:524–538.

Armstrong DM, Harvey RJ, Schild RF (1974) Topographical localization in the olivo-cerebellar projection: an electrophysiological study in the cat. J Comp Neurol 154:287–302.

Atluri PP, Regehr WG (1996) Determinants of the time course of facilitation at the granule cell to Purkinje cell synapse. J Neurosci 16:5661–5671.

– B –

Barmack NH, Yakhnitsa V (2008) Functions of interneurons in mouse cerebellum. J Neurosci 28:1140–1152.

Bastian AJ (2006) Learning to predict the future: the cerebellum adapts feedforward movement control. Curr Opin Neurobiol 16:645–649.

Bastianelli E (2003) Distribution of calcium-binding proteins in the cerebellum. Cerebellum 2:242–262.

Bauer C a, Wisner KW, Baizer JS, Brozoski TJ (2013) Tinnitus, unipolar brush cells, and cerebellar glutamatergic function in an animal model. PLoS One 8:e64726.

Bazzigaluppi P, Ruigrok T, Saisan P, De Zeeuw CI, de Jeu M (2012) Properties of the nucleo-olivary pathway: an in vivo whole-cell patch clamp study. PLoS One 7:e46360.

Bell CC (1981) An efference copy which is modified by reafferent input. Science 214:450–453.

Bell CC, Han VZ, Sugawara Y, Grant K (1997) Synaptic plasticity in a cerebellum-like structure depends on temporal order. Nature 387:278–281.

Bengtsson F, Ekerot C-F, Jörntell H (2011) In vivo analysis of inhibitory synaptic inputs and rebounds in deep cerebellar nuclear neurons. PLoS One 6:e18822.

Bengtsson F, Jörntell H (2009) Sensory transmission in cerebellar granule cells relies on similarly coded mossy fiber inputs. Proc Natl Acad Sci U S A 106:2389–2394.

Bergerot A, Rigby M, Bouvier G, Marcaggi P (2013) Persistent posttetanic depression at cerebellar parallel fiber to purkinje cell synapses. PLoS One 8:e70277.

Berkley KJ, Hand PJ (1978) Projections to the inferior olive of the cat. II. Comparisons of input from the gracile, cuneate and the spinal trigeminal nuclei. J Comp Neurol 180:253–264.

Bidoret C, Ayon A, Barbour B, Casado M (2009) Presynaptic NR2A-containing NMDA receptors implement a high-pass filter synaptic plasticity rule. Proc Natl Acad Sci U S A 106:14126–14131.

Blakemore SJ, Wolpert DM, Frith CD (1998) Central cancellation of self-produced tickle sensation. Nat Neurosci 1:635–640.

Blanco MJ, Peña-Melián A, Nieto MA (2002) Expression of EphA receptors and ligands during chick cerebellar development. Mech Dev 114:225–229.

Blenkinsop T a, Lang EJ (2011) Synaptic action of the olivocerebellar system on cerebellar nuclear spike activity. J Neurosci 31:14708–14720.

Boegman RJ, Parent A, Hawkes R (1988) Zonation in the rat cerebellar cortex: patches of high acetylcholinesterase activity in the granular layer are congruent with Purkinje cell compartments. Brain Res 448:237–251.

Bolk L (1906) Das Cerebellum der Säugetiere. Eine vergleichend anatomische Untersuchung. :[8], 337, [1] p. 183 illus., 3 fold. pl.

Bornschein G, Arendt O, Hallermann S, Brachtendorf S, Eilers J, Schmidt H (2013) Paired-pulse facilitation at recurrent Purkinje neuron synapses is independent of calbindin and parvalbumin during high-frequency activation. J Physiol 591:3355–3370.

Bouhours B, Trigo FF, Marty A (2011) Somatic depolarization enhances GABA release in cerebellar interneurons via a calcium/protein kinase C pathway. J Neurosci 31:5804–5815.

Bower JM, Beermann DH, Gibson JM, Shambes GM, Welker W (1981) Principles of organization of a cerebro-cerebellar circuit. Micromapping the projections from cerebral (SI) to cerebellar (granule cell layer) tactile areas of rats. Brain Behav Evol 18:1–18.

Bower JM, Kassel J (1990) Variability in tactile projection patterns to cerebellar folia crus IIA of the Norway rat. J Comp Neurol 302:768–778.

Boyd IA, Martin AR (1956a) Spontaneous subthreshold activity at mammalian neural muscular junctions. J Physiol 132:61–73.

Boyd IA, Martin AR (1956b) The end-plate potential in mammalian muscle. J Physiol 132:74–91.

Braak E, Braak H (1993) The new monodendritic neuronal type within the adult human cerebellar granule cell layer shows calretinin-immunoreactivity. Neurosci Lett 154:199–202.

Braitenberg V (1967) Is the cerebellar cortex a biological clock in the millisecond range? Prog Brain Res 25:334–346.

Braitenberg V, Atwood RP (1958) Morphological observations on the cerebellar cortex. J Comp Neurol 109:1–33.

Branco T, Staras K (2009) The probability of neurotransmitter release: variability and feedback control at single synapses. Nat Rev Neurosci 10:373–383.

Brenowitz SD, Regehr WG (2007) Reliability and heterogeneity of calcium signaling at single presynaptic boutons of cerebellar granule cells. J Neurosci 27:7888–7898.

Brickley SG, Cull-Candy SG, Farrant M (1996) Development of a tonic form of synaptic inhibition in rat cerebellar granule cells resulting from persistent activation of GABAA receptors. J Physiol 497 (Pt 3:753–759.

Brodal A, Kawamura K (1980) Olivocerebellar projection: a review. Adv Anat Embryol Cell Biol 64:IVIII, 1–140.

Brodal P, Bjaalie JG (1992) Organization of the pontine nuclei. Neurosci Res 13:83–118.

Brown IE, Bower JM (2001) Congruence of mossy fiber and climbing fiber tactile projections in the lateral hemispheres of the rat cerebellum. J Comp Neurol 429:59–70.

Brown SP, Safo PK, Regehr WG (2004) Endocannabinoids inhibit transmission at granule cell to Purkinje cell synapses by modulating three types of presynaptic calcium channels. J Neurosci 24:5623–5631.

Brunel N, Hakim V, Isope P, Nadal J-P, Barbour B (2004) Optimal information storage and the distribution of synaptic weights: perceptron versus Purkinje cell. Neuron 43:745–757.

Bucurenciu I, Kulik A, Schwaller B, Frotscher M, Jonas P (2008) Nanodomain coupling between Ca2+ channels and Ca2+ sensors promotes fast and efficient transmitter release at a cortical GABAergic synapse. Neuron 57:536–545.

Burgoyne RD (2007) Neuronal calcium sensor proteins: generating diversity in neuronal Ca2+ signalling. Nat Rev Neurosci 8:182–193.

– C –

Carter AG, Regehr WG (2002) Quantal events shape cerebellar interneuron firing. Nat Neurosci 5:1309–1318.

Casado M, Isope P, Ascher P (2002) Involvement of presynaptic N-methyl-D-aspartate receptors in cerebellar long-term depression. Neuron 33:123–130.

Cathala L, Brickley S, Cull-Candy S, Farrant M (2003) Maturation of EPSCs and intrinsic membrane properties enhances precision at a cerebellar synapse. J Neurosci 23:6074–6085.

Cathala L, Misra C, Cull-Candy S (2000) Developmental profile of the changing properties of NMDA receptors at cerebellar mossy fiber-granule cell synapses. J Neurosci 20:5899–5905.

Cesana E, Pietrajtis K, Bidoret C, Isope P, D'Angelo E, Dieudonné S, Forti L (2013) Granule cell ascending axon excitatory synapses onto Golgi cells implement a potent feedback circuit in the cerebellar granular layer. J Neurosci 33:12430–12446.

Chadderton P, Margrie TW, Häusser M (2004) Integration of quanta in cerebellar granule cells during sensory processing. Nature 428:856–860.

Chaumont J, Guyon N, Valera AM, Dugué GP, Popa D, Marcaggi P, Gautheron V, Reibel-Foisset S, Dieudonné S, Stephan A, Barrot M, Cassel J-C, Dupont J-L, Doussau F, Poulain B, Selimi F, Léna C, Isope P (2013) Clusters of cerebellar Purkinje cells control their afferent climbing fiber discharge. Proc Natl Acad Sci U S A.

Chédotal A, Pourquié O, Ezan F, San Clemente H, Sotelo C (1996) BEN as a presumptive target recognition molecule during the development of the olivocerebellar system. J Neurosci 16:3296–3310.

Chung S-H, Marzban H, Hawkes R (2009a) Compartmentation of the cerebellar nuclei of the mouse. Neuroscience 161:123–138.

Chung S-H, Marzban H, Watanabe M, Hawkes R (2009b) Phospholipase Cbeta4 expression identifies a novel subset of unipolar brush cells in the adult mouse cerebellum. Cerebellum 8:267–276.

Chung S-HS-H, Sillitoe R V, Croci L, Badaloni A, Consalez G, Hawkes R (2009c) Purkinje cell phenotype restricts the distribution of unipolar brush cells. Neuroscience 164:1496–1508.

Clements JD, Silver R a (2000) Unveiling synaptic plasticity: a new graphical and analytical approach. Trends Neurosci 23:105–113.

Coesmans M, Weber JT, De Zeeuw CI, Hansel C (2004) Bidirectional parallel fiber plasticity in the cerebellum under climbing fiber control. Neuron 44:691–700.

Cohen D, Yarom Y (1998) Patches of synchronized activity in the cerebellar cortex evoked by mossy-fiber stimulation: questioning the role of parallel fibers. Proc Natl Acad Sci U S A 95:15032–15036.

Cohen D, Yarom Y (2000) Cerebellar on-beam and lateral inhibition: two functionally distinct circuits. J Neurophysiol 83:1932–1940.

Comolli A (1910) Per una nuova divisione del cervelletto dei mammifer. Arch Ital Biol 9:247–273.

Courtemanche R, Pellerin J-P, Lamarre Y (2002) Local field potential oscillations in primate cerebellar cortex: modulation during active and passive expectancy. J Neurophysiol 88:771–782.

Courville J, Faraco-Cantin F, Diakiw N (1974) A functionally important feature of the distribution of the olivo-cerebellar climbing fibers. Can J Physiol Pharmacol 52:1212–1217.

Cramer SW, Gao W, Chen G, Ebner TJ (2013) Reevaluation of the beam and radial hypotheses of parallel fiber action in the cerebellar cortex. J Neurosci 33:11412–11424.

Crepel F, Jaillard D (1990) Protein kinases, nitric oxide and long-term depression of synapses in the cerebellum. Neuroreport 1:133–136.

Crook J, Hendrickson A, Robinson FR (2006) Co-localization of glycine and gaba immunoreactivity in interneurons in Macaca monkey cerebellar cortex. Neuroscience 141:1951–1959.

Crowley JJ, Carter AG, Regehr WG (2007) Fast vesicle replenishment and rapid recovery from desensitization at a single synaptic release site. J Neurosci 27:5448–5460.

– D –

D'Angelo E, Casali S (2012) Seeking a unified framework for cerebellar function and dysfunction: from circuit operations to cognition. Front Neural Circuits 6:116.

D'Angelo E, De Zeeuw CI (2009) Timing and plasticity in the cerebellum: focus on the granular layer. Trends Neurosci 32:30–40.

D'Angelo E, Nieus T, Maffei a, Armano S, Rossi P, Taglietti V, Fontana a, Naldi G (2001) Theta-frequency bursting and resonance in cerebellar granule cells: experimental evidence and modeling of a slow k+-dependent mechanism. J Neurosci 21:759–770.

D'Angelo E, Rossi P, Armano S, Taglietti V (1999) Evidence for NMDA and mGlu receptor-dependent long-term potentiation of mossy fiber-granule cell transmission in rat cerebellum. J Neurophysiol 81:277–287.

Dastjerdi F V, Consalez GG, Hawkes R (2012) Pattern formation during development of the embryonic cerebellum. Front Neuroanat 6:10.

De Solages C, Szapiro G, Brunel N, Hakim V, Isope P, Buisseret P, Rousseau C, Barbour B, Léna C (2008) High-frequency organization and synchrony of activity in the purkinje cell layer of the cerebellum. Neuron 58:775–788.

De Zeeuw CI, Hoebeek FE, Bosman LWJ, Schonewille M, Witter L, Koekkoek SK (2011) Spatiotemporal firing patterns in the cerebellum. Nat Rev Neurosci 12:327–344.

De Zeeuw CI, Simpson JI, Hoogenraad CC, Galjart N, Koekkoek SK, Ruigrok TJ (1998) Microcircuitry and function of the inferior olive. Trends Neurosci 21:391–400.

Dean P, Porrill J, Ekerot C-F, Jörntell H (2010) The cerebellar microcircuit as an adaptive filter: experimental and computational evidence. Nat Rev Neurosci 11:30–43.

Debanne D (2004) Information processing in the axon. Nat Rev Neurosci 5:304–316.

Debanne D, Bialowas A, Rama S (2013) What are the mechanisms for analogue and digital signalling in the brain? Nat Rev Neurosci 14:63–69.

Del Castillo J, Katz B (1954) Quantal components of the end-plate potential. J Physiol 124:560–573.

Dieudonne S (1998) Submillisecond kinetics and low efficacy of parallel fibre-Golgi cell synaptic currents in the rat cerebellum. J Physiol 510 (Pt 3:845–866.

Dieudonné S, Dumoulin A (2000) Serotonin-driven long-range inhibitory connections in the cerebellar cortex. J Neurosci 20:1837–1848.

DiGregorio D a, Nusser Z, Silver RA (2002) Spillover of glutamate onto synaptic AMPA receptors enhances fast transmission at a cerebellar synapse. Neuron 35:521–533.

Dingledine R, Borges K, Bowie D, Traynelis SF (1999) The glutamate receptor ion channels. Pharmacol Rev 51:7–61.

Dittman JS, Kreitzer a C, Regehr WG (2000) Interplay between facilitation, depression, and residual calcium at three presynaptic terminals. J Neurosci 20:1374–1385.

Dizon MJ, Khodakhah K (2011) The role of interneurons in shaping Purkinje cell responses in the cerebellar cortex. J Neurosci 31:10463–10473.

Donoghue JP, Leibovic S, Sanes JN (1992) Organization of the forelimb area in squirrel monkey motor cortex: representation of digit, wrist, and elbow muscles. Exp Brain Res 89:1–19.

Doussau F, Humeau Y, Benfenati F, Poulain B (2010) A novel form of presynaptic plasticity based on the fast reactivation of release sites switched off during low-frequency depression. J Neurosci 30:16679–16691.

Ducić I, Caruncho HJ, Zhu WJ, Vicini S, Costa E (1995) gamma-Aminobutyric acid gating of Cl- channels in recombinant GABAA receptors. J Pharmacol Exp Ther 272:438–445.

Dugué GP, Brunel N, Hakim V, Schwartz E, Chat M, Lévesque M, Courtemanche R, Léna C, Dieudonné S (2009) Electrical coupling mediates tunable low-frequency oscillations and resonance in the cerebellar Golgi cell network. Neuron 61:126–139.

Dumoulin a, Triller A, Dieudonné S (2001) IPSC kinetics at identified GABAergic and mixed GABAergic and glycinergic synapses onto cerebellar Golgi cells. J Neurosci 21:6045–6057.

– E –

Eccles J, Llinas R, Sasaki K (1964) Golgi cell inhibition in the cerebellar cortex. Nature 204:1265–1266.

Eccles JC (1973) The cerebellum as a computer: patterns in space and time. J Physiol 229:1–32.

Eccles JC, Ito M, Szentágothai J (1967) The cerebellum as neuronal machine (Springer-Verlag, ed).

Edinger L (1910) Über die Einteilung des Cerebellums. Anat Anz 35:319–323.

Eggermann E, Bucurenciu I, Goswami SP, Jonas P (2012) Nanodomain coupling between Ca^{2+} channels and sensors of exocytosis at fast mammalian synapses. Nat Rev Neurosci 13:7–21.

Eilers J, Takechi H, Finch E a, Augustine GJ, Konnerth A (1997) Local dendritic Ca2+ signaling induces cerebellar long-term depression. Learn Mem 4:159–168.

Ekerot C, Jörntell H (2003) Parallel fiber receptive fields: a key to understanding cerebellar operation and learning. Cerebellum 2:101–109.

Ekerot CF, Jörntell H (2001) Parallel fibre receptive fields of Purkinje cells and interneurons are climbing fibre-specific. Eur J Neurosci 13:1303–1310.

Ekerot C-F, Larson B (1979) The dorsal spino-olivocerebellar system in the cat. I. Functional organization and termination in the anterior lobe. Exp Brain Res 36:201–217.

Ekerot CF, Larson B, Oscarsson O (1979) Information carried by the spinocerebellar paths. Prog Brain Res 50:79–90.

Ekerot CF, Oscarsson O, Schouenborg J (1987) Stimulation of cat cutaneous nociceptive C fibres causing tonic and synchronous activity in climbing fibres. J Physiol 386:539–546.

Engbers JDT, Anderson D, Asmara H, Rehak R, Mehaffey WH, Hameed S, McKay BE, Kruskic M, Zamponi GW, Turner RW (2012) Intermediate conductance calcium-activated potassium channels modulate summation of parallel fiber input in cerebellar Purkinje cells. Proc Natl Acad Sci U S A 109:2601–2606.

– F –

Fatt P, Katz B (1952) Spontaneous subthreshold activity at motor nerve endings. J Physiol 117:109–128.

Foster K a, Crowley JJ, Regehr WG (2005) The influence of multivesicular release and postsynaptic receptor saturation on transmission at granule cell to Purkinje cell synapses. J Neurosci 25:11655–11665.

Fujita H, Morita N, Furuichi T, Sugihara I (2012) Clustered fine compartmentalization of the mouse embryonic cerebellar cortex and its rearrangement into the postnatal striped configuration. J Neurosci 32:15688–15703.

– G –

Gall D, Prestori F, Sola E, D'Errico A, Roussel C, Forti L, Rossi P, D'Angelo E (2005a) Intracellular calcium regulation by burst discharge determines bidirectional long-term synaptic plasticity at the cerebellum input stage. J Neurosci 25:4813–4822.

Gall D, Roussel C, Nieus T, Cheron G, Servais L, D'Angelo E, Schiffmann SN (2005b) Role of calcium binding proteins in the control of cerebellar granule cell neuronal excitability: experimental and modeling studies. Prog Brain Res 148:321–328.

Gao W, Chen G, Reinert KC, Ebner TJ (2006) Cerebellar cortical molecular layer inhibition is organized in parasagittal zones. J Neurosci 26:8377–8387.

Gao Z, van Beugen BJ, De Zeeuw CI (2012) Distributed synergistic plasticity and cerebellar learning. Nat Rev Neurosci 13:619–635.

Garwicz M, Ekerot CF (1994) Topographical organization of the cerebellar cortical projection to nucleus interpositus anterior in the cat. J Physiol 474:245–260.

Garwicz M, Ekerot C-F, Schouenborg J (1992) Distribution of Cutaneous Nociceptive and Tactile Climbing Fibre Input to Sagittal Zones in Cat Cerebellar Anterior Lobe. Eur J Neurosci 4:289–295.

Garwicz M, Jorntell H, Ekerot CF (1998a) Cutaneous receptive fields and topography of mossy fibres and climbing fibres projecting to cat cerebellar C3 zone. J Physiol 512 (Pt 1:277–293.

Garwicz M, Jorntell H, Ekerot CF (1998b) Cutaneous receptive fields and topography of mossy fibres and climbing fibres projecting to cat cerebellar C3 zone. J Physiol 512 (Pt 1:277–293.

Gebre S a, Reeber SL, Sillitoe R V (2012) Parasagittal compartmentation of cerebellar mossy fibers as revealed by the patterned expression of vesicular glutamate transporters VGLUT1 and VGLUT2. Brain Struct Funct 217:165–180.

Geiger JR, Jonas P (2000) Dynamic control of presynaptic Ca(2+) inflow by fast-inactivating K(+) channels in hippocampal mossy fiber boutons. Neuron 28:927–939.

Gellman R, Houk JC, Gibson AR (1983) Somatosensory properties of the inferior olive of the cat. J Comp Neurol 215:228–243.

Gerrits NM, Voogd J, Nas WS (1985) Cerebellar and olivary projections of the external and rostral internal cuneate nuclei in the cat. Exp Brain Res 57:239–255.

Geurts FJ, Timmermans J, Shigemoto R, De Schutter E (2001) Morphological and neurochemical differentiation of large granular layer interneurons in the adult rat cerebellum. Neuroscience 104:499–512.

Gibson JR, Beierlein M, Connors BW (1999) Two networks of electrically coupled inhibitory neurons in neocortex. Nature 402:75–79.

Gilbert PF, Thach WT (1977) Purkinje cell activity during motor learning. Brain Res 128:309–328.

Glickstein M, Sultan F, Voogd J (2011) Functional localization in the cerebellum. Cortex 47:59–80.

Goto J-I, Inoue T, Kuruma A, Mikoshiba K (2006) Short-term potentiation at the parallel fiber-Purkinje cell synapse. Neurosci Res 55:28–33.

Gould HJ (1986) Body surface maps in the somatosensory cortex of rabbit. J Comp Neurol 243:207–233.

Granit R, Phillips CG (1956) Excitatory and inhibitory processes acting upon individual Purkinje cells of the cerebellum in cats. J Physiol 133:520–547.

Grishkat HL, Eisenman LM (1995) Development of the spinocerebellar projection in the prenatal mouse. J Comp Neurol 363:93–108.

Groenewegen HJ, Voogd J (1977) The parasagittal zonation within the olivocerebellar projection. I. Climbing fiber distribution in the vermis of cat cerebellum. J Comp Neurol 174:417–488.

Grossman Y, Parnas I, Spira ME (1979) Differential conduction block in branches of a bifurcating axon. J Physiol 295:283–305.

Gundappa-Sulur G, De Schutter E, Bower JM (1999) Ascending granule cell axon: an important component of cerebellar cortical circuitry. J Comp Neurol 408:580–596.

– H –

Hallermann S, Fejtova A, Schmidt H, Weyhersmüller A, Silver RA, Gundelfinger ED, Eilers J (2010) Bassoon speeds vesicle reloading at a central excitatory synapse. Neuron 68:710–723.

Hallermann S, Silver RA (2013) Sustaining rapid vesicular release at active zones: potential roles for vesicle tethering. Trends Neurosci 36:185–194.

Hámori J (1981) Synaptic input to the axon hillock and initial segment of inhibitory interneurons in the cerebellar cortex of the rat. Cell Tissue Res 217:553–562.

Han VZ, Grant K, Bell CC (2000) Reversible associative depression and nonassociative potentiation at a parallel fiber synapse. Neuron 27:611–622.

Hartell N a (1996) Strong activation of parallel fibers produces localized calcium transients and a form of LTD that spreads to distant synapses. Neuron 16:601–610.

Harvey RJ, Napper RM (1988) Quantitative study of granule and Purkinje cells in the cerebellar cortex of the rat. J Comp Neurol 274:151–157.

Harvey RJ, Napper RM (1991) Quantitative studies on the mammalian cerebellum. Prog Neurobiol 36:437–463.

Häusser M, Clark B a (1997) Tonic synaptic inhibition modulates neuronal output pattern and spatiotemporal synaptic integration. Neuron 19:665–678.

Häusser M, Raman IM, Otis T, Smith SL, Nelson A, du Lac S, Loewenstein Y, Mahon S, Pennartz C, Cohen I, Yarom Y (2004) The beat goes on: spontaneous firing in mammalian neuronal microcircuits. J Neurosci 24:9215–9219.

Hawkes R, Colonnier M, Leclerc N (1985) Monoclonal antibodies reveal sagittal banding in the rodent cerebellar cortex. Brain Res 333:359–365.

Hawkes R, Gallagher E, Ozol K (1997) Blebs in the mouse cerebellar granular layer as a sign of structural inhomogeneity. 1. Anterior lobe vermis. Acta Anat (Basel) 158:205–214.

Hawkes R, Herrup K (1995) Aldolase C/zebrin II and the regionalization of the cerebellum. J Mol Neurosci 6:147–158.

Hawkes R, Leclerc N (1989) Purkinje cell axon collateral distributions reflect the chemical compartmentation of the rat cerebellar cortex. Brain Res 476:279–290.

Heck D, Sultan F (2002) Cerebellar structure and function: making sense of parallel fibers. Hum Mov Sci 21:411–421.

Heck DH, Thach WT, Keating JG (2007) On-beam synchrony in the cerebellum as the mechanism for the timing and coordination of movement. Proc Natl Acad Sci U S A 104:7658–7663.

Heckroth J a, Eisenman LM (1988) Parasagittal organization of mossy fiber collaterals in the cerebellum of the mouse. J Comp Neurol 270:385–394.

Hess DT, Voogd J (1986) Chemoarchitectonic zonation of the monkey cerebellum. Brain Res 369:383–387.

Hillyard DR, Monje VD, Mintz IM, Bean BP, Nadasdi L, Ramachandran J, Miljanich G, Azimi-Zoonooz A, McIntosh JM, Cruz LJ (1992) A new Conus peptide ligand for mammalian presynaptic Ca2+ channels. Neuron 9:69–77.

Hirono M, Saitow F, Kudo M, Suzuki H, Yanagawa Y, Yamada M, Nagao S, Konishi S, Obata K (2012) Cerebellar globular cells receive monoaminergic excitation and monosynaptic inhibition from Purkinje cells. PLoS One 7:e29663.

Huang C-C, Sugino K, Shima Y, Guo C, Bai S, Mensh BD, Nelson SB, Hantman AW (2013) Convergence of pontine and proprioceptive streams onto multimodal cerebellar granule cells. Elife 2:e00400.

Hull C a, Chu Y, Thanawala M, Regehr WG (2013) Hyperpolarization induces a long-term increase in the spontaneous firing rate of cerebellar Golgi cells. J Neurosci 33:5895–5902.

Hull C, Regehr WG (2012) Identification of an inhibitory circuit that regulates cerebellar Golgi cell activity. Neuron 73:149–158.

Humeau Y, Doussau F, Vitiello F, Greengard P, Benfenati F, Poulain B (2001a) Synapsin controls both reserve and releasable synaptic vesicle pools during neuronal activity and short-term plasticity in Aplysia. J Neurosci 21:4195–4206.

Humeau Y, Popoff MR, Kojima H, Doussau F, Poulain B (2002) Rac GTPase plays an essential role in exocytosis by controlling the fusion competence of release sites. J Neurosci 22:7968–7981.

Humeau Y, Vitale N, Chasserot-Golaz S, Dupont JL, Du G, Frohman M a, Bader MF, Poulain B (2001b) A role for phospholipase D1 in neurotransmitter release. Proc Natl Acad Sci U S A 98:15300–15305.

– I –

Isope P, Barbour B (2002) Properties of unitary granule cell-->Purkinje cell synapses in adult rat cerebellar slices. J Neurosci 22:9668–9678.

Ito M (2006) Cerebellar circuitry as a neuronal machine. Prog Neurobiol 78:272–303.

Ito M (2008) Control of mental activities by internal models in the cerebellum. Nat Rev Neurosci 9:304–313.

Ito M, Kano M (1982) Long-lasting depression of parallel fiber-Purkinje cell transmission induced by conjunctive stimulation of parallel fibers and climbing fibers in the cerebellar cortex. Neurosci Lett 33:253–258.

Ito M, Sakurai M, Tongroach P (1982) Climbing fibre induced depression of both mossy fibre responsiveness and glutamate sensitivity of cerebellar Purkinje cells. J Physiol 324:113–134.

Ivry RB, Keele SW, Diener HC (1988) Dissociation of the lateral and medial cerebellum in movement timing and movement execution. Exp Brain Res 73:167–180.

– J –

Jaarsma D, Diño MR, Ohishi H, Shigemoto R, Mugnaini E (1998) Metabotropic glutamate receptors are associated with non-synaptic appendages of unipolar brush cells in rat cerebellar cortex and cochlear nuclear complex. J Neurocytol 27:303–327.

Jacoby S, Sims RE, Hartell N a (2001) Nitric oxide is required for the induction and heterosynaptic spread of long-term potentiation in rat cerebellar slices. J Physiol 535:825–839.

Jakab RL, Hámori J (1988) Quantitative morphology and synaptology of cerebellar glomeruli in the rat. Anat Embryol (Berl) 179:81–88.

Ji Z, Hawkes R (1994) Topography of Purkinje cell compartments and mossy fiber terminal fields in lobules II and III of the rat cerebellar cortex: spinocerebellar and cuneocerebellar projections. Neuroscience 61:935–954.

Jörntell H, Ekerot C-F (2002) Reciprocal bidirectional plasticity of parallel fiber receptive fields in cerebellar Purkinje cells and their afferent interneurons. Neuron 34:797–806.

Jörntell H, Ekerot C-F (2003) Receptive field plasticity profoundly alters the cutaneous parallel fiber synaptic input to cerebellar interneurons in vivo. J Neurosci 23:9620–9631.

Jörntell H, Ekerot C-F (2006) Properties of somatosensory synaptic integration in cerebellar granule cells in vivo. J Neurosci 26:11786–11797.

Jörntell H, Garwicz M, Ekerot CF (1996) Relation between cutaneous receptive fields and muscle afferent input to climbing fibres projecting to the cerebellar C3 zone in the cat. Eur J Neurosci 8:1769–1779.

Jörntell H, Hansel C (2006) Synaptic memories upside down: bidirectional plasticity at cerebellar parallel fiber-Purkinje cell synapses. Neuron 52:227–238.

– K –

Kaas JH (2012) Evolution of columns, modules, and domains in the neocortex of primates. Proc Natl Acad Sci U S A 109 Suppl:10655–10660.

Kakizawa S, Yamasaki M, Watanabe M, Kano M (2000) Critical period for activity-dependent synapse elimination in developing cerebellum. J Neurosci 20:4954–4961.

Kanichay RT, Silver RA (2008) Synaptic and cellular properties of the feedforward inhibitory circuit within the input layer of the cerebellar cortex. J Neurosci 28:8955–8967.

Karavanova I, Vasudevan K, Cheng J, Buonanno A (2007) Novel regional and developmental NMDA receptor expression patterns uncovered in NR2C subunit-beta-galactosidase knock-in mice. Mol Cell Neurosci 34:468–480.

Kassel J, Shambes GM, Welker W (1984) Fractured cutaneous projections to the granule cell layer of the posterior cerebellar hemisphere of the domestic cat. J Comp Neurol 225:458–468.

Katz B, Miledi R (1968) The role of calcium in neuromuscular facilitation. J Physiol 195:481–492.

Katz B, Miledi R (1972) The statistical nature of the acetycholine potential and its molecular components. J Physiol 224:665–699.

Khosrovani S, Van Der Giessen RS, De Zeeuw CI, De Jeu MTG (2007) In vivo mouse inferior olive neurons exhibit heterogeneous subthreshold oscillations and spiking patterns. Proc Natl Acad Sci U S A 104:15911–15916.

Korn H, Axelrad H (1980) Electrical inhibition of Purkinje cells in the cerebellum of the rat. Proc Natl Acad Sci U S A 77:6244–6247.

Krahe R, Gabbiani F (2004) Burst firing in sensory systems. Nat Rev Neurosci 5:13–23.

Krnjevic K, Miledi R (1959) Presynaptic failure of neuromuscular propagation in rats. J Physiol 149:1–22.

Künzle H (1975) Autoradiographic tracing of the cerebellar projections from the lateral reticular nucleus in the cat. Exp Brain Res 22:255–266.

– L –

Lainé J, Axelrad H (2002) Extending the cerebellar Lugaro cell class. Neuroscience 115:363–374.

Larouche M, Hawkes R (2006) From clusters to stripes: the developmental origins of adult cerebellar compartmentation. Cerebellum 5:77–88.

Larsell O (1952) The morphogenesis and adult pattern of the lobules and fissures of the cerebellum of the white rat. J Comp Neurol 97:281–356.

Leclerc N, Doré L, Parent A, Hawkes R (1990) The compartmentalization of the monkey and rat cerebellar cortex: zebrin I and cytochrome oxidase. Brain Res 506:70–78.

Lemkey-Johnston N, Larramendi LM (1968) Types and distribution of synapses upon basket and stellate cells of the mouse cerebellum: an electron microscopic study. J Comp Neurol 134:73–112.

Lev-Ram V, Jiang T, Wood J, Lawrence DS, Tsien RY (1997) Synergies and coincidence requirements between NO, cGMP, and Ca2+ in the induction of cerebellar long-term depression. Neuron 18:1025–1038.

Lev-Ram V, Makings LR, Keitz PF, Kao JP, Tsien RY (1995) Long-term depression in cerebellar Purkinje neurons results from coincidence of nitric oxide and depolarization-induced Ca2+ transients. Neuron 15:407–415.

Lev-Ram V, Wong ST, Storm DR, Tsien RY (2002) A new form of cerebellar long-term potentiation is postsynaptic and depends on nitric oxide but not cAMP. Proc Natl Acad Sci U S A 99:8389–8393.

Libster AM, Yarom Y (2013) In and out of the loop: external and internal modulation of the olivo-cerebellar loop. Front Neural Circuits 7:73.

Linden DJ, Dickinson MH, Smeyne M, Connor J a (1991) A long-term depression of AMPA currents in cultured cerebellar Purkinje neurons. Neuron 7:81–89.

Llano I, Gerschenfeld HM (1993) Inhibitory synaptic currents in stellate cells of rat cerebellar slices. J Physiol 468:177–200.

Llinas R, Baker R, Sotelo C (1974) Electrotonic coupling between neurons in cat inferior olive. J Neurophysiol 37:560–571.

Llinás R, Sugimori M (1980) Electrophysiological properties of in vitro Purkinje cell dendrites in mammalian cerebellar slices. J Physiol 305:197–213.

Llinás R, Yarom Y (1986) Oscillatory properties of guinea-pig inferior olivary neurones and their pharmacological modulation: an in vitro study. J Physiol 376:163–182.

Llinás RR (2009) Inferior olive oscillation as the temporal basis for motricity and oscillatory reset as the basis for motor error correction. Neuroscience 162:797–804.

Loewenstein Y, Mahon S, Chadderton P, Kitamura K, Sompolinsky H, Yarom Y, Häusser M (2005) Bistability of cerebellar Purkinje cells modulated by sensory stimulation. Nat Neurosci 8:202–211.

Lonart G, Schoch S, Kaeser PS, Larkin CJ, Südhof TC, Linden DJ (2003) Phosphorylation of RIM1alpha by PKA triggers presynaptic long-term potentiation at cerebellar parallel fiber synapses. Cell 115:49–60.

– M –

Mann-Metzer P, Yarom Y (1999) Electrotonic coupling interacts with intrinsic properties to generate synchronized activity in cerebellar networks of inhibitory interneurons. J Neurosci 19:3298–3306.

Mann-Metzer P, Yarom Y (2000) Electrotonic coupling synchronizes interneuron activity in the cerebellar cortex. Prog Brain Res 124:115–122.

Marani E (1977) The subcellular distribution of 5'-nucleotidase activity in mouse cerebellum. Exp Neurol 57:1042–1048.

Marr D (1969) A theory of cerebellar cortex. J Physiol 202:437–470.

Marzban H, Khanzada U, Shabir S, Hawkes R, Langnaese K, Smalla K-H, Bockers TM, Gundelfinger ED, Gordon-Weeks PR, Beesley PW (2003) Expression of the immunoglobulin superfamily neuroplastin adhesion molecules in adult and developing mouse cerebellum and their localisation to parasagittal stripes. J Comp Neurol 462:286–301.

Mason CA, Gregory E (1984) Postnatal maturation of cerebellar mossy and climbing fibers: transient expression of dual features on single axons. J Neurosci 4:1715–1735.

Mathy A, Ho SSN, Davie JT, Duguid IC, Clark BA, Häusser M (2009) Encoding of oscillations by axonal bursts in inferior olive neurons. Neuron 62:388–399.

Matsushita M, Ragnarson B, Grant G (1991) Topographic relationship between sagittal Purkinje cell bands revealed by a monoclonal antibody to zebrin I and spinocerebellar projections arising from the central cervical nucleus in the rat. Exp Brain Res 84:133–141.

Matthews G, Fuchs P (2010) The diverse roles of ribbon synapses in sensory neurotransmission. Nat Rev Neurosci 11:812–822.

McKay BE, Engbers JDT, Mehaffey WH, Gordon GRJ, Molineux ML, Bains JS, Turner RW (2007) Climbing fiber discharge regulates cerebellar functions by controlling the intrinsic characteristics of purkinje cell output. J Neurophysiol 97:2590–2604.

Midtgaard J (1992) Membrane properties and synaptic responses of Golgi cells and stellate cells in the turtle cerebellum in vitro. J Physiol 457:329–354.

Mintz IM, Sabatini BL, Regehr WG (1995) Calcium control of transmitter release at a cerebellar synapse. Neuron 15:675–688.

Mitchell SJ, Silver RA (2003) Shunting inhibition modulates neuronal gain during synaptic excitation. Neuron 38:433–445.

Mittmann W, Häusser M (2007) Linking synaptic plasticity and spike output at excitatory and inhibitory synapses onto cerebellar Purkinje cells. J Neurosci 27:5559–5570.

Mittmann W, Koch U, Häusser M (2005) Feed-forward inhibition shapes the spike output of cerebellar Purkinje cells. J Physiol 563:369–378.

Morissette J, Bower JM (1996) Contribution of somatosensory cortex to responses in the rat cerebellar granule cell layer following peripheral tactile stimulation. Exp Brain Res 109:240–250.

Mugnaini E, Sekerková G, Martina M (2011) The unipolar brush cell: a remarkable neuron finally receiving deserved attention. Brain Res Rev 66:220–245.

Mukamel E a, Nimmerjahn A, Schnitzer MJ (2009) Automated analysis of cellular signals from large-scale calcium imaging data. Neuron 63:747–760.

Murase S, Hayashi Y (1996) Expression pattern of integrin beta 1 subunit in Purkinje cells of rat and cerebellar mutant mice. J Comp Neurol 375:225–237.

Murthy VN, Sejnowski TJ, Stevens CF (1997) Heterogeneous release properties of visualized individual hippocampal synapses. Neuron 18:599–612.

Myoga MH, Regehr WG (2011) Calcium microdomains near R-type calcium channels control the induction of presynaptic long-term potentiation at parallel fiber to purkinje cell synapses. J Neurosci 31:5235–5243.

Napper RM, Harvey RJ (1988) Number of parallel fiber synapses on an individual Purkinje cell in the cerebellum of the rat. J Comp Neurol 274:168–177.

– N –

Neki A, Ohishi H, Kaneko T, Shigemoto R, Nakanishi S, Mizuno N (1996) Metabotropic glutamate receptors mGluR2 and mGluR5 are expressed in two non-overlapping populations of Golgi cells in the rat cerebellum. Neuroscience 75:815–826.

Nishiyama H, Linden DJ (2004) Differential maturation of climbing fiber innervation in cerebellar vermis. J Neurosci 24:3926–3932.

Nunzi M., Russo M, Mugnaini E (2003) Vesicular glutamate transporters VGLUT1 and VGLUT2 define two subsets of unipolar brush cells in organotypic cultures of mouse vestibulocerebellum. Neuroscience 122:359–371.

Nunzi M-G, Shigemoto R, Mugnaini E (2002) Differential expression of calretinin and metabotropic glutamate receptor mGluR1alpha defines subsets of unipolar brush cells in mouse cerebellum. J Comp Neurol 451:189–199.

– O –

O'Brien J, Unwin N (2006) Organization of spines on the dendrites of Purkinje cells. Proc Natl Acad Sci U S A 103:1575–1580.

O'Donoghue DL, King JS, Bishop G a (1989) Physiological and anatomical studies of the interactions between Purkinje cells and basket cells in the cat's cerebellar cortex: evidence for a unitary relationship. J Neurosci 9:2141–2150.

Orduz D, Llano I (2007) Recurrent axon collaterals underlie facilitating synapses between cerebellar Purkinje cells. Proc Natl Acad Sci U S A 104:17831–17836.

Oscarsson O (1979) Functional units of the cerebellum - sagittal zones and microzones. Trends Neurosci 2:143–145.

Ottersen OP, Davanger S, Storm-Mathisen J (1987) Glycine-like immunoreactivity in the cerebellum of rat and Senegalese baboon, Papio papio: a comparison with the distribution of GABA-like immunoreactivity and with [3H]glycine and [3H]GABA uptake. Exp Brain Res 66:211–221.

Ottersen OP, Storm-Mathisen J, Somogyi P (1988) Colocalization of glycine-like and GABA-like immunoreactivities in Golgi cell terminals in the rat cerebellum: a postembedding light and electron microscopic study. Brain Res 450:342–353.

Ozden I, Lee HM, Sullivan MR, Wang SS-H (2008) Identification and clustering of event patterns from in vivo multiphoton optical recordings of neuronal ensembles. J Neurophysiol 100:495–503.

Ozden I, Sullivan MR, Lee HM, Wang SS-H (2009) Reliable coding emerges from coactivation of climbing fibers in microbands of cerebellar Purkinje neurons. J Neurosci 29:10463–10473.

– P –

Palay SL, Chan-Palay V (1974) Cerebellar cortex: cytology and organization. New-York: Springer.

Palkovits M, Magyar P, Szentágothai J (1971) Quantitative histological analysis of the cerebellar cortex in the cat. II. Cell numbers and densities in the granular layer. Brain Res 32:15–30.

Palkovits M, Mezey E, Hámori J, Szentágothai J (1977) Quantitative histological analysis of the cerebellar nuclei in the cat. I. Numerical data on cells and on synapses. Exp Brain Res 28:189–209.

Park C, Falls W, Finger JH, Longo-Guess CM, Ackerman SL (2002) Deletion in Catna2, encoding alpha N-catenin, causes cerebellar and hippocampal lamination defects and impaired startle modulation. Nat Genet 31:279–284.

Person AL, Raman IM (2012a) Purkinje neuron synchrony elicits time-locked spiking in the cerebellar nuclei. Nature 481:502–505.

Person AL, Raman IM (2012b) Synchrony and neural coding in cerebellar circuits. Front Neural Circuits 6:97.

Pichitpornchai C, Rawson J a, Rees S (1994) Morphology of parallel fibres in the cerebellar cortex of the rat: an experimental light and electron microscopic study with biocytin. J Comp Neurol 342:206–220.

Pijpers A, Apps R, Pardoe J, Voogd J, Ruigrok TJH (2006) Precise spatial relationships between mossy fibers and climbing fibers in rat cerebellar cortical zones. J Neurosci 26:12067–12080.

Piochon C, Levenes C, Ohtsuki G, Hansel C (2010) Purkinje cell NMDA receptors assume a key role in synaptic gain control in the mature cerebellum. J Neurosci 30:15330–15335.

Pugh JR, Jahr CE (2011) Axonal GABAA receptors increase cerebellar granule cell excitability and synaptic activity. J Neurosci 31:565–574.

– Q –

Qiu D, Knöpfel T (2009) Presynaptically expressed long-term depression at cerebellar parallel fiber synapses. Pflugers Arch 457:865–875.

Quy PN, Fujita H, Sakamoto Y, Na J, Sugihara I (2011) Projection patterns of single mossy fiber axons originating from the dorsal column nuclei mapped on the aldolase C compartments in the rat cerebellar cortex. J Comp Neurol 519:874–899.

– R –

Raman IM, Bean BP (1999) Ionic currents underlying spontaneous action potentials in isolated cerebellar Purkinje neurons. J Neurosci 19:1663–1674.

Ramon y Cajal S (1911) Histologie du système nerveux de l'homme & des vertébrés (Maloine A, ed).

Rancz E a, Ishikawa T, Duguid I, Chadderton P, Mahon S, Häusser M (2007) High-fidelity transmission of sensory information by single cerebellar mossy fibre boutons. Nature 450:1245–1248.

Redies C, Neudert F, Lin J (2011) Cadherins in cerebellar development: translation of embryonic patterning into mature functional compartmentalization. Cerebellum 10:393–408.

Reeber SL, Sillitoe R V (2011) Patterned expression of a cocaine- and amphetamine-regulated transcript peptide reveals complex circuit topography in the rodent cerebellar cortex. J Comp Neurol 519:1781–1796.

Regehr WG (1997) Interplay between sodium and calcium dynamics in granule cell presynaptic terminals. Biophys J 73:2476–2488.

Reid C a, Clements JD (1999) Postsynaptic expression of long-term potentiation in the rat dentate gyrus demonstrated by variance-mean analysis. J Physiol 518 (Pt 1:121–130.

Reinert KC, Dunbar RL, Gao W, Chen G, Ebner TJ (2004) Flavoprotein autofluorescence imaging of neuronal activation in the cerebellar cortex in vivo. J Neurophysiol 92:199–211.

Richter K, Langnaese K, Kreutz MR, Olias G, Zhai R, Scheich H, Garner CC, Gundelfinger ED (1999) Presynaptic cytomatrix protein bassoon is localized at both excitatory and inhibitory synapses of rat brain. J Comp Neurol 408:437–448.

Rokni D, Llinas R, Yarom Y (2007) Stars and stripes in the cerebellar cortex : a voltage sensitive dye study. 1:1–9.

Rosenblatt F (1958) The perceptron: a probabilistic model for information storage and organization in the brain. Psychol Rev 65:386–408.

Rossi DJ, Hamann M (1998) Spillover-mediated transmission at inhibitory synapses promoted by high affinity alpha6 subunit GABA(A) receptors and glomerular geometry. Neuron 20:783–795.

Roth A, Häusser M (2001) Compartmental models of rat cerebellar Purkinje cells based on simultaneous somatic and dendritic patch-clamp recordings. J Physiol 535:445–472.

Rowland NC, Jaeger D (2005) Coding of Tactile Response Properties in the Rat Deep Cerebellar Nuclei. :1236–1251.

Ruigrok TJ, Osse RJ, Voogd J (1992) Organization of inferior olivary projections to the flocculus and ventral paraflocculus of the rat cerebellum. J Comp Neurol 316:129–150.

Ruigrok TJH, Pijpers A, Goedknegt-Sabel E, Coulon P (2008) Multiple cerebellar zones are involved in the control of individual muscles: a retrograde transneuronal tracing study with rabies virus in the rat. Eur J Neurosci 28:181–200.

– S –

Sakurai M (1987) Synaptic modification of parallel fibre-Purkinje cell transmission in in vitro guinea-pig cerebellar slices. J Physiol 394:463–480.

Salin P a, Malenka RC, Nicoll R a (1996) Cyclic AMP mediates a presynaptic form of LTP at cerebellar parallel fiber synapses. Neuron 16:797–803.

Santamaria F, Tripp PG, Bower JM (2007) Feedforward inhibition controls the spread of granule cell-induced Purkinje cell activity in the cerebellar cortex. J Neurophysiol 97:248–263.

Saviane C, Silver RA (2006) Fast vesicle reloading and a large pool sustain high bandwidth transmission at a central synapse. Nature 439:983–987.

Schilling K, Oberdick J, Rossi F, Baader SL (2008) Besides Purkinje cells and granule neurons: an appraisal of the cell biology of the interneurons of the cerebellar cortex. Histochem Cell Biol 130:601–615.

Schmidt H, Brachtendorf S, Arendt O, Hallermann S, Ishiyama S, Bornschein G, Gall D, Schiffmann SN, Heckmann M, Eilers J (2013) Nanodomain coupling at an excitatory cortical synapse. Curr Biol 23:244–249.

Schoen SW, Graeber MB, Reddington M, Kreutzberg GW (1987) Light and electron microscopical immunocytochemistry of 5'-nucleotidase in rat cerebellum. Histochemistry 87:107–113.

Schonewille M, Gao Z, Boele H-J, Veloz MFV, Amerika WE, Simek AAM, De Jeu MT, Steinberg JP, Takamiya K, Hoebeek FE, Linden DJ, Huganir RL, De Zeeuw CI (2011) Reevaluating the role of LTD in cerebellar motor learning. Neuron 70:43–50.

Schonewille M, Luo C, Ruigrok TJH, Voogd J, Schmolesky MT, Rutteman M, Hoebeek FE, De Jeu MTG, De Zeeuw CI (2006) Zonal organization of the mouse flocculus: physiology, input, and output. J Comp Neurol 497:670–682.

Schwartz EJ, Rothman JS, Dugué GP, Diana M, Rousseau C, Silver RA, Dieudonné S (2012) NMDA receptors with incomplete Mg^{2+} block enable low-frequency transmission through the cerebellar cortex. J Neurosci 32:6878–6893.

Scott TG (1963) A unique pattern of localization within the cerebellum. Nature 200:793.

Shambes GM, Beermann DH, Welker W (1978a) Multiple tactile areas in cerebellar cortex: another patchy cutaneous projection to granule cell columns in rats. Brain Res 157:123–128.

Shambes GM, Gibson JM, Welker W (1978b) Fractured somatotopy in granule cell tactile areas of rat cerebellar hemispheres revealed by micromapping. Brain Behav Evol 15:94–140.

Shin S-L, Hoebeek FE, Schonewille M, De Zeeuw CI, Aertsen A, De Schutter E (2007) Regular patterns in cerebellar Purkinje cell simple spike trains. PLoS One 2:e485.

Shinoda Y, Sugihara I, Wu HS, Sugiuchi Y (2000) The entire trajectory of single climbing and mossy fibers in the cerebellar nuclei and cortex. Prog Brain Res 124:173–186.

Sigworth FJ (1980) The variance of sodium current fluctuations at the node of Ranvier. J Physiol 307:97–129.

Sillitoe R V, Benson M a, Blake DJ, Hawkes R (2003) Abnormal dysbindin expression in cerebellar mossy fiber synapses in the mdx mouse model of Duchenne muscular dystrophy. J Neurosci 23:6576–6585.

Sillitoe R V, Chung S-H, Fritschy J-M, Hoy M, Hawkes R (2008) Golgi cell dendrites are restricted by Purkinje cell stripe boundaries in the adult mouse cerebellar cortex. J Neurosci 28:2820–2826.

Sillitoe R V, Vogel MW, Joyner AL (2010) Engrailed homeobox genes regulate establishment of the cerebellar afferent circuit map. J Neurosci 30:10015–10024.

Silver IA, Erecińska M (1990) Intracellular and extracellular changes of [Ca2+] in hypoxia and ischemia in rat brain in vivo. J Gen Physiol 95:837–866.

Silver R a, Cull-Candy SG, Takahashi T (1996) Non-NMDA glutamate receptor occupancy and open probability at a rat cerebellar synapse with single and multiple release sites. J Physiol 494 (Pt 1:231–250.

Silver R a, Momiyama A, Cull-Candy SG (1998) Locus of frequency-dependent depression identified with multiple-probability fluctuation analysis at rat climbing fibre-Purkinje cell synapses. J Physiol 510 (Pt 3:881–902.

Silver RA (2003) Estimation of nonuniform quantal parameters with multiple-probability fluctuation analysis: theory, application and limitations. J Neurosci Methods 130:127–141.

Silver RA, Traynelis SF, Cull-Candy SG (1992) Rapid-time-course miniature and evoked excitatory currents at cerebellar synapses in situ. Nature 355:163–166.

Simat M, Parpan F, Fritschy J (2007) Heterogeneity of glycinergic and gabaergic interneurons in the granule cell layer of mouse cerebellum. J Comp Neurol 500:71–83.

Simonneau M, Tauc L, Baux G (1980) Quantal release of acetylcholine examined by current fluctuation analysis at an identified neuro-neuronal synapse of Aplysia. Proc Natl Acad Sci U S A 77:1661–1665.

Sims RE, Hartell N a (2005) Differences in transmission properties and susceptibility to long-term depression reveal functional specialization of ascending axon and parallel fiber synapses to Purkinje cells. J Neurosci 25:3246–3257.

Simsek-Duran F, Linden DJ, Lonart G (2004) Adapter protein 14-3-3 is required for a presynaptic form of LTP in the cerebellum. Nat Neurosci 7:1296–1298.

Singec I, Knoth R, Ditter M, Frotscher M, Volk B (2003) Neurogranin expression by cerebellar neurons in rodents and non-human primates. J Comp Neurol 459:278–289.

Snider R, Stowell A (1944) Receiving areas of the tactile, auditory, and visual systems in the cerebellum. J Neurophysiol 7:331–357.

Sotelo C, Chédotal A (2005) Development of the olivocerebellar system: migration and formation of cerebellar maps. Prog Brain Res 148:1–20.

Sperry RW (1950) Neural basis of the spontaneous optokinetic response produced by visual inversion. J Comp Physiol Psychol 43:482–489.

Steuber V, Mittmann W, Hoebeek FE, Silver RA, De Zeeuw CI, Häusser M, De Schutter E (2007) Cerebellar LTD and pattern recognition by Purkinje cells. Neuron 54:121–136.

Stuart G, Häusser M (1994) Initiation and spread of sodium action potentials in cerebellar Purkinje cells. Neuron 13:703–712.

Sugihara I (2011) Compartmentalization of the deep cerebellar nuclei based on afferent projections and aldolase C expression. Cerebellum 10:449–463.

Sugihara I, Fujita H, Na J, Quy PN, Li B-Y, Ikeda D (2009) Projection of reconstructed single Purkinje cell axons in relation to the cortical and nuclear aldolase C compartments of the rat cerebellum. J Comp Neurol 512:282–304.

Sugihara I, Quy PN (2007) Identification of aldolase C compartments in the mouse cerebellar cortex by olivocerebellar labeling. J Comp Neurol 500:1076–1092.

Sugihara I, Shinoda Y (2004) Molecular, topographic, and functional organization of the cerebellar cortex: a study with combined aldolase C and olivocerebellar labeling. J Neurosci 24:8771–8785.

Sugihara I, Shinoda Y (2007) Molecular, topographic, and functional organization of the cerebellar nuclei: analysis by three-dimensional mapping of the olivonuclear projection and aldolase C labeling. J Neurosci 27:9696–9710.

Sugihara I, Wu HS, Shinoda Y (2001) The entire trajectories of single olivocerebellar axons in the cerebellar cortex and their contribution to Cerebellar compartmentalization. J Neurosci 21:7715–7723.

Sultan F, Bower JM (1998) Quantitative Golgi study of the rat cerebellar molecular layer interneurons using principal component analysis. J Comp Neurol 393:353–373.

Sultan F, Braitenberg V (1993) Shapes and sizes of different mammalian cerebella. A study in quantitative comparative neuroanatomy. J Hirnforsch 34:79–92.

Szapiro G, Barbour B (2007) Multiple climbing fibers signal to molecular layer interneurons exclusively via glutamate spillover. Nat Neurosci 10:735–742.

Szentágothai J, Rajkovits K (1959) Über den Ursprung der Kletterfasern des Kleinhirns. Z Anat Entwicklungsgesch 121:130–141.

– T –

Ting JT, Phillips PEM, Begley TP (2007) Neurotransmitter Release. In: Wiley Encyclopedia of Chemical Biology, pp 1–12. John Wiley & Sons, Inc.

Traynelis SF, Silver R a, Cull-Candy SG (1993) Estimated conductance of glutamate receptor channels activated during EPSCs at the cerebellar mossy fiber-granule cell synapse. Neuron 11:279–289.

Trott JR, Armstrong DM (1987) The cerebellar corticonuclear projection from lobule Vb/c of the cat anterior lobe: a combined electrophysiological and autoradiographic study. II. Projections from the vermis. Exp Brain Res 68:339–354.

– V –

Valera AM, Doussau F, Poulain B, Barbour B, Isope P (2012) Adaptation of granule cell to Purkinje cell synapses to high-frequency transmission. J Neurosci 32:3267–3280.

Van Beugen BJ, Nagaraja RY, Hansel C (2006) Climbing fiber-evoked endocannabinoid signaling heterosynaptically suppresses presynaptic cerebellar long-term potentiation. J Neurosci 26:8289–8294.

Van der Want JJ, Wiklund L, Guegan M, Ruigrok T, Voogd J (1989) Anterograde tracing of the rat olivocerebellar system with Phaseolus vulgaris leucoagglutinin (PHA-L). Demonstration of climbing fiber collateral innervation of the cerebellar nuclei. J Comp Neurol 288:1–18.

Van Woerden GM, Hoebeek FE, Gao Z, Nagaraja RY, Hoogenraad CC, Kushner S a, Hansel C, De Zeeuw CI, Elgersma Y (2009) betaCaMKII controls the direction of plasticity at parallel fiber-Purkinje cell synapses. Nat Neurosci 12:823–825.

Vervaeke K, Lorincz A, Gleeson P, Farinella M, Nusser Z, Silver RA (2010) Rapid desynchronization of an electrically coupled interneuron network with sparse excitatory synaptic input. Neuron 67:435–451.

Vervaeke K, Lorincz A, Nusser Z, Silver RA (2012) Gap junctions compensate for sublinear dendritic integration in an inhibitory network. Science 335:1624–1628.

Voogd J (1967) Comparative aspects of the structure and fibre connexions of the mammalian cerebellum. Prog Brain Res 25:94–134.

Voogd J (1969) The importance of fiber connections in the comparative anatomy of the mammalian cerebellum. In: Neurobiology of cerebellar evolution and development (Llinas R, ed), pp 493–514. American Medical Association.

Voogd J, Glickstein M (1998) The anatomy of the cerebellum. Trends Neurosci 21:370–375.

Voogd J, Pardoe J, Ruigrok TJH, Apps R (2003) The distribution of climbing and mossy fiber collateral branches from the copula pyramidis and the paramedian lobule: congruence of climbing fiber cortical zones and the pattern of zebrin banding within the rat cerebellum. J Neurosci 23:4645–4656.

Voogd J, Ruigrok TJH (2004) The organization of the corticonuclear and olivocerebellar climbing fiber projections to the rat cerebellar vermis: the congruence of projection zones and the zebrin pattern. J Neurocytol 33:5–21.

– W –

Walter JT, Alviña K, Womack MD, Chevez C, Khodakhah K (2006) Decreases in the precision of Purkinje cell pacemaking cause cerebellar dysfunction and ataxia. Nat Neurosci 9:389–397.

Walter JT, Dizon M-J, Khodakhah K (2009) The functional equivalence of ascending and parallel fiber inputs in cerebellar computation. J Neurosci 29:8462–8473.

Walter JT, Khodakhah K (2006) The linear computational algorithm of cerebellar Purkinje cells. J Neurosci 26:12861–12872.

Wang VY, Zoghbi HY (2001) Genetic regulation of cerebellar development. Nat Rev Neurosci 2:484–491.

Wang X, Chen G, Gao W, Ebner TJ (2011) Parasagittally aligned, mGluR1-dependent patches are evoked at long latencies by parallel fiber stimulation in the mouse cerebellar cortex in vivo. J Neurophysiol 105:1732–1746.

Wang YT, Linden DJ (2000) Expression of cerebellar long-term depression requires postsynaptic clathrin-mediated endocytosis. Neuron 25:635–647.

Wassef M, Sotelo C (1984) Asynchrony in the expression of guanosine 3':5'-phosphate-dependent protein kinase by clusters of Purkinje cells during the perinatal development of rat cerebellum. Neuroscience 13:1217–1241.

Wassef M, Sotelo C, Thomasset M, Granholm AC, Leclerc N, Rafrafi J, Hawkes R (1990) Expression of compartmentation antigen zebrin I in cerebellar transplants. J Comp Neurol 294:223–234.

Watanabe D, Nakanishi S (2003) mGluR2 postsynaptically senses granule cell inputs at Golgi cell synapses. Neuron 39:821–829.

Welsh JP, Lang EJ, Suglhara I, Llinás R (1995) Dynamic organization of motor control within the olivocerebellar system. Nature 374:453–457.

Wilkin GP, Csillag A, Balázs R, Kingsbury AE, Wilson JE, Johnson AL (1981) Localization of high affinity [3H]glycine transport sites in the cerebellar cortex. Brain Res 216:11–33.

Wise AK, Cerminara NL, Marple-Horvat DE, Apps R (2010) Mechanisms of synchronous activity in cerebellar Purkinje cells. J Physiol 588:2373–2390.

Wolpert DM, Miall RC, Kawato M (1998) Internal models in the cerebellum. 2:338–347.

Wu HS, Sugihara I, Shinoda Y (1999) Projection patterns of single mossy fibers originating from the lateral reticular nucleus in the rat cerebellar cortex and nuclei. J Comp Neurol 411:97–118.

– X –

Xia J, Chung HJ, Wihler C, Huganir RL, Linden DJ (2000) Cerebellar long-term depression requires PKC-regulated interactions between GluR2/3 and PDZ domain-containing proteins. Neuron 28:499–510.

Xu-Friedman M a, Harris KM, Regehr WG (2001) Three-dimensional comparison of ultrastructural characteristics at depressing and facilitating synapses onto cerebellar Purkinje cells. J Neurosci 21:6666–6672.

Xu-Friedman M a, Regehr WG (2003) Ultrastructural contributions to desensitization at cerebellar mossy fiber to granule cell synapses. J Neurosci 23:2182–2192.

– Z –

Zhang SJ, Jackson MB (1993) GABA-activated chloride channels in secretory nerve endings. Science 259:531–534.

Zong H, Espinosa JS, Su HH, Muzumdar MD, Luo L (2005) Mosaic analysis with double markers in mice. Cell 121:479–492.

8 APPENDIX

8.1 CLUSTERS OF CEREBELLAR PURKINJE CELLS CONTROL THEIR AFFERENT CLIMBING FIBER DISCHARGE.

Clusters of cerebellar Purkinje cells control their afferent climbing fiber discharge

Joseph Chaumont[a], Nicolas Guyon[b], Antoine M. Valera[a], Guillaume P. Dugué[b], Daniela Popa[b], Paikan Marcaggi[b], Vanessa Gautheron[c], Sophie Reibel-Foisset[d], Stéphane Dieudonné[b], Aline Stephan[e], Michel Barrot[a], Jean-Christophe Cassel[f], Jean-Luc Dupont[a], Frédéric Doussau[a], Bernard Poulain[a], Fekrije Selimi[c,1], Clément Léna[b,1], and Philippe Isope[a,1,2]

[a]Institut des Neurosciences Cellulaires et Intégratives, Centre National de la Recherche Scientifique, Unité Propre de Recherche 3212, Université de Strasbourg, 67084 Strasbourg, France; [b]Institut de Biologie de l'Ecole Normale Supérieure, Centre National de la Recherche Scientifique, Unité Mixte de Recherche 8197, Institut National de la Santé et de la Recherche Médicale, Unité 1024, 75005 Paris, France; [c]Center for Interdisciplinary Research in Biology, Collège de France, Centre National de la Recherche Scientifique, Unité Mixte de Recherche 7241, Institut National de la Santé et de la Recherche Médicale, Unité 1050, 75005 Paris, France; [d]Chronobiotron, Unité Mixte de Service 3415, Centre National pour la Recherche Scientifique, Université de Strasbourg, 67084 Strasbourg, France; [e]Institut de Génétique Moléculaire et Cellulaire, Centre National de la Recherche Scientifique, Unité Mixte de Recherche 7104, Institut National de la Santé et de la Recherche Médicale, Unité 964, Université de Strasbourg, 67400 Illkirch, France; and [f]Laboratoire de Neurosciences Cognitives et Adaptatives, Centre National de la Recherche Scientifique, Unité Mixte de Recherche 7364, Université de Strasbourg, 67084 Strasbourg, France

Edited by Shigetada Nakanishi, Osaka Bioscience Institute, Suita, Japan, and approved August 29, 2013 (received for review February 5, 2013)

Climbing fibers, the projections from the inferior olive to the cerebellar cortex, carry sensorimotor error and clock signals that trigger motor learning by controlling cerebellar Purkinje cell synaptic plasticity and discharge. Purkinje cells target the deep cerebellar nuclei, which are the output of the cerebellum and include an inhibitory GABAergic projection to the inferior olive. This pathway identifies a potential closed loop in the olivo-cortico-nuclear network. Therefore, sets of Purkinje cells may phasically control their own climbing fiber afferents. Here, using in vitro and in vivo recordings, we describe a genetically modified mouse model that allows the specific optogenetic control of Purkinje cell discharge. Tetrode recordings in the cerebellar nuclei demonstrate that focal stimulations of Purkinje cells strongly inhibit spatially restricted sets of cerebellar nuclear neurons. Strikingly, such stimulations trigger delayed climbing-fiber input signals in the stimulated Purkinje cells. Therefore, our results demonstrate that Purkinje cells phasically control the discharge of their own olivary afferents and thus might participate in the regulation of cerebellar motor learning.

motor control | olivo-cerebellar loop | complex spikes

The cerebellar cortex is involved in a wealth of functions, from the control of posture to higher cognitive processes (1–3). Purkinje cells (PCs) are key processing units of the cerebellar cortex (4): each PC receives more than 175,000 parallel fiber synaptic inputs carrying information about the ongoing sensorymotor context. It also receives a single inferior olive afferent, the climbing fiber, which triggers a complex spike (CS), modulates PC firing (5), controls synaptic input plasticity, and has been proposed to carry error and clock signals to the cerebellum (2, 4–8). PCs are grouped in multiple parasagittal microzones, each receiving projections from separate areas of the inferior olive and projecting to subregions of the cerebellar nuclei (CN) (9–12). In the CN, PCs make inhibitory contacts on excitatory neurons that project to various premotor areas and propagate cerebellar computations to the motor system. Anatomical evidence indicates that PC terminals also contact CN inhibitory neurons that target inferior olive cells (13, 14). This nucleo-olivary pathway is topographically organized in multiple parallel projections to the inferior olive subnuclei (15), suggesting the existence of closed olivary-cortico-nuclear loops. Therefore, the discharge of a population of PCs in a microzone might not only shape the output of the cerebellum but also control its afferent climbing-fiber signal. Previous studies have shown that stimulation of the nucleo-olivary pathway significantly reduces olivary cell firing (16–18) and that pharmacological and genetic manipulations of PCs or olivary cell activity induce reciprocal modulations of the firing rate of PCs and climbing fibers (19, 20). These results indicate that PCs may tonically modulate the nucleo-olivary pathway. However, whether the cerebellar cortex can phasically recruit this pathway and whether this circuit functions as a closed loop is currently unknown. We thus set out to study the impact of phasic stimulations of PCs on cortico-nucleo-olivary loops. To control selectively PC firing rates, we engineered a mouse line expressing Channelrhodopsin-2 (ChR2) specifically in PCs. By combining optogenetic stimulation and in vivo electrophysiological recordings, we show that stimulating a set of PCs in a region of the cerebellar cortex triggers a restricted inhibition in the cerebellar nuclei and a transient disinhibition of the inferior olive cells that project to this set of PCs.

Results

L7-ChR2-eYFP Mice Engineering. A genetically modified mouse (L7-ChR2) that expresses ChR2(H134R)-Yellow Fluorescent Protein (YFP) under the control of the regulatory elements of the *pcp2* gene was created using the bacterial artificial chromosome modification strategy (*SI Methods*, Fig. 1*A*, and Fig. S1*A*) (21). Specific expression of the ChR2-YFP fusion protein in all PCs of the cerebellar cortex was detected by YFP fluorescence on cerebellar sections and confirmed by anti-calbindin immunostaining (Fig. 1*B* and Fig. S1*B*). GABA immunostaining and whole-cell patch-clamp recordings in acute cerebellar slices showed no expression in molecular layer interneurons or Golgi cells (Fig. 1*D*). Behavioral tests were performed to assess motor performance of the mutant mice. No difference was found

Significance

The inferior olive, one of the major source of inputs to the cerebellum, sends climbing fibers to Purkinje cells, the key processing units of cerebellar-dependent motor control. Using an optogenetic strategy, we demonstrate that Purkinje cells disinhibit their climbing-fiber afferents via a poly-synaptic circuit. These findings identify a functional closed-loop organization in the olivo-cerebellar circuits that is potentially important for cerebellar motor learning.

Author contributions: F.S., C.L., and P.I. designed research; J.C., N.G., A.M.V., G.P.D., P.M., V.G., S.R.-F., F.D., F.S., and P.I. performed research; S.D., A.S., M.B., J.-C.C., B.P., F.S., and C.L. contributed new reagents/analytic tools; J.C., G.P.D., D.P., J.-L.D., F.S., C.L., and P.I. analyzed data; and J.C., C.L., and P.I. wrote the paper.

The authors declare no conflict of interest.

This article is a PNAS Direct Submission.

[1]F.S., C.L., and P.I. contributed equally to this work.

[2]To whom correspondence should be addressed. E-mail: philippe.isope@inci-cnrs.unistra.fr.

This article contains supporting information online at www.pnas.org/lookup/suppl/doi:10.1073/pnas.1302310110/-/DCSupplemental.

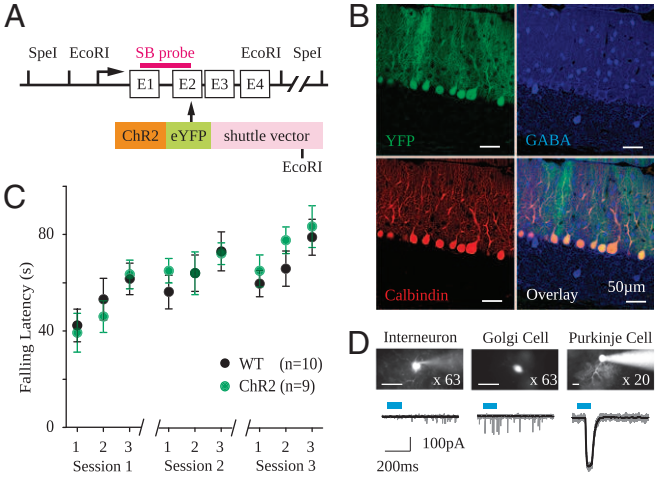

Fig. 1. Generation and characterization of L7-ChR2(H134R)-eYFP mice. (*A*) Diagram of the modified BAC containing the ChR2(H134R)-eYFP cDNA under the control of the L7/pcp2 gene regulatory elements. (*B*) Transgene expression monitored by YFP fluorescence in cerebellar sections (*Upper Left*); (*Lower Left*) calbindin immunolabeling; (*Upper Right*) GABA immunolabeling; (*Lower Right*) overlay. (*C*) Falling latencies in the rotarod test during three sessions of three trials at 0–45 rpm (tested by multifactorial ANOVA, $P = 0.392$; WT, $n = 10$; ChR2, $n = 9$). (*D*) Molecular layer interneurons, Golgi cells, and Purkinje cells recorded in acute cerebellar slices visualized using Alexa 594 in the pipette and wide-field illumination at 473 nm. (Scale bar: 20 µm.) No current was observed in molecular layer interneurons ($n = 4$) and Golgi cells ($n = 6$).

between L7-ChR2 mice and wild-type littermates (Fig. 1*C*), indicating that this transgene expression does not perturb motor functions.

Control of Purkinje Cells by Light. To characterize PC activation by ChR2, in vitro recordings were performed on acute cerebellar slices using whole-cell patch-clamp. Wide-field illumination with blue light (Fig. 2*A* and *SI Methods*) systematically activated an inward current in all PCs tested ($n = 65$; Fig. 2 *B–D*). By restricting the field of illumination (*SI Methods*), we could show that ChR2 channels are expressed throughout PC dendrites (Fig. 2*B*) and estimate their density to be 150–300 channels per µm^2 illuminated [Fig. S2, assuming a unitary conductance of 100 fS (22)]. We then set out to characterize the current induced in PCs by illumination as a function of irradiance and pulse duration. For a pulse duration of 1 ms, increasing irradiance enhanced the amplitude of the photocurrent up to several hundred picoamps (Fig. 2*C* and *SI Methods*) with a decay time constant of 17.3 ± 8.5 ms ($n = 11$). For longer pulses (100 ms), the current rapidly desensitized to a stationary current at 58 ± 3% of the peak for stimulation frequency below 0.05 Hz ($n = 5$) (Fig. 2 *C*, *iv*), in agreement with previous work (23). The pulse frequency used in most of the experiments reported in this work was above 0.05 Hz, leading to a smaller peak current but a similar stationary current (Fig. 2*C*). Current-clamp recordings showed that light-evoked current carrying a charge above 14.7 ± 10 pC ($n = 4$) elicited an action potential in PCs (Vm = −60 mV) and that action potentials were repeated during burst illuminations of up to 10 Hz for irradiance above 8 mW/mm^2 (Fig. 2*D*). These results demonstrate that, despite its very low conductance, the density of ChR2 channels is high enough to produce large currents and reliably elicit action potentials in PCs of L7-ChR2 mice.

Next, the activation of PCs was characterized in vivo using juxtacellular recordings in anesthetized mice. Blue-light illumination was delivered through optical fibers coupled to a LED and positioned in the vicinity of the brain surface (*SI Methods* and Fig. 2*E*). In contrast to in vitro conditions, the irradiance received by the PCs in vivo depends strongly on the scattering of light in the tissue and varies as a function of the depth and orientation of the dendrite of the PC. PCs were identified by the occurrence of complex spikes (CSs), produced by the climbing-fiber input, and by the frequency of spontaneous simple spikes (mean CS rate = 0.44 ± 0.63 Hz; mean simple spike rate = 39.7 ± 3.9 Hz, $n = 19$, $n = 16$ mice). Increasing irradiance intensity led to an increase in simple spike firing rate in all cells ($n = 14$) whose somata lie in the first hundreds of micrometers from the surface of the tissue (Fig. 2 *F* and *G*). This increase in simple spike-firing rate could continue up to 500 ms (the longest duration tested) and reach up to 250 Hz. Further increasing the intensity induced a depolarization block consisting of a burst of spikes at light onset followed by a complete suppression of PC firing during the remaining time of illumination (Fig. 2*F*). Because of the diffusion of light (*SI Methods*; and see Fig. S5), depolarization block was not observed for cells distant from the tip of the optic fiber by more than 300 µm even at tip irradiance above 30 mW/mm^2. Also, no depolarization block was elicited with short pulses of light (≤2 ms). To quantify the onset of the effect of illumination, the latency of the first spike after the onset of illumination was measured. This latency was significantly shortened to a median delay of 5.5 ms ($n = 19$) (Fig. 2*H*) for irradiance as low as 2.5 mW/mm^2, and further decreased to a minimum median of 3.0 ms for an irradiance intensity of 19 mW/mm^2 (Fig. 2*H*). At the offset of the illumination, the time required to resume basal firing rate ranged between 10 and 30 ms (Fig. 2*I*). These findings demonstrate that ChR2-expressing PCs can be excited by light with high temporal precision in vivo.

Inhibition of Cerebellar Nuclei Neurons by Purkinje Cells. To assess whether the photostimulation of PCs was able to modulate the activity of their target neurons in the cerebellar nuclei (CN), in vivo extracellular recordings were performed with tetrodes in the CN while illuminating the ipsilateral cerebellar cortex (*SI Methods* and Fig. 3 *A* and *B*). To increase the probability of stimulating the group of PCs that target the recording site in the CN, we used illumination parameters that maximize the number of PCs excited (optical fiber of 600 µm diameter, 100-ms pulses, irradiance at 60 mW/mm^2) (*SI Methods*). Using these conditions, only 10% of activated PCs are likely to experience intensities that trigger a depolarization block (*SI Methods*; and see Fig. S5). By illuminating the lateral part of Crus I, sites that induced inhibition in recorded units from the interposed nucleus were found (26/48 tested sites; 21 animals) (Fig. 3 *C–G*). The suppression of firing was often accompanied by a small deflection in the field potential, presumably due to synaptic activation (red arrow, Fig. 3*C*). Usually, several cells were recorded simultaneously by the tetrode at each recording site (3.7 ± 1.7 cells per site) (Fig. 3*B*). Among the 97 cells recorded at responding sites (i.e., where at least one cell was inhibited), 70 cells were inhibited by Crus I illumination whereas 27 did not respond (average of 76 ± 26% inhibited cells at each site). These cells exhibited a mean firing rate of 18.0 ± 13.1 Hz and a coefficient of variation of 0.58 ± 0.29 for the interspike interval.

To quantify the effectiveness of the inhibition, the parameters of illumination were then varied (Fig. 3*E* and Fig. S3). Decreasing the intensity of irradiance to 19 mW/mm^2 did not change the proportion of responding cells at responding sites in the CN (72.8 ± 31% responding cells from 57 cells recorded at 25 responding sites in four mice), showing that this intensity is enough to recruit the minimum number of PCs necessary for CN inhibition. The duration of full inhibition (complete suppression of firing) increased with pulse duration and irradiance intensity (Fig. 3*E*). For 25-ms pulses, a complete inhibition of some CN units could be observed at irradiance higher than 3 mW/mm^2. The mean latency to full inhibition was slow but variable (mean = 18.9 ± 11.7 ms at 19 mW/mm^2 and 19.7 ± 12.15 ms at 60 mW/mm^2) (Fig. S3 *D–F*), which is consistent with the requirement of a large number of activated PCs for complete inhibition of CN firing. Finally, trains of 20-Hz and 30-Hz light pulses induced a rhythmic modulation of CN firing (Fig. S4). Taken together,

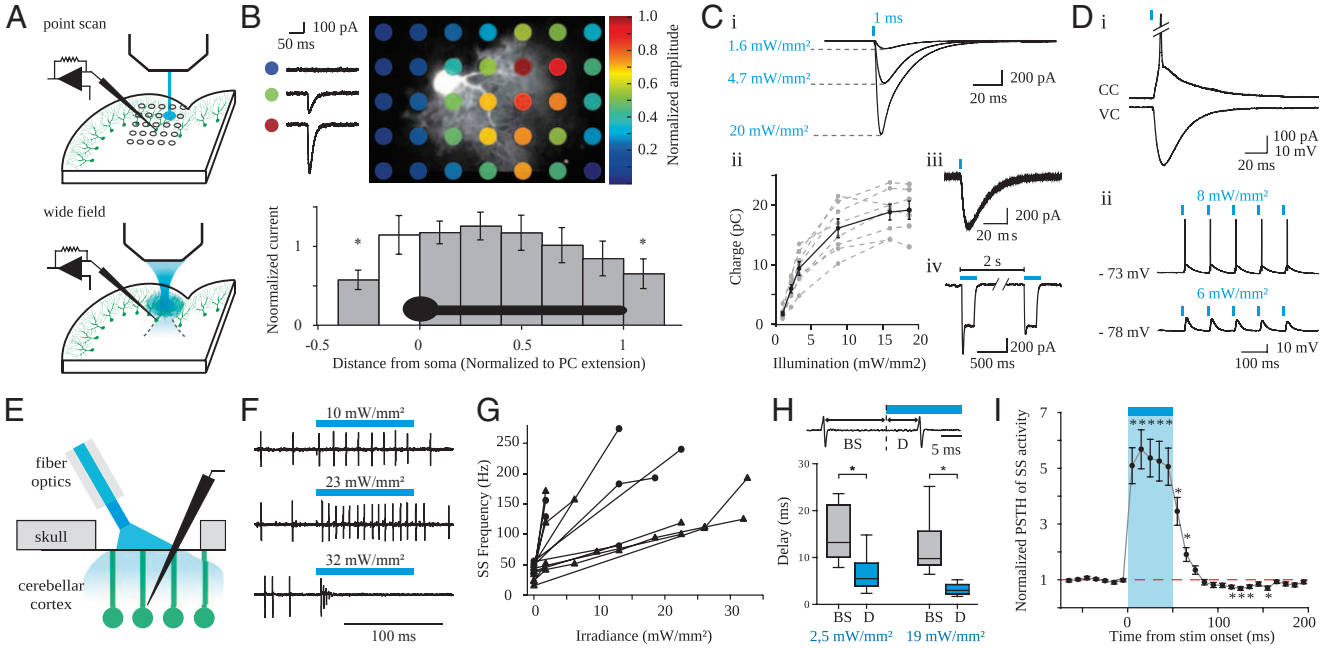

Fig. 2. Electrophysiological characterization of L7-ChR2(H134R)-eYFP mice in vitro and in vivo. (*A*) Schematics of acute cerebellar slices illustrating whole-cell recordings combined with laser-point scan photostimulation (*Upper*) or wide-field illumination (*Lower*). (*B, Upper*) Point-scan photostimulation (1-ms pulses) of Purkinje-cell dendrites and average current elicited at identified color-code points. (*Lower*) normalized current (± SEM) plotted against the distance from the soma ($n = 7$, Mann-Whitney test, $P < 0.05$). (*C, i*) Average whole-cell currents recorded in a PC with 1-ms wide-field LED illumination at various irradiances. (*ii*) Average charge against irradiance ($n = 8$ cells; black, mean ± SEM). (*iii*) Example of 10 successive traces superimposed from one cell. (*iv*) Desensitization of peak current at 0.5 Hz (100-ms pulses). Panels *iii* and *iv* are from different cells. (*D, i*) Action potential recorded in current-clamp mode elicited by a 1-ms light pulse (top) and corresponding photocurrent recorded in voltage clamp (bottom). (*ii*) Action potential initiation for burst of illumination (1-ms pulses at 10 Hz). (*E*) Schematic of in vivo juxtacellular recordings of PCs combined with optical fiber illumination. (*F*) Example traces recorded in juxtacellular mode during 100-ms pulses. (*G*) Relationship between PC firing rate and irradiance intensity ($n = 14$ cells). Triangle, cells deeper than 400 μm. (*H*) Delay of occurrence (D) of the first spike during illumination, compared with the preceding spike (BS) at various irradiances ($n = 20$ cells, 16 mice). Box plots show median values and 25/75% percentiles. Control median delay = 10.9 ms (quartiles: 8.4, 17.1); median delay = 5.5 ms (quartiles: 3.9, 8.8) at 2.5 mW/mm^2 and 3 ms (quartiles 2.2, 4.2) at 19 mW/mm^2, Kruskal–Wallis One-Way ANOVA, $P < 0.001$. Pairwise multiple comparison, Dunn's method, *$P < 0.05$. Median delays during illumination were not significantly different. (*I*) Time course of the effect of illumination on the firing rate. Post stimulus time histograms (PSTHs) were normalized to the baseline frequency before averaging. Only cells with strong increases in firing rate (greater than twofold increase) were used in this panel. Kruskal–Wallis One-Way ANOVA, $P < 0.001$. Pairwise multiple comparisons, Dunn's method. *$P < 0.05$.

these data show that illumination of PCs allows a dynamic control of CN firing (24) and that the duration of inhibition increases with the intensity and duration of light stimulations. Because PC inhibition has been proposed to produce a rebound excitation in CN neurons (25), we examined whether the instantaneous frequency was significantly enhanced relative to baseline values when the cells resumed their firing. The inhibition produced by PC inputs did not trigger a detectable rebound excitation even at high irradiance (60 mW/mm^2) in most CN cells (about 90%) but was followed by either a progressive or a direct return of CN discharge to its baseline value after the end of the stimulation (Fig. S3). To test the spatial specificity of the responses, the light source at the surface of the cerebellum was displaced from Crus I to Crus II, once a responding site was found; in most cells, the light-induced inhibition was lost ($n = 12/14$ cells recorded, six recording sites, four mice) (Fig. 3*F*), consistent with the zonal anatomical organization of the cortico-nuclear pathway. We then mapped the region of the CN inhibited by activation of ~1000–3000 PCs in Crus I (pulse duration: 100 ms, irradiance 19 mW/mm^2; see Fig. 3*A*, Fig. S5, and *SI Methods*). The cellular responses were explored by systematic penetrations in ranges of stereotaxic coordinates [antero-posterior (AP) −5.9 to 6.4, medio-lateral (ML) 1.5; 2.5, depth 2.1, 3.3], and the most responsive sites were located in a small area (AP −6.2, −6.4, ML 1.7, 1.9, depth 2.7; 3.2) ($n = 106$ cells, 53 recording sites, four mice) (Fig. 3*G* and Fig. S3).

Activation of Purkinje Cells Controls Inferior Olivary Neurons Discharge. We then set out to assess whether the stimulation of a population of PCs can stop the firing of CN neurons and then influence the discharge of inferior olivary neurons. Complex spikes (CS) in PCs were monitored in juxtacellular recordings in vivo as a readout of olivary cells discharge. The recorded PC and its neighbors were then excited using small optical fibers (diameter 50–200 μm), and the irradiance was adjusted to obtain a strong activation without depolarization block (mean = 20.6 ± 11.7 mW/mm^2). Local illumination by pulses of light lasting 35–500 ms elicited a CS in 25 out of 42 PCs ($n = 25$ mice) (Fig. S6) with a mean latency of 138 ± 39 ms after the onset of the stimulation (Fig. 4 *A* and *B*). No response was observed for pulse durations of 10 and 20 ms. For pulse durations of 100 ms or less, most stimulation-induced CSs were elicited tens of milliseconds after the end of illumination, thus ruling out the possibility that CSs are a direct (artifactual) consequence of light stimulation. Indeed, no effect of illumination was detected in wild-type control mice either in PCs or in other cell types ($n = 4$ PCs, 7 non-PCs, presumably inhibitory interneurons from four wild-type mice). Interestingly, once a rebound CS was observed, the response rate was independent of the size of the fiber used ($F(1,23) = 2.85$, $P = 0.10$) and the irradiance at the tip of the optic fiber ($F(1,52) = 0.73$, $P = 0.40$). Therefore, data obtained using different irradiance intensities and fiber diameters were pooled together. No difference was observed in the onset of the CS responses for pulse durations between 35 and 500 ms whereas the offset of the response increased with pulse duration (Fig. 4*C*), suggesting that the beginning and the end of the

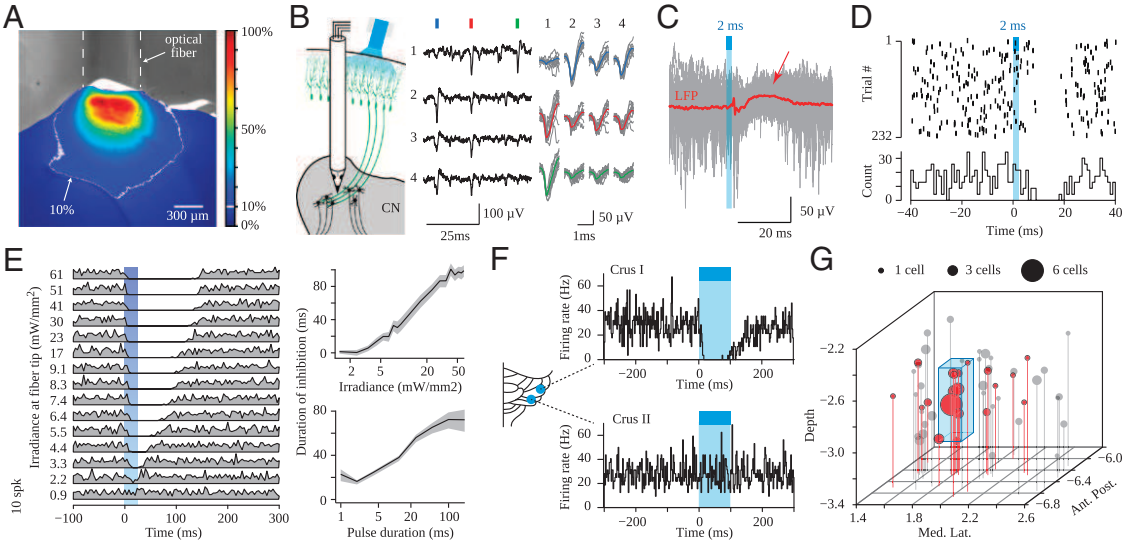

Fig. 3. Effective silencing of cerebellar nuclear cells by photostimulation of Purkinje cells in vivo. (*A*) Propagation of blue light in the cerebellar cortex (color coded part of the image) for a 600-µm optical fiber placed on the surface of the cerebellum (grayscale part of the image). In the color-coded part, the color of each pixel corresponds to its value expressed as a percentage of the intensity of the brightest pixel. The 10% isoline is delineated in white (i.e., corresponding to ∼2 mW/mm^2 if the brightest pixel immediately under the fiber corresponds to 20 mW/mm^2). (*B*) Illustration of tetrode recordings in cerebellar nuclei. (*Left*) Schematics of the experiment. (*Center*) Example traces (vertical ticks of different colors signal different spikes; numbers identify the four channels of the tetrode). (*Right*) Average unfiltered waveforms on the four channels (same color code as for *Center*), superimposed on 10 successive events (gray traces). (*C*) Example of a recording obtained on one channel in the interposed nucleus. The average extracellular potential (LFP, local field potential, red) recorded in CN is superimposed on 30 successive sweeps (gray lines) aligned on the onset of photo-stimulation (2 ms, 60 mW/mm^2). Note the suppression of extracellular (negative) spikes after the stimulation. The average LFP was calculated from 232 sweeps. The red arrow signals the deflection of LFP. (*D*) Example of a raster plot (*Upper*) and corresponding PSTH (*Lower*; bin, 1 ms), showing a complete suppression of firing following the stimulation (blue bar); the example is the same as in *C*. (E, *Left*) Example of PSTHs for one cell tested with different light intensities (pulse duration, 25 ms). (*Right*) Average duration of full inhibition plotted against the irradiance at the fiber tip (at 25 ms) or pulse duration (at 60 mW/mm^2) (n = 74 cells) (*SI Methods*). The shaded area indicates the SEM. (*F*) Example cell inhibited in response to the illumination of Crus I (*Upper,* PSTH), but not Crus II (*Lower*, PSTH). Bin, 5 ms. Blue bar, light pulse (100 ms, 60 mW/mm^2). (*G*) A 3D view of the distribution of CN recording sites where inhibited cells were found (red) or not (gray) during Crus I illumination (100 ms, 19 mW/mm^2) on the ipsilateral cerebellar Crus I region (AP, −6.1; ML, 3.3). The 3D rectangle arrow identifies the region where most responsive sites are clustered. See Fig. S3 planar projections.

response are locked respectively to the beginning—with a long delay—and to the end of the stimulation. Therefore, CS were evoked by pulses of irradiance around 20 mW/mm^2 using a 100-µm optical fiber that should activate about 200–500 PCs (Fig. 4*A* and Fig. S5). Taken together, these results indicate that, provided a critical number of PCs were illuminated for a minimal period (35 ms), the disinhibition of olivary neurons resulted in CSs evoked with a minimal delay of 80–100 ms. Moreover, experiments in which the optical fiber was moved along the transverse axis above the surface showed that the evoked CS response (i.e., the inferior olive disinhibition) decreased and disappeared together with the simple spike response (i.e., the direct activation of the recorded cell) (Fig. 4*E*). These results indicate that the set of PCs that control the climbing fiber afferent to a PC is localized close to that PC (Fig. 4*F*), consistent with the topographical organization of the cortico-nucleo-olivary circuit.

There is a substantial jitter in the time of occurrence of the CS after the onset of illumination (several tens of milliseconds) (Fig. 4 *B* and *D*), suggesting a temporal fluctuation of the responsiveness of the inferior olivary neurons to disinhibition. There was indeed a correlation between the probability of occurrence of the CS following the stimulation of PCs and the CS baseline firing rate (Fig. S6*B*), indicating that PC illumination is more efficient when olivary cells are more depolarized. Because inferior olivary neurons are known to express subthreshold oscillations spontaneously (26), we examined whether such oscillations would condition the timing of the CS evoked by PCs stimulations. Poststimulus time histograms were constructed by aligning individual trials on the time of the first CS after the onset of stimulation (Fig. 4*D*, green ticks; 100 ms pulse, n = 8), and the evoked CS were found to occur preferentially ∼225 ms and ∼450 ms after a preceding spontaneous CS (Fig. 4*D*, *Bottom*). These results show that the disinhibition of olivary neurons triggers CS spikes in phase with an ∼4-Hz subthreshold oscillation.

Discussion

In this study, a transgenic mouse line expressing ChR2 specifically in PCs is described and used to investigate the functional organization of the olivo-cerebellar circuit. The level of ChR2 (H134) expression yielded reliable and sustained currents (23, 27) in PCs and increased the cells' discharge. Focal illumination in one specific part of the cerebellar cortex (crus I) transiently inhibited 75% of the cells recorded simultaneously from the same tetrode in a restricted area of the cerebellar nuclei. Lowering the intensity of stimulation did not change the percentage of responsive cells at responsive sites, suggesting that the non-responsive cells receive weaker PC inputs, as it has been suggested for nuclear GABAergic interneurons (28). Although light stimulations took a few milliseconds to evoke spikes in PCs, the complete suppression of firing in CN cells was variable among cells and was reached on average in ∼20 ms, indicating the need for a high convergence of presynaptic PCs or a temporal summation of inhibitory PC inputs to fully inhibit CN neurons. Surprisingly, although sustained inhibition was induced in CN neurons following activation of PCs, rebound excitation (29, 30) was observed in only ∼10% of the cells, in agreement with the study of Alviña et al. (31). Anesthesia might alter physiological properties of CN neurons. However, recent studies (25, 32) have demonstrated that rebound excitation in CN neurons requires the extensive activation of the presynaptic PCs. Thus, a more likely interpretation is that our protocol of illumination leads to poorly synchronized PC discharges and/or fails to recruit enough presynaptic PCs.

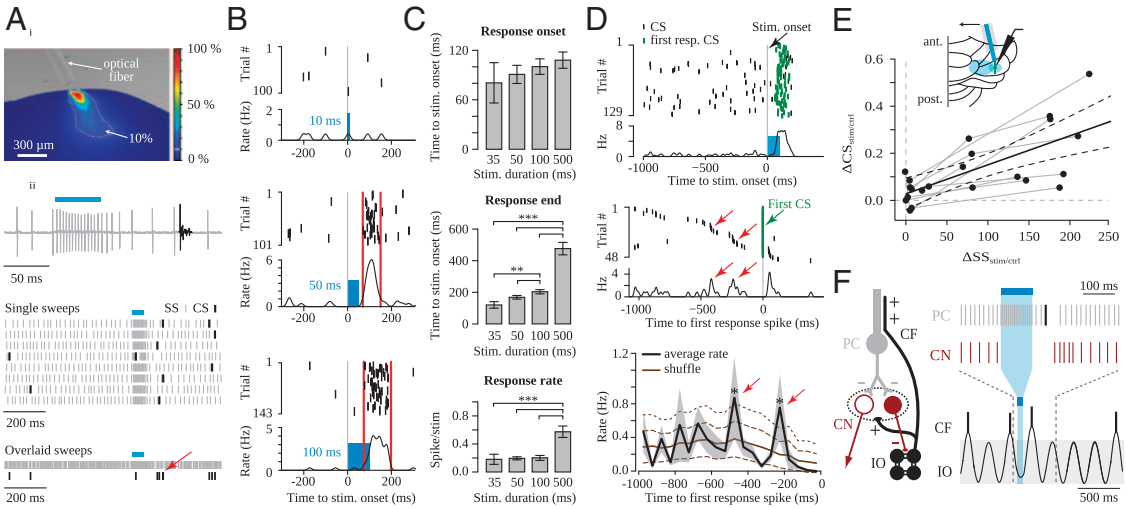

Fig. 4. Photostimulation of Purkinje cells controls inferior olivary cell discharge. (*A*, *i*) Blue–light propagation observed in a transverse section of the cerebellar cortex using a 100-µm optical fiber. The same code as in Fig. 3*A*. (*ii*) Individual trace from in vivo juxtacellular PC recordings and corresponding raster plot for both simple spikes (gray ticks) and CSs (black ticks, the signature of olivary cell discharge in PCs). Light illumination elicited CSs in the recorded PC. The arrow indicates the evoked complex spikes. (*B*) Example raster plot and average peri-stimulation firing rate (obtained from the density of spikes convolved with a Gaussian kernel with a 10-ms variance) of CSs recorded with 10-, 50-, and 100-ms illumination pulses (blue rectangles). Red lines identify the time periods with significant increase in the CS firing rate relative to baseline. (*C*) Mean latency from stimulation onset to response onset (*Top*, no significant difference, $F_{1,56} = 0.074$, $P = 0.79$) and response end (*Middle*, significant difference across conditions, $F_{1,56} = 465$, $P < 10^{-4}$), and mean response rate (spike/stim, *Bottom*, significant difference across conditions, $F_{1,56} = 56$, $P < 10^{-4}$) for 35-, 50-, 100-, and 500-ms pulses ($n = 4$, 13, 19, and 11 cells, respectively; 50–200 trials by conditions). *, **, ***$P < 0.05$, 0.01, and 0.001, respectively. (*D*) Influence of the recent history of CS firing on the timing of the disinhibitory response. For each cell, the PSTH (*Top*) was recalculated to realign the trials on the time of the first CS after stimulus onset (*Middle*, green CSs are aligned, trials without CS are not represented). In the example (*Middle*), the trials are sorted by decreasing ISIs before the response CS showing that the first response spikes occurred preferentially after specific ISIs (red arrows); in some trials, the illumination triggered two CSs yielding a peak at positive times. The realigned PSTH were averaged for eight cells (*Bottom*) and compared with the expected values after randomly shifting the preresponse CS (±300 ms). The disinhibitory response occurred preferentially after specific intervals (*) after the last prestimulation CS spikes. Dashed and dotted lines represent shuffled PSTH ± 1 SD and 2 SD respectively. (*E*) Increase of CS frequency against the modulation of simple spike frequency after blue-light illumination at different optical-fiber position. Points acquired from the same cell are connected by a gray line. A linear fit (black line, $r^2 = 0.7$) with confidence interval at 95% (dashed black line) is superimposed on the data showing the correlation between direct PC activation and CS response (and the simultaneous disappearance of both responses when the fiber is moved away). (*F*) Diagram of the synaptic connections in the olivo-cortico-nucleo-olivary loop and illustration of discharge in Purkinje cells, CN neurons, and olivary cells based on our results. Blue light activates PCs (simple spike firing rate increased during stimulation, gray ticks) that stop CN neuron discharge and consequently disinhibit inferior olive neurons. A CS is then observed in PCs. Ticks illustrate neuronal discharge.

The stimulation of PCs during tens of milliseconds elicited olivary discharge with an onset latency close to 100 ms and an offset latency that increased with stimulation duration. Such long-latency phenomenon has been previously suggested in behaving monkeys (33) by analyzing the simple spike discharge preceding complex spikes. In our experiments, the CS response started while the CN neurons were still inhibited, which rules out the recruitment of an (indirect) excitatory output of the CN to the inferior olive (15, 34). However, the evoked CS is consistent with properties of the nucleo-olivary inhibitory pathway (35), which is dominated by asynchronous release (17) leading to long latencies for inhibition (18); this mode of transmission should delay the transmission of changes in CN firing rate and filter out very transient suppressions of CN firing. Moreover, the variability of the latency of the CS response across trials seems to be partly due to intrinsic subthreshold fluctuations (26) (in our case, 4-Hz oscillation) of the membrane potential of inferior olivary neurons. Indeed, the maximal probability of occurrence of CS response was found in phase with olivary oscillations. Overall, the characteristics of the CS response to increased PC discharge are consistent with a disinhibition of the inferior olive via the nucleo-olivary pathway. Our results are also consistent with a topographical organization of the cortico-nucleo-olivary pathway. CN neurons inhibition was lost when the illumination was moved to a neighboring lobule. Moreover, the CS response in the recorded PCs disappeared as soon as direct excitation (evidenced by simple spike modulation) was lost when the optic fiber was moved away in the transverse direction. The combination of these results and those from previous studies (9, 16, 24, 26, 27, 30–32, 36) strongly argue for the existence of closed cortico-nucleo-olivary loops where spatially restricted sets of PCs control their afferent climbing fibers. The spatial extension of the set of PCs excited by our smallest illumination (around 300 µm diameter) is closer to the scale of cerebellar zones than of microzones (11). Indeed, recent imaging studies in vivo describing synchronized CSs during sensory stimulation identified microbands narrower than 100 µm (37, 38). Testing whether the control of the CS is segregated across such microzones may require the use of specific strategies (39) to restrict the expression of the opsin to single microzones and therefore circumvent the difficulty of illuminating very narrow bands of cells. The closed cortico-nucleo-olivary loops will favor the triggering of a CS volley in a subset of PCs shortly after their firing rate is increased. Moreover, because the nucleo-olivary inhibitory pathway targets gap junctions between olivary cells and promotes their decoupling (7, 40), the inhibition of this pathway should promote CS synchrony (19, 41). This feedback excitatory loop could also modulate plasticity in the cerebellar cortex, for example, at the parallel fiber to PC synapse because the delay between the onset of the increased PCs firing and the rebound CS (around 100 ms) matches the optimal interval between parallel-fiber and climbing-fiber discharges required for the induction of long-term depression (42, 43). Indeed, the nucleo-olivary pathway has been proposed to play important roles in conditioning (44, 45), and an appealing possibility is that the cortico-nuclear pathway controls the contribution of the nucleo-olivary pathway to motor learning. A wide range of theoretical and experimental evidence has led to the proposal that learning mechanisms in the cerebellar cortex

underlie the formation and the storage of internal models of the sensory-motor system (46). These models convert desired movements into motor commands or predict sensory outcomes of planned movements (47); the adjustment of the models is performed by supervised learning via the climbing fibers. The cortico-nucleo-olivary pathway described in our study provides a way to propagate the predictions computed in the cerebellar cortex to the inferior olive, where it can be compared, with an appropriate delay, with the actual outcome of the ongoing task carried by other inputs to the inferior olive. Therefore, the closed cortico-nucleo-olivary loops may play an essential role in adjusting the internal models in the cerebellum.

Methods

All experimental procedures conform to Centre National de la Recherche Scientifique and National Institutes of Health guidelines on animal experimentation. A BAC transgenic mouse expressing channelrhodopsin-2(H134R) under the control of the regulatory elements of the L7-pcp2 gene was generated (21) (*SI Methods* and Fig. S1). In vivo extracellular recordings of PCs were performed in anesthetized animals (*SI Methods*). Means were given ± SD unless otherwise stated.

ACKNOWLEDGMENTS. We thank Pr Karl Deisseroth for kindly providing the pAAV-double floxed-hChR2(H134R)EYFP-WPRE-pA vector. We thank the Mouse Clinical Institute, Laurence Huck, and Cassidy Fiford for technical assistance. We thank Samuel Garcia for support on software and Boris Barbour and Nancy Grant for comments on this manuscript. This work was supported by the Centre National pour la Recherche Scientifique, Ecole Normale Supérieure, Institut National de la Santé et de la Recherche Médicale, Université de Strasbourg, Ministère de la Recherche, Agence Nationale pour la Recherche Grants ANR-09-MNPS-038 CeCoMod, ANR-2010-JCJC-1403-1 MicroCer, and ANR-GUI-AAP-04 Sensocode; the INTERREG IV Rhin Supérieur Program; and the European Funds for Regional Development, TIGER project. Publication costs are supported by the Neurex network (www.neurex.org).

1. Ito M (2006) Cerebellar circuitry as a neuronal machine. *Prog Neurobiol* 78(3-5):272–303.
2. Thach WT, Goodkin HP, Keating JG (1992) The cerebellum and the adaptive coordination of movement. *Annu Rev Neurosci* 15:403–442.
3. Dean P, Porrill J, Ekerot C-F, Jörntell H (2010) The cerebellar microcircuit as an adaptive filter: Experimental and computational evidence. *Nat Rev Neurosci* 11(1): 30–43.
4. Ito M (1984) *The Cerebellum and Neural Control* (Raven, New York).
5. De Zeeuw CI, et al. (2011) Spatiotemporal firing patterns in the cerebellum. *Nat Rev Neurosci* 12(6):327–344.
6. Llinás RR (2011) Cerebellar motor learning versus cerebellar motor timing: The climbing fibre story. *J Physiol* 589(Pt 14):3423–3432.
7. Yarom Y, Cohen D (2002) The olivocerebellar system as a generator of temporal patterns. *Ann N Y Acad Sci* 978:122–134.
8. Barmack NH (2006) Inferior olive and oculomotor system. *Prog Brain Res* 151:269–291.
9. Oscarsson O (1979) Functional units of the cerebellum—sagittal zones and microzones. *Trends Neurosci* 2:143–145.
10. Voogd J, Glickstein M (1998) The anatomy of the cerebellum. *Trends Neurosci* 21(9): 370–375.
11. Apps R, Hawkes R (2009) Cerebellar cortical organization: A one-map hypothesis. *Nat Rev Neurosci* 10(9):670–681.
12. Glickstein M, Sultan F, Voogd J (2011) Functional localization in the cerebellum. *Cortex* 47(1):59–80.
13. Nelson BJ, Adams JC, Barmack NH, Mugnaini E (1989) Comparative study of glutamate decarboxylase immunoreactive boutons in the mammalian inferior olive. *J Comp Neurol* 286(4):514–539.
14. Teune TM, van der Burg J, de Zeeuw CI, Voogd J, Ruigrok TJ (1998) Single Purkinje cell can innervate multiple classes of projection neurons in the cerebellar nuclei of the rat: A light microscopic and ultrastructural triple-tracer study in the rat. *J Comp Neurol* 392(2):164–178.
15. Teune TM, van der Burg J, van der Moer J, Voogd J, Ruigrok TJ (2000) Topography of cerebellar nuclear projections to the brain stem in the rat. *Prog Brain Res* 124: 141–172.
16. Bengtsson F, Hesslow G (2006) Cerebellar control of the inferior olive. *Cerebellum* 5(1):7–14.
17. Best AR, Regehr WG (2009) Inhibitory regulation of electrically coupled neurons in the inferior olive is mediated by asynchronous release of GABA. *Neuron* 62(4): 555–565.
18. Bazzigaluppi P, Ruigrok T, Saisan P, De Zeeuw CI, de Jeu M (2012) Properties of the nucleo-olivary pathway: An in vivo whole-cell patch clamp study. *PLoS ONE* 7(9): e46360.
19. Marshall SP, Lang EJ (2009) Local changes in the excitability of the cerebellar cortex produce spatially restricted changes in complex spike synchrony. *J Neurosci* 29(45): 14352–14362.
20. Chen X, et al. (2010) Disruption of the olivo-cerebellar circuit by Purkinje neuron-specific ablation of BK channels. *Proc Natl Acad Sci USA* 107(27):12323–12328.
21. Gong S, et al. (2003) A gene expression atlas of the central nervous system based on bacterial artificial chromosomes. *Nature* 425(6961):917–925.
22. Lin JY (2011) A user's guide to channelrhodopsin variants: Features, limitations and future developments. *Exp Physiol* 96(1):19–25.
23. Berndt A, et al. (2011) High-efficiency channelrhodopsins for fast neuronal stimulation at low light levels. *Proc Natl Acad Sci USA* 108(18):7595–7600.
24. Person AL, Raman IM (2012) Purkinje neuron synchrony elicits time-locked spiking in the cerebellar nuclei. *Nature* 481(7382):502–505.
25. Bengtsson F, Ekerot CF, Jörntell H (2011) In vivo analysis of inhibitory synaptic inputs and rebounds in deep cerebellar nuclear neurons. *PLoS ONE* 6(4):e18822.
26. Khosrovani S, Van Der Giessen RS, De Zeeuw CI, De Jeu MT (2007) In vivo mouse inferior olive neurons exhibit heterogeneous subthreshold oscillations and spiking patterns. *Proc Natl Acad Sci USA* 104(40):15911–15916.
27. Zhao S, et al. (2011) Cell type–specific channelrhodopsin-2 transgenic mice for optogenetic dissection of neural circuitry function. *Nat Methods* 8(9):745–752.
28. Uusisaari M, Knöpfel T (2011) Functional classification of neurons in the mouse lateral cerebellar nuclei. *Cerebellum* 10(4):637–646.
29. Tadayonnejad R, et al. (2010) Rebound discharge in deep cerebellar nuclear neurons in vitro. *Cerebellum* 9(3):352–374.
30. Aizenman CD, Linden DJ (1999) Regulation of the rebound depolarization and spontaneous firing patterns of deep nuclear neurons in slices of rat cerebellum. *J Neurophysiol* 82(4):1697–1709.
31. Alviña K, Walter JT, Kohn A, Ellis-Davies G, Khodakhah K (2008) Questioning the role of rebound firing in the cerebellum. *Nat Neurosci* 11(11):1256–1258.
32. Hoebeek FE, Witter L, Ruigrok TJ, De Zeeuw CI (2010) Differential olivo-cerebellar cortical control of rebound activity in the cerebellar nuclei. *Proc Natl Acad Sci USA* 107(18):8410–8415.
33. Miall RC, Keating JG, Malkmus M, Thach WT (1998) Simple spike activity predicts occurrence of complex spikes in cerebellar Purkinje cells. *Nat Neurosci* 1(1):13–15.
34. Ruigrok TJ, de Zeeuw CI, van der Burg J, Voogd J (1990) Intracellular labeling of neurons in the medial accessory olive of the cat. I. Physiology and light microscopy. *J Comp Neurol* 300(4):462–477.
35. Lang EJ, Sugihara I, Llinás R (1996) GABAergic modulation of complex spike activity by the cerebellar nucleoolivary pathway in rat. *J Neurophysiol* 76(1):255–275.
36. Sugihara I, et al. (2009) Projection of reconstructed single Purkinje cell axons in relation to the cortical and nuclear aldolase C compartments of the rat cerebellum. *J Comp Neurol* 512(2):282–304.
37. Ozden I, Sullivan MR, Lee HM, Wang SS (2009) Reliable coding emerges from coactivation of climbing fibers in microbands of cerebellar Purkinje neurons. *J Neurosci* 29(34):10463–10473.
38. Ghosh KK, et al. (2011) Miniaturized integration of a fluorescence microscope. *Nat Methods* 8(10):871–878.
39. Tsubota T, Ohashi Y, Tamura K (2013) Optogenetics in the cerebellum: Purkinje cell-specific approaches for understanding local cerebellar functions. *Behav Brain Res*, 10.1016/j.bbr.2013.04.019.
40. de Zeeuw CI, Holstege JC, Ruigrok TJ, Voogd J (1989) Ultrastructural study of the GABAergic, cerebellar, and mesodiencephalic innervation of the cat medial accessory olive: Anterograde tracing combined with immunocytochemistry. *J Comp Neurol* 284(1):12–35.
41. Welsh JP, Llinás R (1997) Some organizing principles for the control of movement based on olivocerebellar physiology. *Prog Brain Res* 114:449–461.
42. Safo P, Regehr WG (2008) Timing dependence of the induction of cerebellar LTD. *Neuropharmacology* 54(1):213–218.
43. Wang SS, Denk W, Häusser M (2000) Coincidence detection in single dendritic spines mediated by calcium release. *Nat Neurosci* 3(12):1266–1273.
44. Rasmussen A, Jirenhed DA, Hesslow G (2008) Simple and complex spike firing patterns in Purkinje cells during classical conditioning. *Cerebellum* 7(4): 563–566.
45. Kim JJ, Krupa DJ, Thompson RF (1998) Inhibitory cerebello-olivary projections and blocking effect in classical conditioning. *Science* 279(5350):570–573.
46. Ito M (2008) Control of mental activities by internal models in the cerebellum. *Nat Rev Neurosci* 9(4):304–313.
47. Kawato M (1999) Internal models for motor control and trajectory planning. *Curr Opin Neurobiol* 9(6):718–727.

Supporting Information

Chaumont et al. 10.1073/pnas.1302310110

SI Methods

BAC Modification and Transgenic Mice. A 1-kb homology box located 5′ of the ATG of the *pcp2* gene was amplified by PCR from bacterial artificial chromosome (BAC) RP24-186D18 and subcloned in the pLD53.SC2 shuttle vector. The cDNA encoding hChR2(H134R)EYFP was amplified from the vector pAAV-double floxed-hChR2(H134R)EYFP-WPRE-pA (kindly provided by K. Deisseroth, Stanford University, Standford, California), and placed behind the pcp2 homology box. The resulting pcp2/hChR2(H134R)EYFP shuttle vector was used to modify the BAC RP24-186D18 by homologous recombination according to previously published protocols (1). The recombination design allows the replacement of the pcp2 ATG by the cDNA construct in the BAC, effectively placing the expression of the channelrhodopsin hChR2(H134R)EYFP construct under the control of the regulatory elements of the pcp2 gene. Correct modification of the RP24-186D18 BAC was visualized by Southern blot on BAC DNA digested by EcoRI, separated on 0.8% agarose gel, and probed with digoxigenin-labeled pcp2 homology box. Pulsed-field gel electrophoresis was performed on BAC DNA digested by SpeI. A correctly modified BAC was selected (Fig. 1*A*) based on the pattern observed by Southern blot and pulsed-field gel analysis (including no visible reorganization of the BAC). This BAC was amplified and purified using a cesium chloride gradient. DNA was then dialyzed in oocyte injection buffer for generation of transgenic mice (injection performed by the Institut Clinique de la Souris, Illkirch, France). Founders were genotyped using two sets of primers ensuring the integrity of the inserted BAC: one set in the BAC backbone (forward: 5′GTGATATCGCGGAAGGAAAA3′; reverse: 5′AGGATATACGGCAGGCATTG3′), another set encompassing the L7 homology box and the ChR2 cDNA (forward: 5′GCTTCTTCAACCTGCTGACC3′; reverse: 5′aaaaatgtgttcgcgccata3′).

In Vitro Recordings. All experimental procedures conformed to Centre National de la Recherche Scientifique and National Institutes of Health guidelines on animal experimentation. Slices were prepared from juvenile L7-ChR2-eYFP mice (postnatal 15 to 24) as described in ref. 2. Following anesthesia by isoflurane inhalation, animals were killed by decapitation, the cerebellum was dissected out and placed in a cold artificial cerebrospinal fluid (ACSF) (4 °C) bubbled with carbogen [95% O_2, 5% CO_2 (vol/vol)], containing in mM: NaCl 120; KCl 3; $NaHCO_3$ 26; NaH_2PO_4 1.25; $CaCl_2$ 2.5; $MgCl_2$ 2. Glucose 10, Minocyclin 0.00005 (Sigma-Aldrich). The 330 μm-thick sagittal slices were prepared (Microm HM 650V, Microm) in potassium-based medium, containing in mM: K-gluconate 130; KCl 14.6; EGTA 2; Hepes 20; Glucose 25; minocyclin 0.00005, and D-AP5 0.05. This method was used to protect acute brain slices during cutting (3). After cutting, slices were soaked a few seconds in a sucrose-based medium at 34 °C, containing in mM: sucrose 230; KCl 2.5; $NaHCO_3$ 26; NaH_2PO_4 1.25; glucose 25; $CaCl_2$ 0.8; $MgCl_2$ 8; minocyclin 0.00005; and D-APV 0.05. Slices were maintained in a water bath at 34 °C in bubbled ACSF. Experiments were done at 34 °C using the same bubbled ACSF. Drugs were obtained from Tocris-Cookson or Ascent Scientific. Purkinje cells (PCs) were whole-cell patch-clamped both in voltage and current clamp mode using 3- to 4-MΩ pipettes with a Multiclamp 700 amplifier (Molecular Devices), and optimal series resistance (R_s) compensation (80% of 5–10 MΩ typically) was applied. R_s was monitored in all experiments, and cells were held at −60 mV (Figs. 1 and 2) or −70 mV (Fig. S2). The pipette solution contained (in mM): $KMeSO_4$ 135; NaCl 6, Hepes 10; MgATP 4; Na_2GTP 0.4, with pH adjusted to 7.3 with KOH and osmolarity to 300 mOsm. Voltages were not corrected for the liquid junction potential, which was calculated to be 9 mV (i.e., the real membrane potential was 9 mV more hyperpolarized than reported). Currents in Purkinje cells were low-pass filtered at 2 kHz, and then sampled at 20-50 kHz. Acquisition of data and control of light illumination were performed using the WinWCP 4.2.x freeware (John Dempster, University of Strathclyde, Glasgow, UK).

In Vitro Photostimulation. For experiments of Fig. 2 *C* and *D*, PCs were photostimulated using wide field LED-based illumination (collimated LED M470L2-C1 powered by a T-cube LEDD1B driver from Thorlabs or a collimated black LED 460 nm from Prizmatix) through the objective (20×, NA = 0.5) of the microscope (BX51 Olympus). Irradiance was measured with a PM100D power meter equipped with an S120C photodiode sensor (Thorlabs) under the objective, and the illuminated area was estimated to a disk of 600 μm. In Fig. 2*B*, a 473-nm diode-pumped solid-state (DPSS) laser (CrystaLaser) was used for laser scan illumination on an Olympus microscope. In Fig. S2, photostimulation at 460nm (Lumen Dynamics X-cite XLED1) was carried out on an optogenetic workstation based on a Leica DM6000 FS fixed-stage microscope, with patterned illumination (digital micromirror device; AndorTM Mosaic). The position and shape of illumination masks were verified by using a mirror slide straight after the experiment. The homogeneous illumination over masks of defined size enabled the accurate calibration of the irradiance. Recorded PCs were loaded with alexa 568 to draw the masks and estimate their depth (on average ∼30 μm below the slice surface).

Surgery. Mice were anesthetized using urethane (1.9 g/kg i.p.) and mounted in a stereotaxic frame (Model 942; David Kopf Instruments; or SR-6M; Narishige). Their body temperature was maintained at 36–37 °C throughout the experiment using a heating blanket controlled by rectal temperature (CMA 450, CMA or TC-1000; CWE Inc). Before scalp incision, 3% lidocaine was injected s.c. at the incision site. After incision, the skull was exposed, and a craniotomy was drilled above the right cerebellar hemisphere. During surgery, a long pass filter (cut on 550 nm) on white-light apparatus was used to avoid spurious ChR2 activation. The surface of the cerebellum was kept moist with a saline solution throughout the experiment. For juxtacellular recordings, mice were ventilated (SAR-830/P, BIOSEB; Dwyer). All in vivo electrophysiological experiments were performed on anesthetized mice.

Rotarod. To evaluate motor coordination, mice were placed on immobile rotarod cylinders, which ramped up from 0 to 45 rotations per minute (IITC) in 180 s. The timer was stopped when the mouse fell off the cylinder or did a whole turn with it. For a given session, this procedure was repeated three consecutive times. The full experiment comprised three sessions per animal, separated by 90 min.

in Vivo Juxtacellular Recordings and Data Analysis. Juxtacellular recordings in anesthetized mice were made as in ref. 4 using 15–30 MΩ resistance borosilicate glass pipettes (Warner Instruments), filled with a 0.5 M NaCl solution and mounted on motorized micromanipulators (Luigs and Neumann). Data were recorded and filtered between 300 Hz and 5 kHz and sampled at 20 kHz using an amplifier in current clamp mode (ELC 03XS; NPI). Acquisition of data and control of light illumination were

performed using the WinWCP 4.2.x freeware (John Dempster). Spike sorting and data storage were designed with OpenElectrophy open source software in a sql environment (http://neuralensemble.org/OpenElectrophy/) [Garcia and Fourcaud-Trocmé (5)].

Cerebellar Nuclei Recordings. For electrophysiological recordings, a commercial quartz tetrode (Thomas Recordings) was lowered into the right nucleus interpositus (from Bregma, −6.2 to −6.4 mm antero-posterior (AP), 1.5–2.0 mm medio-lateral (ML), and 2.4–2.8 mm below brain surface). As we showed earlier, these tetrodes produce more reliable penetrations of the cerebellar cortex and less tissue damage than conventional wire tetrodes (6). Each tetrode was covered with dye (Vybrant DiI; Life Technologies), and its position in the nucleus interpositus was verified by post hoc analysis of cryostat brain sections. Extracellular potentials measured by the tetrode were amplified and digitized using a System 3 workstation purchased from Tucker Davis Technologies.

In Vivo Photostimulation of Purkinje Cells. Light was delivered to discrete areas of the exposed cerebellar surface using a high-brightness blue light emitting diode (LED) coupled with optical fibers of different diameters (50, 100, 200, and 600 μm, numerical aperture 0.22, 0.22, 0.48, and 0.37), purchased from Prizmatix or Doric Lenses. The LED had a peak wavelength of 460 or 463 nm and a spectral bandwidth (full-width at half maximum) of 27 or 24 nm. Light pulses were generated using a universal LED controller (Prizmatix; SLC-AA02-US; Mightex Systems) triggered from the electrophysiology acquisition software (WinWCP or Tucker-Davis). Optical power at the fiber tip was measured with a PM100D power meter equipped with an S120C photodiode sensor (Thorlabs). The waveform and timing of individual light pulses were monitored using a silicon photodiode (SM1PD1A; Thorlabs). All values of irradiance in the text correspond to the value at the tip of the optic fiber. For photostimulation of Purkinje cells, the tip of the optical fiber was positioned in close vicinity or in contact with the cerebellar surface (except in the experiments where the fiber was moved while recording the cell).

Initially, a 200-μm fiber was used to study Purkinje-cell response to blue light in juxtacellular recordings and control the emission of spikes by olivary cells as shown in Fig. 4. In an attempt to restrict the spread of light, a set of experiments with a fiber of 100 μm diameter (and a few experiments using a fiber of 50 μm) was performed. In these experiments, the irradiance at the tip of the optical fiber was adjusted to compensate for light diffusion between the optical fiber and the recorded PC (and its neighbors), so that it generated a strong increase in the frequency of simple spikes but remained below the threshold triggering depolarization block in the recorded PC.

A 600-μm-diameter fiber combined with high irradiance was used for the recordings in the cerebellar nuclei: in these experiments we needed to stimulate a larger area to increase the chance to stimulate the few tens of Purkinje cells that contact the cerebellar nuclei (CN) units recorded.

In the experiment of Fig. 4*E* for which the fiber was moved while recording the PC, the fiber had to be kept distant from the surface to avoid the loss of the cell, thus yielding more diffuse activation [these data were analyzed by comparing the occurrence of the light-evoked complex-spike (CS) response to the modulation of the simple-spike discharge as a signature of a direct effect].

Estimation of the Number of Stimulated Purkinje Cells. To estimate the number of cells activated during photostimulation, we first assessed the volume of tissue that received enough light to increase the simple spike firing rate and then calculated the number of Purkinje cells in this volume.

We first performed a series of experiments as in ref. 7 using freshly dissected hemisectioned cerebellum maintained in saline and embedded in 2% agarose gel to hold the surface horizontal. An opening in the agarose gel surrounding the tissue was made around CrusII to bring an optical fiber next to the cerebellar surface. The optical fibers (100 μm core 0.22 NA and 600 μm core 0.37 NA) were positioned against the *pia* in a plane parallel to the section and with a distance and angle relative to the surface as in the in vivo CN recordings (Fig. 3) and evoked CS experiments (Fig. 4 *A–D*). The cut surface was imaged from the top using a CCD camera; this measure provides a coarse estimate of the power density distribution in the depth of the cerebellar cortex. Series of images were collected while the optical fiber was translated vertically to change the distance between the axis of the fiber and the plane of the section (Fig. S5), thus exploring the lateral extension of the power density profiles.

We then estimated the volume receiving enough light to activate Purkinje cells (i.e., irradiances $\geq$ 2 mW/mm^2) in experiments aimed at studying the nuclear and olivary responses (Figs. 3*A* and 4*A*). For irradiance of 20 mW/mm^2 at the fiber tip (intensity used for mapping the CN responsive area and mean intensity in the study of olivary disinhibition), we identified on all images the pixels with intensities above 10% of the intensity of the brightest pixel immediately underneath the fiber. (This provides probably an overestimation of the volume because, for this brightest pixel, the irradiance is probably lower than the irradiance at the fiber tip, and thus the 10% threshold corresponds to an even lower irradiance threshold.) For the 100-μm fiber, this volume has a roughly conical shape, with a maximal width of 360 μm in the transverse direction and 800 μm in the sagittal direction. For the 600-μm fiber, we found a roughly spherical volume with a diameter of 1,300 μm. Purkinje cells are organized in layers that are intersecting these volumes. For planar layers, this intersection will have an elliptic surface of at most 0.2 mm^2 for the 100-μm fiber, and a circular surface of at most 1.3 mm^2 for the 600-μm fiber. In the mouse, the total surface of the Purkinje-cell layer has been estimated to ∼190 mm^2 (8) or 80 mm^2 (9). According to these authors, the patch of activated Purkinje cells will represent 0.1–0.25% (respectively 0.7–1.6%) of the total Purkinje-cell layer surface when using a 100-μm (respectively 600 μm) optical fiber. Using a density of Purkinje cell of 1,018 per mm^2 [Napper and Harvey (10)], this estimation would yield ∼200 Purkinje cells per layer for the 100-μm fiber and ∼1,300 Purkinje cells per layer for the 600-μm fiber at 20 mW/mm^2. For irradiance of 60 mW/mm^2 (used to study CN responses), the volume receiving enough light to activate Purkinje cells had a radial extension of 1 mm and maximal depth of 1.5 mm (with thus ∼3,000 Purkinje cells per layer activated), whereas the volume exposed to intensities above 10 mW/mm^2 (which provides a conservative volume where depolarization block may occur) has a radial extension of 450 μm and maximal depth of 750 μm, and thus represents only ∼10% of the activated volume. The 60 mW/mm^2 condition will thus increase the volume stimulated by a factor of 5 compared to the 20 mW/mm^2 condition.

Because we computed the widest intersection of a planar Purkinje-cell layer, these numbers provide only order-of-magnitude estimates and not accurate numerical predictions; depending on the recording site, the topology of the lobule may bring one or two layers within the photostimulated volume. Therefore, we may consider that with a 100-μm fiber, we will activate 200–500 Purkinje cells whereas these numbers may be closer to 1,000–3,000 Purkinje cells with a 600-μm optic fiber at 20 mW/mm^2 and 5,000–10,000 Purkinje cells at 60 mW/mm^2.

CN Data Analysis. Single units were isolated as described previously (4, 11). Briefly, spikes were detected by thresholding of a high-pass filtered version (1 kHz) of the continuous recording, and the

main parameters of their waveforms were extracted. The data were then hand clustered by polygon-cutting in 2-dimensional projections of the parameter space using Xclust (Matt Wilson, Massachusetts Institute of Technology, Cambridge, MA). The quality of clustering was evaluated by inspecting the auto-correlograms of the units. To assess the presence of inhibition and to quantify its intensity, we applied more than 150 light pulses of various durations and intensities at 1 Hz or 0.3 Hz. Peri-stimulus-histograms (PSTHs) with bins of 2 ms were constructed. The latency to full inhibition corresponded to the time to the first empty bin after light onset, and the duration of full inhibition was obtained by counting the empty bins during or immediately after the light pulse. The instantaneous frequency was computed for each time bin (5 ms) by computing the geometric mean of the inverse of the interspikes interval that preceded all of the spikes occurring within this time bin. The ability of rhythmic trains of light pulses to constrain the firing of CN units is reflected by the presence of oscillations in the PSTHs during the stimulation. We therefore computed the power spectral density of PSTHs from experiments with 20 pulses of 12 ms and irradiance of 16.6 mW/mm^2 at 20 Hz/30 Hz; the peak value in the spectrum was normalized to the total power in the 0- to 100-Hz window.

Statistical Analysis. Means are given ± SD in the text unless otherwise stated. See figure legends for statistics in figures. Significance levels are indicated in figures as follows: (*) $P < 0.05$, (**) $P < 0.01$, (***) $P < 0.001$. The parameters (onset, offset, response rate) of the light-evoked CSs were obtained from the density of spikes convolved with a Gaussian kernel with a 20-ms variance; this convolution provides a curve similar to a peri-stimulus histogram with bin 20 ms; the baseline average (1 s before stimulation) was substracted from the spike density and the result was divided by the SD of the baseline. Significant departure from baseline over a search period T was detected when this studentized spike density departed by more than a z-score critical value corresponding to $P = 0.05/(T/bin)$. We used a search period starting at light onset and ending 250 ms after the light offset. The response rate is defined as the number of CS observed during the identified time interval of significant deviation from baseline, divided by the number of trial. For the study of the dependence of the timing of CSs to the recent history of CS firing (Fig. 4*D*), we constructed, for each cell in which CS frequency was above 0.1 Hz and for which at least 20 light-evoked CS were recorded, a PSTH aligned to the first CS response in each trial (with a response). Shuffled PSTHs were obtained by shifting each trial with a random number in the interval (−0.3; 0.3) ms. The average PSTHs were then compared with the average of 300 shuffled PSTHs.

Immunochemistry. Mice were perfused with 4% paraformaldehyde, and their brains were postfixed in 4% paraformaldehyde overnight. Sagittal Slices of 35 μm thickness were cut with a vibratome (Leica VT1000). Sections were washed three time with PBS and non-specific staining was blocked for 24 h using PBS contaning 1% BSA, 4% normal goat serum, and 0.5% triton. Slices were incubated for 48 h at 4 °C with the following antibodies: mouse anti-calbindin monoclonal antibody (1:1,000; Sigma Aldrich) and rabbit anti-GABA polyclonal antibody (1:1,000; Sigma Aldrich). Then sections were washed with PBS (5 × 10 min) and incubated for 2 h at room temperature with Alexa Fluor 633-conjugated goat anti-rabbit antibody (1:500; Invitrogen) and Alexa Fluor 555-conjugated goat anti-mice antibody (1:500; Invitrogen).

1. Gong S, et al. (2003) A gene expression atlas of the central nervous system based on bacterial artificial chromosomes. *Nature* 425(6961):917–925.
2. Valera AM, Doussau F, Poulain B, Barbour B, Isope P (2012) Adaptation of granule cell to Purkinje cell synapses to high-frequency transmission. *J Neurosci* 32(9):3267–3280.
3. Dugué GP, Dumoulin A, Triller A, Dieudonné S (2005) Target-dependent use of co-released inhibitory transmitters at central synapses. *J Neurosci* 25(28):6490–6498.
4. Pinault D (1996) A novel single-cell staining procedure performed in vivo under electrophysiological control: Morpho-functional features of juxtacellularly labeled thalamic cells and other central neurons with biocytin or Neurobiotin. *J Neurosci Methods* 65(2):113–136.
5. Garcia S, Fourcaud-Trocmé N (2009) OpenElectrophy: An electrophysiological data- and analysis-sharing framework. *Front Neuroinform* 3:14.
6. Gao H, Solages Cd, Lena C (2012) Tetrode recordings in the cerebellar cortex. *J Physiol Paris* 106(3-4):128–136.
7. Huber D, et al. (2008) Sparse optical microstimulation in barrel cortex drives learned behaviour in freely moving mice. *Nature* 451(7174):61–64.
8. Sultan F, Braitenberg V (1993) Shapes and sizes of different mammalian cerebella. A study in quantitative comparative neuroanatomy. *J Hirnforsch* 34(1):79–92.
9. Van Essen DC (2002) Surface-based atlases of cerebellar cortex in the human, macaque, and mouse. *Ann N Y Acad Sci* 978:468–479.
10. Napper RM, Harvey RJ (1988) Quantitative study of the Purkinje cell dendritic spines in the rat cerebellum. *J Comp Neurol* 274(2):158–167.
11. de Solages C, et al. (2008) High-frequency organization and synchrony of activity in the purkinje cell layer of the cerebellum. *Neuron* 58(5):775–788.

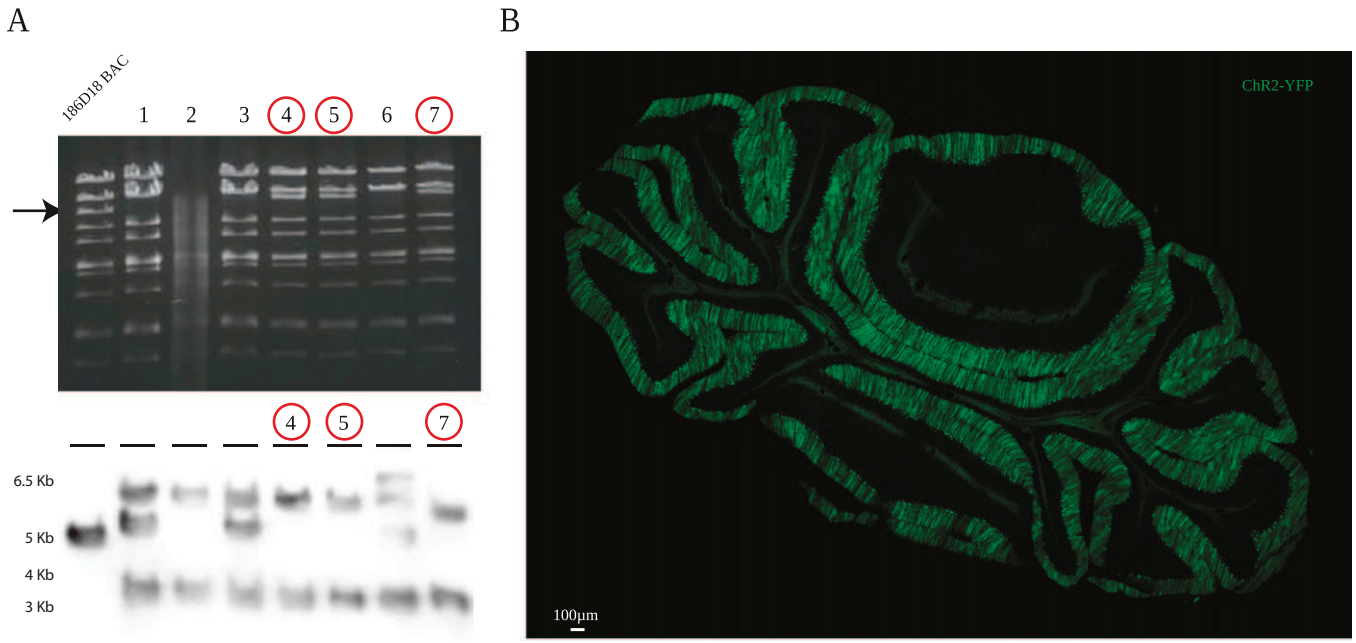

Fig. S1. Construction of L7-ChR2(H134R)-eYFP mice. (*A*) Pulsed-field gel analysis (*Upper*) of SpeI-digested BAC DNA confirmed correct insertion of the shuttle vector at the level of the *pcp2* ATG starting codon in exon 2 and ruled out major reorganization of the BAC (only one band shifted compared with the profile of the original BAC vector 186D18, arrow). Correct insertion of the shuttle vector was also checked by Southern blot analysis (*Lower*) using the homology box as a probe (SB probe, Fig. 1) and EcoRI-digested BAC DNA. The correctly recombined clones are circled in red. (*B*) L7-ChR2(H134R)-eYFP expression in cerebellar sections at P40 (50 μm).

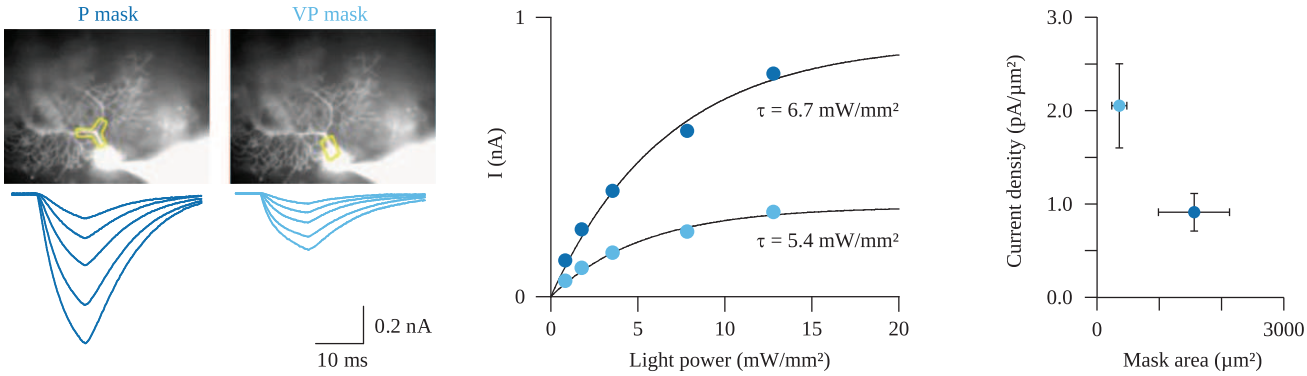

Fig. S2. Density of ChR2 currents in L7-ChR2(H134R)-eYFP Purkinje cells. (*Left*) Representative whole-cell recording from one PC. Currents evoked by 10 ms illumination (460 nm LED) at increasing irradiances (0.83, 1.79, 3.56, 7.84, and 12.80 mW/mm^2) over spatial patterns (masks) defined by a digital micromirror device (Mosaic; Andor Technology). The positions of proximal (P) and very proximal (VP) masks were verified by using a mirror slide, and their contours are shown over the recorded PC (loaded with Alexa 568). (*Center*) A 10-ms illumination peak current and their exponential fit plotted against irradiance for the two masks. (*Right*) Density current recorded using the two masks.

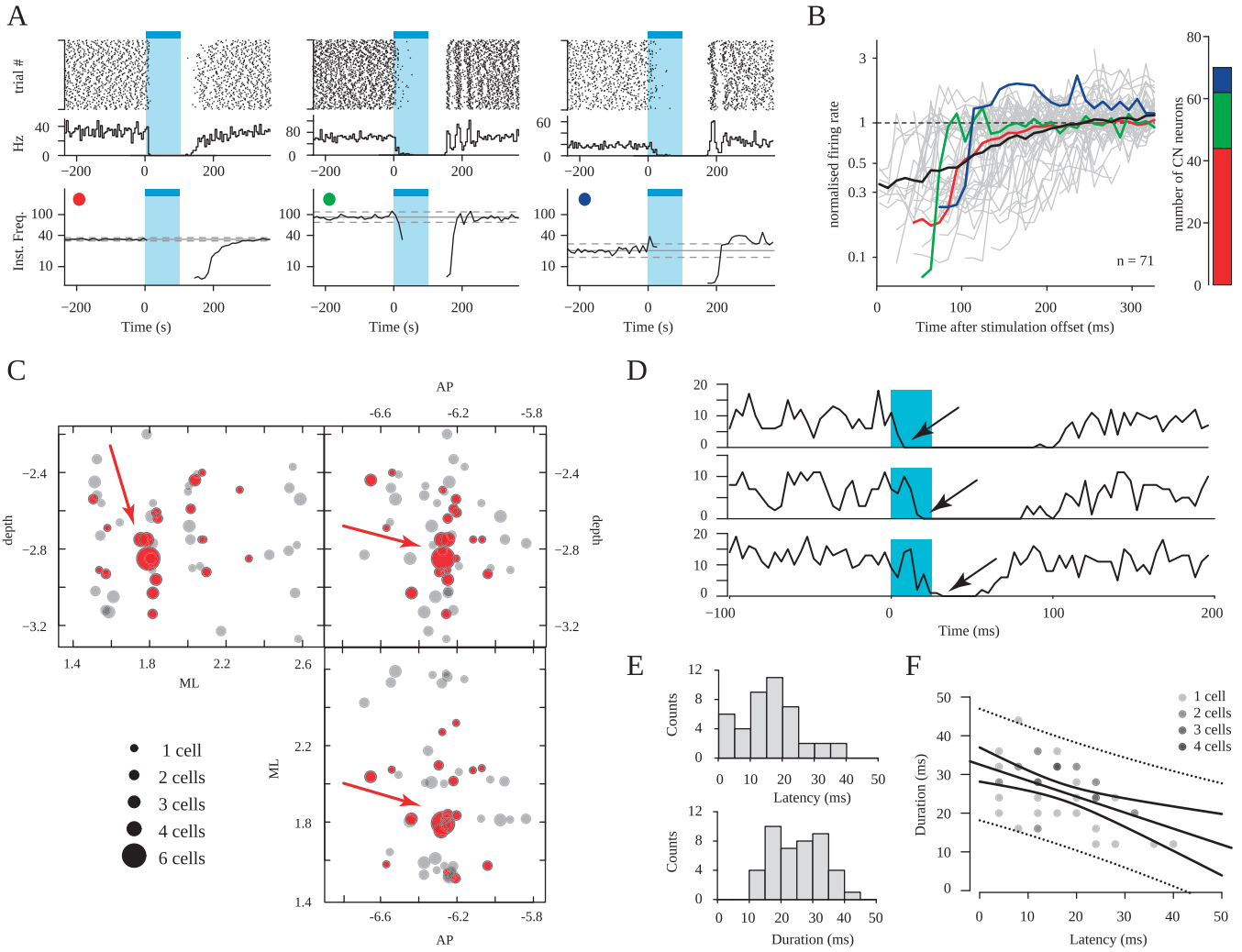

Fig. S3. Temporal and spatial properties of the light-triggered inhibition of cerebellar nuclear neurons. (*A* and *B*) Postsuppression firing behavior of cerebellar nuclear cells following photostimulation of Purkinje cells. (*A*) Three examples of cells displaying complete suppression of their firing in response to illumination of the ipsilateral Crus I region (100-ms light pulses, 60 mW/mm^2). For each cell, a raster plot (*Upper*) is represented on top of the corresponding PSTH (*Center*; bin, 5 ms) and average instantaneous frequency profile (*Lower*; bin, 10 ms; gray lines correspond to mean ± 2 SD of the baseline values). Unlike the first cell (red dot), the two other cells (green and blue dot) readily resumed their firing with a strong locking relative to the stimulation. However, only the third cell (blue dot) exhibited a modest but significant peak in the instantaneous frequency, suggestive of a postsuppression "rebound excitation." (*B*) Superimposed (gray) and average (black) instantaneous frequency traces of 70 cells during the postsuppression period (bin, 10 ms). Traces from example cells are plotted in red, green, and blue, respectively. The bar graph summarizes the distribution of the cells in the three categories depending on their postinhibitory behavior: no rebound and progressive return to baseline firing rate (red, $n = 44$); no rebound and time-locked return to baseline firing (green, $n = 18$); rebound (blue, $n = 8$). (*C*) Distribution of the coordinates of CN recording sites where inhibited cells were found (red) or not (black) during illumination of the ipsilateral cerebellar Crus I region [antero-posterior (AP), 6.1; medio-lateral (ML), 3.3; pulse = 100 ms, irradiance = 19 mW/mm^2]. The number of cell recorded at each site is represented as the diameter of the points. The red arrow identifies the region where most responsive sites are clustered. See Fig. 3G for a 3D view of the same data. (*D*) Examples of peri-stimulus histograms from three different CN neurons with latency to full inhibition (black arrow) smaller than 10 ms, between 10 and 20 ms, and longer than 20 ms, from top to bottom panels respectively (25 ms, 19 mW/mm^2, bin = 4 ms). (*E*) Histograms showing the distribution of latency and duration of full inhibition (for 43 cells, 25 ms, 19 mW/mm^2, bin = 4ms). (*F*) Plot showing the anti-correlation of these response parameters (linear fit: $r^2 = 0.24$, $P = 8.10^{-4}$).

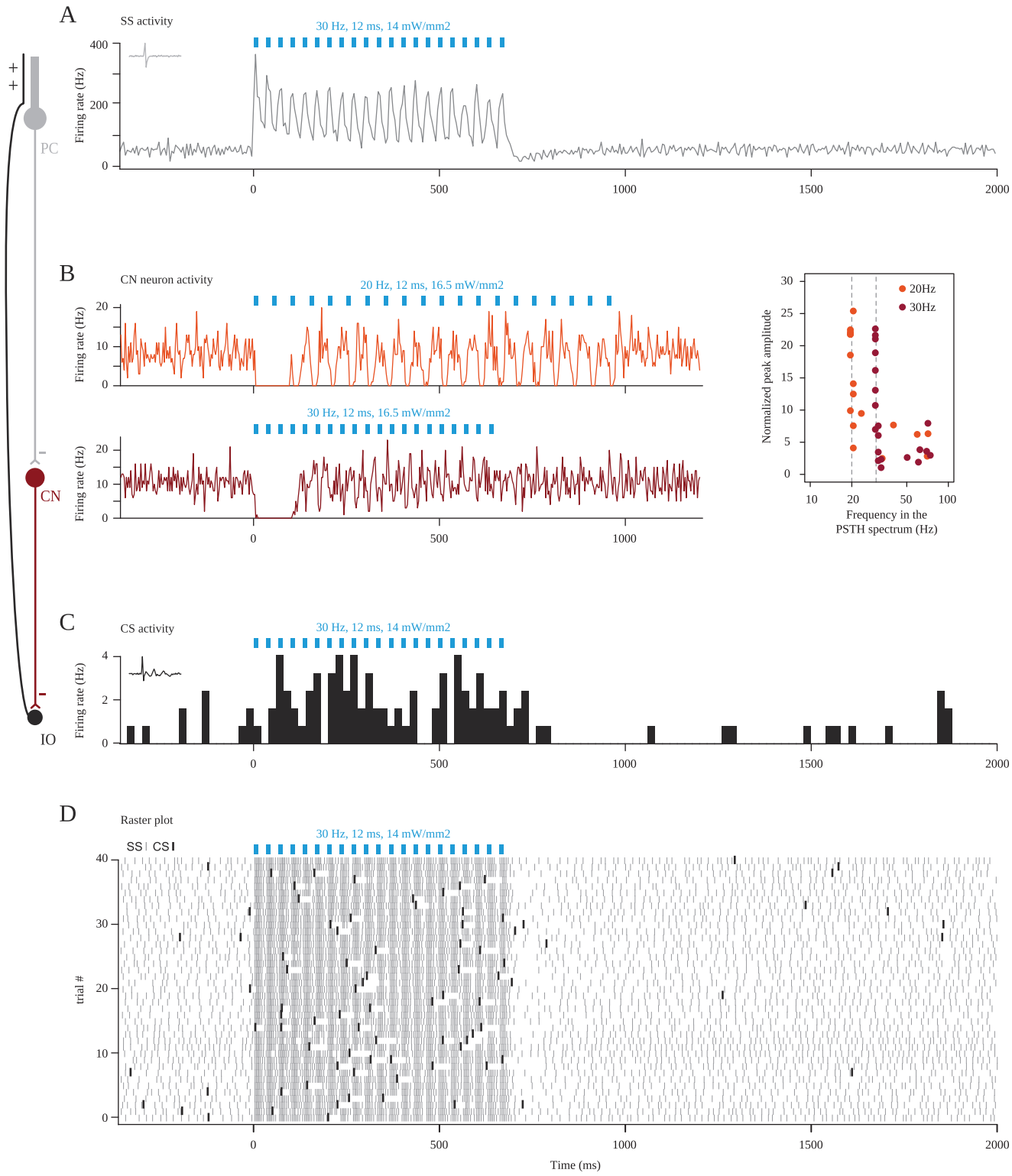

Fig. S4. Burst of light pulses elicits CSs in PCs in vivo. (*A*) Simple spike PSTH in one PC (bin: 5 ms) during 30 Hz illumination (12 ms light pulse, 14 mW/mm^2, blue bars). (*B*, *Left*) PSTH of one CN neuron (bin: 1 ms) in response to trains of illuminations (12-ms light pulses, 16.5 mW/mm^2, blue bars). After a short period of complete inhibition, the cell discharge was locked to the illumination pulses. (*Right*) For all 22 cells tested with stimulations pulses, the power spectral density of the PSTH (*SI Methods*) was calculated during the illumination; the presence of a peak at the same frequency as the stimulation evidences a time-locked inhibition of the cells. (*C*) PSTH of light-induced CSs in a PC (bin: 20 ms) during 30-Hz stimulation (same stimulation and same cell as in *A*). (*D*) Raster plot of simple spikes (gray ticks) and CS (black ticks) activity during 30-Hz stimulation of the cell in *A* and *C*. CN and PC are recordings from different set of experiments.

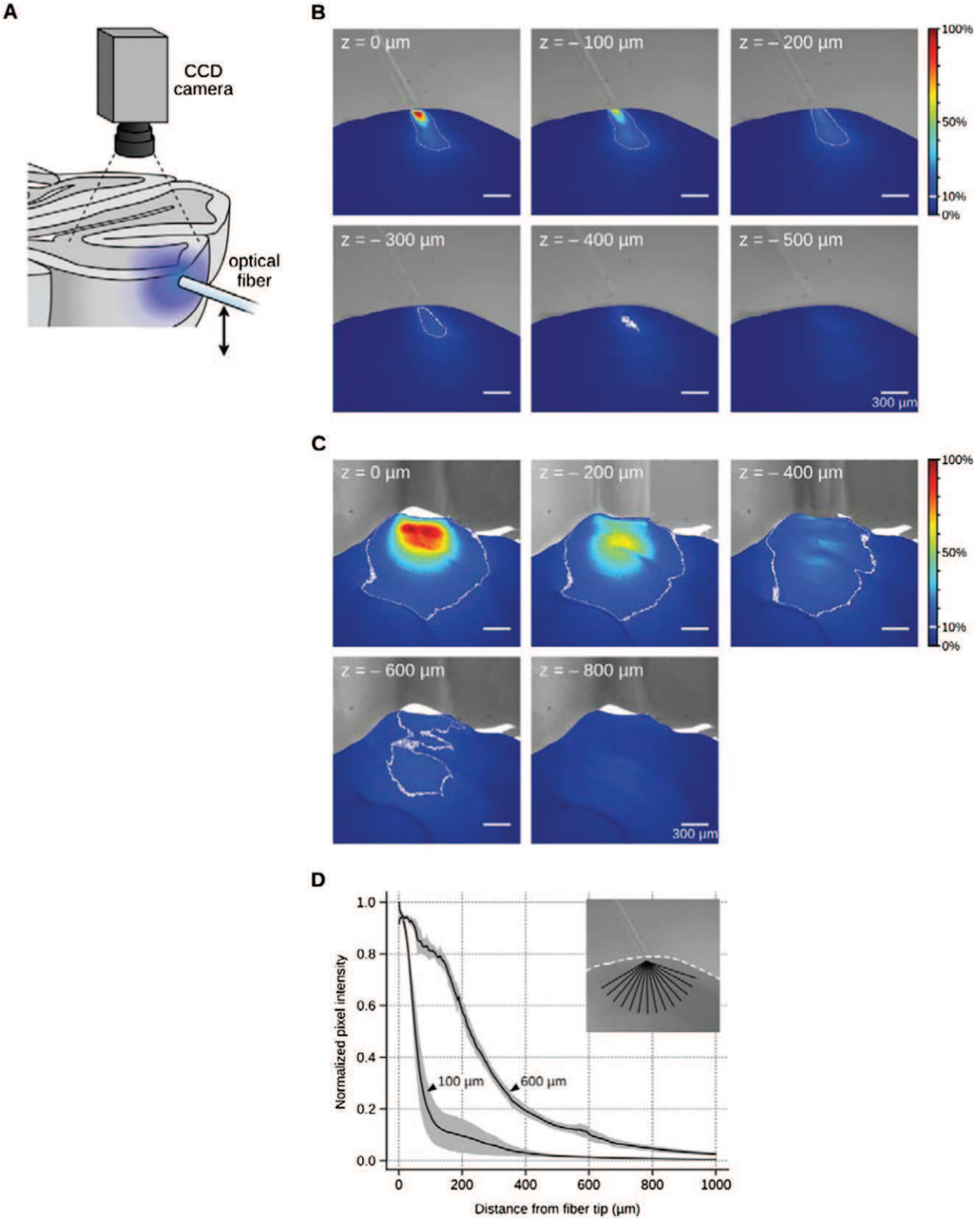

Fig. S5. Light power density mapping using cerebellar hemisections. (*A*) Schematic of the experimental setup. The cut surface was imaged from the top using a CCD camera whereas the tissue was illuminated from the side through an optical fiber coupled to blue (470 nm) LED. The fiber was translated vertically (two headed arrow) to assess the lateral propagation of light. (*B*) Series of images taken for different vertical fiber positions using a 100-µm optical fiber with an angle of incidence of ~30° and a distance to the *pia* of around 100 µm. The position of the fiber relative to the cut surface is indicated in white. Pictures were taken in the dark with a power at the fiber tip of 125 µW. The intensity of each pixel is expressed as a percentage of the intensity of the brightest pixel of the image series and color coded. The 10% isoline is delineated in white on each image. The color-coded image of the tissue is superimposed on a grayscale picture

Legend continued on following page

of the fiber obtained with a brightfield side illumination. Here, the hemisection was done coronally. (*C*) A similar series of images taken for different vertical fiber positions, using a 600-μm optical fiber. Here, the fiber was affixed perpendicularly to the *pia*, and the hemisection was performed parasagitally. The power at the fiber tip was 200 μW. The white patches in the grayscale picture are due to reflections of the brightfield side illumination on the surface of the liquid. (*D*) Decay of the pixel intensity as a function of distance from the brightest pixel. Pixel intensity profiles were measured for the upper fiber position (z = 0 μm) along 70 evenly distributed lines drawn through the tissue. All lines originated from the brightest pixel underneath the fiber tip (as indicated in the top right *Inset*). The average curves calculated from these profiles are plotted for the experiments shown in *B* and *C*. Note the much steeper decay of pixel intensity for the 100-μm fiber. The shaded area represents the SD for the 70 profiles along the lines radiating from the most intense pixel.

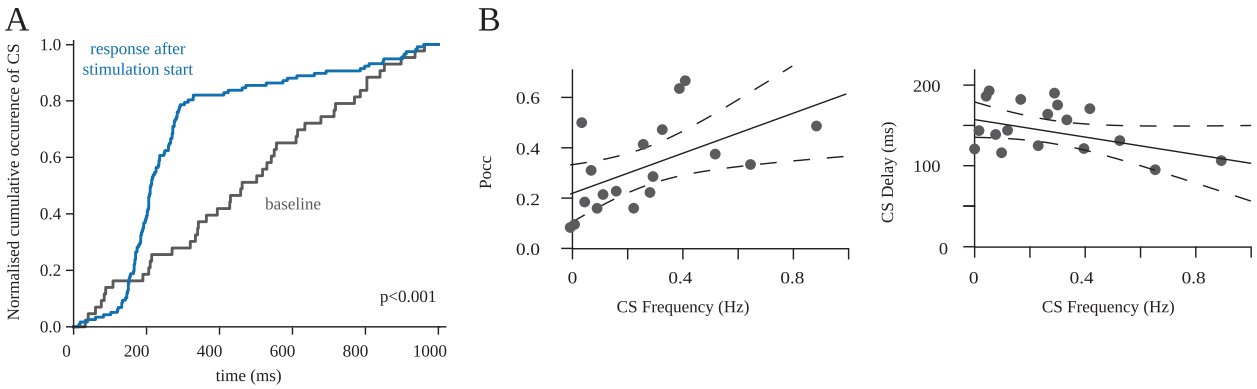

Fig. S6. Purkinje-cell synchronization triggers complex spike responses. (*A*) Normalized cumulative PSTH of light-induced CS for one cell (bin: 2ms) during 1 s before (gray) and after stimulation start (blue). Cumulative PSTHs were significantly different for 25/42 PCs (Kolmogorov–Smirnov; $P < 0.001$). (*B*) Scatter plot of the probability of occurrence (Pocc, *Left*) or the delay (*Right*) of the light-induced CSs as a function of the baseline CS firing rate.

8.2 RÉSUMÉ EN FRANÇAIS

Organisation spatiale et temporelle des entrées granulaires dans le cortex cérébelleux.

Antoine VALERA

Résumé du manuscrit en français

1 INTRODUCTION GENERALE – LE CERVELET : STRUCTURE ET FONCTION

Le cervelet est une structure du système nerveux central impliquée dans le contrôle de l'équilibre, de la posture, la coordination motrice et les apprentissages moteurs. Il est divisé en deux structures : les noyaux profonds cérébelleux, seule sortie du cervelet, et le cortex cérébelleux. Lors de l'exécution de ces tâches motrices, le cervelet reçoit une copie de l'ordre moteur en provenance des aires corticales motrices ainsi que des informations sensorielles provenant de l'ensemble de l'organisme (muscles, tendons, articulations, mais aussi des informations visuelles, vestibulaires, etc.). Le traitement simultané du contexte sensoriel et de l'ordre moteur permet l'exécution précise de mouvements complexes, la correction d'éventuelles erreurs motrices et le stockage de séquences de mouvements en vue de réexécutions ultérieures (apprentissages moteurs). Le dysfonctionnement du cervelet entraine des pathologies telles que des ataxies, des dysmétries ou des tremblements.

Les cellules de Purkinje forment l'unique sortie du cortex cérébelleux, et intègrent donc l'ensemble des informations qui y sont traitées. Ces dernières, spontanément actives, voient leur activité modulée par les deux entrées synaptiques excitatrices du cortex cérébelleux: la voie des fibres grimpantes provenant de l'olive inférieure, et la voie fibres moussues – cellules en grain, qui provient de divers noyaux precérébelleux. L'activité des cellules de Purkinje est également modulée par des interneurones inhibiteurs (cellules étoilées et cellules en panier, toutes deux activées par les fibres parallèles) ainsi que par les collatérales des axones d'autres cellules de Purkinje. Les fibres grimpantes contactent donc directement les cellules de Purkinje, tandis que les fibres moussues projettent d'abord sur les cellules en grain, lesquelles exercent ensuite leur activité excitatrice sur les cellules de Purkinje. La première partie de cette thèse comprend une introduction générale de l'anatomie du cervelet et des propriétés anatomo – fonctionnelles de certains de ses principaux composants cellulaires (cellules en grains, cellules de Purkinje, cellules de Golgi et interneurones de la couche moléculaire).

Le cervelet est impliqué dans des tâches motrices mobilisant de nombreux muscles au court de mouvements séquentiels complexes. Chaque région du cortex cérébelleux est spécialisée dans le contrôle d'un ou de plusieurs muscles bien définis. Lors d'une tâche nécessitant plusieurs muscles/groupes de muscles, ces différentes régions vont être coordonnées afin de moduler correctement le mouvement. Les zones contrôlant des groupes de muscles adjacents dans l'organisme ne sont pas nécessairement localisées dans des régions adjacentes du cortex cérébelleux – on parle de somatotopie fracturée – et l'association entre ces région peut se faire par l'intermédiaire des fibres parallèles. L'organisation spatiale des différentes entrées du cortex cérébelleux, ainsi que l'organisation spatiale de nombreux marqueurs histochimiques sont décrites dans la seconde partie de l'introduction. L'une des grandes questions qui demeure est de savoir

comment l'information entrante est traitée dans le cortex cérébelleux et quelle est la taille du module fonctionnel, c'est – à – dire du plus petit microcircuit pouvant traiter l'information provenant des cellules en grain. L'étude de l'organisation modulaire du cortex cérébelleux est traitée dans l'article *Cerebellar Modules Are Coordinated By Granule Cell Inputs* (en préparation).

Le contrôle et l'ajustement de mouvements fins et coordonnés nécessite une très grande précision temporelle dans le traitement de l'information. De plus les informations sensorielles convoyées par les entrées fibres moussues arrivent sous forme de bouffées de potentiels d'action à très haute fréquence (bursts), pouvant atteindre 1000 Hz. La troisième partie de l'introduction présente l'état des connaissances sur les processus de codage temporel dans la voie fibre moussue – cellule en grain – cellule de Purkinje, ainsi que les processus modulant la libération vésiculaire de neurotransmetteurs lors de bursts (plasticités à court terme, rôle du Ca^{2+}). La transmission synaptique dans cette gamme de fréquence est très mal connue, et la description des plasticités à court terme régissant la transmission glutamatergique à la synapse cellule en grain – cellule de Purkinje est l'objet de l'article *Adaptation of Granule Cell to Purkinje Cell Synapses to High – Frequency Transmission* (publié).

2 ORGANISATION SPATIALE DU CERVELET

2.1 PRESENTATION DU CONTEXTE

2.1.1 ORGANISATION MODULAIRE DANS LE CERVELET

Le cortex cérébelleux est composé de 10 lobules. Les entrées fibres grimpantes et fibres moussues sont organisées en bandes parasagittales traversant plusieurs lobules, et la position des bandes dépend de l'origine précise des projections. Cette organisation somatotopique des entrées est conservée d'un animal à l'autre, ainsi que d'une espèce à l'autre. De la même façon, certaines protéines s'expriment en suivant un patron de bandes parasagittales où la protéine est alternativement exprimée ou non dans les cellules de Purkinje, donnant ainsi un aspect zébré au tissu. Ces bandes, appelées bandes *zébrines*, sont également remarquablement conservées entre les individus et d'une espèce de mammifère à l'autre. Les zébrines ne correspondent pas à une classe de protéines particulière, mais sont uniquement définies par leur répartition hétérogène dans le cortex cérébelleux. Il peut s'agir d'enzymes, de récepteurs membranaires, de tampons calciques etc… Plusieurs dizaines de zébrines ont déjà été décrites dont la plupart suivent le patron de distribution de l'aldolase C (aussi appelées Zebrin II) ou son patron en miroir. Cependant, d'autres patrons zébrines que l'aldolase C existent, suggérant que chaque cellule de Purkinje possède une identité protéique spécifique dépendant de son appartenance ou non aux différents patrons zébrines.

Les projections des fibres grimpantes et des fibres moussues sont anatomiquement corrélées avec le patron d'expression de l'aldolase C, et les frontières de bandes zébrines délimitent des régions traitant différentes modalités/types d'information. Dès lors, ces frontières zébrines constituent de bons outils pour essayer de définir le module fonctionnel. Les cellules situées d'un côté d'une frontière zébrines traitent-elles de façon privilégiée les entrées fibres moussues arrivant sur les cellules en grain dans le même module, par rapport aux entrées parvenant sur les cellules en

grain situées de l'autre côté de cette frontière zébrine ? Les règles sont elles les mêmes pour tous les types cellulaires du cortex cérébelleux ? Comment les fibres parallèles qui, de part leur structure, sont nécessairement trans-modulaires vont-elles contacter différents modules ? Les cellules en grain du cervelet situées à un endroit donné établissent-elles toujours des synapses fonctionnelles vers les mêmes cellules de Purkinje d'un animal à l'autre ?

2.1.2 HYPOTHESE DE TRAVAIL

Notre postulat d'origine était que l'organisation du cortex cérébelleux en termes de modules fonctionnels, à l'image de ce qui se passe pour les entrées fibres grimpantes, respecte également les frontières des bandes zébrines. Ces frontières histochimiques marqueraient donc également la frontière fonctionnelle d'un module donné. Nous disposons d'une souris transgénique expriment une protéine de fusion EAAT4 – GFP. La protéine EAAT4, un transporteur du glutamate, est exprimée suivant le patron d'expression de l'aldolase C (patron zébrine II) et permet donc la localisation de la cellule enregistrée. La GFP permet la visualisation des bandes directement durant l'expérimentation et le positionnement de l'enregistrement et des stimulations de façon précise d'un animal à l'autre. Outre leur rôle potentiel de limite fonctionnelle, les bandes zébrines peuvent également servir de système de coordonnées, de part leur grande conservation d'un animal à l'autre. De ce fait, s'il existe une organisation modulaire ne respectant pas les frontières des bandes zébrines mais respectant d'autres limites encore non-identifiée, nous devrions également être en mesure de définir cette organisation grâce à un positionnement précis des cellules. Nous avons donc effectué une cartographie des projections cellules en grain vers les autres types cellulaires présents dans le cortex cérébelleux afin de voir si des connexions privilégiées ont lieu au sein d'une même bande, et si des règles organisationnelles générales peuvent être dégagées. Afin d'avoir la plus faible variabilité possible, nous nous sommes focalisés sur le vermis médian antérieur pour nos expériences. Cette région reçoit des entrées sensorielles spinales bien définies, et contrôle essentiellement les muscles du tronc et les muscles proximaux des membres.

2.1.3 DEVELOPPEMENT TECHNIQUE

Pour réaliser ce projet j'ai dû développer un système de stimulation précis, reproductible et contrôlé par logiciel. Il est également nécessaire de pouvoir identifier la position des cellules en grain stimulées et de la cellule enregistrée. La cellule d'intérêt est enregistrée en voltage clamp, et de la biocytine est présente dans la solution intracellulaire afin de pouvoir localiser la cellule *a posteriori* et éventuellement de procéder à une reconstruction morphologique. Seule la transmission glutamatergique ionotropique sur les récepteur AMPA est étudiée grâce à divers agents pharmacologiques. Le milieu extracellulaire contient également du glutamate cagé photoactivable. Un petit groupe de cellules en grain peut ainsi être stimulé grâce à bref flash laser effectué à une position contrôlée, libérant localement du glutamate et excitant temporairement les cellules en grain proximales. Si ces grains sont connectés, un courant postsynaptique excitateur est détecté, indiquant l'existence d'une connexion fonctionnelle entre ces 2 régions. La zone de stimulation est ensuite

décalée de quelques microns, et l'opération est répétée. L'ensemble de la procédure permet de définir des régions connectées fonctionnellement, et des régions non connectées, et de déterminer une carte fonctionnelle.

L'analyse des données est complexe, et j'ai développé un logiciel permettant l'analyse des résultats et leur positionnement automatique par rapport aux bandes zébrines.

2.2 RESULTATS : CARTOGRAPHIE FONCTIONELLES DES PROJECTIONS DES CELLULES EN GRAIN.

2.2.1 CONNEXION CELLULE EN GRAIN – CELLULE DE PURKINJE.

La première connexion étudiée est la connexion cellule en grain cellule de Purkinje. C'est la connexion la plus directe entre l'entrée fibres moussues et la sortie du cervelet. Dans la région étudiée, les fibres moussues provenant du noyau cunéiforme externe et du tractus spinocérébelleux entrent dans la couche granulaire sous forme de bandes parasagittales alternées. Aucune indication jusque là ne permettait de dire si une Purkinje donnée ne reçoit que des informations provenant d'une même origine précérébelleuse, ou si l'information provenant de différents tractus peut être associée par l'intermédiaire des fibres parallèles par exemple. Actuellement, les seules données disponibles dans la littérature suggèrent qu'une cellule de Purkinje est plus fortement contactée par les cellules en grain locales que par les cellules en grains distales. Le taux de connexion décroit ensuite progressivement avec la distance. Aucune hétérogénéité reproductible de la connectivité cellule en grain – cellule de Purkinje n'avait jusque là été mise en évidence.

Durant ma thèse j'ai pu montrer que pour une cellule de Purkinje localisée dans un endroit précis, les patrons de connexions des cellules en grains ne sont pas distribués aléatoirement. Plusieurs groupes peuvent être définis. Bien qu'il existe une forte variabilité interindividuelle, les cellules en grains recevant la même modalité via les fibres moussues semblent être connectées plus fortement à une cellule Purkinje donnée que des cellules en grains recevant des entrées sensorielles très différentes. Puisque les fibres parallèles peuvent théoriquement, de par leur morphologie, associer n'importe quelle cellule en grain avec une cellule de Purkinje donnée, l'existence de telles hétérogénéités semble être l'expression d'un mécanisme de sélection.

La question de savoir si ces associations privilégiées entre différentes régions est d'origine développementale ou si elle est liées à des apprentissages survenant durant la vie de l'animal n'est pas entièrement résolue. Cependant 1) des enregistrements de paires de cellules de Purkinje suggèrent que dans un même animal, les motifs d'entrées de deux cellules de Purkinje voisines sont bien plus proches que d'un animal à l'autre 2) des expériences d'induction de plasticité montrent que les poids synaptiques sont modifiables, suggérant que les motifs observés sont bien le résultat de sélections 3) la plupart des cellules suivent le motif moyen, mais certaines s'en éloignent fortement. De plus, même si peu de régions sont complètement non-répondantes, le poids des entrées entre zone répondantes et non répondantes présente de très fortes hétérogénéités. Ces trois indices suggèrent que des connexions privilégiées peuvent apparaître entre des régions traitant des entrées

sensorielles voisines mais que l'ensemble des associations est sans doute possible, permettant une grande souplesse dans les apprentissages moteurs.

Ainsi cette étude est la première à montrer que l'organisation de la connexion cellule en grain – cellule de Purkinje présente des patrons de connexion reproductibles, suggérant l'existence d'un traitement régionalisé, et donc modulaire de l'information.

2.2.2 CONNEXION CELLULE EN GRAIN – CELLULE DE GOLGI.

Compte tenu de l'organisation morphologique de la cellule de Golgi, qui dispose à la fois de dendrites basolatérales capables d'échantillonner les entrées locales et de dendrites apicales capables de recevoir des entrées distales par les fibres parallèles, nous avons cherché à voir si cette cellule avait une organisation des entrées similaire à celle des cellules de Purkinje, ou si elle ne traitait que des informations locales, comme le suggère certains modèles du fonctionnement cérébelleux.

Nous avons été surpris d'observer que la quasi-totalité des entrées granulaires sur la cellule de Golgi provenaient des cellules en grain locales, confortant ainsi l'hypothèse que la cellule de Golgi est un interneurone local, probablement intramodulaire. Ce résultat conforte une des hypothèses initiales du modèle de Marr et Albus sur le fonctionnement du cortex cérébelleux, selon lequel la cellule de Golgi peut contrôler le gain du système, via un rétrocontrôle inhibiteur sur les grains locaux.

Dans quelques cas, des entrées distales de petite taille ont pu être observées, suggérant que les dendrites apicales peuvent également collecter des entrées excitatrices provenant de sites lointains via les fibres parallèles, et donc de modules différents. Ces entrées sont relativement faibles en comparaison des entrées locales, et la compréhension du rôle exact des dendrites apicales de la cellule de Golgi nécessite une étude plus approfondie.

Un complément à notre approche a été la reconstruction morphologique des cellules de Golgi enregistrées, notamment dans le but de voir si leur plexus axonal présente des modification ou distorsions morphologiques à proximité des frontières de modules. Aucune règle générale n'a pu être mise en évidence, mais la quantification morphologique des extensions cellulaires montre que ces cellules gardent une taille modérée, et donc que l'inhibition des cellules en grain par la cellule de Golgi est nécessairement locale.

2.2.3 CONNEXION CELLULE EN GRAIN – INTERNEURONES DE LA COUCHE MOLECULAIRE

Les interneurones de la couche moléculaire, cellules étoilées et cellules en panier, sont traditionnellement associés à l'inhibition *feedforward* des fibres parallèles sur les cellules de Purkinje. L'extension de leur axone et de leurs dendrites suit un axe parasagittal. Néanmoins, le fait que les interneurones de la couche moléculaire soient contactés par les fibres parallèles suggère qu'ils puissent être activés aussi bien par les cellules en grain locales que par les cellules en grain distales.

L'approche méthodologique utilisée a été la même que pour les cellules de Purkinje, et des motifs particuliers semblent se dégager ici aussi. Les interneurones de la couche moléculaire sont activés par des régions spécifiques de la couche granulaire, même si le nombre de cellules en grain connectées semblent plus restreint que dans le cas des cellules de Purkinje. Une entrée locale est couramment observée. Les entrées distales ont quant à elles une organisation différente des entrées sur les cellules de Purkinje, et semblent présenter un patron opposé, ou, du moins, distinct de celui de la connexion cellule en grain – cellule de Purkinje.

Ces cellules ont également été reconstruites, afin de déterminer leur morphologie précise, et notamment l'extension maximale de leur axone. Dans la majeure partie des cas, les axones des interneurones restent localisés autour du soma, avec une extension médiolatérale équivalente à une ou 2 cellules de Purkinje au maximum. Le patron très précis des connexions cellule en grain – interneurones de la couche moléculaire suggère que les interneurones sont liés à un groupe très restreint de cellules de Purkinje, dont ils modulent précisément l'activité. Une observation importante indique que les interneurones sont parfois couplés avec d'autres interneurones voisins, par gap jonction, et que le réseau de couplage ainsi formé reste toujours parasagittal, et ne s'étend jamais selon un axe transversal.

2.3 VARIATIONS DE DENSITES DES SOUS TYPES DE CELLULES DE GOLGI DANS LE CORTEX CEREBELLEUX

Un troisième volet de ma thèse s'est concentré sur la distribution des sous types de cellules de Golgi dans le cortex cérébelleux. Dans la suite du travail d'Héloïse Cruveiller, et de Jean – Luc Dupont, nous avons quantifié les variations de densité de deux sous types de cellules de Golgi : Les cellules de Golgi exprimant le transporteur à la glycine ($GlyT_2^+$) et les cellules de Golgi exprimant la Neurogranine (Neu^+). Alors que la densité des cellules de Golgi, mais aussi celle de ses sous types était jusque là considérée comme homogène à travers tout le cervelet, nous avons montré d'importantes variations de la densité des cellules de Golgi $GlyT_2^+$ et Neu^+, selon un axe medio – latéral, mais aussi selon un axe antero-postérieur.

Les distributions observées sont particulièrement corrélées aux motifs des entrées fibres moussues (par exemple aux entrées provenant du noyau cunéiforme externe ou du tractus lombaire), et aux motifs de connexions entre cellules de grain et cellules de Purkinje.

L'ensemble de ces travaux semblent suggérer une organisation modulaire du cervelet au niveau fonctionnel et au niveau des profils immuno – histochimiques de certaines cellules qui n'avait pas encore été décrite dans la littérature.

Ces travaux donnent de nouvelles clés pour la lecture du fonctionnement cérébelleux et la modélisation de son fonctionnement, et suggère également une plus grande prudence quant à la réalisation de nouvelles expériences, qui devront désormais intégrer l'aspect non-homogène et spatialement organisé de cette structure.

3 ETUDE DE LA TRANSMISSION HAUTE FREQUENCE A LA SYNAPSE CELLULE EN GRAIN CELLULE DE PURKINJE

3.1 TRANSMISSION A HAUTE FREQUENCE DANS LE CERVELET.

Les cellules en grain, dont le soma et les dendrites sont situés dans la couche granulaire sont les seules cellules excitatrices du cortex cérébelleux (mis à part les *cellules unipolaires en brosse*, une sous population de cellules présente uniquement dans les lobules postérieurs). De par leur long axone parcourant la couche moléculaire sur plusieurs millimètres, ces cellules traversent l'arbre dendritique de plusieurs centaines de cellules de Purkinje, faisant synapse avec la moitié d'entre elles. Ces synapses sont pour la plupart silencieuses (80%), et de faible poids synaptique (10 pA). De ce fait, la synapse cellule en grain – cellule de Purkinje a longtemps été considérée comme étant peu fiable, du fait de sa faible probabilité de libération. Dans ce modèle traditionnel, la transmission d'un signal bref se fait via l'activation d'un nombre important de fibres parallèles ou par une activité très soutenue.

Des enregistrements *in vivo* réalisés récemment suggèrent que les cellules en grain sont capables de produire des *burst* à très haute fréquence, jusqu'à 1000 Hz. Or, les mécanismes de libération synaptique à de si hautes fréquences sont mal connus. A ces fréquences, des mécanismes tels que la déplétion du stock de vésicules libérables ou la désensibilisation des récepteurs postsynaptiques peuvent empêcher une transmission précise de l'information. La conséquence serait un filtrage passe-bas du signal. Afin de comprendre comment les entrées provenant des cellules en grain sont intégrées par la cellule de Purkinje, et donc par la sortie cortex cérébelleux, nous nous sommes intéressés à cette transmission synaptique à haute fréquence.

3.2 RESULTATS : IDENTIFICATION DES MECANISMES DE PLASTICITE A COURT TERME A HAUTE FREQUENCE.

Pour étudier ce sujet, nous avons utilisé un modèle d'enregistrements électrophysiologiques *in vitro*, sur des rats juvéniles (P18 – P21). L'ensemble des plasticités connues ont été bloquées pharmacologiquement, et les expériences ont consisté à stimuler électriquement les somas des cellules en grain à différentes fréquences, de façon plus ou moins soutenue, et dans des conditions extracellulaires variables afin de décrire toute la gamme de fonctionnement de cette synapse.

Nous avons confirmé par des enregistrements en paires cellules en grain – cellule de Purkinje, puis via des stimulations extracellulaires de petites populations de cellules en grain, que la probabilité initiale de libération à cette synapse est relativement élevée, et, en conséquence, le taux d'échec de libération de neurotransmetteur est faible, suggérant une transmission fiable de chaque potentiel d'action. De plus, la transmission est fiable dès le premier courant postsynaptique excitateur. Malgré une probabilité de libération initiale élevée, la synapse cellules en grain – cellule de Purkinje est capable d'augmenter le nombre de vésicules libérées d'un coup sur l'autre (facilitation à court terme), et ce même à 500 Hz ou pendant des trains soutenus. Ces résultats suggèrent que les cellules de Purkinje peuvent intégrer des entrées granulaires sans perte d'information sur une gamme allant jusqu'à 1000 Hz, comme cela a été montré à la synapse fibres

moussues – cellules en grain. Cette voie fibres moussues – cellules en grain – cellule de Purkinje pourrait ainsi constituer un filtre passe-haut pour le codage des informations par les cellules de Purkinje. J'ai démontré, en utilisant l'analyse de variance – un outil statistique permettant d'extraire des informations sur la transmission synaptique à partir des fluctuations de l'amplitude des réponses – que cette transmission est due à une augmentation transitoire, dépendante de la fréquence, du nombre de sites de libération de vésicules de neurotransmetteurs. Ceci est possible via l'activation de vésicules initialement résistante à la libération. Ces sites seraient également réapprovisionnés très rapidement en nouvelles vésicules depuis le stock de réserve, permettant ainsi une libération soutenue.

Deux hypothèses peuvent expliquer la mobilisation de ce stock. La vague calcique générée par la bouffée de potentiels d'action dans l'élément présynaptique pourrait permettre la libération de vésicules synaptiques situées à de plus grandes distances des canaux calciques que les vésicules libérées lors d'un unique potentiel d'action. Alternativement, des vésicules non compétentes pourraient être rendues libérables suite au premier potentiel d'action, via des mécanismes intracellulaires impliquant des messagers tels que des phosphatases ou des kinases. Sans pouvoir exclure une contribution du premier mécanisme, les derniers résultats suggèrent que le mécanisme permettant la libération soutenue de glutamate à cette synapse est essentiellement dû au recrutement de sites silencieux lors de *bursts* à haute fréquence via des processus actifs.

4 CONCLUSION

En conclusion, la transmission de l'information par les cellules en grain dans le cortex cérébelleux est spatialement très organisée. Nos enregistrements montrent que les cellules de Purkinje peuvent théoriquement être contactées par 175 000 cellules en grain, et ce jusqu'à plusieurs mm suivant une orientation médiolatérale. De petites populations de cellules en grain ciblent des populations de cellules de Purkinje et d'interneurones de la couche moléculaire bien précises, y compris à de grandes distances, par l'intermédiaire des fibres parallèles. En revanche, les cellules de Golgi sont essentiellement activées par les cellules en grain locales. Bien que non démontré, il est possible que l'existence de connexions privilégiées entre certaines cellules en grain et certaines cellules de Purkinje soit le reflet des mécanismes de plasticité qui se sont déroulés durant la vie de l'animal, puisque les poids synaptiques sont modifiables, et que des zones non-connectées peuvent être réveillées suite à l'utilisation d'un protocole de plasticité i*n vitro*. Cette organisation spatiale reflète probablement l'effet d'apprentissages moteurs survenus au préalable. Nous proposons que la reproductibilité des cartes spatiales entre animaux soit expliquée par l'organisation somatotopique des entrées moussues et grimpantes, qui sont similaires d'un animal à l'autre, et par l'existence de mouvements appris comparables entre animaux vivants dans des milieux similaires. Le mode de transmission de l'information à la synapse cellule en grain cellule de Purkinje permet une transmission fiable et soutenue du message. Les hautes fréquences sont faiblement filtrées, et de ce fait, même l'activation d'une fraction extrêmement restreinte des 175 000 fibres parallèles peut être suffisante pour moduler l'activité de la cellule de Purkinje, et donc du cortex cérébelleux. Une carte spatiale extrêmement précise des connexions fonctionnelles et une transmission fiable de l'information par les cellules sélectionnées est probablement fondamentale dans l'exécution des fonctions cérébelleuses telles que les apprentissages moteurs ou la coordination motrice.

5 COMMUNICATIONS SCIENTIFIQUES AU COURS DE LA THESE

PUBLICATIONS

In preparation — ***Valera Antoine M**, Binda Francesca, Pawlowski Sophie, Dupont Jean – Luc, Casella Jean – François, Cruveiller Héloise, Rothstein Jeffrey, Poulain Bernard and Isope Philippe.*
Cerebellar modules are coordinated by granular inputs

In preparation — *Dupont J. – L. , Cruveiller H. , **Valera A.M.**, Pawlowski S. , Poulain B. & Isope P*
Heterogeneous Distribution of Golgi Cell Subtypes in the Cerebellar Cortex

2013 — *J. Chaumont, N. Guyon, **A. M. Valera**, P. Marcaggi, V. Gautheron, S. Reibel – Foisset, D. Popa, S. Dieudonné, G. P. Dugué, A. Stephan, M. Barrot, J – C Cassel, J – L. Dupont, F. Doussau, B. Poulain, F. Selimi, C. Lena, P. Isope, **PNAS***
Optogenetic Coactivation of Purkinje Cells Controls Climbing Fiber Discharge in the Cerebellar Cortex.

2012 — ***Valera A.M**, Doussau F., Poulain B, Barbour B., & Isope P.*
Adaptation of Granule Cell to Purkinje Cell Synapses to High – Frequency Transmission. ***J. Neurosci., 2012,***

2012 — *Lonchamp E, Gambino F, Dupont JL, Doussau F, **Valera A,** Poulain B, Bossu JL, **Plos One, 2012***
Pre and Postsynaptic NMDA Effects Targeting Purkinje Cells in the Mouse Cerebellar Cortex.

2010 — *Kaufling J, Waltisperger E, Bourdy R, **Valera A**, Veinante P, Freund – Mercier MJ, Barrot M.**, Br. J. Pharmacol. 2010***
Pharmacological recruitment of the GABAergic tail of the ventral tegmental area by acute drug exposure.

POSTER COMMUNICATIONS

2013 — Neurex meeting 2013, Strasbourg
***Valera A.M.**, Dupont J. – L., Cruveiller H., Pawlowski S. A., Binda F., Casella J. – F, Rothstein J., Poulain B. & Isope P.*
Functional Organization of Synaptic Inputs on Mouse Cerebellar Golgi Cells and Purkinje Cells, Related to Zebrin Band Patterns

2012 — 23rd SFN annual meeting 2012, New Orleans.
***Valera A.,** Dupont J. – L., Cruveiller H., Léna C., Pawlowski S. A., Binda F., Rothstein J., Poulain B. & Isope P.*
Functional Organization of Synaptic Inputs on Mouse Cerebellar Golgi Cells Related to Zebrin Band Patterns

2012 — 9th FENS, Barcelona 2012.
***Valera A.,** Dupont J. – L., Cruveiller H., Léna C., Pawlowski S. A., Binda F., Rothstein J., Poulain B. & Isope P.*
Functional Organization of Synaptic Inputs on Mouse Cerebellar Golgi Cells Related to Zebrin Band Patterns
*Doussau F., **Valera A.,** Poulain B. & Isope P*
Low – Frequency Depression at the cerebellar granule cell to Purkinje cell synapse
*Chaumont J., Selimi F., Guyon N., Gautheron G., Reibel – Foisset S., Popa D., **Valera A.**, Dieudonné S., Barrot M., Cassel J – C., Poulain B., Doussau F., Léna C. and Isope P.*
Modulation of cerebellar spatio – temporal activity by optogenetic stimulation of channelrhodopsin specifically expressed in Purkinje cells

2011 — 10th Neurosciences colloquium, Marseille 2011.
***Valera, A.**, Barbour, B., Poulain, B., Isope, P.*
Characterization of short term plasticity during high frequency bursts at parallel fiber – Purkinje cells synapse

2010 — 8th FENS, Amsterdam 2010.
***Valera A**., Barbour B., Poulain B. & Isope P.*
Characterization of short term plasticity during high frequency bursts at parallel fiber – Purkinje cells synapse.
*Kneib M., Gambino F., **Valera A**., Cruveiller H., Rothstein J., Isope P. & Humeau Y.*
Segmentation of inhibition in the cerebellar cortex.

Summary

The cerebellum is a structure involved in the control of posture, gait, motor coordination and motor learning. It integrates both sensory and motor information through two pathways: the climbing fibre-Purkinje cell pathway and the mossy fibre-granule cell-Purkinje cell pathway. Mossy fibre inputs carry sensorimotor context such as somesthesic information from specific receptive fields. Projections arrive in scattered locations in the cerebellar cortex which result in a fractured somatotopy. Sensory information carried by mossy fibres is transmitted to granule cells, which can fire high frequency bursts up to 1000 Hz. Many aspects of the spatiotemporal integration in the mossy fibre pathway structure are still unknown. During my PhD, I addressed two questions:

1: What are the short term plasticities that occur at the granule cell axon (parallel fibre) to Purkinje cell synapse during high frequency bursts and sustained trains? Is the information reliably transmitted in the whole physiological range of frequencies?

2: How are granule cell to Purkinje cell connections spatially organised? Are granule cells homogeneously connected along the mediolateral axis, or are there some hotspots of higher connection probability? Can we describe the cerebellar functional module, that is, the smallest processing unit, at the microcircuit level? This question was further extended to the other granule cell targets: molecular layer interneurons and Golgi cells.

Using whole cell patch clamp recordings in rat cerebellum acute slices, I found that high frequency information processed in the mossy fibre-granule cell pathway is conserved at the parallel fibre to Purkinje cell synapse. Small bursts of action potential could evoke strong Excitatory Postsynaptic Currents (EPSCs) at the Purkinje cell soma. The reliable transmission at the parallel fibre to Purkinje cell synapse can follow high frequency rates, with high initial release probability, paired-pulse facilitation up to 700 Hz, and sustained facilitation during tens of pulses. We found, by using variance mean analysis, that this fast release is possible during bursts through the recruitment of reluctant vesicles that boost vesicular release. Moreover, fast release can be sustained through fast vesicles reloading.

In a second study, by using precise RuBi-Glutamate uncaging onto granule cells, and by recording either Purkinje cells, molecular layer interneurons or Golgi cells, I found that in the anterior vermis of the mouse cerebellum, granule cell to Purkinje cell connection follows a precise spatial organisation. Specific sets of Purkinje cell, that can be identified using histochemical markers, receive inputs from small granule cell hotspots. Local granule cells generally elicit a strong input, but distal granule cells located in specific regions can also be strongly connected. The connection pattern between two neighbouring cells is highly correlated in a single animal. Inter-individual variability is important, probably because of individual motor learning performed in each animal, but similarities can be found, suggesting a shared general organisational map in the cerebellar cortex. Similar experiments performed on molecular layer interneurons showed an distinct pattern, suggesting that a given patch of granule cell either directly activate or indirectly inhibit distal Purkinje cells. Recordings of Golgi cells expressing glycine transporter 2 ($GlyT^{2+}$), a subpopulation of Golgi cells that are not homogeneously distributed, revealed that Golgi cells essentially receive inputs from local granule cells, whereas EPSCs from parallel fibres were weak and rare. This result suggests that basolateral dendrites and apical dendrites perform distinct computations in the network.